An Investigation of the Mechanisms of Wind Generated Surface Waves.

MA'MOUN ALI MOHAMMAD JANAJRAH

A thesis submitted in partial fulfilment of the requirements of the University of Hertfordshire for the degree of Doctor of Philosophy

The programme of research was carried out in the School of Aerospace, Automotive and Design Engineering, Faculty of Engineering and Information Sciences, University of Hertfordshire

Hatfield

2009

Abstract

The goal of wind-waves research is to predict the waves field and its effect on the environment. That environment could be natural or imposed by human endeavour. The mechanism of wind generated waves is described in the present work as a wind-bulk flow interaction rather than as a mechanical process which only transfers the wind energy to the wave. In the light of this description, the generation and growth of surface waves are functions of the physical properties of the interface, density of the bulk flow perturbations and wind shear stress.

While the present models for the prediction of surface growth and evolution show some consistence - in some cases - with observations that were conducted in laboratories and in real fields, the work presented in this thesis justifies and explains the inconsistency or contradictions in other cases between the observations and the predictions. Also, physical interpretations for observations, for example wave growth with fetch, are suggested in the present work.

To illustrate the physical mechanism responsible for wave generation and growth under the effect of wind action, two approaches are used. The first involves studying the effect of the physical properties of the water surface on atmospheric input into the bulk and thus the effect on the formation and growth of capillary waves. The second involves studying the correlation between the wave formation and growth and the density of the bulk perturbations.

Wide ranges of previous data are used to analyse the effect of the physical properties of the water surface on wave generation and growth mechanism for the first approach. Also, a group of experiments using the PIV system (Particle Image Velocimetry) were conducted to study the correlation between the wind speed, bulk flow evolution and wind-waves' generation and growth for the second approach.

The main physical parameters which are responsible for the generation and growth of capillary waves are determined. The Ohnesorge number is modified to predict the generation and growth of surface waves. In the second part, additional physical parameters of the bulk flow are introduced to illustrate the correlation between the wind generated waves and bulk flow evolution. A new parameter is used to scale the

transition of the bulk flow from laminar flow to turbulent flow or the transition of the water surface from an undisturbed surface to a fully disturbed surface.

The history of wind-wave research is relatively short. Although there were basic developments in the 18th century, a concentrated effort really began as a result of the military imperative of the Second World War. These developments were however, largely empirical. A theoretical frame work began to develop with the studies of wind-wave generation in the last century. The present work is conducted to fill some gaps in wind generated surface waves research and to introduce new approaches to simplify understanding wind-waves field and its effect on the environment.

Key words: surface waves, physical properties of the water surface, wave growth rate, bulk perturbations, PIV system.

Acknowledgments

This thesis presents the results of my work performed at the University of Hertfordshire for a period of three years. I would like to express my gratitude to Dr. Raj K. Calay for the trust she had in me before and during my research project. Her supervision and guidance were an important factor in completing this thesis. I would like to thank my second supervisor Dr Andy Lewis and Dr Omer Badran for their contribution and feedback.

My gratitude also to Fadl Isa, David Bell, Chris Dyer, Ian Currie and Steve Lines for their support during my work.

Finally, my special thanks go to my parents and to my wife Hanan for their encouragements and support during all three years of my PhD.

Table of Content

Nomenclature

a	Wave amplitude
c	Phase speed
c_i	Imaginary part of phase speed
λ	Wave length
k	Wave number $2\pi/\lambda$
k_m	Maximum wave number
g	Gravitational acceleration
$g_\perp$	Normal components to the gravity forces
δ	Average surface displacement and
h_m	Mean depth of water flow
W	Surface cell size, $[W] = \sqrt{\sigma/\rho g_\perp}$
R	Average radius of water surface curvature
U_∞	Wind velocity outside of the boundary layer
U_{cr}	Critical wind speed
U_z	Wind speed at height z from the water surface.
U_m	Mean flow velocity of wind
U_λ	Wind speed at height equal λ from the water surface
$U_\circ$	Surface velocity
ω	Angular velocity
T	Temperature
U_i	Inception wind speed
β_d	Viscous damping rate
Δ_c	Damping coefficient

β_t	Temporal damping rate
ν_w	Kinematic viscosity of the water
ν	Kinematic viscosity of the air
$\bar{\nu}$	Mean value of kinematics viscosity of water and air $\bar{\nu} = (\nu + \nu_w)/2$
ρ_a	Density of the air
ρ_w	Density of the water.
μ_a	Dynamic viscosity of air
μ_w	Dynamic viscosity of water
t	Time
Oh	Ohnesorge number
R_r	Reynolds number
R_{er}	Roughness Reynolds number
W_e	Weber number
F_r	Froude number
$W_e(t)$	Turbulent Weber number
$F_r(t)$	Turbulent Froude number
$R_r(t)$	Turbulent Reynolds number
y_1	Viscous sublayer thickness
$Z_\circ$	Roughness length
U_1	Wind velocity at the edge of the viscous sublayer
K	Kárman constant 0.41
τ	Momentum flux
C_D	Drag coefficient
C_{DN10}	Drag coefficient, $N10$ indicates neutral atmospheric stratification at height 10 m from the water surface
C_f	Friction factor

$\acute{u}$	Turbulent fluctuations of horizontal components
$\acute{w}$	Turbulent fluctuations of vertical components
PIV	Particle Image Velocimetry
σ	Surface tension
σ_0	Surface tension of the pure water
$\mathcal{X}$	Surface elasticity
γ	Energy growth rate
f	Wave frequency
$\boldsymbol{\theta}$	Thee angle between the wind and the waves
β	Growth rate parameter
kc_i	Theoretical growth rate
C_g	Group velocity
A_w	Overall leeward surface area of the surface waves
A_U	Overall area of undisturbed water surface
F	Fetch length
$S_{in}(f,\theta)$	Atmospheric input
CCD	Charged Couple Device
$\boldsymbol{\zeta}$	Ratio of kinetic energy density of wind and air
δ_w	Boundary layer thickness 'water side'
V_{RMS}	Root mean square of the bulk velocity
α	Velocity vector angle
Rot (z)	Vorticity
S_w	Swirling strength
$\tau_s,$	Shear strength

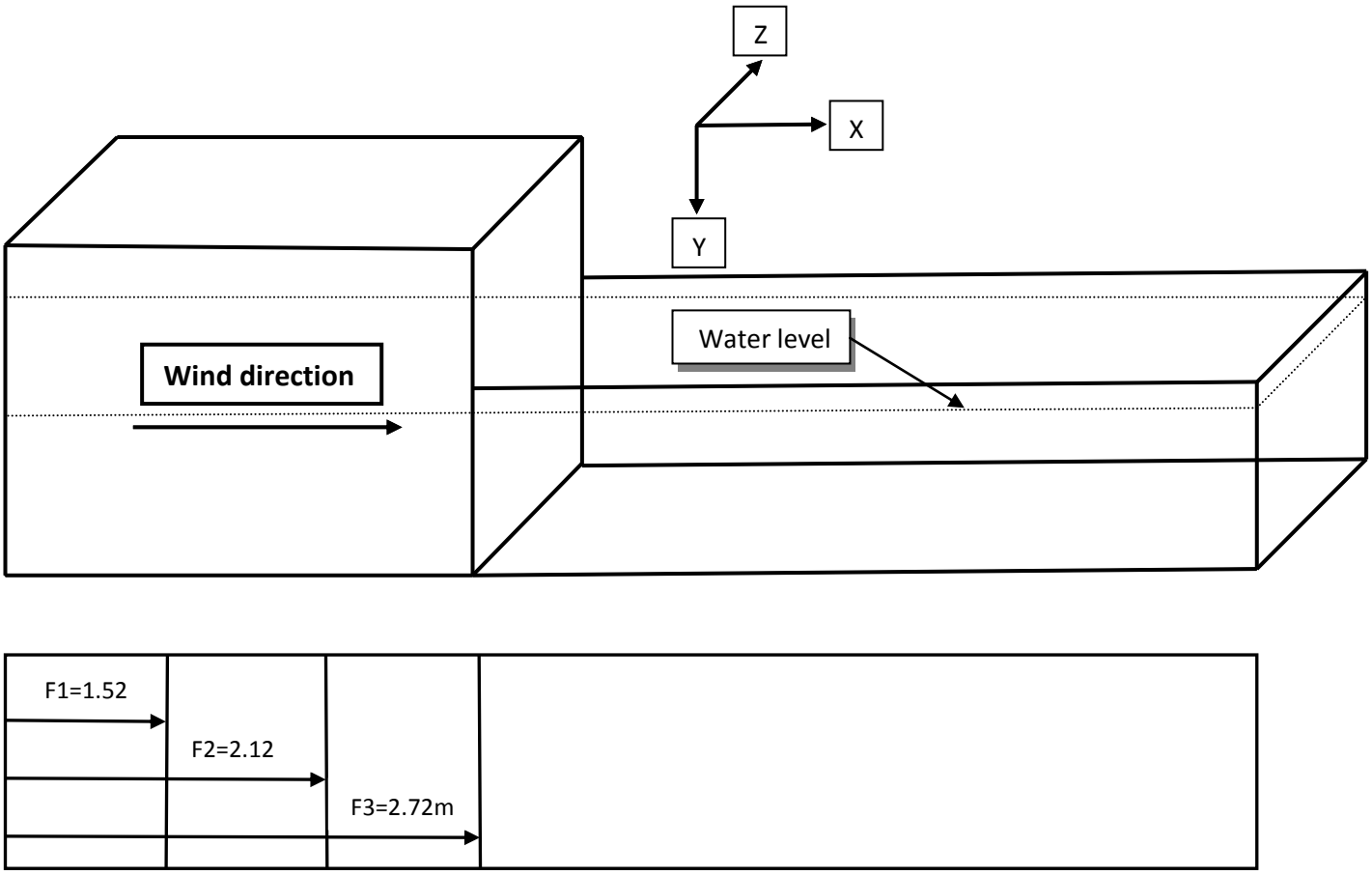

Schematic diagram for the wind tunnel and water channel that used in the current experiments using PIV system.F1, F2 and F3 are the fetch length for the three measuring zones. Details of PIV experiments will be discussed in chapter 3 and 4.

Chapter 1

Effect of the physical properties of water on the wave generation mechanism

I Background

Wind generated surface waves are almost the oldest topic in fluid mechanics and one which requires a better understanding of the conditions at different wind-water surfaces. Despite the large body of theoretical and numerical models to explain the observation of wave evolution over the whole range of wind and wave speeds, the basic questions - such as how the wind generates ocean waves and how these waves evolve - are still not understood according to Belcher et al (1994).

The causal relationship between the wind and surface waves is obvious to even the most casual observers, Young (1999). In a superb review of knowledge at the time, Ursell (1956) remarked ‘‘wind blowing over the water generates waves in the water by a physical process which cannot be regarded as known’’. Plate and Chang (1969) conducted experiments in a laboratory under different conditions and came to a conclusion that no evidence exists which can be used to support existing theories on the inception of the very first ripples; “they have, however, brought out some facts which were not observed before, such as the dependency of the frequency of the first waves on surface shear stress”. Some 34 years after Ursell (1956), Donelan and Hui (1990) reported ‘‘… our ideas of the wind input into the waves is still rather primitive. The theoretical ideas of the fifties have not been capable of explaining the observed growth rate and essentially no new ideas have followed’’. After a few years, Donelan and Hui, Belcher et al (1994) have reviewed the history of wind generated ocean waves and reported ‘‘… yet the large body of literature currently available tends to present a confusing and often contradictory picture. Most of the investigators agree however that the best available theoretical and numerical models are unable to explain observations of wave evolution over the whole range of wind and wave speeds’’. Young (1999) reviewed the previous theories of wind generated surface waves and added ‘‘… our understanding of the detailed processes which lead to a flux of energy

from wind to the wave is incomplete, ….Our existing knowledge, incomplete as it is, yields models which have proven to be remarkably reliable''.

More recently Elsayed (2005) has reviewed several studies were conducted to analyse wind-wave interaction; among those are (Phillips (1957), (1958), Miles (1957), (1959a, b), (1967), Lighthill (1962), Kraus and Businger (1994). Elsayed introduced a new technique 'wavelet bicoherence' to analyse wind-wave interaction. Elsayed reported ''… the studies analysed the generation of the waves during the wind action and the mechanism of primary transfer of energy from wind to water, but still the mechanism by wind generates the waves is not yet understood''.

Lorenz et al (2005) reviewed the available theories of wind generated surface waves. They conducted experimental investigations to describe for the first time the generation of the capillary waves at a pressure of 15-1000 mbar. They reported; ''the problem is difficult to solve by analytical means since the transfer of wind momentum to water surface depends on roughness, which in turn depends on wave growth so far''.

II Wind generated surface wave theories

There are a number of theories that have been suggested to explain the mechanism of the wind generated surface waves. Generally, theories of the wind generation of ocean waves have involved one of two mechanisms: (1) surface instability, for example Kelvin (1910) and Helmholtz (1868), Jeffreys (1925) and Miles (1957) or (2) random excitation by atmospheric pressure fluctuations (resonance mechanism). For example the theories of Eckart (1953) and Philips (1957). The theoretical and experimental investigations that came after these theories were involved in validating, modifying or invalidating the above theories, for instance Plate et al (1969), Larson and Wright (1975), Wu et al (1977,1979), Kawai (1979a,b), Snyder et al (1981), Kahma and Donelan (1988), Young (1999).

The coupling between the surface waves and coherent wave induced pressure fluctuations is the basis of the instability theory. According to this theory, exponential growth rate of energy of a particular wave component increases with time or fetch.

The phase shift angle between the induced pressure fluctuation component and surface elevation is the key difference between the theories related to instability theory. In the Kelvin-Helmholtz theory the phases shift angle is 180 degrees. The observations at sea were very far from theoretical predictions. The theory predicted a higher wind speed to generate surface waves than encountered at sea. The difference was justified by Snyder and Cox (1966) as the coupling between the surface elevation and the induced perturbation was inefficient when the induced perturbation component lags the surface elevation component by 180 degrees. Jeffery and Miles assumed the perturbation component lags the surface elevation component by an angle of 90 degrees. The Jeffery and Miles theories were more efficient than the Kelvin-Helmholtz theory. The theory of Jeffery (sheltering theory) postulates a separation of the flow in the lee of a wave crest which gives rises to fluctuations of atmospheric pressure that is proportional to the wave slope. The wave slope was defined as (ak), where a and k are the wave amplitude and wave number respectively. The other feature of this theory is that the energy transfer is a function of the difference between the wind speed and phase speed; when the phase speed becomes higher than the wind speed, the energy transfer from the waves to the wind and the wave tends to decay. Banner and Melville (1976) indicated that the sheltering theory is unlikely to contribute significantly to the air-water energy flux, since the separation occurs above waves only with the onset of wave breaking. The shear flow theory of Miles neglected any direct interaction between atmospheric turbulence and surface waves, but he allowed for a velocity shear in the mean air flow. Miles (1957) solved the inviscid form of the Orr-Somerfield equation, showing that the energy transfer depends upon the ratio of curvature of the wind profile to its slope at a *critical height* above the surface where $U = c$; U and c is the wind speed at sufficient height from the water surface and phase speed. The coherent wave induced atmospheric pressure fluctuation is considered in Miles theory; the measuring of the pressure over the waves was used in laboratory investigations to measure the wave's growth rate.

Phillips (1957) developed a theory for the generation of waves on the basis of resonance between the surface wave and turbulent pressure field. According to Phillips theory, the energy growth of a particular wave component is linear and increases with fetch or time. Snyder and Cox (1966) found that the growth of energy transfer should be particularly large for wave components satisfying the relation

$$k.U_m - \omega(k) = 0$$

Where $k, \omega(k)$ and U_m is the propagation vector of the component, the corresponding angular frequency and the mean wind velocity measured at appropriate height above the water surface. The required pressure fluctuations to excite the water surface should be large enough to create surface waves. Young (1999) studied Phillips theory (1957) and Miles theory (1957), (1962) and concluded that the Phillips' linear term is important only in triggering initial growth from a calm water surface. Once waves are generated, the waves induced pressure variations which result in exponential growth quickly dominated.

Janssen (1991) showed that the surface shear is determined by the wind speed and the wave spectrum. Janssen modified Miles theory and compared it with observations of Plant (1982), Shemdim and Hsu (1967), Larson and Wright (1975) Wu et al (1977, 1979) Snyder et al (1981) and strong agreement with the theory was found. Belcher et al (1994) plotted the same data using linear scales rather than the logarithmic scales that were used by Janssen (1991); significant scatter was observed.

In some cases, the observations of wave growth rate are consistent with Miles-Janssen theory. Young (1999) commented on such results that even though these observations are consistent with instability theory; "they don't explain the physical process responsible for the wave induced pressure; they do not conclusively confirm the physical mechanism responsible for atmospheric input to the waves".

Also the theory of Miles has proved successful in operational wave models such as Wamdai (1988). Komen et al (1994).

Recently Teixeira and Belcher (2005) developed an analytical model for the initial stage of surface wave generation at an air-water interface by turbulent shear flow in either the air or in the water. They concluded that the turbulence in the water may be more important for the initiation of surface waves than previously expected, because the associated pressure fluctuations are much more efficient. Their model suggests that the stage that follows immediately the *laminar–turbulent transition* of the flow may be the key stage in surface wave initiation. Their results are consistent with recent laboratory experiments by Caulliez et al (1998) which support the idea of an

explosive growth after the transition to turbulence of shear current induced by the wind.

III Introduction

Wind generated surface waves are understood as forming when the wind blows over the water surface and its momentum transfers through the surface to the bulk and generates perturbations throughout. The appearance of the surface waves start if the disturbing effects of the wind shear stress at the surface and the induced bulk flow perturbations exceed the effect of the stabilising and restoring forces of gravity, capillary forces and viscous forces. The growth rate and the characteristics of the surface waves depend on the physical properties of the surface, strength of the induced bulk perturbations and wind shear stress. The waves cannot be generated under the effect of wind action if the strength of the induced bulk flow perturbations is insignificant even if the wind speed is sufficient to generate surface waves.

In the light of this concept, the wind generated surface wave process can be described as wind-wave interaction rather than a mechanical action which only transfers the wind energy to the wave. The wind-wave interaction occurs due to the mechanical action, chemical action, and thermal action as illustrated below. Through the wind-wave interaction the wind-wave acts as a united couple and the cohesion of such a couple depends on the physical properties of the surface.

The chemical action involves natural reactions between the water particles and air particles. An interface lamina between the two phases of wind and water is produced through of such reactions. The characteristics of the interface lamina between the two phases affect by the chemical composition of the water and the air, water surface temperature and the dimensions of the water body. The physical properties of the interface lamina play a significant role in wind-wave generation mechanism. The thermal action affects the wave generation mechanism due to the actions of heat and mass transfer. The bulk-surface and surface-air temperature difference affect the heat transfer and mass transfer from the water to the wind. The mechanical effect indicates the transfer of wind energy to wave due to the action of shear current induced by the wind. The growth rate of the latter depends on the rate of the energy transfer from the wind to the water.

To illustrate the physical mechanism responsible for wave generation and growth under effect of the wind action two approaches are used. The first one, studying the effect of the physical properties of water surface on the mechanism responsible for atmospheric input and capillary waves formation; the second, studying the correlation between the wave formation and growth and the density of the bulk perturbations.

The physical properties of the water surface significantly affect the capillary wave (very short length wave) generation mechanism. Understanding the correlation between the physical properties of the water surface and the capillary wave formation mechanism helps to explain the effect of the former on the wave generation mechanism. The capillary waves affect the formation of the waves, their damping and growth once formed and the tendency of longer waves to break. The parameters that affect the generation and growth of capillary waves are explored. Understanding the generation of the capillary waves mechanism may justify and illustrate the disparities between the characteristics of wind generated surface waves under the effect of different conditions. In wind induced surface waves on a water surface initially calm, the capillary waves form the bases of the mature waves. The wavelength and amplitude of capillary waves are increased as the wind speed is increased. The ratio of wave amplitude to wavelength is important to predict the behaviour of the capillary waves under the effect of wind action.

Capillary waves also play a significant role in wave-wave interaction. When the capillary waves are generated on the surface of longer waves, the nonlinear interaction between longer waves and capillary waves affects the wind momentum flux and wave growth rate. The wave-wave interaction increase as the capillary waves attain a higher growth rate.

The dependence of the wave growth on the fetch length was observed experimentally and predicted theoretically. A unique interpretation of the dependence of wave growth on fetch was proposed based on predicting the growth of the interface kinematic viscosity with fetch. The dimensional analysis approach was used to show the dependence of the interface kinematic viscosity on fetch length. It is hypothesised that the homogeneity of the wind-wave coupling increases as the difference between the kinematic viscosity of the wind and the water surface decreases. This action

influences significantly the transfer of wind momentum to the wave and the wave growth rate.

To emphasise that the growth rate of the surface waves are a function of the physical properties of the water surface and the bulk flow regime, a new pattern of Ohnesorge number (Oh) is proposed to scale the wave growth rate. The new pattern of Oh comprises the effect of the capillary forces, viscous forces and inertia forces. This feature made the Oh number suitable for studying the characteristics of the bulk and the surface.

The correlation between the wind speed, wave formation and the bulk perturbations density was observed experimentally. Experimental work was conducted in wind tunnel facilities (a combinations of water channel and wind tunnel to deliver the wind over water surface) using the PIV (particle image Velocimetry) system as a measuring system to measure the flow parameter under the action of wind. Since the correlation between the onset of the wind waves and the bulk flow transition from laminar to turbulent was observed and predicted analytically, a new method based on analysing the angular movement of the water particles under effect of wind action was proposed to scale bulk flow transition from laminar to turbulent.

This study is divided into four chapters: in the first chapter the effect of the physical properties of the water surface on the wave formation and growth is explored. Such physical effects can be traced through analysing the characteristics of the capillary waves on water surface after introducing a significant change in the physical properties of the water bulk and surface. Also the physical properties of the surface can be changed naturally due to the wind-water interaction. For example, the diffusion of the active materials from the bulk to the surface reduces the surface tension whereas the kinematic viscosity increases as the fetch length increase as proposed.

The parameters that are affected by the characteristics of wind-water interface such as surface velocity, wave velocity, surface structure, viscous sublayer thickness, roughness thickness, drag coefficient, etc, are explored. Previous data were used to analyse the effect of the physical properties on such parameters based on new assumptions and suggestions.

In Chapter 2, the wave growth rate and damping rate is explored. The relevant parameters such as surface elasticity, bulk viscosity, wavelength, friction velocity, wave's frequency, fetch length, that affect the growth and damping rate of surface wave are analysed based on previous data. The purpose of this methodology is to determine the key parameters that affect the wave damping and growth.

In Chapter 3, the effect of the wind action at different speeds on the kinematics and dynamics of the bulk is explored. A group of experiments using the PIV system to measure the parameters of the bulk flow under action of wind were conducted in the Fluid Mechanics Laboratory at Hertfordshire University. Wind tunnel facilities were used to achieve this purpose. The behaviour of relevant parameters such as bulk flow velocity, vorticity, swirling strength, shear strength, velocity vector angle (defined later) under action of wind is studied over several magnitude of wind speed.

In Chapter 4, the same parameters studied in Chapter 3 are analysed at three fetch lengths (the length at which wind blows over the water surface) under the effect of the same speeds. Only the maximum magnitude for each parameter is considered in this analysis. The maximum magnitudes are determined after plotting each parameter against the position along the water channel (PIV measure zone) at six different speeds. The aim of considering only the maximum values is to reduce the error that may occur due to the inaccuracy of the measurement system or due to the structure of the experiment facilities. The consideration of maximum values also helps in obtaining the maximum effects of wind action on the kinematics and dynamics of the bulk.

These approaches to interpreting the wave's generation and evolution may justify the disparity or sometimes the contradiction in wave growth magnitudes between observation and prediction or between the observations conducted under a variety of conditions.

A better interpretation of the physics of the wave generation mechanism under the effect of different conditions of wind and water bodies helps in the following sectors:

- Improving the efficiency of waves-energy generating systems
- Improving ship design to achieve safe sailing with minimum power consumption.

- Predicting the sea state and
- Protecting the sea beach and water reservoir banks from scouring effect.

IV Motivation of this study

A principal motivation for studying wind generated surface waves is the disparity of the observed and predicted values in the characteristics of wind generated surface waves. These disparities can be categorised into two main types: the disparity between the results that are obtained from analytical and numerical models, and the disparity between the results that are observed under a variety of conditions. In the first type, the disparity refers to the main assumptions and approximations and to the background theories that were used to build the analytical and numerical models. In the second type, the field of measurements plays a significant role in the quality of the collected data before analysing and presenting them.

Broadly, the investigations are conducted in laboratories and in real fields. The real fields include open oceans, rivers, lakes and water reservoirs. In laboratory investigations, the conditions of the experiments are much easier to govern. Also the ability of repeating the same measurements under the same conditions in the laboratories is much easier than the real fields. The shortcomings of laboratory measurements are due to the restrictions of the water channels and flumes dimensions and the inability to realise natural conditions such as relative humidity, wind direction and speed, atmospheric pressure, temperature, etc. For instance, there is a variation between the characteristics of initial waves that are generated under the effect of high relative humidity, high temperature, high atmospheric pressure and clear weather and those generated under the effect of low relative humidity, low temperature, low atmospheric pressure, and cloudy weather even if the measurements are conducted in the same water body and under the same wind speed without significant changes in wind direction.

Also the variations in data quality between the real observations and laboratory observations are due to the extensiveness of the water bodies and the characteristics of the water. The former affects the fetch length and the background perturbations which may occur in large water bodies due to bulk-surface temperature difference, density difference, etc. The latter affects the characteristics of the interface and the wind-

water interaction particularly under the effect of slow and moderate wind speed. In laboratory investigations, tap water or distilled water is mostly used to observe waves under the action of wind. However, the characteristics of the water vary in real fields from one water body to another. For instance, in open oceans, the water contains minerals and active materials at a higher concentration than in fresh water. These materials diffuse to the surface by different mechanisms and change the structure and characteristics of the interface. These parameters affect the atmospheric input to the bulk and consequently, the characteristics of wind generated surface waves. The shortcomings of real field measurements are due to the difficulty of controlling the experimental conditions as required in some cases and the repeatability of the same measured parameters under the same conditions.

The inability to directly measure important parameters such as wind momentum flux to the bulk is a significant problem. It affects estimation of the wave growth rate and prediction of the sea state. Such problems cause a lack of understanding of the mechanism of wind generated waves and cause a discrepancy between the results of the investigation.

In addition to the above reasons for the disparity between the results of the investigation, the accuracy of the measurement systems, data analysing techniques and methods of measurement play major roles in the quality of the measured data. The wind and wave parameters are measured directly using particular probes in some cases or indirectly using different techniques. The latter are used if direct measurement systems are not possible or if the direct measurements cause a lack in the accuracy of the measured data. In the current study, a PIV (Particle Image Velocimetry) system was used as an indirect system to measure the water flow characteristics under the action of wind

V Aim of present work

The aim of this study is to find a better interpretation for the physical mechanism of wind generated surface waves. This aim is divided into sub aims as shown below to achieve the main aim:

1. Provide insight into the physical mechanism responsible for the atmospheric inputs to the waves and to the bulk flow

2. Determine the most relevant parameters that affect the wave formation and growth under the effect of wind action.
3. Finding a dimensionless number to scale the wave growth on undisturbed water surfaces or on rough surfaces.
4. Justify the disparity or the discrepancy in other cases between the observations or between the observations and the predictions of the characteristics the surface waves.
5. Suggest a physical interpretation of observed phenomena such as wave growth with fetch.
6. Simplify understanding of a complicated phenomenon.

VI Methodology

- Analytical work

In the first two chapters, published experimental data relevant to the effect of the physical properties of water surface and wave growth rate is analysed to enhance understanding of wind-wave generation under the effect of different conditions. The correlation between parameters related to wave growth and physical properties of the water surface is analysed. The most relevant parameters responsible for growth of the wind wave are determined based on such analysis.

- Experimental work

Experimental laboratory work was conducted in wind tunnel facilities using a PIV system to measure the velocity fields under the action of different wind speeds. The evolutions of bulk flow parameters under the action of different wind speeds were analysed to find the most relevant parameters to the generation and growth of the surface waves. In Chapter 3, the measured data was analysed on a single fetch. However, the fetch length is considered in Chapter 4.

The philosophy of this methodology is finding the correlation between wind shear stress, bulk flow evolution, and physical properties of the water surface and wave generation mechanism.

1.0 How do the physical properties of the water surface affect the wave generation mechanism?

Three essential factors exist simultaneously in the generating of natural surface waves; wind with a significant speed, water with a significant depth and a reservoir with its three dimensions (fetch length with respect to width and water depth). The characteristics of surface waves generated by wind action broadly depend on the characteristics of these factors. Most of the parameters that were considered in the experimental and analytical research that were initiated to observe or to predict the initiation and evolution of the surface waves involve one of these factors. For example, when the wind blows over the water surface, the resulting surface waves are affected by the wind speed, direction, turbulence, duration, air temperature, etc. Secondly, the surface-waves can be generated on seawater, fresh water or on contaminated water. The chemical composition of the water affects the characteristics of the wind-water interface and therefore the wind induced turbulence into the water bulk. Also the growth rate of the surface waves as a function of the bulk flow regime (from laminar to strong turbulence) were observed experimentally and considered analytically in mathematical and numerical models. Finally, the effect of the water body size due to fetch length and water depth on the characteristics of surface waves is well known to even the most casual observer in this field; for instance, the difference between the characteristics of shallow water waves and deep water waves and the difference between the characteristics of surface waves on limited fetch length and on long fetch length of water bodies were observed.

The above three factors are critical in the wind produced surface waves process; the surface waves cannot be generated naturally in the absence of anyone of them. The investigations and the analytical studies that were initiated to discuss the surface wave phenomenon cannot comprise all of these factors at once. The researchers generally considered particular cases to give insight to some parameters related to one of the above factors, for instance, turbulence in water, turbulence in the wind, etc.

To consider the effect of the three factors together on surface-wave generation mechanism, as possible, it is assumed that the characteristics of the water surface (wind-water interface) under the effect of wind action are affected by the characteristics of the three factors at once. For example, it assumes that the viscosity of the surface film which is a main parameter in the atmospheric input to the bulk

flow under effect of steady wind is a function of wind speed (friction velocity), fetch length, water depth and the viscosity of the bulk. Recently, Miraghaie & Smolentsev (2003) studied the structure of the interface which appeared as a cell-type structure. The structure of the interface that is stabilized by surface tension and gravity is a function of the bulk flow regime if no surface disintegration occurs. Davies and Rideal (1963) reported 'the boundary between two homogeneous phases is lamina or film of characteristic thickness where the material in the surface phase shows properties differing from those of the material in the contiguous homogeneous layers. According to Davies and Rideal, the physical properties of the interface comprise the physical properties of both the water side and wind side and it assumed that they are affected by the size of the water body as will be shown later.

The effect of physical properties of the water surface on the wave generation mechanism are considered in this study as comprehensive parameters because they combine the characteristics of the main factors which are required to generate and evolve surface waves. It is postulated that studying the physical properties of the water surface helps to explain observations of wave evolution over the whole range of wind speeds particularly when the wave is generated from an undisturbed surface. This approach may give insight to the physical mechanism responsible for atmospheric input to the waves, thus the surface wave's formation mechanism. At the end, a better interpretation for wind generated surface waves mechanism may be achieved. The importance of studying the effect of the physical properties of water surface in surface waves generation mechanism can be deduced from the following points:

1. The intimate correlation between the capillary wave - which is very important in wave formation and evolution - and the physical properties of wind-water interface
2. The disparity between observed values of the growth rate of the initial surface waves on contaminated water surface and the - considerably smaller - values obtained from clean water surfaces (non contaminated surface).

3. The disparity between observed values of the growth rate of surface waves and the - considerably smaller - values obtained from analytical and numerical models.

1.1 How do the physical properties of the water surface change?

The physical properties of the water surface under the effect of wind action are affected by the active material or surfactants that are present naturally in water samples and diffuse steadily to the free surface, Phongikaroon and Judd (2006). These materials both reduce the surface tension and give the surface elastic properties, which enable it to resist compression, Scot (1981). The questions that arise here are :

- How do the active materials diffuse to the surface?
- How does the active material diffusion to the surface affect the surface wave's generation and growth?
- Under which conditions are the active materials more likely to diffuse towards the surface?
- How do the properties of the surface affect the curvature and the slope of the wind velocity profile?

1.2 Basic definition

According to Rosen (1978), the term interface indicates a boundary between any immiscible phases. However, the term surface denotes an interface where one phase is gas - usually air. In this study, both terms are used to indicate the wind-water interface. Rosen has defined the interfacial free energy as the minimum amount of work required to create the interface. The interfacial (surface) tension between two phases is the interfacial free energy per unit area. The minimum work W_{in} to create an additional amount of an interface is given by the equation $W_{in} = \sigma \times A$, where σ, A are the surface tension and the additional amount of the interfacial area respectively. According to previous studies; active materials reduce the interfacial free energy rather than increase it. The active materials are adsorbed at the interface in an

oriented fashion. The performance of the active materials in the interfacial process depends on their concentration at the interface, orientation at the surface and the associated energy change. Davies and Rideal (1963) found, when a molecule passes across the gas-liquid interface it encounters resistances due to diffusion in the gas phase R_G, across the region constituting the interface R_I and through the liquid R_L . They found that the value of R_I increased significantly in the presence of active materials compared to the case of a clean surface. The value of R_G can be reduced significantly by stirring the air above the interface. According to the above theory, the wind-water interaction is reduced as R_I is increased in the presence of a high concentration of active materials in the bulk. The correlation between the bulk flow evolution and the characteristics of the wind over the surface depend on the strength of cohesion of wind-water coupling as will be shown later.

1.3 How do the active materials diffuse to the water surface?

To explain the diffusion mechanism of the bulk molecules to the surface, Rosen (1978) suggested that, at the interface there is always an unequal distribution of electrical charges between the two phases. This distribution causes one side of the interface to acquire a net charge of a particular sign and the other side to acquire a net charge of the opposite sign giving rise to potential across the interface layer. This layer was called the electrical double layer. To maintain overall electrical neutrality at the interface, the net charge on both sides must be balanced. The potential energy of the surface molecules is greater than the corresponding potential energy of the bulk flow molecules. This is because the attractive interaction between molecules at the surface and those in the interior of the liquid is greater than with the widely separated molecules in the air. Because of this difference in potential energy, an amount of work equal to this difference must be extended to bring molecules from the interior to the surface. The surface tension is a measure of this work. The active materials need less work to diffuse to the surface than the water molecules. Rosen (1978) defined the surface tension as the minimum amount of work required to bring sufficient molecules to the surface to expand it by unit area. According to Jarvis (1965) the active materials that are naturally present in sea water can be adsorbed at the water surface of the sea forming so called slicks and cause a significant change in the other

surface properties and damp the gravity waves. Recently, Phongikaroon and Judd (2006) reported that the surface-active materials or surfactants are naturally present in bodies of water. They diffuse to the free surface forming a thin layer that causes a change in the characteristics of the interface lamina and influences wave motion. In the light of the above explanation, less surface tension is expected for the water bodies that have a high concentration of active materials since in the presence of active materials, less work is required to generate the interface. Also the associated perturbations in the bulk flow due to diffusion of the active material to the surface will be less.

The attraction between the water molecules and the air molecules is suggested through conducting experiments to study effect of the wind action on the flow characteristics. The suggestion sprung from observations in experiments to study the effect of the wind action on the characteristics of the bulk flow. A group of experiments were conducted in wind tunnel facilities (water channel and wind tunnel to deliver the air over the water surface) using a PIV (Particle Image Velocimetry) system as a nonintrusive method of measuring the flow bulk velocity. Tracers needed to be added to the water to trace the bulk flow in all directions. It was found that these tracers have an angular movement with respect to a plane parallel to water surface in addition to the linear movement. It is suggested that the attraction between the tracers and the wind particles is due to the presence of opposite electrical charges on the tracers and on the air molecules, thus causing the tracers' angular movements. To emphasize this suggestion, a simple experiment was conducted by approaching a charged object close to a weak water stream. A notable deviation of the water stream from the normal direction was observed until the charges on the object were equalised by the charges in the water stream. The details of the PIV experiments will be discussed later in Chapter 3 and 4. It can be concluded from the above illustration that the characteristics of the wind-water interface are affected by the presence of the active materials (charged molecules) in the water bulk and by the density of the electrical charges in the air side. It is known that the concentration of the active materials in sea water is higher than those in fresh water. This gives a primitive idea to understanding the difference in the observations in experiments on oceans and on fresh water bodies. The diffusion rate of the active materials towards the surface is assumed to be a function of the density of the electrical charges in the air side which

is influenced by the atmospheric conditions. For example, the density of electrical charges distributed in space on a dry dusty day is higher than those on a clear wet day.

The associated components of liquid flow normal to the surface during a passage of a wave are illustrated by Brown (1936) who stated that induced waves increased the rate of adsorption of surface-active impurities (from very low concentration in the bulk) by up to seven times. This may be due to increase in the wind-water interaction area; as the water surface becomes rough the water surface area increases which influences the process of wind-water interaction. Furthermore, the rate of adsorption of gases into liquid is greatly accelerated if the surface is disturbed by the waves; Downing and Truesdale (1955)**.** In the light of the above illustrations, the resulting of the interface layer is a function of the active material concentration in the water, the associated energy change and the density of the electrostatic charges on the air side. These parameters will determine the capability of the interface layer to resist the distortion under effect of the wind shear stress action and eddy propagation near the surface. The resulting strong interface layer may cause a blockage of heat and mass transfer from the water to the wind and immobilise the atmospheric input to bulk flow. In other words, the strong interface layer isolates the bulk from wind action and affects the wave formation mechanism. According to Davies and Rideal (1963) the formation of the waves, their damping once formed and the tendency of longer waves to break are all phenomena that are affected by the monolayer (active materials) on the surface. They added that the damping of short wavelengths that disturb the surface of large waves are much affected by the monolayer at the surface. This affects the consequent large wave breaking and reduces wave growth due to reduced wave-wave interaction. The following observations illustrate the importance of the physical properties of the surface on the mechanism of wind generated surface wave.

1.4 Observation of surface wave's in water bodies with different surface prosperities.

The calming of the waves at sea during a storm was noted by Pliny who recorded the practice of the seamen of his time of pouring oil on the turbulent sea to calm the waves. In (1762) Franklin was told by an old sea Captain that,' the Bermudans before

they dive to spear fish below the surface of the sea, would first calm the ripples with a little oil to eliminate the otherwise distractive pattern of sun-light produced by the waves used oil to calm the waves. Later Franklin (1773) used oil to calm the ripples and waves at Lake Derwent Water (a lake of moderate size in England).

Keulegan (1951) conducted experiments using soapy water (water with soap) in wind tunnel facilities where the wind velocity was increased gradually, and it was found that no matter how great the wind velocity, the surface of the water resisted the formation of the wave, even at a wind velocity of 12 ms^{-1} or $u_* = 0.6\, ms^{-1}$ ($u_* \approx 0.05\, U_\infty$). Keulegan observed the same phenomenon when he repeated the experiments for several depths of the water from 4 to 14.5 cm and when he introduced a detergent to the water. Keulegan introduced a special manipulation to produce waves in the same channel with substantial dimensions. The produced waves were propagated windward to last the quarter of the channel whereas the rest of the channel was undisturbed, then the waves were damped completely. The wind caused the wave to be formed at a speed of the order 3 ms^{-1} when Keulegan used clean water (without contaminations). Van Dorn (1953) found the critical wind speed (the minimum wind speed required to generate visible waves) for soapy water was 6 ms^{-1}. Two speculations were made by Kawai (1979) on the cause of the increase of the critical wind speed for soapy water; surface tension and characteristics of surface film. According to Kawai (1979) surface tension is a possible factor in explaining the increase of the critical wind speed. The wavelength of the initial wave is so short, so the dispersion relation is strongly controlled by surface tension and the critical wind speed might be altered to a large extent. Since both the surface tension and surface film are formed by adsorption of the solute by the surface, it is not possible to separate them experimentally. Kawai studied the case analytically and compared his results with Miles (1967) who expressed the effect of surface film in terms of surface elasticity, surface viscosity and solubility of surface material and pointed out that the surface film increased the damping rate of surface waves. Kawai (1979) came to the conclusion that the increase in the actual value of critical wind speed is presumably caused by the surface film and no effect of the surface tension on the critical wind speed. The questions that arise here are: What did the soap do in Keulegan experiments that caused the elimination of the effect of wind shear stress on the surface? How does the soap change the mechanism of wind generated surface waves

as on clean water surface? Which parameters are responsible for wind generated waves?

During the experiments that were conducted using a PIV system in wind tunnel facilities to observe the flow characteristics beneath the water surface, it was observed that within one or two days of filling the water channel the contaminants create surface film on the water surface. After running the wind tunnel where the max wind speed was of the order of 4.5 ms^{-1}, the water surface remained unruffled and the flow beneath the surface seemed very calm until the wind shear stress pushed the film downwind of the channel. To find an interpretation for this phenomenon some other experiments were conducted after filling the water channel for more than 10 days to create a strong contaminated layer on the surface. Some amount of dye was injected in the middle of the water channel at a depth of 25 cm from the surface of the water (the total depth of the water was 45 cm) to observe the flow regime. The fan of the wind tunnel was run from rest to deliver wind over the water surface with a maximum wind speed of the order 4.5 ms^{-1}. The wind tunnel attained the max wind speed after 1.5 minutes; the water surface remained unruffled and the flow remained laminar until the wind stress pushed the film downwind after 6 minutes. However, approximately half of this time was needed to disturb the surface and bulk flow when the water surface was clean. Two important conclusions can be extracted from the last experiments using dye in the water: the importance of properties of the surface in wave generation mechanism and the relationship between the bulk flow regime and surface wave generation. The surface of the bulk remained unruffled until the flow transition from laminar to turbulent occurred. The same phenomenon was observed by Kahma and Donelan (1988) while conducting experiments to measure the inception of surface waves and the critical wind speed using wind tunnel facilities. The contaminants from the air created a strong surface film and the surface remained unruffled even at a wind speed of the order 9 ms^{-1} until the wind shear stress pushed the film downwind of the flume. Kahma and Donelan (1988) measured the surface tension of the contamination surface; it was as low as 50 mNm^{-1}; (surface tension of pure water at 25ºC ≈ 72.8 mNm^{-1}).

Mansfield (1973) conducted experiments using a closed channel to observe the flow beneath the water surface under the action of wind. He observed that a steady surface velocity developed as part of a flow extending to the channel bed when a clean water

surface was used. With concentrated solutions of surfactants on the surface (characterized by low surface tension), an entirely different flow was produced. The flow was confined to the boundary adjacent to the surface, and the surface velocity $U_\circ$ increased with the downwind distance X as $U_\circ \propto \sqrt{X^3}$.

Fitzgerald (1964) measured the surface drift velocity of a clean water under the action of shear exerted by a wind and the empirical relationship of $U_\circ \propto 0.033U_\infty$ *was* suggested, where $U_\circ$ *and* U_∞ are surface velocity and wind speed out of the boundary layer respectively. However, in the presence of surfactants, the surface velocity was 50% above the previous value. The increase in drift velocity was justified by Fitzgerald (1964) as a result of surface tension gradient at the interface. Davies et al (1968) conducted experiments using wind tunnel facilities, and they reported that the ripple becomes appreciable on the surface at a wind velocity of about 1.6 ms^{-1} if the water surface is clean, and only above 3.2 ms^{-1} if there is a captive monolayer on the surface (low surface tension). At equal air velocities the amplitude of the induced ripple, when a monolayer is present was only about 9 per cent of that on a clean water surface. Davies et al (1968) justified the differences by the surface tension gradient to balance the wind stress. Gottifredi and Jameson (1970) used artificially-generated mm-scale waves for different viscosity solutions, and they found the lower viscosity solutions had higher wave growth rates, and higher surface tension led to more rapid wave growth. The liquid density was not appreciably varied in their experiments and one bar air pressure was used throughout.

Pockels (1891) showed experimentally that the ripple damping was affected by spreading monolayer on the surface. He reported that the surface tension of strongly contaminated water surface is variable-that is, it varies with the size of the surface.

From the observations of wind generated surface waves as the characteristics of the interface lamina change, it is supposed that the characteristics of the interface lamina affect the following parameters; surface velocity, critical wind speed, the density of the induced perturbations in the bulk, drag coefficient, viscous sublayer thickness, wavelength, surface structure, wave damping and growth rate, wave velocity, maximum wave amplitude.

1.5 Surface velocity

The dependence of surface velocity $U_\circ$ on the wind velocity has been investigated experimentally by many investigators for the various conditions of the surface from that of clean water to a fully damped condition. The most important feature of their results is the difference of the dependence the surface velocity on the surface tension that reduced using different kinds of active materials. For example it was found for the clean water case, the values of the ratio $U_\circ/U_\infty$ were around 0.03 such as Fitzgerald (1963) and, Van Dorn (1953) for Reynolds number $Re > 30{,}000$ (if Reynolds number defined as $Re = \frac{U_\circ H}{\nu}$ where H is the liquid depth) and Gottifredi and Jameson (1970) for $U_\infty > 2ms^{-1}$. Fitzgerald (1963), Van Dorn (1953) found that the value of the ratio $U_\circ/U_\infty$ was independent of the presence or absence of waves on the surface. For the damping surface which was produced in Fitzgerald's (1963) experiment by the addition of detergent to the water; the magnitude of the value of the ratio $U_\circ/U_\infty$ rose linearly with wind speed reaching a maximum value of 0.045 for wind speed of the order 5.5 ms^{-1}. Also, he found that the value of the ratio $U_\circ/U_\infty$ was dependent on the concentration of the detergent. McArthur (1962) suggested that the value of $U_\circ/U_\infty$ in the presence of a surface film undergoes an acceleration for a given wind speed (increases with time). For a concentrated solution of surfactants Mansfield (1973) found that the surface velocity increased with downwind distance X as $U_\circ \propto \sqrt{X^3}$. In contrast to these observations Gottifredi and Jameson (1970) found that in the presence of surfactants (SLS solutions) $U_\circ$ was lower than the corresponding value for clean water surface for wind speed less than $5ms^{-1}$, however for high concentration solutions and for wind speed of the order 4.5 ms^{-1} the $U_\circ/U_\infty$ reached 0.046. Petkov et al (1996) found the surface velocity in the presence of surfactant layers of SDS and HTAP was about two times lower than the clean water surface. In Mansfield (1973) and Fitzgerald (1963) observations, in the presence of surfactants, it was noted that the laminar flow condition near the surface did not extend right down in the water body.

In the above observations, all the solutions of surfactants and detergent materials that were used in the experiments reduced the surface tension. However, the surface velocity attained different magnitudes with respect to the clean water case under the effect of the corresponding conditions. To interpret the above observations, the

characteristics of the used surfactants should be examined. In the case of increasing the surface velocity as in Mansfield and Fitzgerald observations the surfactants were detergent materials which are a kind of soapy solutions. However, the other chemical solutions such as those used in Gottifredi and Jameson and Petkov et al caused a decrease in surface velocity with respect to a clean water surface. The soap material in Keulegan (1951) observations caused an observable change in the surface wave formation mechanism. It seems that the detergent materials cause a significant reduction in wind-bulk flow interaction and only the mechanical action remains active. Due to such process the wind shear stress causes a significant increase in surface velocity and in very thin contagious layer, however, insignificant change occurs in the bulk. Based on the assumption that a significant increase in bulk perturbation should occur to generate wind-waves, the waves cannot be generated in presence of detergent materials. In terms of the physical properties of the water surface it can be concluded that not only the surface tension is responsible for surface wave generation, there are other parameters such as viscosity that have different effects on the wave generation mechanism. Secondly, to generate surface waves the wind–bulk flow interactions should occur to create perturbations through the bulk to feed energy to the surface waves which was eliminated completely by using detergent in the water. Otherwise both the wind flow and bulk flow appear as two independent flows.

1.6 Wave velocity

The velocity c of the wave of length λ on the surface of a deep liquid is given by Thomson and William (1871) as

$$c^2 = \frac{g\lambda}{2\pi} + \frac{2\pi\sigma}{\rho_w \lambda} \quad \text{(1.1)}$$

Equation (1.1) can be written in form

$$c^2 = \frac{g}{k} + \frac{\sigma k}{\rho_w} \quad \text{(1.2)}$$

If λ is very small the first term is unimportant compared to the second term, then the waves are capillary waves. If λ is large, the first term is dominant and the waves are

called gravity waves. Equation (1.1) and for capillary waves (λ<0.5 cm) the reduction of surface tension reduces the speed of the waves (energy of the wave). The contribution of the surface tension to the wave's velocity depends on the wavelength. The effect of surface tension on wave velocity reduces systematically as the wavelength increases. Velocity of waves on a clean surface, corresponding wavelength and percentage of c^2due to surface tension is shown in the table according to observation of Thomson and William (1871)

Table (1.1): The surface tension contribution to the wave velocity of (Thomson and William 1871)

λ (cm)	c cms^{-1}	Percentage of c^2 due to surface tension term
0	∞	∞
0.1	67.8	100
0.3	39.4	99.97
0.5	31.5	97.0
0.59	29.5	92.2
1.0	24.8	89.5
1.71	23.1	74.5
2.0	23.2	50.0
5.0	29.5	42.4
10.0	40.0	10.5
100	125	2.86
1000	395	0.03

It is evident from the previous observations that the presence of the active materials in the water causes the surface tension to attain lesser values compared to clean water. The latter confines the growth of the capillary waves that can be formed on an initially undisturbed surface or on the surface of longer waves. This affects the growth of the gravity waves and the tendency of longer waves to break due to wave-wave interaction. It is suggested that the damping mechanism of capillary waves depends on the length of initial waves. Determining the factors or the parameters that cease and control the length of initial waves helps in understanding the mechanism of wave growth. The reduction in the surface tension in presence of the active materials in the water is one of the parameters that cause a reduction in the length of the capillary wave to minimal values. Explaining the parameters that affect the magnitude of the

wavelength of the capillary waves plays a key role in interpreting the evolution of gravity waves under the effect of wind action. Lorenz et al (2005) studied the generation of the capillary waves under the effect of different conditions by varying the wind speed and atmospheric pressure. They concluded that ‘‘the capillary waves are instrumental in causing larger waves while no claim of proportionality of higher dependence can yet be made’’. They postulated that gravity waves seem to follow the capillary wave trend. Based on Lorenz et al’s assumption, if the capillary waves attained larger wavelength, the gravity waves will attain larger amplitude before breaking because they will attain larger wavelength and vice versa. It was reported that the waves tend to break if their amplitude is higher than one seventh of their wavelength. The wavelength forms the base of the wave's structure, and the maximum height that the waves can attain depends upon the size of the wavelength. If the reduction of the surface tension causes a reduction in the wavelength of the capillary waves what are the parameters that may increase the wavelength?

Other parameters rather than surface tension, such as viscosity, should be considered in studying the effect of the characteristics of the interface on the wave generation mechanism. The viscosity affects the drag coefficient, wave friction factor (stress coefficient). The drag coefficient parameterises the wind momentum flux as will be defined later. Petkov et al (1996) conducted experiments to measure the surface viscosity in the presence of surfactants. It was found that the surface viscosity attained higher values compared to a clean water surface.

Petkov et al traced the trajectories of small glass particle floating on a water surface in the absence and in the presence of surfactants layer. The results were plotted as the distance against the time and the velocity of the particle against the capillary forces. In the presence of the surfactants, the curves x (t) attained a smaller slope compared with curves for pure water, and the particles have two times lower (at the same force) velocity compared to pure water. These results were illustrated by Petkov et al as due to the friction within the adsorption layer. Correspondingly, they found that the dimensionless drag coefficients were more than two times larger in the presence of the surfactants. The results obtained by Petkov illustrate the importance of the surface viscosity in the formation of the capillary waves, their damping once formed and the tendency of longer waves to break**.**

From the above discussion, in the presence of some kinds of active materials in the water, the surface tension reduced and the capillary waves tended to dampen due to a reduction in the wavelength and the corresponding wave amplitude. However other observations showed that in the presence of other kinds of active materials, the surface viscosity increases and the wave growth increases due to an increase in the dimensionless drag coefficient. It is believed that the surface tension and viscosity are the most relevant parameters that affect the generation and the evolution of surface waves. The appropriate dimensionless number that balances the effect of both viscosity and surface tension is the Ohnesorge number which is defined as

$$Oh = \frac{We}{Re} = \frac{\rho_w v_w}{\sigma} V = \frac{\mu_w}{\sigma} V \quad \text{(1.3)}$$

Based on the values of Oh number, the characteristics of the waves may be deduced as they tend to grow or tend to damp as will be shown in section 1.7.

The understanding of the conditions that have a significant effect on the values of surface tension and viscosity may explain the unusual sea state under the effect of a particular wind speed.

1.7 Surface structure

Three dimensionless numbers are usually used in studying the flow regimes and the surface structure; these numbers are Reynolds, Weber and Froude numbers. The Re, We and Fr number are defined respectively as:

$$Re = \frac{\rho_w h_m}{\mu_w} V = \frac{inerti\ a\ forces}{Viscous\ \ Forces} \quad \text{(1.4)}$$

$$We = \frac{1}{(\frac{\sigma}{\rho h_m})^{1/2}} V = \frac{Inertia\ \ Forces}{Surface\ \ Tension} \quad \text{(1.5)}$$

$$Fr = \frac{1}{(g h_m)^{1/2}} V = \frac{Inertia\ \ Forces}{Gravity\ \ Forces} \quad \text{(1.6)}$$

Some authors use the We and Fr numbers as square of the original ones as $We = \frac{\rho h_m V^2}{\sigma}$ and $Fr = \frac{V^2}{g h_m}$. Where $\rho_w, h_m, V, \sigma, \mu_w$ and g are the water density, mean flow

depth, mean flow velocity, surface tension, dynamic viscosity of the water and acceleration due gravity.

Reynolds number scales the transition between laminar and turbulent flows. When the value of Reynolds number exceeds the critical value, laminar flow becomes chaotic and turbulent.

The Froude number can be considered to be the ratio of fluid velocity to velocity of surface waves since water in shallow water basins propagates at a velocity of $(gh)^{1/2}$.

Weber gives a measure of the ratio of the inertia forces of fluid element to surface tension.

As shown in the previous section, both surface tension and viscosity are the most relevant parameters that affect the generation and evolution of capillary waves. Viscosity is a relevant parameter to the Re number, while the surface tension is a relevant parameter to the We number. The dimensionless number that combines the Re and We numbers is the Oh number or in other words, the *Oh* number involves the effect of surface tension and viscosity. The original Oh number is defined as

$$Oh = \frac{We}{Re} = \frac{\mu_w}{(h_m \rho_w \sigma)^{1/2}} \quad \text{(1.7)}$$

If the second We number definition (the square of the original We number) is used then the new definition of the Oh number is given in the form

$$Oh = \frac{We}{Re} = \frac{\rho_w v_w}{\sigma} V = \frac{\mu_w}{\sigma} V \quad \text{(1.8)}$$

A higher value of the Oh number at a particular wind speed indicates that viscous forces are dominant. However, a lower value indicates that capillary forces are dominant. The last Oh definition does not involve any distance variables (flow depth or fetch length) which are already included in the *We* and *Re* numbers. If the *Re* and We numbers are calculated separately, then *Oh* number is calculated or Oh is calculated by the last expression of $Oh = \frac{\mu_w}{\sigma} V$, the same results will be achieved. This means that viscosity and surface tension are functions of the dimensions of the water body.

As mentioned above, Brown (1935) presumed that the bulk viscosity of the solution dose not vary with time, whereas the surface structure does. He then concluded that the damping of capillary dimension waves is a function of the surface structure. For example, the surfaces with high elasticity (low surface tension) indicate high surface resistance to structure distortion. So that the parameters that are used to scale the surface structure can be used to scale the damping of the capillary wave. The Oh number is an appropriate dimensionless number that can be used to scale the interface structure transition from weak turbulence (undisturbed interface) to strong turbulence (highly disturbed but not destroyed), thus scales the damping of the capillary wave**.**

To explain the importance of the *Oh* number in scaling the structure of the water surface which is relevant to the physical properties of the surface, another evaluation for Miraghaie & Smolentsev (2003) study is presented in this work. Hereinafter referred to Miraghaie & Smolentsev as MS.

MS studied experimentally a water-air interface in an inclined open-channel flow as the interface changed from weak to strong turbulence. They used the terminologies of 'weak', and 'strong', turbulence to characterise the interface in which the water-air interface is almost not disturbed, and , on the contrary, highly agitated by bulk eddies but not destroyed respectively. They justify the transition from weak to strong turbulence based on the stabilizing effect of capillary and gravity forces against the disrupting influence of the turbulent kinetic energy.

During the transition, the surface developed cell like structures. According to MS the occurrence of the surface structures and dimensions of such structures are mostly due to bulk turbulence-free surface interactions rather than the wave motion. This conclusion was based on measuring the cell celerity (velocity) which agreed well with mean flow velocity. However, phase speed gravity and capillary waves can be significantly different from the mean flow speed. It is doubted that the flow can be called free surface (neglecting the effect of wind shear) as described by MS since the flow velocity was high and the shear occur due moving the surface in high velocity with respect to the air. In opposition to MS conclusion it is assumed that the wave motion contributed to structured distortion.

The dimensionless parameters of Re, Fr and We were used in MS investigations to study the turbulence-interface interactions, and the spatial forms of turbulent Weber

number $We(t)$ and turbulent Froude number $Fr(t)$ that were suggested by Brocchini and Peregrine (2001) as;

$$We(t) = \frac{\rho_w h}{2\sigma} u_* \quad \text{(1.9)}$$

$$Fr(t) = \frac{u_*}{\sqrt{2gh_m}} \quad \text{(1.10)}$$

were used to scale the interface transition from weak to strong turbulence; in the regime of weak turbulence $We(t) \ll 1$, $Fr(t) \ll 1$ .In strong turbulence $We(t) \gg 1$, $Fr(1) \gg 1$; the stabilizing effect due to capillary or gravity forces cannot restrain the effect of turbulent eddies near the surface. The values of the dimensionless parameters were changed by varying the inclination angle of the flume (the mean flow velocity) and the flow rate**.** As the parameters Fr and We grow, the stabilizing effect due to gravity and capillary forces against the disrupting influence of turbulence decreases, and transition from weak to strong turbulence occurs. Decreasing the stabilizing effects at the water surface is an appropriate condition for capillary waves to grow. However, studying the state of the surface structure helps to predict the growth of the capillary waves since the former is also affected by the flow turbulence. In MS experiment the following range for turbulent Froude and Weber numbers was invistigated: $0.33 < We(t) < 1.98$ and $0.15 < Fr(t) < 0.52$. These values fit with the transitional regime.

Three dimensions were evaluated in the experiments: the average surface deflection (δ/h_m), where δ and h_m are the average surface displacement and flow depth, the surface cell size (w), and the average radius of curvature R. All the three parameters can be associated, to some degree, with the eddy size near the free surface. In the following tables, the measurements of MS experiments and the associated calculations based on these results are shown. The Oh number was calculated as: $Oh = \frac{\mu_w}{\sigma} V = \frac{We}{Re}$. The turbulent Reynolds and turbulent Weber were calculated as $We(t) = \frac{\rho h_m}{2\sigma} u_*$ and $Re(t) = \frac{u_* h_m}{40\ \nu_w}$. The last expression of Re(t) will explained later.

Table (1.2) MS (2003) experiments flow parameter and the corresponding calculations

Run	δ/h (m)	w/[w]	w (m)	δ (m)	h_m (m)	U_m ms^{-1}	α(°)
1	0.054	2.286	0.0062	0.00051	0.0093	1.43	3.5
1	0.065	1.917	0.0052	0.00083	0.0127	1.93	3.5
2	0.073	2.02	0.0055	0.00062	0.0085	1.65	5
2	0.079	1.84	0.005	0.00093	0.0117	2.14	5
3	0.10298	1.575	0.0043	0.00069	0.0067	2.06	10
3	0.0989	1.428	0.0039	0.00095	0.0096	2.63	10
3	0.099	1.392	0.0038	0.0011	0.0111	2.99	10
4	0.1103	1.378	0.0038	0.00064	0.0058	2.33	15
4	0.1096	1.3442	0.0037	0.00091	0.0083	2.95	15
4	0.1195	1.378	0.0038	0.00116	0.0097	3.31	15
5	0.132	1.18	0.0033	0.00066	0.005	2.45	20
5	0.1368	1.216	0.0034	0.00104	0.0076	3.25	20
5	0.1333	1.288	0.0036	0.0012	0.009	3.64	20
6	0.1333	1.244	0.0032	0.0006	0.0045	2.54	25
6	0.1416	1.19	0.0034	0.00102	0.0072	3.5	25
6	0.154	1.27	0.0035	0.00131	0.0085	3.93	25
7	0.1441	0.99	0.0029	0.00062	0.0043	2.67	30
7	0.153	1.2	0.0035	0.00101	0.0066	3.64	30
7	0.17	1.27	0.0037	0.00136	0.008	4.13	30

The friction velocity was calculated according to Pope (2000) as

$$\frac{V}{u_*} \approx 5log_{10}\,\mathrm{Re} - 2.4 \quad \text{(1.11)}$$

Table (1.3) MS (2003) experiments flow parameters and the corresponding calculations

Run	R/hm	u_* ms^{-1}	Fr	Fr (t)	Oh	Re	$Re(t)$	$We(t)$
1	47	0.0725	22.3	0.17	0.0196	13250	16.789	0.335
1	39.5	0.0916	30	0.183	0.0264	24500	28.967	0.7318
2	20.3	0.083	32.7	0.2	0.0226	14000	17.567	0.402
2	10.7	0.101	39.9	0.21	0.0293	25000	29.424	0.8197
3	5.27	0.104	65.3	0.28	0.0282	13750	17.35	0.4977
3	2.42	0.124	74.3	0.286	0.036	25250	29.64	1.0138
3	1.57	0.137	83.6	0.293	0.041	33250	37.866	1.43
4	3.22	0.1179	98.5	0.35	0.032	13500	17.027	0.5537
4	1.61	0.14	110	0.35	0.04	24500	28.934	1.117
4	1.21	0.152	119	0.35	0.045	32250	36.713	1.539
5	3.05	0.125	129	0.4	0.033	12250	15.56	0.536
5	1.36	0.1542	150	0.4	0.044	24750	29.18	1.241
5	0.95	0.167	160	0.42	0.045	32750	37.42	1.7239
6	2.75	0.13	161	0.5	0.035	11500	14.5667	0.522
6	1.1	0.148	192	0.397	0.048	25000	26.53	1.083
6	0.82	0.18	203	0.44	0.054	33500	38.09	1.891
7	2.48	0.137	196	0.47	0.036	11500	14.668	0.5543
7	1.03	0.173	237	0.48	0.05	24000	28.431	1.3566
7	0.74	0.19	250	0.48	0.056	33000	37.848	1.983

Where α, U_m, h_m, δ, w and R represent the flume inclining angle, mean flow velocity, mean flow depth, the average surface displacement, cell size and radius of curvature respectively.$[w] = (\frac{\sigma}{\rho g_\perp})^{0.5}$, $g_\perp$ is the normal components to the gravity forces. The dimension $[w]$ was used by MS in scaling the cell size to introduce the effect of the surface tension. The data of MS and the corresponding calculation of dimensionless numbers and relevant calculations is shown in table (1.2) and (1.3).

MS have studied the average surface deflection, cell size and average radius of curvature as a function of Fr number. The Fr was selected because U_m was increased by varying α and flow rate, which caused a significant reduction in the gravity forces and consequently a significant change in Fr number. The corresponding values of the same dimensions were plotted as a function of Ohnesorge number. As shown in the Figures (1.1-1.5), when these dimensions are plotted against the Froude number, the surface deflection grows by about three times, while the other dimension decreases. The decrease in the cell size is about two times. A well consistent with these results was achieved when these dimensions were plotted against Ohnesorge number as shown in Figures (1.1-1.5). The most significant changes for cell size and average radius of curvature occurred within the relatively narrow range of *Fr* from 20 to about 40-50 or Oh number of a range from 0.0196 to about 0.029. This gives an indication of the most relevant ranges of Fr and Oh numbers to the surface structure. For the surface deflection a systematic increase with respect to Fr and Oh numbers is shown. The surface deflection show a much more systematic consistence as a function of Fr number than Oh number. However, the average radius of curvature shows a much more systematic consistence as a function of Oh number than Fr number.

The above experiments were conducted in a particular arrangement in an inclined water flume to achieve turbulent surface transition from weak turbulence to strong turbulence; this caused a reduction in the gravity forces and consequently a growth in the Fr number. Even under the effect of such particular conditions, the Oh number has shown a high capability to scale the transition of the interface from weak turbulence to strong turbulence. These results indicate a higher capability for Oh number to scale the turbulent surface transition under normal conditions where the viscous forces and capillary forces have a higher effect on the interface structure. Since an increase of Oh number indicates an increase in surface distortion and a decrease in restoring forcing

(stabilising forces) which are appropriate conditions to grow the waves; it is postulated that the Oh number can be used to scale the growth of the capillary waves. The higher values of Oh number indicate that the viscous forces are dominant and the waves tend to grow. However, the lower values indicate the capillary forces are dominant and the waves tend to decay. Figures (1.1-1.5) illustrate the above discussion.

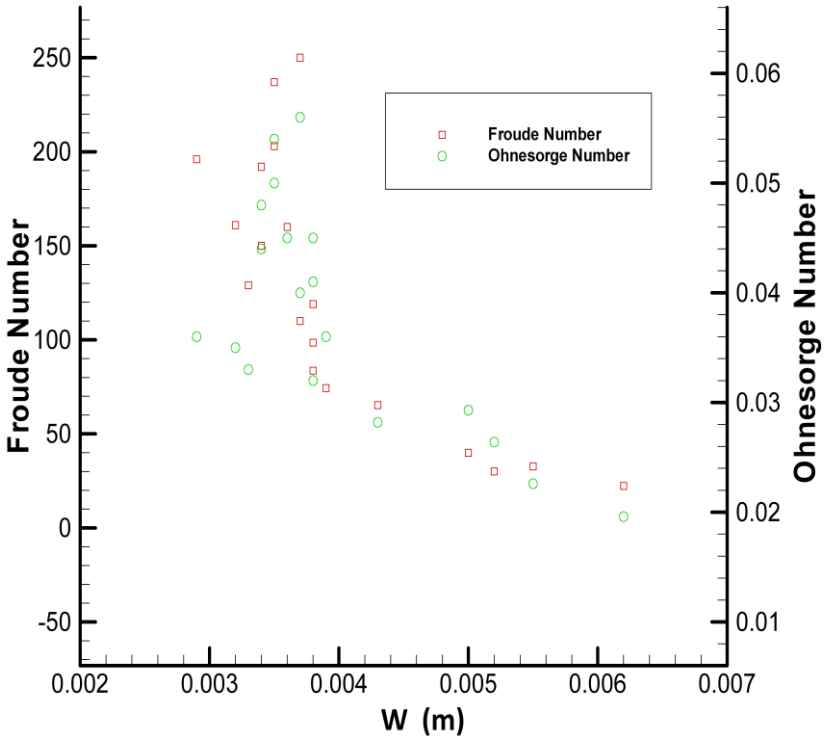

Figure (1.1) Surface cell size (W) as a function of Ohnesorge and Froude numbers

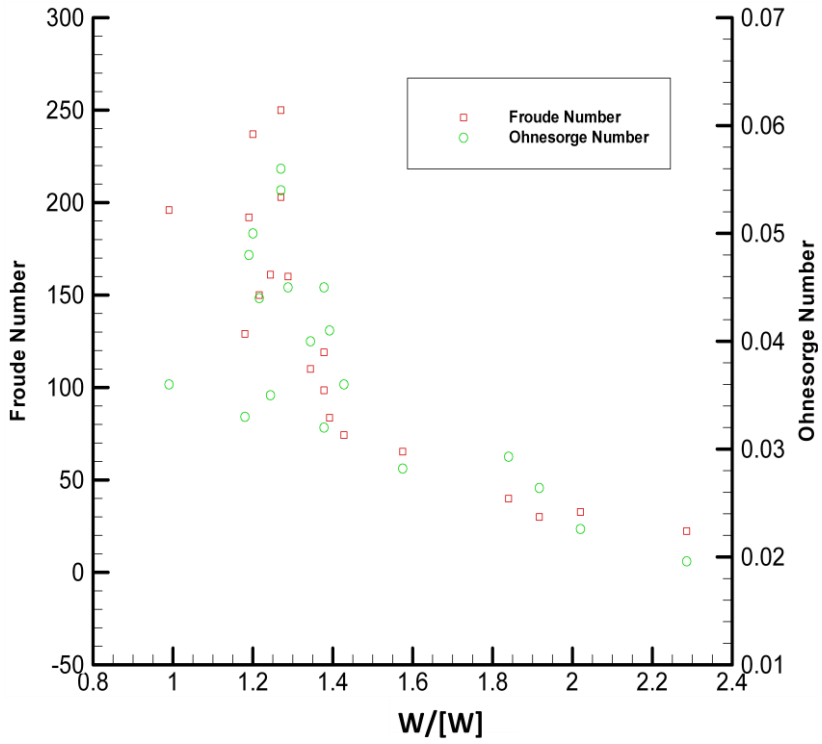

Figure (1.2) Surface cell size scaled with $[W] = \sqrt{\sigma/\rho g_{\perp}}$ as a function of Ohnesorge and Froude numbers

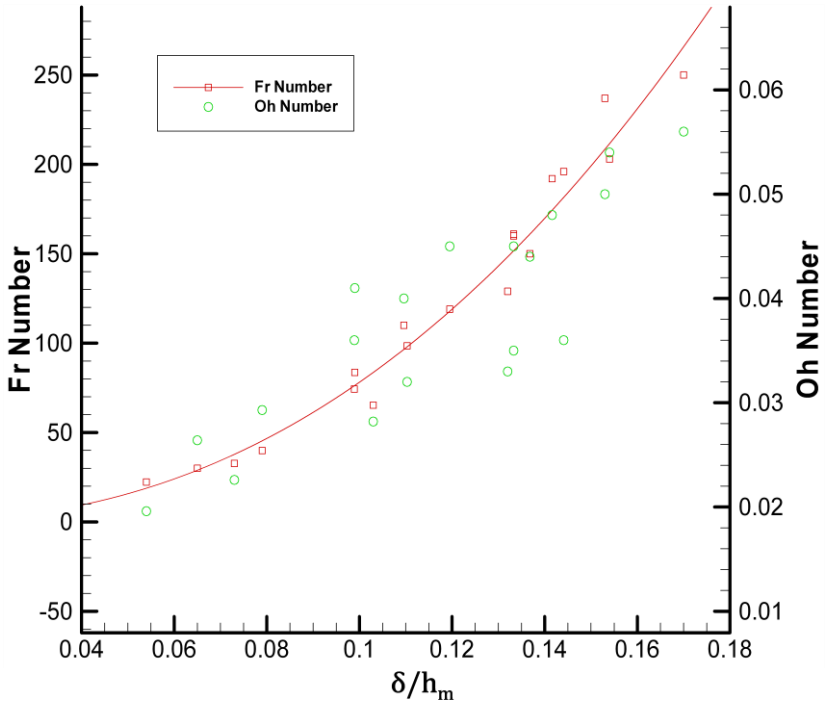

Figure (1.3) Surface displacement normalized by the mean flow depth as a function of Froude and Ohnesorge numbers

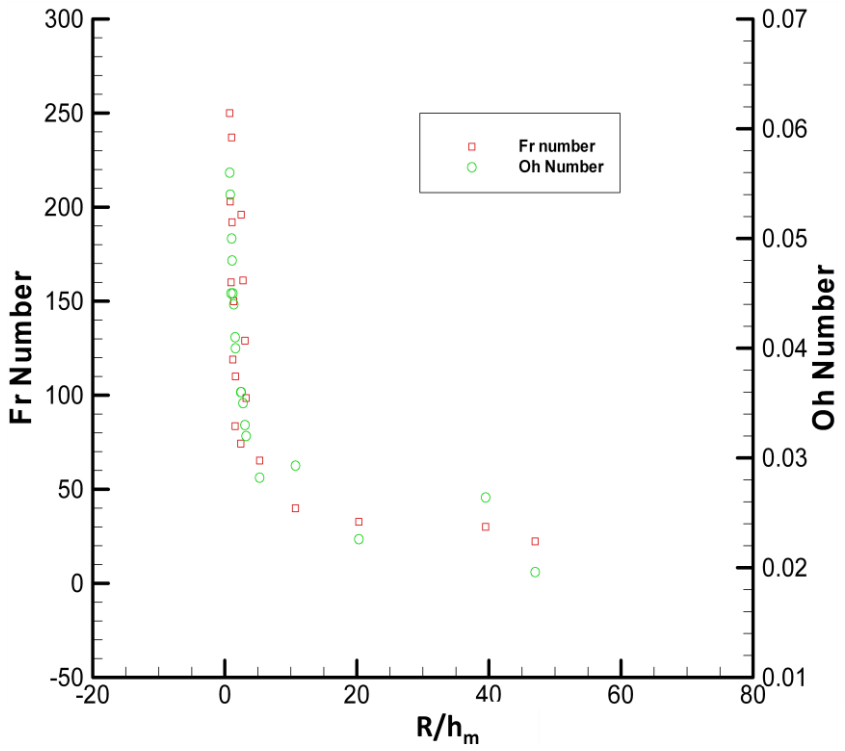

Figure (1.4): Radius of curvature of the turbulent eddy at the free surface scaled by the mean flow depth as a function of Ohnesorge and Froude numbers

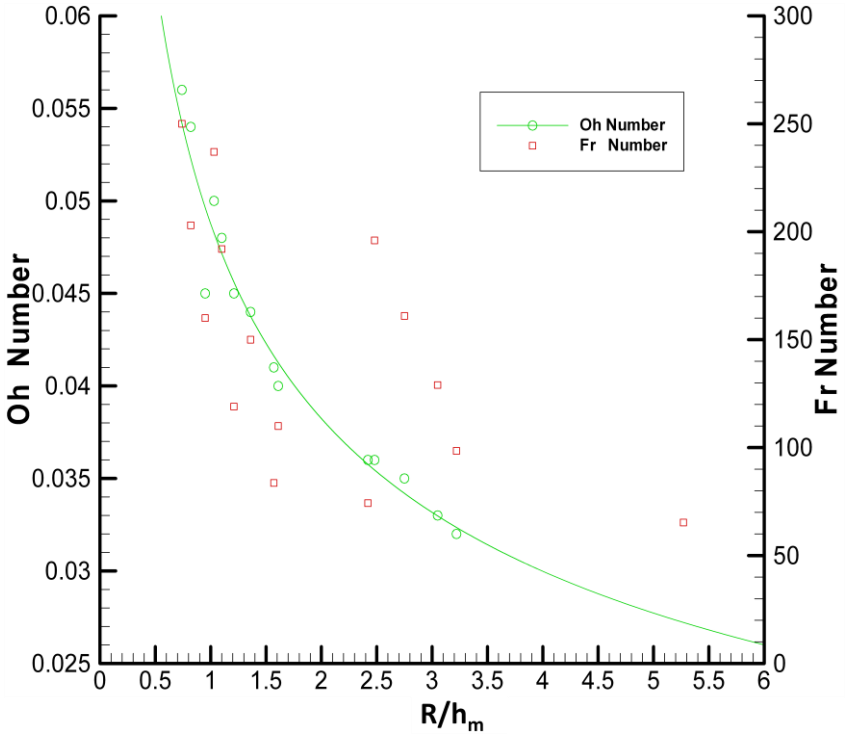

Figure (1.5): An expansion for the previous figure to illustrate the values of the (R/h_m) at higher values of Froude and Ohnesorge numbers

The relationship between the turbulence in the bulk flow and initial wave generation was observed experimentally and predicted theoretically using analytical and numerical models. The above discussion indicated the relationship between the surface structure and the turbulence of the flow through a comparison between the cell celerity and the bulk mean flow velocity. To study the relationship between the turbulence in the bulk flow and the interface structure, it is suggested to plot the above surface dimensions against turbulent Reynolds Re (t) number. The value of $Re(t)$ is calculated from the suggested formula as

$$Oh = \frac{We}{Re} = \frac{We(t)}{Re(t)} \quad (1.12)$$

$We(t)$ is calculated based on Brocchini and Peregrine (2001). It was found that the last expression of Oh number is realized if $Re(t)$is defined as:

$$Re(t) = \frac{u_* h_m}{40 \nu_w} \quad (1.13)$$

Figures (1.6-1.9) below show the relationship between the average surface deflection δ/h_m the surface cell size (w), and the average radius of curvature R as a function of $Re(t)$. The most interesting feature of these Figures is; the $Re(t)$ number can be divided into three main ranges with respect to the interface dimensions as (14.5-17.5), (26-29.5) and (36-38.5). The terms $Re(t)_1$, $Re(t)_2$ and $Re(t)_3$ will be used to indicate the three turbulent ranges and the strength of the flow turbulence respectively. As shown in Figures (1.6-1.9), the strong interface turbulence occurs regardless of the turbulence strength in the bulk flow. The term Δ_{max} which is defined as the maximum change in structural dimension at a particular $Re(t)$range is introduced to analyse the figures below. As a function of $Re(t)$, the Δ_{max} for each interface dimension changes as follow: For w and $w/[w]$ the maximum change in Δ_{max} occurs at $Re(t)_1$. The highest and lowest values of w and $w/[w]$ occur also at $Re(t)_1$ compared with other $Re(t)$ number ranges. At $Re(t)_2$ and $Re(t)_3$, Δ_{max} is reduced systematically and the values of w and $w/[w]$ are shifted to the left (towards the minimal value). In general, a pyramid shape can be obtained as shown in Figure (1.6). For the R/h_m the Δ_{max} occur at $Re(t)_1, Re(t)_2$. The lowest value of R/h_m can be achieved at all ranges of $Re(t)$number and the highest value of R/h_m can be achieved at $Re(t)_1$. For δ/h_m the values of Δ_{max} tend to decrease as

$Re(t)$ increases from $Re(t)_1$ to $Re(t)_3$. The lowest and highest values occur at $Re(t)_1$ and $Re(t)_3$ respectively.

It can be concluded from the above discussion of MS results that the Δ_{max} of each interface dimension is a function Re(t). All the interface dimension values as a function of Re(t) number tend to decrease as the magnitude of Re(t) increases except the value of δ/h_m which tends to increase at higher magnitudes of Re(t) number. These figures give insight to enable the prediction of the values of Δ_{max} for each interface dimension at lower or higher values of $Re(t)$. Figure (1.10) shows the correlation between the surface displacement and both Re and Re (t). This figure shows explicitly the effect of the flow turbulence on the surface displacement. The correlation is systematic as the Re or $Re(t)$ numbers increase from one range to other.

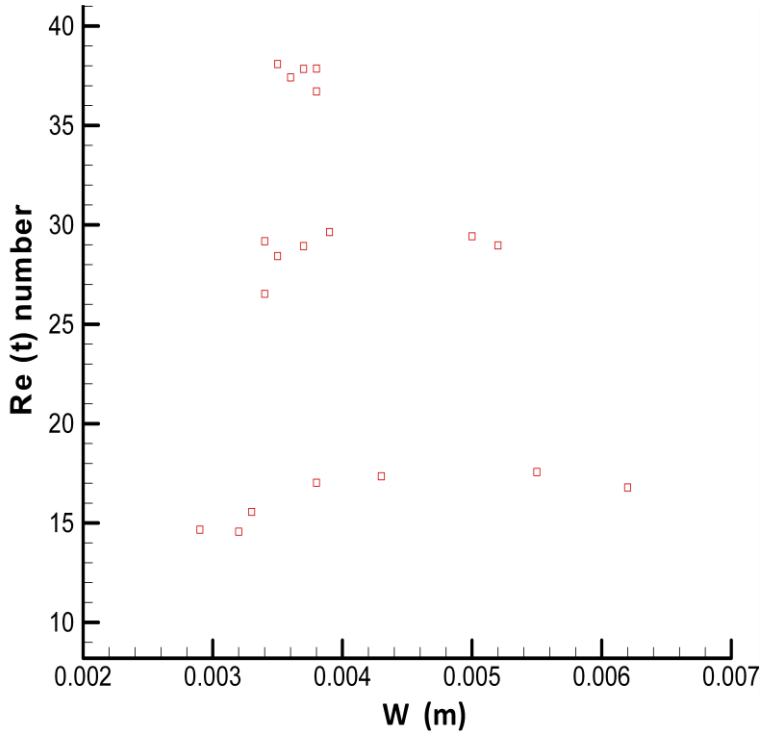

Figure (1.6): Surface cell size (w) as a function of turbulent Reynolds number

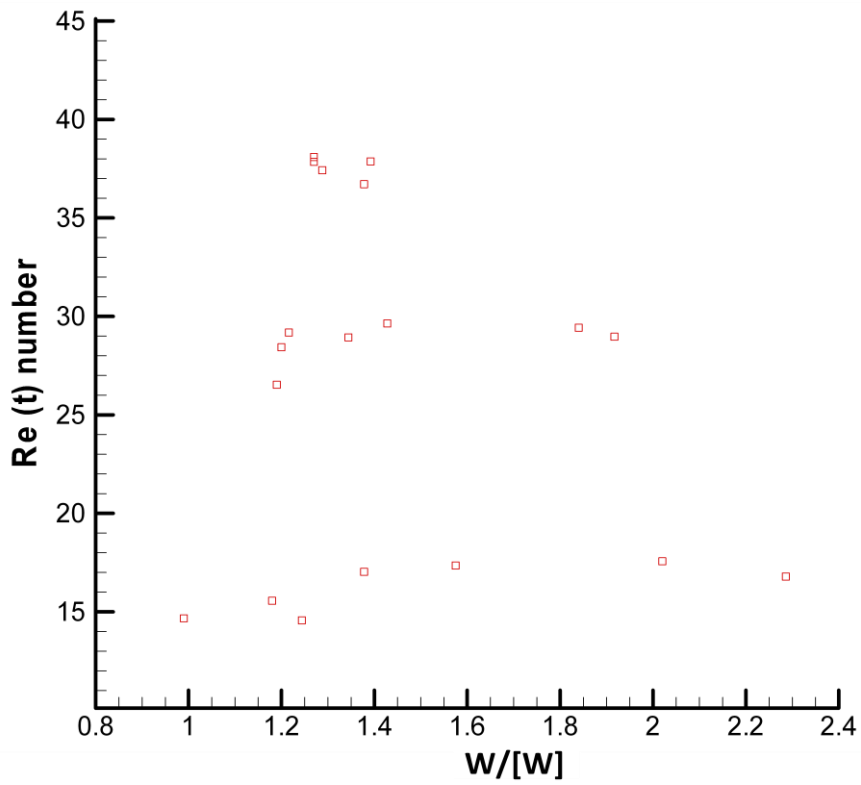

Figure (1.7): Surface cell size scaled with $W = \sqrt{\sigma/\rho g_{\perp}}$ as a function of turbulent Reynolds number

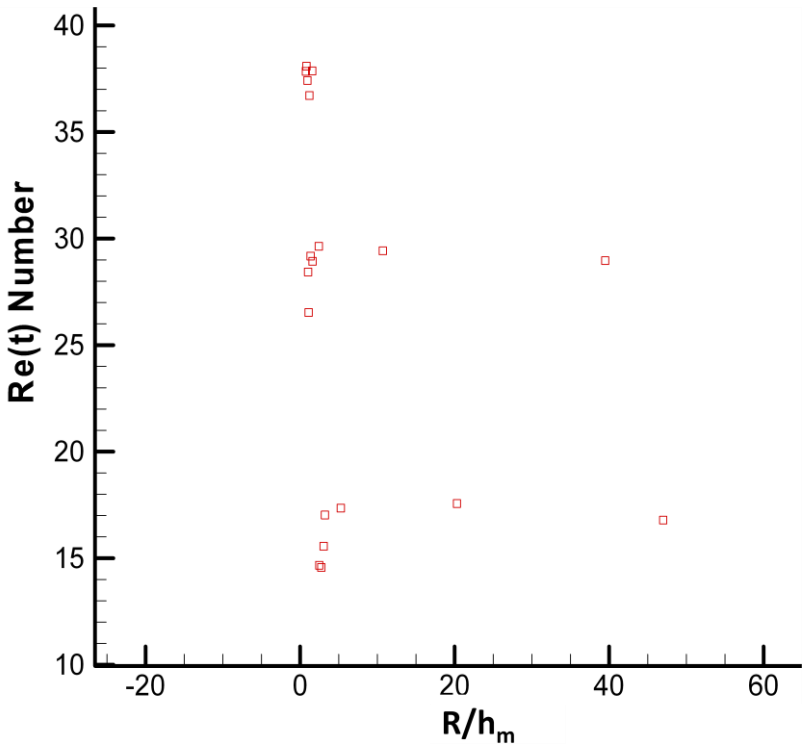

Figure (1.8): **Radius of the curvature of the turbulent eddy at the free surface scaled by the mean flow depth as a function of turbulent Reynolds number**

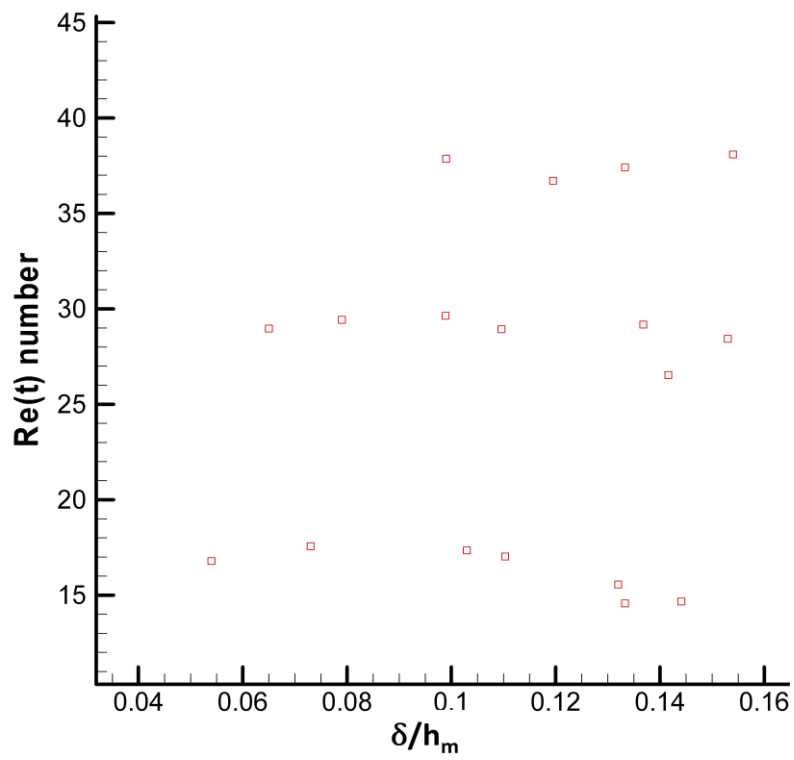

Figure (1.9): **Surface displacement normalized by the mean flow depth as a function of turbulent Reynolds number**

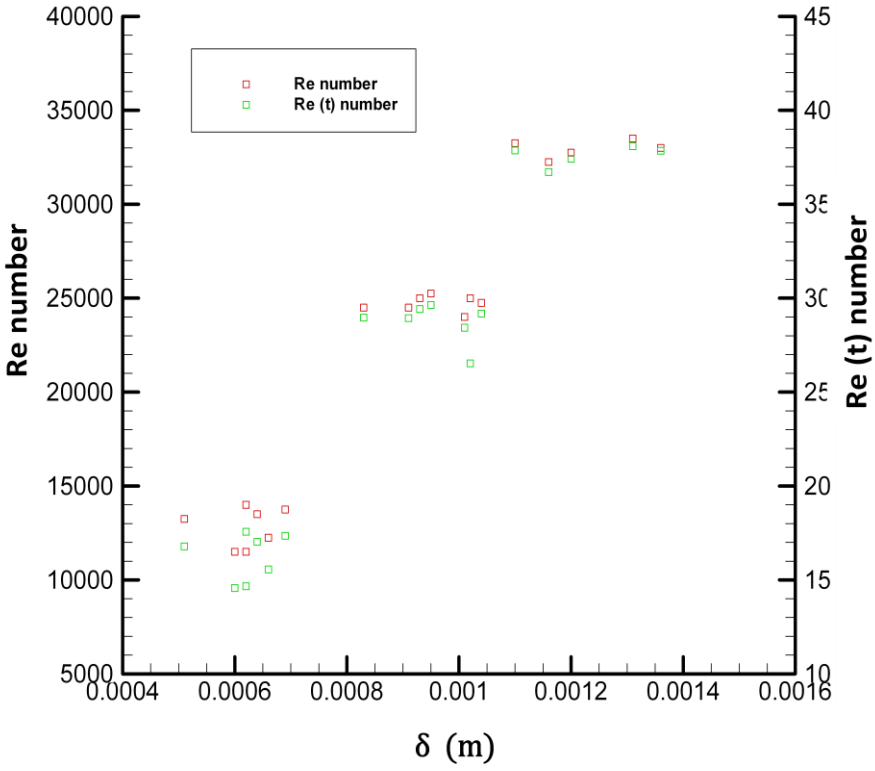

Figure (1.10): Correlation between the Re, Re(t) numbers and the surface displacement.

Figure (1.11) illustrates the relationship between the Oh number and Re number. It is obvious that the relationships between Oh number and Re number has broadly the same trend as the relationships between the interface dimensions and Re(t) particularly δ/h_m versus Re(t) . Figure (1.11) shows that the values of Oh number increase at a particular average of Re number. The overlapping between the values of the Oh number when the average values of Re number increase suddenly from lower range to a higher one is due to the way that the experiments conducted. The experiments conducted in separate runs which caused such overlapping. In general, the maximum value of Oh number can be attained at higher Re number values. It is evident that Oh is a function of Re number and also is a function of the interface dimension (structure) which makes the Oh number suitable to scale the growth of the capillary waves. It is reasonable to infer that the correlation between the bulk-flow turbulence and interface turbulence will be much appropriate at lower magnitudes of Re number.

It should be considered that the above measurements were taken for different runs separately. The systematic correlations between the Oh and Re numbers and the Oh number with structure dimensions are obvious if each run is studied individually as shown in table (1.3).

The summary of the above discussion is; the surface structure and the capillary wave's formation are functions of the stabilising forces and flow turbulent regime. Since Oh number is a function of surface structure and Re number it can be used to scale the formation and evolution of the capillary waves.

It is suggested to employ the Oh number to scale the transition of water surface flow under the effect of wind action from calm (undisturbed) surface to fully disturbed surface when the capillary waves becomes dominant . Since the capillary waves grow on undisturbed surfaces or on the surfaces of longer waves and cause an increase in the wind momentum flux; Oh number may be employed to predict the tendency of longer waves to break. The last formulation of Oh number comprises the flow speed and three physical properties of water; density, kinematic viscosity and surface tension. Or in other words, the capillary, viscous and inertia forces are comprised in the last formulation of Oh number which give the Oh number the capability to scale the wave evolution.

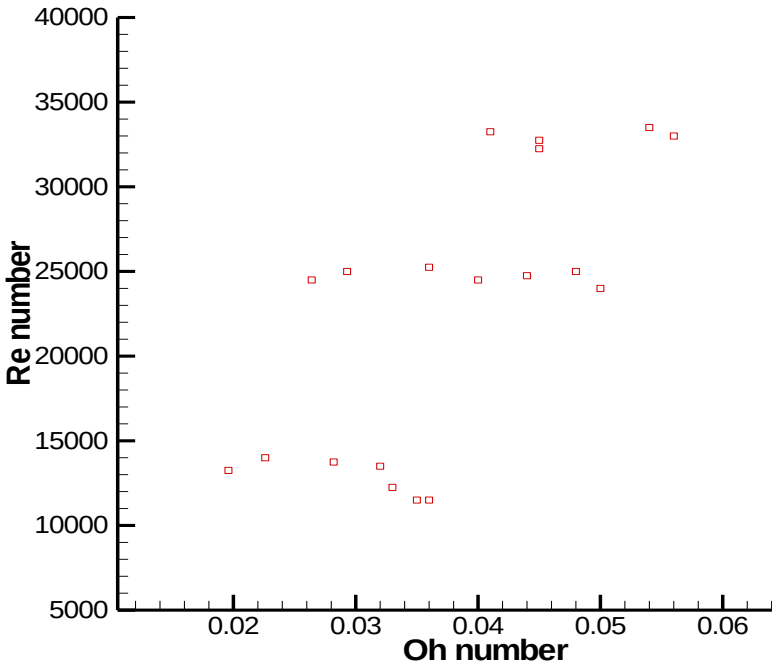

Figure (1.11): Correlation between Re number and Oh number

1.8 Critical wind speed

The critical wind speed U_{cr} is one of the important parameters that is measured in laboratories and in the real field and estimated based on theories. U_{cr} is a relevant parameter in studying the mechanism of wind generated surface waves. The magnitudes of U_{cr} that were obtained from observations were compared with the corresponding magnitudes that were obtained from the theories to confirm particular theoretical hypotheses. Critical wind speed is defined experimentally as: the minimum wind speed required to a produce wave - that is, in principle readily observable, Kahma and Donelan (1988); the speed of the air at a fixed reference location at which the vibration of water becomes visible, Plate et al (1969). Theoretically it is defined as: the speed of wind at which the wave growth rate becomes positive, Kawai (1979). The observed values of U_{cr} in the laboratories and in the real fields varied from those predicted based on theories. Examples of theoretical values, Kawai (1979) 0.93 ms^{-1} ($u_* \approx 4-5$ cm^{-1}) based on shear flow instability theory of Miles (1962); Kahma and Donelan (1988) 0.4 ms^{-1} ($u_* \approx 2$ cm^{-1}) based on Phillips resonance mechanism (1957). In laboratory observation: e.g. Kahma and Donelan (1988) 3.50

ms^{-1} at 4°C, 2.9 ms^{-1} at 35°C ; Keulegan (1951) 3.3 ms^{-1}; Kunishi (1957) 2.4ms^{-1}; Gottifredi and Jameson (1968) 3.5 ms^{-1} for tap water and 2.5ms^{-1} for distilled water; Pierson & Stacy (1973) 3.3ms^{-1}; Wu (1978) 1.6 ms^{-1}; Pokazeyev & Voronin (1982) 3.2-5.4 ms^{-1}. In real field observations: e.g. Scott Russell (1844) 0.85ms^{-1}; Jeffreys (1924) 1.1 ms^{-1}; Roll (1951) 0.4 ms^{-1}; Van Dorn (1953) 2 ms^{-1}.

The discrepancy between the predictions and observations in the values of U_{cr} may be attributable to the theoretical basis that was used in the estimation; for example instability theory assumes that the wave growth rate is exponential and U_{cr} estimated when the growth rate becomes positive (exceeds the viscous damping rate). The discrepancy between the observations that were conducted in laboratories and in real fields is assumed to be attributable to the natural background perturbations that occur in the water bulk; in oceans and large water bodies, natural perturbations occur in water bulk in the absence or presence of the effect of wind action and are due to the extensive water body size, surface lamina formation process, temperature and density differences between the surface and bulk. These perturbations increase the evolution of the bulk flow and form the background energy in a water bulk. The higher magnitudes of these perturbations in a water bulk causes a reduction in the minimum wind speed required to generate visible waves. The relationship between characteristics and the evolution of bulk flow and wave generation and evolution were explored by Mamoun et al (2008). This point will be explained in more detail in the discussion of the results of the PIV experiments in Chapters 3 and 4. Also the relationship between the bulk flow development and U_{cr} value was observed by Mansfield (1973) when the surfactants ceased the wind momentum flux to the bulk.

Following Kahma and Donelan (1988), the discrepancy might be attributable to the differences in experimental conditions and to the definition of critical wind speed.

A new method is suggested to estimate U_{cr} depending on the dynamic values of surface tension and dynamic viscosity of a water body. The method was inferred from tracing the effect of the physical properties of the water surface on the wave generation mechanism. The dimensionless number that measures the balance between viscous forces and surface tension, as shown in the previous section, is the Ohnesorge number (*Oh*).

It is hypothesised that if the magnitude of the critical wind speed, friction speed or mean flow speed for a water body and the magnitude of the ratio μ_w/σ at particular conditions for the same water body are known, the corresponding values under different conditions can be estimated. The main parameter that affects the value of the surface tension and dynamic viscosity is the bulk and surface temperatures. Also the presence of the active materials in the bulk flow or the accumulated contaminates on the surface affect the values of dynamic viscosity and dynamic surface tension. Also the corresponding magnitudes for any liquids can be obtained based on the knowledge of the dynamic viscosity, surface tension and critical speed of the reference. In other words, one accurate reference measurement for the critical (wind, friction, or mean flow) speed will be used to estimate the corresponding values for the water bodies under different conditions. The following formula explains the hypothesis:

$$u_{*_x} = \frac{(\mu_w/\sigma)_x}{(\mu_w/\sigma)_r} \times u_{*_r} \quad \text{..... (1.14)}$$

Where the subscripts r and x refer to the reference and the predicted values respectively. The term u_* can be replaced by U_z or U_m in equation (1.14) to estimate the corresponding values, where U_z and V are the wind speed at height z from the water surface and the mean bulk velocity. The following examples illustrate the above hypothesis:

Kahma and Donelan (1988) revealed the effect of the water temperature on the critical wind speed and inception wind speed values. For example they observed that the critical wind speed increased from 2.9 ms^{-1} at 35$^{\circ}C$ to 3.5 ms^{-1} at 4$^{\circ}C$ and the inception wind speed changed from 0.4 ms^{-1} ms^{-1} at 25$^{\circ}C$ to 0.7 ms^{-1} at 6$^{\circ}C$. the inception wind speed is used by Kahma and Donelan to define the wind velocity at which the wave starts to grow and before they become appreciable to the naked eye.

The ratio of $(\mu_w/\sigma)_x$ at T=4$^{\circ}C$ is 0.02066 and at 35$^{\circ}C$ is 0.01038, and by using the parameters at T=4$^{\circ}C$ as reference parameter. The predicted value of critical wind speed at T =35$^{\circ}C$ using the equation (1.14) is of the order 1.76 ms^{-1}, which is closer to the 1.3 ms^{-1} that is predicted by shear flow instability theory of Miles (1962) if the growth of the waves are assumed as exponential.

For inception wind speed (the waves start to grow but their amplitude cannot be seen be the naked eye) based on the Kahma and Donelan (1988) estimation, the predicted value us ms^{-1} ing equation (1.14) at $25℃$ is of the order 0.43 ms^{-1} which is lower than 0.93 ms^{-1} that is predicted by shear flow instability theory and higher than 0.4 ms^{-1} that predicted by Kahma and Donelan (1988). The summary of the above investigations is shown in Table (1.4).

Table (1.4) summary of the critical and inception wind speed based on the above discussion

T°C	Kahma & Donelan (1988)		Using Equation (1.14)		Shear flow instability theorem	
	U_{cr} ms^{-1}	U_i ms^{-1}	U_{cr} ms^{-1}	U_i ms^{-1}	U_{cr} ms^{-1}	U_i ms^{-1}
4	3.5		2.9			
35	2.9		1.72			
6		0.7		0.7	1.3	0.94
25		0.4		0.43		

Since both the surface tension and dynamic viscosity are sensitive to the temperature, the formula below is derived to find out the value of μ_w/σ for water at different temperatures.

$$\left[\frac{\mu_w}{\sigma_w}\right]_T = 1\Big/\left[\left(\frac{\sigma_{w\,(T=0℃)}}{\mu_{w\,(T=0℃)}}\right)^{1/2} + AT - BT^2\right]^2 \quad \text{..... (1.15)}$$

$A = 0.1$ and $B = 2 \times 10^{-4}$

Equation (1.15) was derived using the data of Fox et al (2004) for the dynamic viscosity and surface tension at different temperature**s.** The typical data at different temperatures are shown in table (1.5). Figure (1.12) shows the correlation between the equation (1.15) and Fox data.

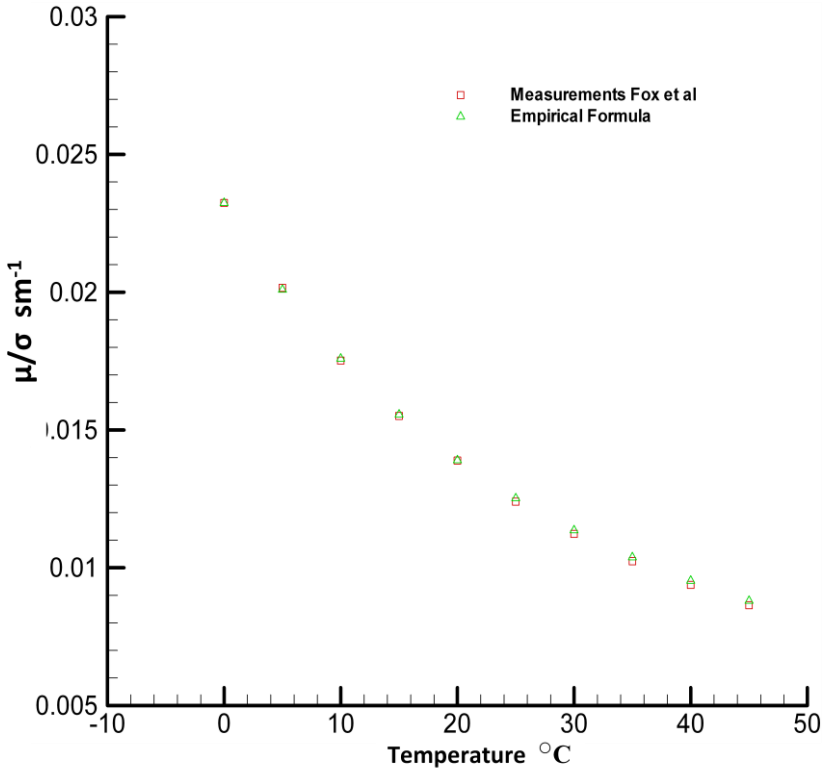

Figure (1.12) Correlation between the ratio of μ/σ and water temperature

Table (1.5) Properties of Water (Fox et al 2004)

Temperature ˚C	Dynamic Viscosity μ (N.s/m^2)	Kinematic Viscosity m^2/s	Surface tension σ (N/m)	μ/σ sm^{-1}	μ/σ eq (1.15) sm^{-1}
0	1.76E-03	1.76E-06	0.0757	0.02324	0.02324
5	1.51E-03	1.51E-06	0.0749	0.02016	0.02009
10	1.30E-03	1.30E-06	0.0742	0.01752	0.01759
15	1.14E-03	1.14E-06	0.0735	0.01551	0.01556
20	1.01E-03	1.01E-06	0.0727	0.01389	0.01390
25	8.93E-04	8.96E-07	0.0720	0.0124	0.01252
30	8.00E-04	8.03E-07	0.0712	0.01123	0.01136
35	7.21E-04	7.25E-07	0.0704	0.01024	0.01038
40	6.53E-04	6.59E-07	0.0696	0.00938	0.00953
45	5.95E-04	6.02E-07	0.0688	0.00864	0.00880

Figure (1.13) shows a comparison of critical wind speed at different temperatures using the surface tension-dynamic viscosity principle (equation (1.14) and Kahma and Donelan (1988) predictions. The magnitude of surface tension and dynamic viscosity

that is used in equation (1.14) is the standard magnitudes according to Table (1.4), however these values are function of the experimental conditions. The difference between the two curves may be attributed to this reason; it is postulated that viscosity and surface tension are function of the fetch length; the kinematic viscosity grows with fetch (as will be shown later) and the surface tension decays with fetch as observed experimentally. If these points are considered it is expected that the gap in Figure (1.13) between the equation (1.14) and Donelan's prediction will be reduced.

Kahma and Donelan (1988) data was plotted based on the observed wave growth rate at fixed temperature assuming the viscous decay rate as $\beta_d = -4k^2\nu_w$ where k is the wave number. Donelan and Kahma (1988) reported that if the growth mechanism of the initial waves is exponential, the inception wind speed should be dependent on temperature. They added; 'because the wave growth rate increases rapidly with k, the wavelength of the initial wave should be longer at lower temperatures'. Kahma and Donelan (1988) measured the surface displacement and slope spectra at $6℃$ and 25 $℃$ and at different wind speeds. The effect of the temperature on the spectra of both parameters at $25℃$ was obvious. On the other hand, a significant increase in U_{cr} value was observed by Kahma and Donelan (1988) when the contaminants formed a strong layer on the water surface with low surface tension as low as 50 mNm^{-1}. By using equation (1.14), the critical wind speed should increase from 3.5 ms^{-1} to 5.02 ms^{-1} at the same temperature if the surface tension is reduced from 72 to 50 $Nm^{-1}$by the contaminants. No measurements were taken for the dynamic viscosity. It is expected that the dynamic viscosity will increase due to the presence of the contaminants and consequently the predicted U_{cr} becomes closer to the observations. The above results show the effect of the physical properties of the water on the wave generation mechanism and the critical wind speed.

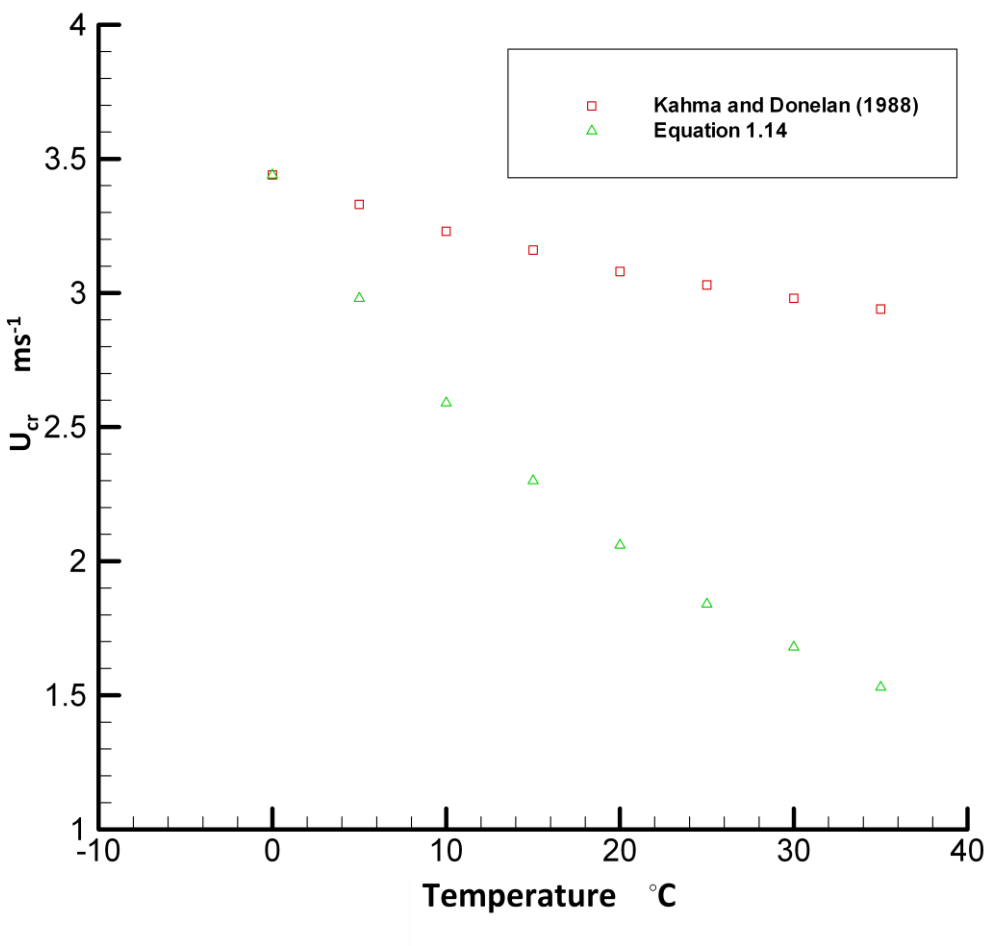

Figure (1.13): Correlation between the critical wind speed and air temperature.

1.9 The effect of kinematic viscosity on wind-water interaction

According to J.T Davies et al (1967) 'the boundary between two homogeneous phases is a lamina or film of characteristic thickness where the material in the 'surface phase' shows properties differing from those of the material in the contiguous homogeneous phases'. When the air flows over the water surface a characteristic lamina occurs between the two phases. The characteristics of such lamina have much importance in studying wind-generated surface waves particularly the infinitesimal wavelets and capillary waves. These waves have much importance in wind-wave interaction and in wave growth rate and decay as discussed above. Most of the equations that are derived to study the characteristics of the interface lamina depend on the properties of the air such as: the equations of viscous sublayer thickness,

roughness thickness, the parameter U_1 (the velocity at the edge of the viscous sublayer), drag coefficient, etc. The most frequently used parameter in these equations is the kinematic viscosity of the air ν. Since the lamina locates very closely to the two phases; It is suggested to introduce a parameter of a mean value of kinematic viscosity of the water and the surrounding air,$\bar{\nu}$ instead of ν. This parameter is estimated as $\bar{\nu} = (\nu + \nu_w)/2.$, where ν_w is the kinematic viscosity of the water. This is because $\bar{\nu}$ combines the effect of ν, and ν_w and both of them respond to the atmospheric change in different magnitudes and directions. For example; if the temperature falls from 20 to 0°C, ν decreases from 1.51×10^{-5} to 1.32×10^{-5} (-12%) whereas ν_w increases from 1.04×10^{-6} to 1.87×10^{-6} (44%) if the properties at 0°C are taken as a reference. The suggestion of using $\bar{\nu}$ in the equations that characterize the properties of the interface layer will be discussed below.

1.9.1 The viscous sublayer thickness

The air flow is characterised as aerodynamically smooth flow if the turbulence near the surface is suppressed and the flow is determined by the viscous shear, the velocity profile is assumed linear (or exponential if the renewal surface is considered). This condition occurs when roughness Reynolds number $R_{er} < 5$, where $R_{er} = zu_*/\nu$. At higher Reynolds number and away from the viscous sublayer ($R_{er} < 30$) the velocity profile changes to logarithmic. At these conditions, the viscous effects become negligible and the total stress is determined by the turbulent transfer, Ataktürk and Katsaros (1999). According to Schlichting (1968), the height at which the asymptotes of linear and logarithmic velocity intersect is taken as the viscous sublayer thickness,

The thickness of the viscous sublayer y_1 was found by Schlichting (1968) as

$$y_1 = \frac{11.6\,\nu}{u_*} \quad \text{..... (1.16)}$$

The virtual origin of the of the logarithmic profile i.e. the roughness length $Z_\circ$ for aerodynamically smooth flow was found by Donelan (1993) as

$$Z_\circ = \frac{0.11\nu}{u_*}, \quad u_* < 2\,(\nu g)^{1/3} \quad \text{..... (1.17)}$$

According to the equations (1.16) and (1.17), $Z_\circ \approx 0.01\, y_1$. The upper bound of the friction velocity in equation (1.17) is affected by the air temperature which in turn affects the value of friction speed, viscous sublayer thickness and roughness length. For example: *at T=0°C,* ν *1.32x10^{-5} m^{-2}s^{-1}, u$_*$ 10.3 cms^{-1},* $y_1 = 149\ mm$ *and* $Z_\circ = 1.41 \times 10^{-3}$ *1.41x10^{-3} and, at T=20°C, ν = 1.513 ×10^{-5} m^{-2}s^{-1}, u$_*$ = 10.6 cms^{-1},* $y_1 = 145\ mm$ *and* $Z_\circ = 1.41 \times 10^{-3}$

The modified formulations of the equations (1.16) and (1.17) by using $\overline{\nu}$ in place of ν according to the assumption that $\overline{\nu}$ is much representative for the kinematics viscosity through the viscous sublayer than ν, since the former combine the viscosity of the air and wind.

$$y_1 = \frac{11.6\overline{\nu}}{u_*} \text{.....} \quad \text{(1.18)}$$

$$Z_\circ = \frac{0.11\overline{\nu}}{u_*}, \quad u_* < 2\,(\nu g)^{1/3} \quad \text{..... (1.19)}$$

Figure (1.14) shows an estimation of viscous sublayer thickness using the equations of Schlichting (1968), Kawai (1979) and the proposed equation (1.18). Kawai (1979b) used a nondimensional parameter r to estimate the thickness of the viscous sublayer which is defined by $r = y_1 u_*/\nu = U_1/u_*$ and the two profiles of Kawai are made for $r = 5$ and 8, this equivalent to ($U_1 = 5u_*$ and $8u_*$). Kawai found that most of the observations lie between these two profiles. The following profiles that are addressed by Kawai 1 and Kawai 2 are plotted based on $r = 5$ and 8 respectively. The profile that is made based on the equation (1.18) lies between the two profiles of Kawai (1979). It seems therefore that using equation (1.18) to approximate the vicious sublayer thickness is appropriate and consistent with the observations since it combines the properties of air and water. The corresponding magnitudes of y_1 based on the above equation are shown in Table (1.6). Table (1.7) shows the magnitudes of viscous sublayer thickness using the same equations in Table (1. 6) for lower friction speeds obtained by Kunishi (1957).

Table 1.6: Viscous sublayer thickness based on the above equations using data of Kawai (1979)

u_* cm^{-1}	$y_1 = \frac{11.6\nu}{u_*}$ mm	$y_1 = \frac{11.6\bar{\nu}}{u_*}$ Mm	$y_1 = \frac{5\nu}{u_*}$ mm	$y_1 = \frac{8\nu}{u_*}$ mm
13.6	1.28	0.68	0.56	0.89
17	1.03	0.54	0.44	0.71
21.4	0.818	0.44	0.35	0.56
24.8	0.7	0.38	0.3	0.49

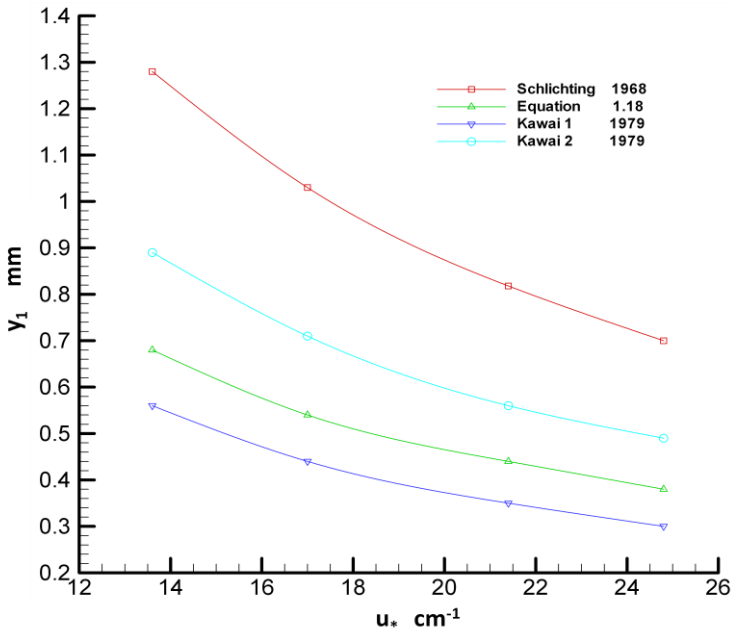

Figure 1.14: Viscous sublayer thickness was calculated using different equations as legend

Table 1.7: Viscous sublayer thickness based on the above equations (friction velocity as measured by Kunishi 1957)

u_* cm^{-1}	$y_1 = \frac{11.6\nu}{u_*}$ mm	$y_1 = \frac{11.6\bar{\nu}}{u_*}$ Mm	$y_1 = \frac{5\nu}{u_*}$ mm	$y_1 = \frac{8\nu}{u_*}$ Mm
2.3	7.61	4.06	3.28	5.25
3.1	5.65	3.01	2.43	3.9
4.2	4.17	2.22	1.79	2.88
4.7	3.72	1.98	1.6	2.57
6.8	2.57	1.37	1.11	1.78
10.3	1.7	0.90	0.73	1.17

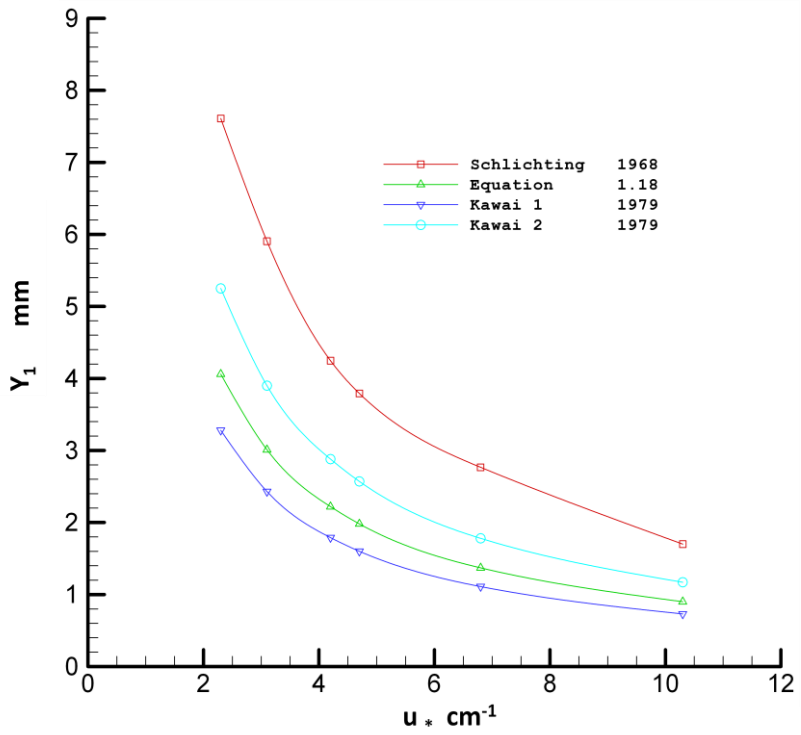

Figure 1.15: Viscous sublayer thickness was calculated using different equations as shown in legend. Kunishi data was used in this figure

Figure (1.15) was plotted based on the data in table (1.7). y_1 has attained higher values and the curve trends are much closer to the logarithmic trend than Figure (1.14) since the wind speed was very low**.** The magnitudes of y_1 based on equation (1.18) seem more reasonable than those calculated based on Schlichting (1968) equation, the latter is quite high compared to the observations; Kawai (1979) reported that most of the observations lay between the two curves that were plotted based on $r = 5, and\ 8$ as shown in Figure (1.15).

1.9.2 The parameter U_1

By using the equation (1.18) to calculate y_1 and Kawai definition of $r = y_1 u_*/\nu = U_1/u_*$ to calculate U_1 ; it was found that the value of $U_1 = 6.18\, u_*$, for all values of r. To examine the validity of using $\overline{\nu}$ in the above equations instead of ν, the equation of Miles (1962b) that was derived on basis of logarithmic law of wind profile to estimate U_1 and modified by Plate (1969) is given here :

$$U_y = U_1 + \frac{u_*}{\mathrm{K}}\left[ln\left(\frac{4\mathrm{K}u_* y}{\nu}\right) - 1\right] \quad \text{(1.20)}$$

After using the term of mean flow velocity equation (1.20) becomes in the form

$$U_y = U_1 + \frac{u_*}{\mathrm{K}}\left[ln\left(\frac{4\mathrm{K}u_* y}{\bar{\nu}}\right) - 1\right] \quad \text{(1.21)}$$

Equation (1.21) will be used to calculate the value of the wind velocity for previous observations using the value of $U_1 = 6.18\, u_*$. The magnitude of wind velocity based on equation (1.21) will be compared with corresponding values measured in laboratories; for example; Kunishi (1957); Hsu and Hsu (1983); Plate (1969); Larson and Wright (1975). In these observations the wind velocity was measured in the laboratories in different conditions in wind tunnel facilities. In Figures (1.16) and (1.17), the wind velocity is calculated for previous measurements based on equation (1.21) and the value of the parameter U_1 is taken as $U_1 = 6.18$. Figure (1.16) shows wind velocity based on equation (1.21) and the corresponding measured values versus friction speed. A good agreement between theory and observation is shown in Figure (1.16).

However, at wind speeds higher than those in Figure (1.16), deviation between observation and theory was observed. To reduce the difference between the observations and theory the operator (ln) was replaced by operator (log) as in the original equation proposed by Miles (1962a). The modified formulation equation (1.20) is in the form:

$$U_y = U_1 + \frac{u_*}{\mathrm{K}}\left[log\left(\frac{4\mathrm{K}u_* y}{\bar{\nu}}\right) - 1\right] \quad \text{(1.22)}$$

Figure (1.17) shows wind velocity versus friction velocity on the same basis as figure (1.16) but for higher wind speeds.

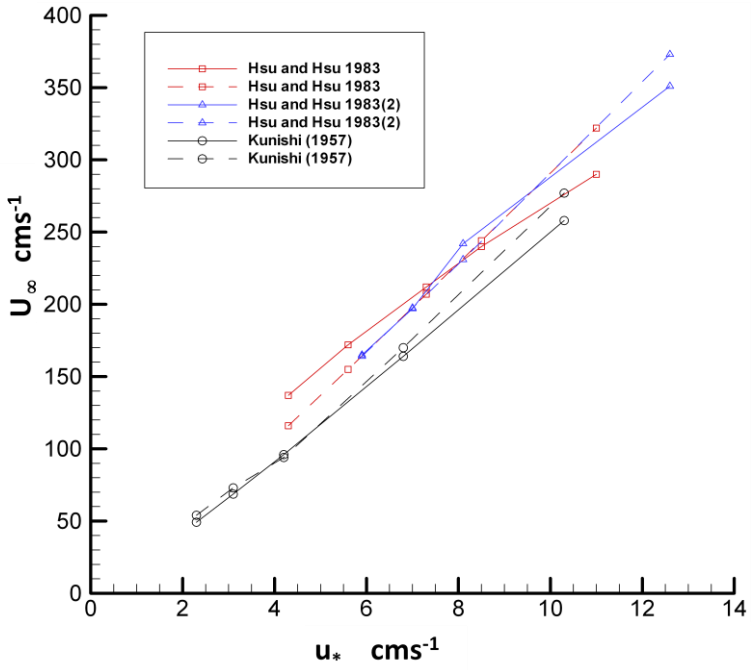

Figure (1.16): Correlation between wind velocity and friction velocity. The solid lines indicate experimental results and dashed lines indicate theoretical predictions using equation. The value of parameter U_1 is $6.18u_*$.

In Figures (1.16) and (1.17) the wind speeds were measured at heights outside the boundary layer. The boundary layer and viscous sublayer did not affect the measurement of the air flow.

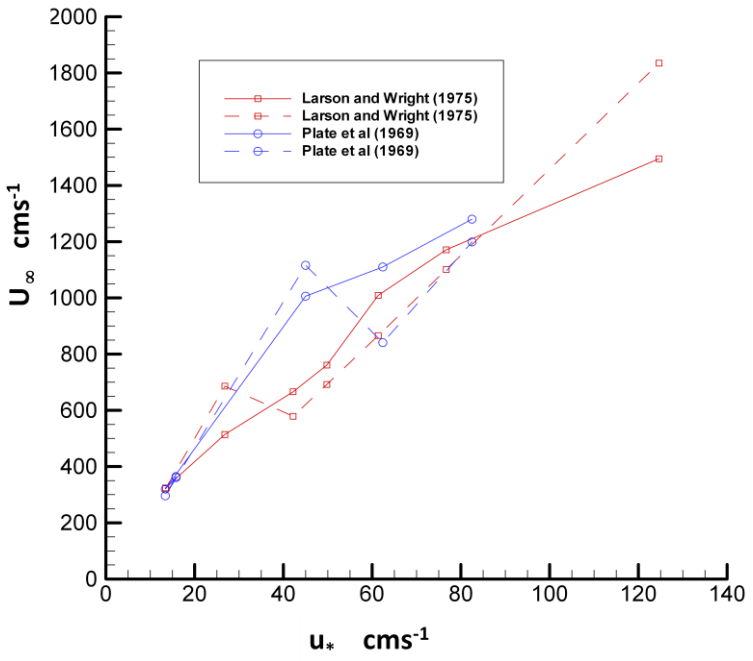

Figure (1.17): Correlation between wind velocity and friction velocity. The solid lines indicate experimental results and dashed lines indicate theoretical predictions. $U_1 = 6.18u_*$.

1.9.3 Drag coefficient

In a bulk aerodynamic formulation the momentum flux is related to the difference in mean wind speed between the surface and some height, z, using a dimensionless drag coefficient C_D

$$\frac{\tau}{\rho} = C_D[U_z - U_\circ]^2 = u_*^2 \quad \text{..... (1.23)}$$

Ataktürk and Katsaros (1999) pointed out that C_D is a function of roughness length and atmospheric stratification. Katsaros (1986) calculated C_D after adjusting the atmospheric stratification to neutral conditions then the remaining effects due stratification are very small. The drag coefficient corresponding to these conditions is calculated according to Katsaros (1986) as

$$C_{DN10} = \text{K}^2 \left[ln\frac{10}{Z_\circ}\right]^{-2} \quad \text{..... (1.24)}$$

Where K and $Z_\circ$ is the von Kárman constant 0.41 and surface roughness length respectively. Geernaert (1990) reported that C_{D10} at low wind speed converges to $C_{DN10} \approx 1 \times 10^{-3}$ and at a given wind speeds is larger for shallow or fetch limited sites; the waves associated with shallow or fetch-limited sites being steeper and moving slower relative to the wind speed. The subscript $N10$ indicates neutral atmospheric stratification at reference height 10 m from the surface. Ataktürk and Katsaros (1999) found that drag coefficient adjusted to neutral atmospheric stratification and at reference height of 10 m depends on roughness length (the height of the virtual origin of logarithmic wind speed profile); the drag coefficient values fluctuated from $(0.5\sim2) \times 10^{-3}$.

From equation (1.23), drag coefficient is a correlation factor between the friction speed, surface speed and momentum flux. The increase in surface speed at a particular wind speed decreases the momentum flux. As stated in section1.5 and 1.8, the surface speed and the critical wind speed were increased significantly when the water surface was covered by a surfactant film which is characterized by low surface tension; the transfer of wind momentum to the water bulk was confined to the surface adjacent layer and an increase in surface speed was observed in some cases.

To estimate the drag coefficient in the viscous sublayer the following equations were employed here. Kawai (1979b) has modified the pattern that was proposed by Miles (1957) to find the wind speed at height z from the surface in the viscous sublayer and presented it in the form:

$$U_z = \left(\frac{u_*^2}{\nu}\right) z + U_\circ, \text{ for } 0 \leq z \leq y_1 \quad \text{(1.25)}$$

From the equation (1.25) the friction velocity of the air can be expressed as

$$u_*^2 = \frac{(U_z - U_\circ)\nu}{z}, \text{ for } 0 \leq z \leq y_1 \quad \text{(1.26)}$$

By equating the equations (1.23) and (1.26), the value of C_D can be expressed in the viscous sublayer as:

$$C_D = \frac{\nu}{z(U_z - U_\circ)} \quad \text{(1.27)}$$

The same principle of using the mean values of kinematic viscosity is suggested for use in determining the drag coefficient.

$$C_D = \frac{\overline{\nu}}{z(U_z - U_\circ)} \quad \text{(1.28)}$$

$U_\circ$ in fully developed region was estimated by Phongikaron et al (2006) about $0.02U_\infty$, Fitzgerald (1963) found that $U_\circ/U_\infty = 0.03$ for all wind speeds.

The most interesting features of the above equations are:

If equation (1.18) is used to calculate the viscous sublayer thickness, equation (1.21) to find the wind velocity at y_1 and equation (1.28) to find the drag coefficient; the drag coefficient is constant and is of the order of 0.0081 for all cases. These results were examined for measurements of Kunishi (1957), Plate et al (1982), Mastenbroek (1996), Hsu and Hsu (1983) and Gottifredi and Jameson (1970) for different frequencies and fetch length. All of these observations have given the same value of the drag coefficient parameter.

Gottifredi and Jameson (1970) defined the friction factor C_f in the form $C_\mathrm{f} = (u_*/U_\infty)^2$. They found that the magnitude of C_f for laboratory experiments was $(2.5\sim4) \times 10^{-3}$. Larson and Wright defined wind stress factor C in the form

$C = (u_*/U_{max})^2$ and the values of C for laboratory experiments was $(2.5 \mp 0.5) \times 10^{-3}$).

If the same equations are used to calculate the viscous sublayer thickness and the velocity of the wind at y_1 the friction factor suggested by Gottifredi and Jameson (1970) is also constant. It is of the order of 0.00837 for all the above observations.

It is concluded that the drag coefficient and friction factor at height y_1 are constant for all observations. Figure (1.18) below shows the momentum flux versus friction velocity based on equation (1.28) to calculate the drag coefficients. If the value of C_D is of the order 0.0081, the momentum flux equation will be in the form

$$\tau = 0.0081\rho_a(U_z - U_\circ)^2,\ z = y_1,\quad U_\circ = 0.03U_z \quad \text{(1.29)}$$

Ataktürk and Katsaros (1999) calculated the momentum flux on lake Washington using the eddy correlation technique as $\tau = \rho\overline{\acute{u}\,\acute{w}}$. Where $\acute{u}$ and $\acute{w}$ is the turbulent fluctuations of horizontal and vertical components and the overbar denotes the space average. The fit line for Ataktürk and Katsaros observations is a shown as a pink colour in Figure (1.18). The regression line equation and the root mean square error e_{rms} for the fit line of the correlation between the friction velocity and momentum flux was of the form (as proposed by Ataktürk and Katsaros)

$$\tau = \rho(0.14(U_{N10})^2 + 0.44U_{N10} - 1.83) \times 10^{-2} \quad \text{(1.30)}$$

$$e_{rms} = 0.013\ N\ m^{-2}.$$

The momentum flux according to the equation (1.29) were calculated using data of Kunishi (1957), Gottifredi and Jameson (1970) at two different fetch lengths, Hsu and Hsu (1983) and Mastenbroak (1996). A very good agreement between the trends of τ versus u_* with Ataktürk and Katsaros (1999) estimation was found. For the corresponding friction speed, the magnitudes of the momentum flux based on equation (1.29) were higher than those estimated by Ataktürk and Katsaros (1999) using the eddy correlation technique. The above observations were made in a number of different conditions, and the applied wind speed varied from one experiment to another. In general the maximum wind speed in the above observations was lower than those recorded in Ataktürk and Katsaros (1999) observations

Ataktürk and Katsaros conducted the experiments during summers of 1986-1989 at Lake Washington. Quadratic dependence of momentum flux on wind speed was observed. The calculations of drag coefficient based on wind speed at $z \gg y_1$ showed in previous investigations an increase and scatter as the wind speed increases. However, a constant value is obtained if the magnitude of wind speed at height y_1 is used in calculating the drag coefficient.

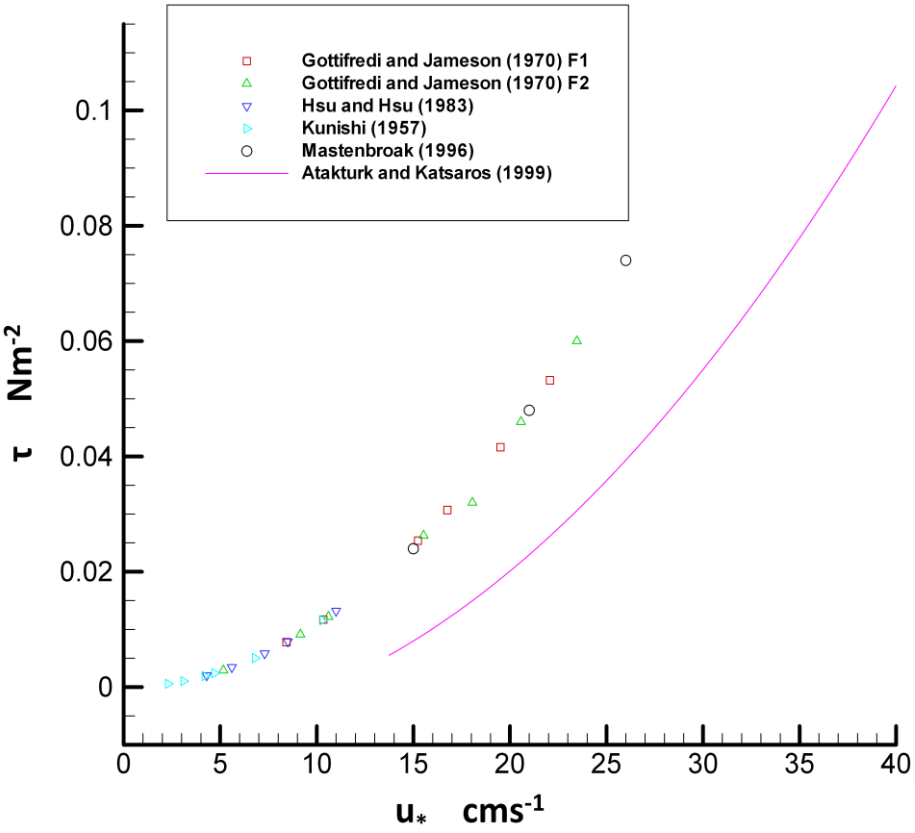

Figure (1.18): Correlation between momentum flux and friction velocity based on constant drag coefficient. The pink line represents fit line for Ataktürk and Katsaros (1999) observations.

1.10 Conclusion

Analysing the effect of the physical properties of the water surface to study the mechanism of wind generated surface waves, is a comprehensive approach since the physical properties of the water and surface waves are affected by the same parameters.

The presence of the active materials on the water surface increases the resistance that the molecules encounter to pass through the interface which causing a reduction in strength of the wind water interaction.

The characteristics of the interface lamina affect by the diffusion of the active materials to the surface. The resulting lamina is a function of the concentration of the active materials in the bulk, the density of the electrical charges and the presence of the waves.

Based on observations of wind generated surface waves at low and moderate wind speed, it is suggested that the characteristics of the interface lamina affect the following parameters; surface velocity, critical wind speed, the wind induced perturbation in the bulk, drag coefficient, viscous sublayer thickness, wavelength, surface structure, wave damping and growth rate, wave velocity, maximum wave amplitude, etc.

The viscosity and surface tension are functions of the dimensions of the water body

Since an increase of Oh number indicates an increase in surface distortion due to a decrease in the effect of the restoring forcing (stabilising forces), which is an appropriate condition for the wave's growth; it is postulated that the Oh number can be used to scale the growth of the capillary waves. The growth of the Oh number indicates that the waves tend to grow where the lesser magnitudes of Oh number indicate that the waves tend to damp out.

The Δ_{max} of each interface dimension is a function of Re (t), i.e. the bulk turbulence is a function of the surface structure and the bulk flow regime can be predicted from the dimensions of the surface structure or from the magnitudes of the Oh number.

The systematic relationships between the; Oh number and the Reynolds number, Oh number and structured dimensions are obvious if each run of MS measurements is taken individually.

Since Oh number comprises the flow speed and three physical properties of water; density, kinematic viscosity and surface tension; the Oh number can be employed to scale the wave growth, surface structure regime and bulk flow regime. The last formulation of Oh number contains the capillary, viscous and inertia forces

The discrepancy between observations of critical wind speed that were conducted in laboratories and in real fields is assumed to be attributable to the natural background perturbations that occur in the water bulk in the absence of wind; in oceans and large water bodies, natural perturbations occur in water bulk in the absence of the wind are due to the extensive water body size, surface lamina formation process, temperature and density differences between the surface and bulk.

The drag coefficient and the friction factor are expected to be constant at height equal the thickness of the viscous sublayer. The momentum flux based on a constant drag coefficient is consisting with other estimation that based on eddy correlation technique.

Since the characteristics of the air through $y_1$combine the characteristic of the water and the air, it is suggested to introduce the parameter $\bar{\nu}$ instead of ν in the equations that related to the viscous sublayer zone; such as $y_1, Z_\circ, U_1$, and C_D. The calculations of these parameters using $\bar{\nu}$ showed a consistence with the observations and predictions.

Chapter 2

Wave growth rate

Introduction

One of the most important aims of studying wind-generated surface waves is finding a precise estimate of the wind-wave growth rate due to the transfer of wind momentum and energy to the water. This is because relevant applications such as predicting sea state depend on finding a precise estimate of wave growth rate.

In modelling the wind generated surface waves, the growth rate is of great importance in predicting the sea state. The wave growth rate was calculated based on observations or mathematical models to estimate the energy and momentum flux from wind to water because the latter cannot be measured directly. The measurements of growth rate were conducted in laboratories and in real fields. For example, in wind tunnel facilities, Gottifredi and Jameson (1970) approximated the growth rate by measuring the amplitude of a wave at two measuring sections with a known distance apart and they compared their results with theoretical calculations. A good agreement with theory was found for $u_* < 20cms^{-1}(U_\infty \approx 4ms^{-1})$. Snyder et al (1981) deduced the growth rate in open oceans by measuring the wind induced pressure close to the water surface. Plant (1982) collected a number of wave growth rate measurements obtained from laboratory measurements and presented the data as (γ/f versus u_*/c). Where γ and f are the energy growth rate according to Miles definition and wave frequency. Plant concluded for a wide range of relative wind speeds, $1 < c/u_* < 20$ that the growth rate parameter β was 32 ∓ 16. An agreement was found with Miles theory when logarithmic scaling was used to present the collections. (Miles 1960) defined the growth rate γ being in the form

$$\gamma = (\rho_a/\rho_w)\,\beta\,\omega(\frac{U_r}{C_w}\cos\theta)^2 \quad \text{..... (2.1)}$$

Where $\boldsymbol{\theta}$ is the angle between the wind and the waves, c_w the phase velocity of free gravity waves and U_r is the reference wind velocity defined by Miles (1959) assuming a logarithmic boundary layer profile in the form.

$$U_z = U_r \log\left(\frac{z}{z_\circ}\right) = 2.5u_* \log\left(\frac{z}{z_\circ}\right) . \quad \text{(2.2)}$$

The growth rate parameter β should be constant according to Miles theory. Janssen (1991) predicts that β is only constant at high frequency.

Belcher et al (1994) represented the Plant collections in linear axis as (β versus c/u_*) and a large scatter was found as shown in Figure (2.1).

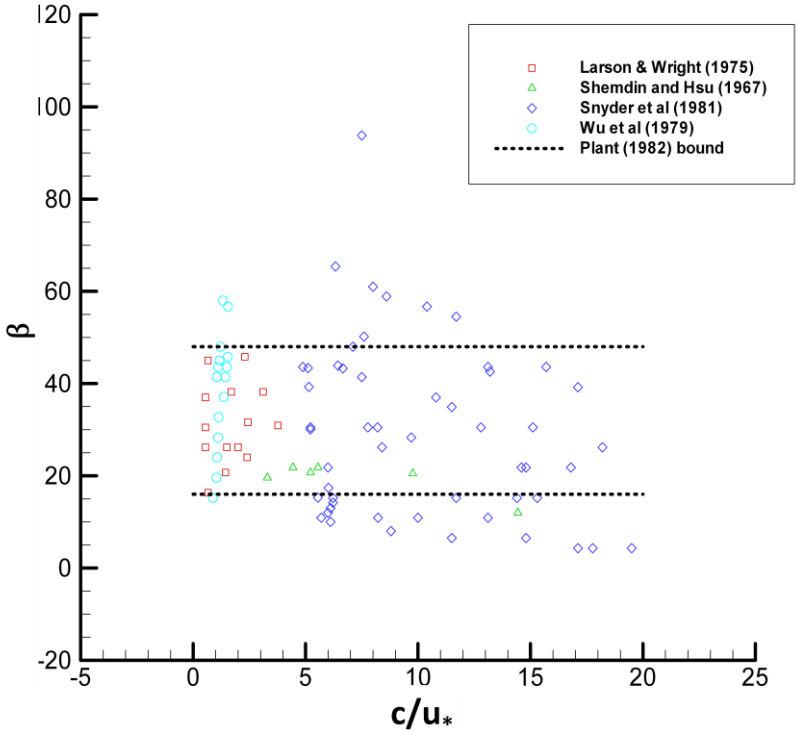

Figure 2.1: Correlation between the wave growth parameter and relative speed of c / u$_*$ for the data collected by Plant (1982) after Belcher et al (1994)

The terms growth rate and damping rate are used to characterise the wave behaviour under the effect of wind action. The latter is used to characterise the situation where the wind blows over the water surface without a detectable increase in wave amplitude. The damping rate occurs due to the effect of the physical properties of the water surface which ceases the growth of capillary and infinitesimal waves as will be shown later in this chapter. It is suggested to categorise the mechanism of wave damping into two parts; the first due to damping the wave amplitude and the second due to damping the wavelength. Based on understanding the effect of physical properties of the water surface on the wave growth mechanism, the damping due to the viscous forces affect the wave amplitude growth and the damping due to capillary

forces affects the wavelength growth. The latter resists wave growth in all stages of a wave evolution; infinitesimal wave, capillary wave, gravity wave and longer wave. The former damps the wave growth of infinitesimal and capillary waves where the wave's amplitude is less than the viscous layer thickness. However, the viscous forces affect the characteristics of a wave at a higher wind speed due to an increase in the wavelength. The viscous forces and capillary forces affect the wavelength in opposite directions, while the former causes an increase in wavelength, the latter causes a reduction in wavelength. If the viscous forces are dominant, it is expected that the waves will attain higher amplitudes if the wind speed is sufficient; however, if the capillary forces are dominant, it is expected that the waves will attain lower amplitudes even if the wind speed is sufficient; this is because the increase of wave slope. The wave slope is defined as $ak\ or\ 2\pi/\lambda$. This definition highlights the importance of the wavelength in the progress of a wave under the effect of wind action. The previous studies considered the effect of the viscous forces and capillary forces only in the initial stages of wave growth (infinitesimal and capillary waves). However, the effect of the capillary and viscous forces should be considered for all stages of wave growth.

For waves which already exist and are under the action of wind, the waves are either in a growing state or a decaying state; for example, when a wave propagates at a speed faster than the wind speed, the energy transfer is from the wave to the wind and the wave decays though the wind remains blowing over the waves. Also wave breaking occurs when they reach the saturation level where the restoring forces exceed the suction forces. It is believed that the wave breaking phenomenon is a function of the characteristics of the waves such as wave slope.

The negative sign will be used to indicate the waves in decaying state or damping state, whereas the positive sign will be used to indicate the growing state. The growth rate can be represented using time unit as s^{-1} or distance unit as cm^{-1}. When the distance unit is used, the wave growth rate is called spatial growth. The temporal wave growth rate term is used in transition conditions, for instance when the wind speed increases abruptly. The correlation between the spatial growth rate and theoretical growth rate proposed by Gaster (1962) as

$$S_T = \frac{2kc_i}{C_g} \quad \ldots\ldots\ldots\ldots\ldots\ldots\ldots\ldots\ldots\ldots\ldots\ldots\ldots\ldots \quad (2.3)$$

Where S_T is the spatial growth rate, kc_i is the theoretical growth rate (k and c_i is the wave number and imaginary part of phase speed) and c_g is the group velocity. The term c_i can take a positive or negative sign; the waves being in growth state if the term c_i is positive.

Since the observations showed a considerable scatter and they did not match with the theories in many cases, the present study aims to find the main parameters which are most responsible for the growth of capillary waves. The latter plays a significant role in wind-water interaction and is instrumental in causing larger waves while no claim of proportionality of higher dependence can yet be made, Lorenz et al (2005). It is believed that understanding of the formation and evolution of the capillary waves gives insight to illustrate the behaviour of gravity waves and a guide to explain the extraordinary states of the sea.

2.1 The correlation between the growth rate and relative speed of (u_*/U_∞)

In the above observations such as in Figure (2.1) 'that showed a large scatter' the growth rates were plotted against relative wind speeds of (c/u_*), however, it is suggested to compare the values of the relative wind speed of (u_*/U_∞) with the values of growth rate that were predicted by theories or using mathematical models. Since u_* is determined from the linear portion of a logarithmic wind velocity profile; it is assumed that the higher value of u_* indicates a strong wind-wave (or wind-water surface in absence of waves) coupling and therefore a higher momentum flux to the water. u_*/U_∞ can be used to correlate the growth rate even if the surface waves do not appear, while c/u_* depends on the phase speed. It is assumed that this ratio is a function of growth rate and a greater value of the growth rate occurs at a greater value of this ratio.

Mastenbroek (1996) studied the growth rate parameter versus the ratio of c/u_* for three numerical models and he found the wave growth rate is a function of the

ratio c/u_* or U_λ/c and reported that the Launder, Reece, and Rodi (LRR) (1975) model gives the best agreement with observations. The LRR model divided the values of the wave growth into three ranges based on the value of the ratio c/u_* or U_λ/c; for a slow moving wave $U_\lambda/c = 5$), a fast moving wave $U_\lambda/c = 1.5$ and waves travelling faster than wind $U_\lambda/c = 0.8$ Table (2.1) summarise the calculation of wave growth using the (LRR) model for different values of the ratio c/u_*. According to LRR model the highest wave of growth occurs at $U_\lambda/c \sim 1.5$, where U_λ is the wind speed at height λ (wavelength) from the surface.

Table (2.1): Wave growth calculation using Launder, Reece, and Rodi (1975) (LRR) model at different wind speed-phase speed ratio after Mastenbroek (1996).

U_λ/c	c/u_*	β	u_*/U_∞
5.0	5.3	14.5	0.0377
1.5	18.0	21.7	0.0370
0.8	33.0	-5.6	0.0378

The ratio of u_*/U_λ is used as an alternative of U_λ/c that was used in Mastenbroek (1996) study. In Table (2.1) the change in the magnitude of u_*/U_λ is insignificant while the growth rate changed significantly. The values of u_*/U_λ in Table (2.1) are determined based on theoretical values. The following studies are called here to interpret the above suggestion.

Kawai (1979) predicted the value of the critical wind speed for two values of non dimensionless parameter r of the thickness of viscous sublayer which is defined as $r = y_1 u_*/\nu$, where y_1 is the viscous sublayer thickness. At $r = 5$ the value of the critical friction speed u_{*cr} lies between 4.7 cms^{-1} and 4.2 cms^{-1}. For $r = 8$, the value of the critical wind speed U_{cr} lies between 4.2 cms^{-1} and 3.7 cms^{-1}. Kawai (1979) compared the predicted critical wind speed with Kunishi (1957) observation which was of the order 9.22 cms^{-1} or wind speed of the order 244 cms^{-1}. The critical friction speed predicted by Kawai (1979) is much smaller than the values that were observed by Kunishi (1957). In order to give an explanation for the discrepancy between the Kawai (1979) prediction and Kunishi (1957) observations; the values of $u_*/U_{0.3}$ for 6

cases of Kunishi (1957) observations are calculated as shown in Table (2.2) and plotted versus wind speed as shown in Figure (2.2)

Table (2.2): Observations of Kunishi (1957) experiment for six different wind speed

	VI	V	IV	III	II	I
$U_{0.3}$ (cms^{-1})	277	170	109	94	73	54
U_*(cms^{-1})	10.3	6.8	4.7	4.2	3.1	2.3
$u_*/U_{0.3}$	0.037	0.04	0.0431	0.0446	0.0424	0.0425

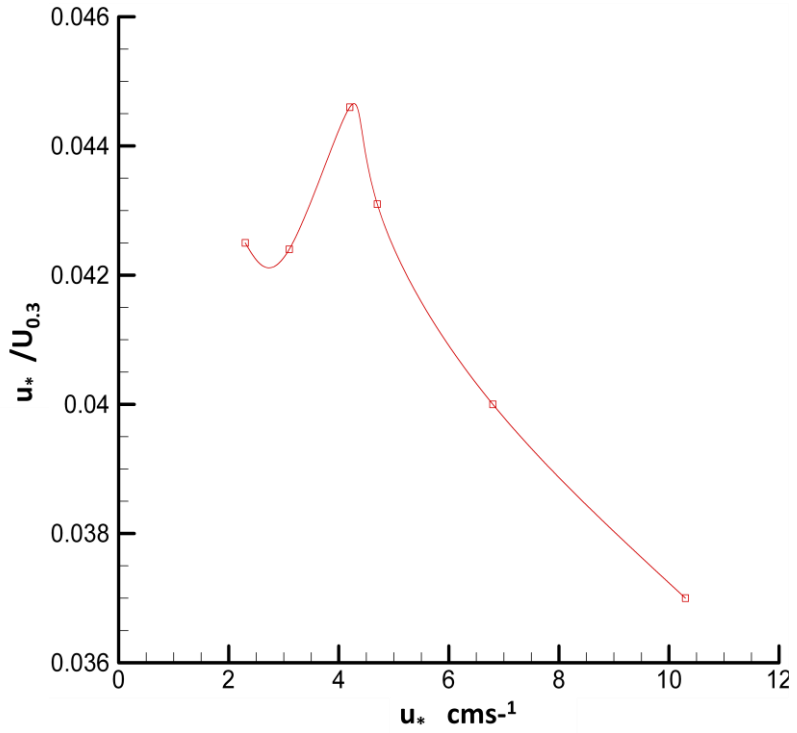

Figure (2.2): Correlation between versus $u_*/U_{0.3}$ and u_* using data of Kunishi (1957).

Figure (2.2) shows that the highest value of $u_*/U_{0.3}$ occurs at $U_{0.3}$ =94 cm^{-1} or u_* 4.2 cm^{-1} which is identical with U_{cr} predicted by Kawai model (1979) at $r = 5$ and shear flow instability theory of Miles (1962). It is supposed this is the actual critical friction speed for the Kunishi (1957) observation and the maximum growth occurs at this speed. It is assumed that the waves growth rate develops gradually based on the wind speed and attains the greatest value at the highest magnitude of $u_*/U_{0.3}$. The above manipulation for the Kunishi (1957) observation may help to clarify the discrepancy between the predicted and the observed values of critical wind speed.

It seems that the ratio of u_*/U_∞ is fetch and time dependent and affected by the physical properties of the water surface since the u_* determined from the linear portion of the wind velocity profile and u_* is a function of shear stress. Kunishi (1957) observed the initial wave after 100 seconds from onset of the wind flow over the water surface. The dependence of wave growth on fetch was observed in laboratories and field measurements, for example Kahma (1981) observed exponential growth of a component of dimensionless spectrum with fetch.

Plate et al (1969) conducted experiments at different fetch lengths and wind speeds using wind tunnel facilities. A summary of the experimental results is shown in Table (2.3)

Table (2.3): Observations of Plate et al (1969) and the corresponding magnitudes of u_*/U_∞

Run	X m	U_∞ ms^{-1}	U_* cm^{-1}	u_*/U_∞.	Remarks
1	4.88	3.66	15.8	0.04317	Usual inlet condition
2	4.88	3.2	13.4	0.04187	With Grid
3	2.44	11.1	62.4	0.0562	Over Initial Ripples
4	8.5	12.8	82.5	0.0644	Over fully developed waves

In run (2), the reading was taken after placing a heavy grid with slat nails in the air flow passage to create a high level of turbulence which caused some decrease in wind velocity and in the ratio of u_*/U_∞. For other runs the value of the ratio u_*/U_∞ increased as the surface state transformed from an undisturbed surface to a fully developed wave surface. The higher value of u_*/U_∞ indicates an increase in the transfer rate of wind momentum to the water according to the assumption above. This assumption agrees well with Plate et al (1969) observations. Over a rough surface or fully developed waves, the rate of the transfer of wind momentum increases consequently increasing the wave growth rate. The placement of a grid nail in the air passage did not affect the value of u_*/U_∞; this arrangement may reduce the wind velocity without introducing a significant increase in the wind turbulence over the water surface. Plate et al (1969) has conducted experiments to study the generation of small water waves by wind reported and that "no evidence which can be used for

support theories on the inception of the very first ripple. They have however, brought out some facts which were not observed before".

The following examples also explain the relationship between u_*/U_λ, U_λ/c and β. Mastenbroek (1996) conducted experiments in a large wind wave tank which was 40 m long, 3 m wide and 1m deep and a closed wind tunnel with wind speeds of up to 7ms^{-1}. Paddle makers were introduced to generate waves with particular wavelengths in addition to the wind action. Table (2.4) shows the results of Mastenbroek experiments and the corresponding values of u_*/U_λ at different wind speeds. The friction velocity was determined from the mean velocity profile.

Table (2.4): Observations of Mastenbroek (1996) and the corresponding magnitudes of u_*/U_∞

Run	U_∞ ms^{-1}	U_λ ms-1	U_* ms^{-1}	λ m	U_λ/c	c/u_*	u_*/U_λ
1	3.5	3.36	0.15	0.92	2.8	8.0	0.0446
2	5.4	5.11	0.21	0.8	4.6	5.3	0.0411
3	6.3	5.92	0.26	0.8	5.3	4.3	0.043

Also Hsu and Hsu (1993) conducted experiments using wind action and mechanical vibrator to generate waves at lower wind speeds than that used in the Mastenbroek experiments and the wave length was kept at 1.6 m. The observations of Hsu and Hsu (1983) are shown in Table (2.5) including the case of Hsu et al (1981).

Table (2.5): Parameters for four sets of observation by Hsu and Hsu (1983) corresponding magnitudes of u_*/U_∞

Run	U_∞ ms^{-1}	U_* ms^{-1}	U_λ/c	u_*/U_λ
1	1.37	0.043	0.88	0.0313
2	1.72	0.056	1.1	0.0325
3	2.12	0.073	1.35	0.0344
I	2.4	0.085	1.54	0.0354
4	2.92	0.11	1.89	0.0376

In Mastenbroek (1996) observation and, following the (LRR) predictions, the maximum wave growth rate should occur for run 1 where the value of U_λ/c is about 2. This result is also consistent with the above hypothesis where the value u_*/U_λ for the first run attains the maximum value compared to all runs.

The correlation between u_*/U_∞ and U_λ/c is obvious in Hsu and Hsu (1993) observations as shown in Table (2.5). According to (LRR) predictions the maximum wave growth rate should occur for run I and 4 where the value of U_λ/c is about 1.5 ~2. The reading denoted by I was taken from Hsu et al (1981). A according to the above hypothesis the highest growth rate occurs for run 4 and I where the value of u_*/U_λ attains the maximum values. The highest value of u_*/U_λ has occurred exactly at a wind speed of the order 2.92 ms^{-1} which is identical with other observations of critical wind seed such as Kahma and Donelan (1989) 3.1ms^{-1}, Atakürk and Katsaros (1999) 3 ms^{-1} and the current study 2.73ms^{-1} as will be shown in chapter three.

From the above discussion, it is concluded that the increase in the magnitude of the ratio u_*/U_∞ causes an increase in wave growth rate. Under conditions of gradual increase of wind speed over water surface which is initially calm, the critical wind speed may occur at maximum value of u_*/U_∞. The calculation of the value u_*/U_∞ has clarified the discrepancy between the Kunishi (1957) observation and the Kawai (1979). The discrepancy may be attributable to the accuracy of the measurement system that was used by Kunishi (1957).

It is important to consider while analysing the value of u_*/U_∞ if the wave is generated by the action of the wind or by using a wave maker only. Peirson et al (2003) conducted two separate experiments to observe the attenuation rate of waves generated by different mechanisms. In the first experiment the wave generated by the action of wind blew over the water surface, while in the second experiment the waves were generated by using a mechanical vibrator located on the water surface. Peirson et al (2003) used a fan delivering air in the opposite direction of the wave motion to attenuate the waves. They found that the attenuation rate of the latter was higher than the former. This may be due to the different nature of the motions generated inside the water flow by the two mechanisms. Limited perturbations will be generated through a water flow when a mechanical vibrator is used to generate the waves. However, the wind momentum will transfer to the whole water body when wind action is used to

generate waves. This will affect the dynamics of the bulk flow and thus the wave energy. The correlation between the wave growth and the characteristics of the bulk under the action of wind will be discussed in chapter 3 and 4. The values of u_*/U_∞ for the above four experiments that were conducted under different conditions are plotted verses U_λ in Figure (2.3).

Kunishi (1957) and Hsu and Hsu (1993) conducted their experiments at the same range of wind speeds. The discrepancy in curves trend between the two experiments may be attributed to the condition of the experiments; in Hsu and Hsu (1993) experiments, a wave maker in addition to the wind action was used to generate surface waves. In the Kunishi (1957) experiment wind action only was used to generate the surface waves. Mastenbroek (1996) also used a wave maker such as Hsu and Hsu (1993) but the experiments were performed at a higher range of wind speeds. Plate (1982) performed his experiments using the action of wind only to generate surface waves at wind speeds higher than the previous experiments. In all cases the maximum value of the ratio u_*/U_∞ occurred at the maximum predicted wave growth rate. A well consistence between LRR model (1975) that considers the ratio of c/U_λ over fully developed waves and the present assumption that considers the ratio of u_*/U_∞ in prediction of the max wave growth rate. The wind speed in the above investigation was measured at different heights from the surface which may cause fewer discrepancies, however, in all cases the measurements were taken a long way from the viscous layer.

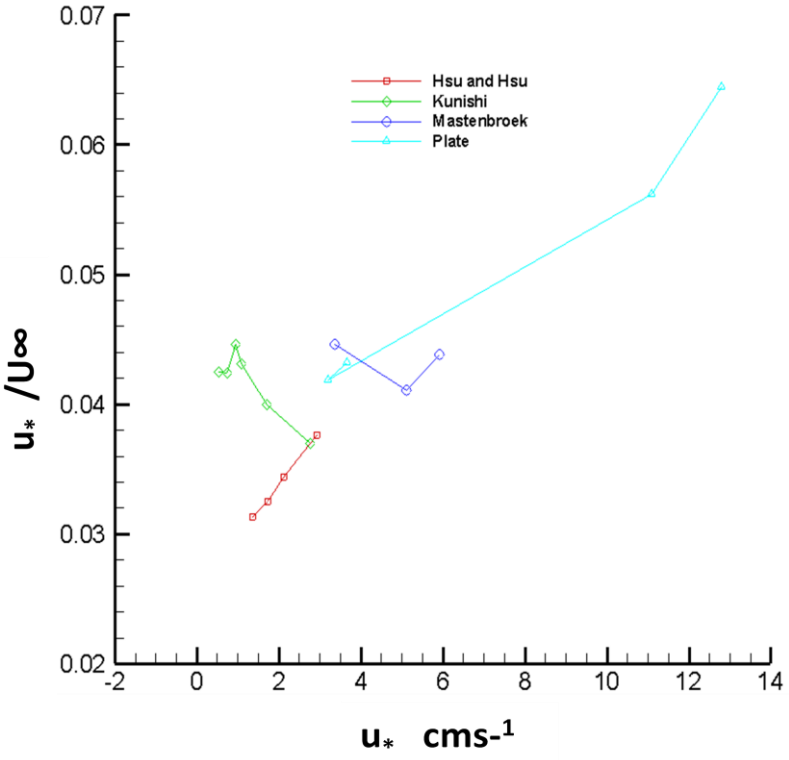

Figure (2.3): Correlation between $U_{0.3}$ versus u_*/U_∞ for the above four investigators as in the legend.

Gottifredi and Jameson (1968) derived the following equation for water covered by active agents to find the amplification of kc_i (theoretical growth rate) for waves if the frequency and wavelength are given using approximate method of Benjamin (1959) and Miles (1962a, b) and by solving the Orr-Sommerfeld equation for the gas flow with appropriate boundary conditions.

$$\frac{2c_i}{c_o} = \frac{-2(1+K_r)}{R_w} + K_i\mathcal{D} + \frac{\rho_a(P_s+iT_sK)}{k\rho\, c_o^2} \quad \text{..... (2.4)}$$

where $K = (1-\mathcal{D}(R_w/2)^{0.5}(1-i))^{-1}$and $c_r \simeq c_o = (g/k + \sigma k/\rho_w)^{0.5}$; $\mathcal{D}$ is the damping number $\mathcal{D} = k\mathcal{X}/\rho c_0$, $\mathcal{X}$ is the Gibbs elasticity assuming; $\mathcal{X} = \sigma_\circ - \sigma_s$ according to Davies & Rideal (1961) where $\sigma_\circ$ and σ_s is the surface tension of the water and the surface tension of the solution. R_w is the wave Reynolds number defined as; $R_w = c/k\nu_w$, c is the wave velocity defined as; $c = c_r + ic_i$. Disturbances will grow if the imaginary part of the phase velocity is positive. P_s and T_s are related to the normal and tangential stresses at the surface of the liquid.

Gottifredi and Jameson (1967) deduced together with the definition of K, that the damping rate in a liquid is increased whether $\mathcal{X}$ is negative or positive.

To deduce the growth rate kc_i form the experimental data, Gottifredi and Jameson (1970) used the form

$$kc_i = \ln(a_2/a_1)\, c_g (x_2 - x_1)^{-1} \quad \text{..... (2.5)}$$

where a is the amplitude of the wave at the two measuring section 1 and 2 a distance $(x_2 - x_1)$ apart. The theory of Miles yields growth rate in time which have to be converted to spatial growth rate by means of the transformation of Gaster (1962) ; $S_T = \frac{2kc_i}{c_g}$. S_T is spatial growth rate and c_g is the group velocity.

The net amplification factor kc_i consists of the sum of two terms; a growth rate m_a due to Miles -Benjamin mechanism and the damping rate m_w resulting from the viscous dissipation of wave energy in the water.

$$kc_i = m_a + m_w \ . \quad \text{..... (2.6)}$$

The growth factor m_a is given by Miles (1962a)

$$m_a = \frac{1}{2}\left(\frac{\rho_a}{\rho_w}\right) \acute{U}_\circ \left[\frac{w_i - F_i - k\delta^*(w_r - F_r) - H_i}{|F-w|^2}\right]_{c=c_\circ} \quad \text{..... (2.7)}$$

Where F and H are complex function of the variable

$$Z = c/\acute{U}_\circ \delta^*$$

$$\acute{U}_\circ \approx u_*^2/\nu_a$$

$$|F - w|^2 = (F_r - w_r)^2 + F_i^2$$

Where m_a, F_r, F_i *and* H_i can be determined from curves given in Figure (3) of Miles (1962a).

$$m_w \ or \ (\beta_d) = -2k^2\nu_w - (2k^3\nu_w c_\circ)^{1/2} exp(-2kd) \quad \text{..... (2.8)}$$

In other references (β_d) estimated is as $\beta_d = -4k^2\nu_w$

The parameter U_1 is used to indicate the velocity at the edge of the viscous sublayer. This parameter can be found from the logarithmic velocity profile as given by Miles (1962a)

$$U_y = U_1 + \frac{u_*}{\mathrm{K}}\left[ln\left(\frac{4\mathrm{K}u_* y}{\nu_a}\right) - 1\right] \quad \text{(2.9)}$$

In Miles equation $\frac{U_1}{u_*} \approx 6.9$

The value of U_1/u_* has a significant effect in the estimation of the growth rate by the theory of Miles.

Table (2.6a) and Table (2.6b) shows the results of Gottifredi and Jameson (1968), u_*^2/U_∞ and u_*/U_∞ were added to the tables to examine the relationship between these ratios and the wave growth rate. The term C_f in Table (2.6a, b) is defined by Gottifredi and Jameson as the friction factor which is estimated as

$$C_\mathrm{f} = (u_*/U_\infty)^2 \quad \text{(2.10)}$$

Larson and Wright defined wind stress coefficient *C* using equation (2.10). The values of C_f were $(2.5 \pm 0.5) \times 10^{-3}$. y_1 (viscous sublayer thickness), C_D (drag coefficient)

Table (2.6a): Summary of the Gottifredi and Jameson for velocity profile parameter for flow over water. u_*^2/U_∞, u_*/U_∞, y_1 and C_D were calculated and added to the table. The oscillator Frequency was 4.61 Hz

Fetch	$U_\infty\ cm^{-1}$	$u_*\ cm^{-1}$	$y_1 \times 10^3$	$C_D \times 10^3$	u_*^2/U_∞	u_*/U_∞	$10^3 C_\mathrm{f}$
2	82	5.16	1.8	5.6	0.32	0.062	3.94
2	155	9.15	1.02	5.2	0.54	0.059	3.48
2	196	10.6	0.88	4.8	0.57	0.054	2.92
2	311	15.53	0.60	4.4	0.77	0.049	2.94
2	351	18.06	0.50	4.7	0.929	0.0514	2.64

2	400	20.57	0.454	4.6	1.057	0.0514	2.64
2	468	23.47	0.397	4.5	1.177	0.0501	2.52
1	151	8.43	1.107	5	0.473	0.0558	3.12
1	188	10.34	0.90	4.9	0.578	0.055	3.03
1	282	15.24	0.61	4.7	0.823	0.054	2.92
1	333	16.76	0.557	4.5	0.843	0.05	2.53
1	376	19.51	0.478	4.6	1.012	0.0518	2.69
1	418	22.07	0.423	4.7	1.165	0.05	2.79

Table (2.6b): The oscillator frequency was 7.62 Hz

Fetch	$U_\infty\ cm^{-1}$	$U_*\ cm^{-1}$	$y_1 \times 10^3$	$C_D \times 10^3$	U_*^2/U_∞	u_*/U_∞	$(u_*/U_\infty)^2$
2	82	5.22	1.789	5.7	0.332	0.063	4.03
2	155	9.23	0.101	5.4	0.549	0.0595	3.55
2	200	11.46	0.815	5.1	0.656	0.0573	3.28
2	307	15.8	0.59	4.6	0.813	0.0514	2.65
2	398	19.94	0.468	0.58	0.999	0.0501	2.58
2	460	27.92	0.334	0.54	1.694	0.06	3.68
1	153	9.78	0.955	4.59	0.625	0.0639	4.08
1	190	10.39	0.898	5.7	0.568	0.0546	2.99
1	284	16.17	0.558	5.1	0.920	0.0569	3.24
1	366	18.89	0.494	4.6	0.974	0.0516	2.66
1	315	22.28	0.419	6.3	1.57	0.07	2.88

Figure (2.4) shows the relationship between u_*/U_∞ versus U_∞. According to the above assumption, the maximum growth rate should occur at wind speeds of the order 151 and 153 cms^{-1} for fetch 1 and frequencies of the order 4.16 and 7.62 Hz respectively. And at wind speeds of the order 82 cms^{-1} for fetch 2 for the same frequencies. However, the maximum growth rate that was observed and calculated by Gottifredi and Jameson (1968) occurred at maximum friction speed as shown in Figure (2.4). The above assumption that u_*/U_∞ is a function of the maximum growth according to LRR model is not consistent with the observations of Gottifredi and

Jameson and with the theoretical growth rate that was calculated by them according to Miles theory.

Figure (2.5) shows the correlation between both of the theoretical and experimental growth rate versus friction speed using the data of Gottifredi and Jameson (1970).The ratio of u_*^2/U_∞ were calculated and added to the Figure. The divergence between theory and experiments is quite large at $u_* > 20$ cm^{-1}. As shown in Figure (2.5) and Figure (2.6) the agreement is acceptable up to u_*=15 cm^{-1}, however above this value the growth rate obtained using experimental formula is less than those predicted by the theory for frequency of the order 7.62 Hz and greater than those predicted by the theory for frequency of the order 4.16 Hz . According to Gottifredi (1970) at frequency of the order 4.61 Hz the theory tends to under predict the growth rate above $u_* > 20$ cm^{-1}. Such a case was observed by Hidy and Plate (1966) where the wavelength increased with increasing wind speed which causes a significant reduction in growth rate due to decrease in the wave slope.

The growth rate as calculated based on equation (2.5) and by using glycerol solution was less than the corresponding growth rate using tap water.

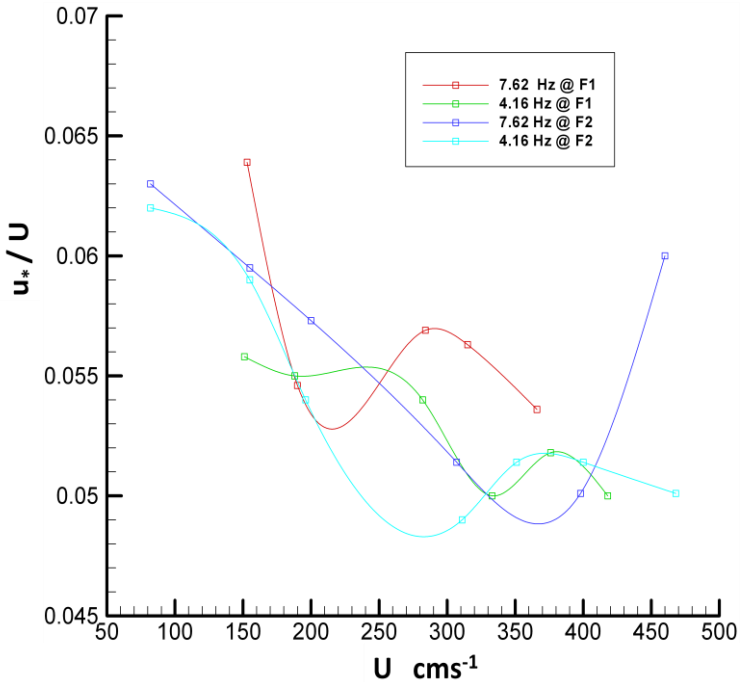

Figure (2.4): Correlation between versus u_*/U and U_∞ for Gottifredi and Jameson (1970)

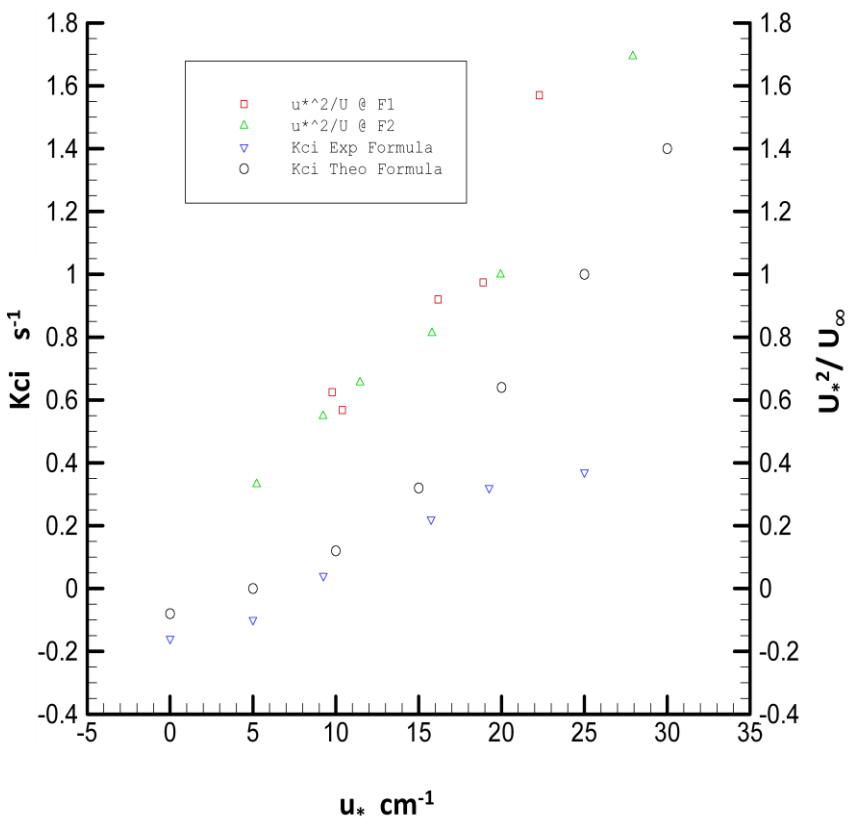

Figure (2.5): correlation between $kci, u_*^2/U_\infty$ and u_*. kci was calculated based on theoretical formula and experimental formula by Gottifredi and Jameson (1970). The frequency was 7.62 Hz

However, the trend of $u_*{}^2/U_\infty$ versus friction velocity showed an agreement with the theory particularly at a frequency of the order 7.62 Hz. As shown in Figure (2.5) and (2.6) the ratio of u_*^2/U_z is a function of wave growth rate and independent of frequency. In the first figure, the consistency between the values and trend of u_*^2/U_z and the theory is evident. In the second figure at a frequency of 4.61 Hz, the values of the ratio u_*^2/U_z exceeded the theoretical growth rate at corresponding friction velocity and tended to attain greater values at a higher friction velocity. This ratio does not give an exact value of the wave's growth rate but indicates the direction of the increase. It seems that the growth rate is a function of $(u_*/U_\infty)^n$, however the value of n is varied according to the experiment conditions and the background theory that was used to analyse the observation or to predict the growth rate.

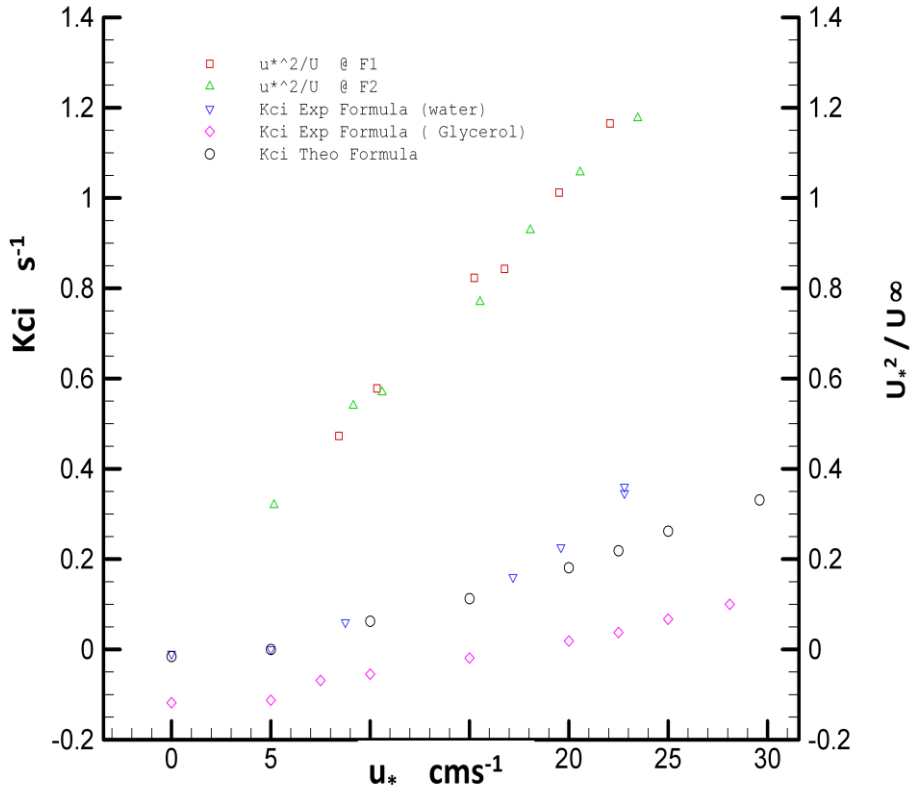

Figure (2.6): correlation between $kci, u_*^2/U_\infty$ and u_*. kci was calculated based on theoretical formula and experimental formula by Gottifredi and Jameson (1970). The frequency was 4.61 Hz

Gottifredi and Jameson (1970) studied the relationship between the wave growth rate and friction velocity at particular frequency for three SLS solutions (low surface tension solutions) with elasticity values of 15,20 and 27 dyne cm^{-1}. Theoretically, the growth rate reduces systematically as the elasticity increases. For a solution with less elasticity, the growth rate approaches the pure water behaviour as the friction velocity increases ($u_* > 20$ cms^{-1}). However for the most concentrated solutions (the highest elasticity), the growth did not approach the values of pure water even at $u_* > 20$ cms^{-1}. In general, the measured kc_i agree well with the theory up to values of friction velocity of the order 20 cms^{-1}. These results can be generalized for a large range of frequencies and different magnitudes of viscosities. Sutherland (1968) measured the growth rate of wind generated waves and found the results agreed well with Miles (1962a) at frequencies less than 3.5 s^{-1}.

To sort out the most relevant parameters to wave growth rate; the figures below illustrate the relationship between the growth rate as a function of fetch, frequency, wavelength and relative speed of $(U_1/u_*)^2$ in separate figures.

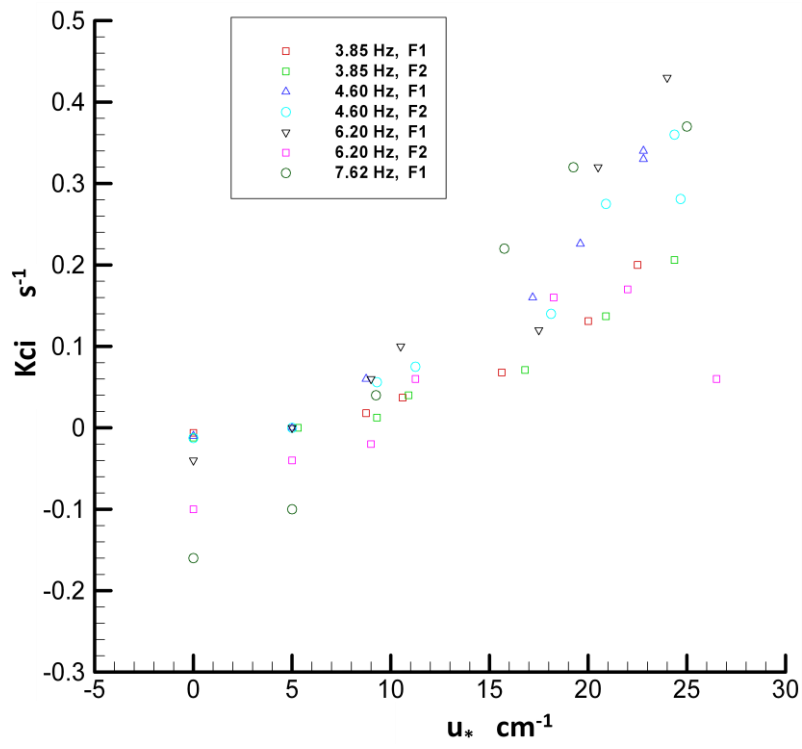

Figure (2.7): correlation between kci,and u_* for different frequencies and two fetch length. kci was calculated based on equation (2.5). The magnitudes of the frequencies are shown in the legend.

Figure (2.7) shows the growth rate as a function of friction velocity for data measured at two different fetches and three frequencies. This figure is plotted based on Gottifredi and Jameson (1970) measurements; the distance between the two fetches was 60 cm and a mechanical vibrator was used to generate surface waves besides the wind action. The effect of the fetch length on growth rate is insignificant for frequencies of 3.85 and 4.6 Hz, however, for frequency of 6.2 Hz the growth rate at F2 (second fetch) decayed at u_*>20cm^{-1} while the growth rate at F1 continued in the same trend. Larson and Wright (1974) measured the growth rates of wind-induced water waves in wind tunnel facilities. The wind speed ranged from 0.5 - 5 m/s and the measurements were taken at fetches of the order 1.0, 3.0 and 8.4 m. The low power dependence of friction velocity and waves growth rate was deduced by Larson and Wright as $kci \propto u_*^n$ where $n = 1.484 \mp 0.027$is the slope of (kci, u_*) in log scale. The growth rate was defined by Larson and Wright as $kci = kci_m - 4\nu k^2$ where kci_m is the temporal growth rate. They did not observe a dependence of the growth rate on the fetch.

To clarify the effect of the frequency on the wave growth rate as friction velocity increased at particular fetch the Figure (2.7) is expanded into two figures; Figure (2.8) shows the correlation between kci and u_* for measurements were taken at F1 and three different frequencies, Figure (2.9) shows the same correlation at F2 and the same frequencies.

At F1 and $u_* < 20cm^{-1}$ the growth rate increases slightly as the frequency increases from 3.85 to 4.6 Hz whereas the growth rate fluctuates at $f = 6.2$ Hz. At $u_*>20cm^{-1}$ a significant increase in wave growth rate occurs for $f = 4.6$ and 6.2 Hz. At F2 and $u_*<20cm^{-1}$the growth rate slightly increases as the frequency increases from 3.85 to 4.6 Hz and no significant change occurs at $f = 6.2$ Hz. At $u_*>20cm^{-1}$ the growth decays at $f = 6.2$ Hz and seems to continue in the same trend at $f = 4.6$ Hz. Figure (2.10) shows the correlation between the theoretical growth rate and Frequency for Plant et al (1969) data. Plant et al calculated the growth rate based on the equations (2.6-2.8). A significant increase occurs as the frequency increases particularly at frequencies higher than 10 Hz. For the results that were obtained by Gottifredi and Jameson, the wave tends to decay at higher friction velocities and frequencies at F2 may be attributable to the wavelength which becomes shorter as frequency increases. The shorter wavelength attains the maximum height and tends to decay before the longer one. This is due to increase in the wave slope. One point that should be noted is that the background of wave growth rate at zero friction speed at $f = 4.6$ Hz is lower than the other frequencies.

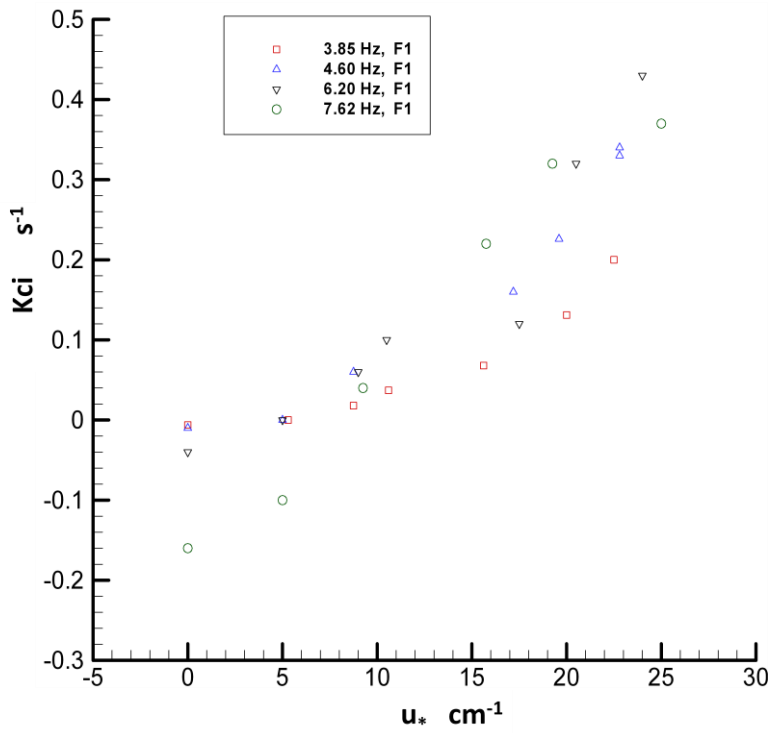

Figure (2.8) Correlation between kci and u_* for measurements taken at F1 and three different frequencies

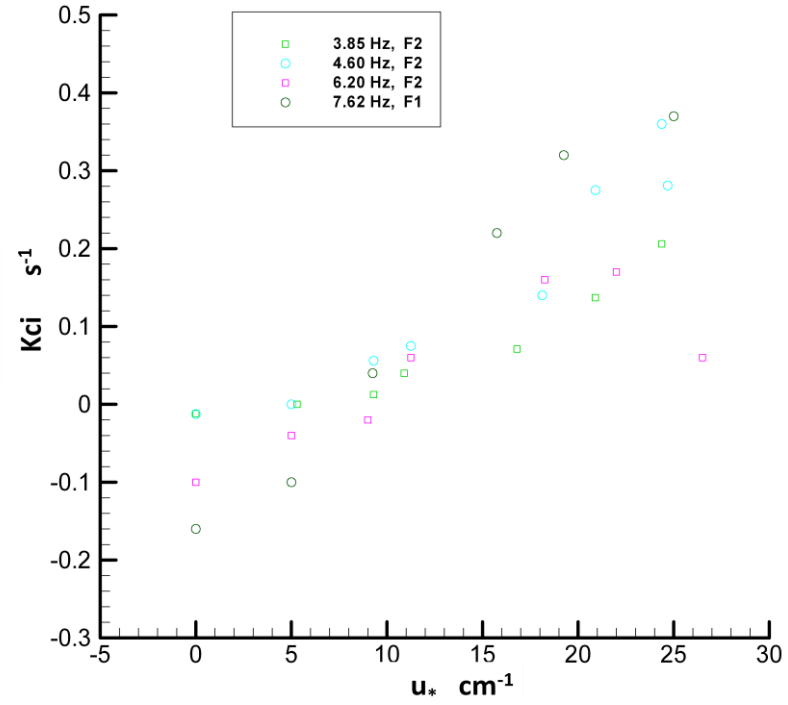

Figure (2.9) Correlation between kci and u_* for measurements taken at F2 and three different frequencies

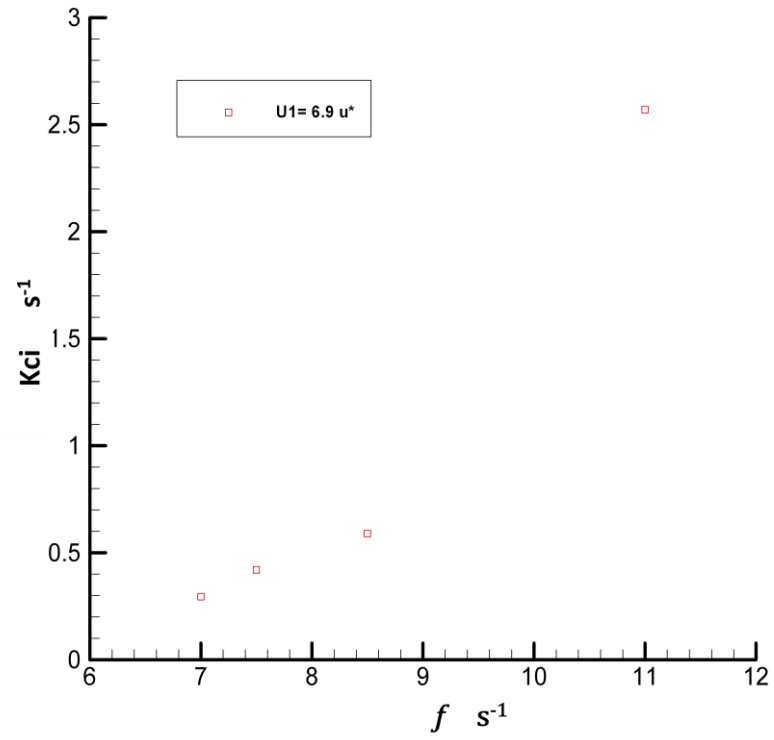

Figure (2.10): Correlation between the $kci\ and\ f$ for data collected by Plant (1982)

Kawai studied the correlation between the friction velocity and frequency and he found that the frequency of initial waves is apparently dependent on friction velocity; the latter is a function of growth rate. Based on Kawai findings the growth rate is a function of wave frequency. However, the relevance of the other parameter such as wavelength and the size of frequency fluctuation should be considered to explain the relationship between the growth rate and frequency.

To study the effect of the parameter U_1 on the theoretical value of wave growth rate the results of different studies are called for here. The estimation of the values of U_1 are varied from one study to another; for example Mile theory (1962b) 5.6-8u_*; Hidy and Plate (1966) 6 to 10u_*; Kawai (1979b) 5 to 8u_* ; Gottifredi and Jameson (1970) 4.5 to 6u_* as on smooth surface and 1.96u_* for rough surface (high wind speed and short wavelength). Miles (1962b) derived the equation on the basis of logarithmic law of wind profile to estimate U_1 ; Plate Modified Miles formulation in the form

$$(u)y = U_1 + \frac{u_*}{\mathrm{K}}\left[ln\left(\frac{4\mathrm{K}u_* y}{\nu_a}\right) - 1\right] \quad \text{..... (2.11)}$$

Though U_1 was used in some studies as a reference velocity, others used it as a free parameter of no physical importance.

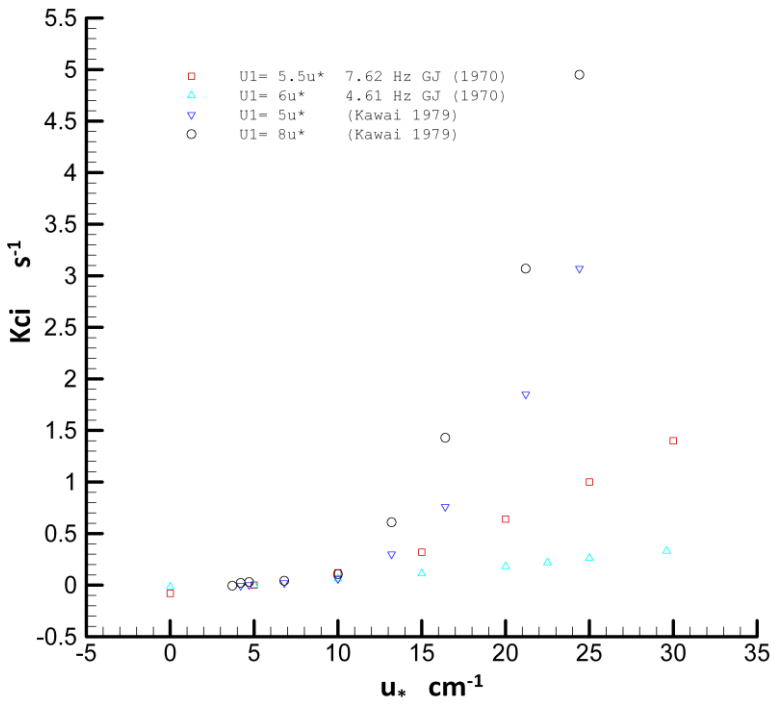

Figure (2.11): Correlation between kci and u_*fro different values of the parameter U1as shown in the legened

Figure (2.11) shows the wave growth rate as a function of friction velocity for results of Gottifredi and Jameson (1970) model and Kawai (1979) model. Gottifredi and Jameson presented the growth rate results for two different frequencies and two values of the parameter U_1 as U_1=5.5 u_* and U_1=6.0u_*. The growth rate at U_1=5.5 u_* and $f = 4.6$ Hz is higher than the growth rate at U_1=6.0 u_* and $f = 6.2$ Hz at the same range of friction velocity. The increase in the growth rate may be due to increase in the frequency rather than the parameter U_1. Kawai (1979) proposed a coupled shear flow model (shear in the water and in the air) in terms of instability mechanism and suggested an increase in wave growth rate due to increase in the value of the parameter U_1. An increase of the parameter U_1 indicates an increase in the viscous sublayer thickness because the velocity increases as the distance from the surface increases. Higher values of the parameter U_1 indicate that the wind velocity profile is much closer to the logarithmic profile. The observations show that as the wind speed increases the logarithmic profile is lost gradually and the viscous sublayer thickness also decreases. These conditions limit the value of the parameter U_1. The value of U_1 should be selected according to the condition of the observations which may not be covered by the theory. In section (1.9.2) the parameter U_1 is determined from the viscous sublayer thickness based on the assumption that the interface

viscosity is equal to the mean value of the viscosity of the air and viscosity of the water.

The last parameter is the wavelength or wave number. Larson and Wright studied the wave's growth rate in terms of wave number, fetch length and friction velocity. They observed that the wave's growth rate ceased abruptly after exponential growing over several orders of magnitude. Larson and Wright plotted the growth rate versus wave number for several orders of wind speed; they found for each wind speed the growth rate has relative maximum k_m near $k \simeq 3.6\, cm^{-1}$. Larson and Wright deduced that the short waves are tightly coupled to the wind and renders the growth rate to be qualitatively very large. Figure (2.12) below shows the correlation between the growth rate and wave number for a range of friction speeds.

It is suggested to add a definition of critical wave number k_{cr} (or wavelength λ_{cr}) as; the waves number (wavelength) at which the growth rate is maximum for a particular friction velocity. It is obvious that k_{cr} is a function of the physical properties of water. The initial wavelength is a function of the viscous forces and capillary forces. The wind speed at which a wavelength attains the critical magnitude depends on the initial wavelength

The above discussion of previous investigations has revealed that the growth rate is a function of: surface elasticity, bulk viscosity, wavelength (wave number), friction velocity, and wave's frequency, fetch length, the parameter U_1 and relative wind speed u_*^n / U_z . The dependence of growth rate on the above parameters is varied depending on the experimental conditions and on the theory that is used to analyse the observations. a comparison of the observations shows a scatter and disparity in some cases if the magnitude of one of the above parameters does not match the corresponding parameter in other observation.

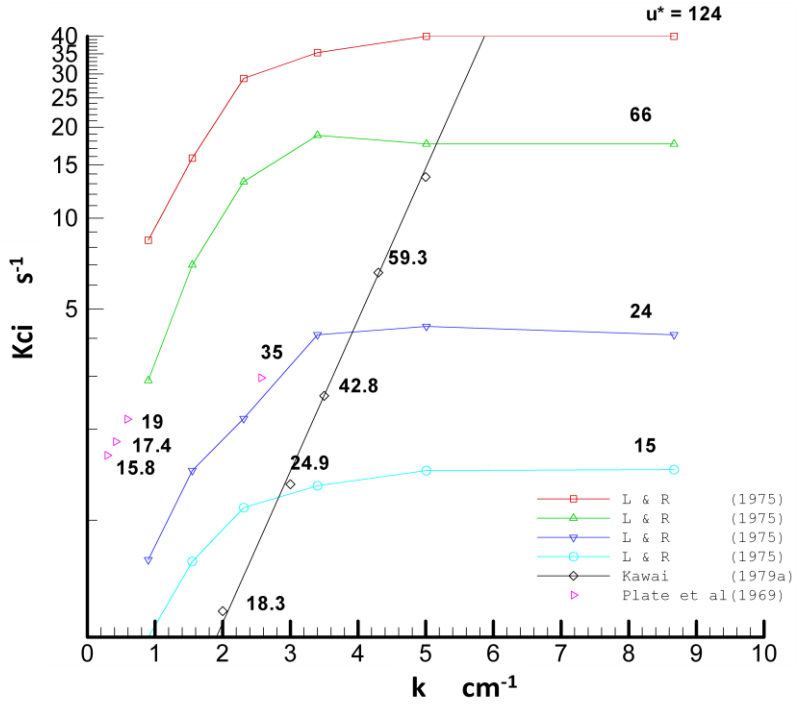

Figure (1.12): Correlation between kci and k for several investigations as shown in the legend. The growth rate was calculated for several order of u_*

It seems that the frequency has a significant effect on growth rate at high orders. Also the same discussions revealed that the growth rate is independent of the fetch length. The latter is presumably accepted for short fetch water bodies where the fetch length is insufficient to produce tight wind-water coupling. Such coupling may occur at sufficient fetch length due to a reduction in the difference between the kinematic viscosity of the wind and water surface. This may cause an increase in the wind-water coupling tightness due to enhanced homogeneity of the interfaced layers of air and water surface. Under effect of such conditions, the transferred rate of wind momentum to water will be enhanced. This point will be discussed in section 2.3

The key parameter which is assumed to affect the growth rate significantly under the effect of different conditions is the wavelength. Better interpretations for parameters that affect the length of the initial waves helps to understand the growth rate and wave generation mechanism under the effect of different conditions. This parameter is recommended to be considered thoroughly in studying the effect of other parameters on wave growth and damping rate.

2.2 Wave damping rate

Larson and Wright (1975) discussed the strength of the wind-wave interaction in terms of the ratio of $\beta/(2\omega)$ where ω the frequency of capillary waves. They found that the tight coupling of wind-water occurs as $\beta/(2\omega)$ attains the maximum value which was 0.2 at u_*=124 $cm^{-1}$and $k = k_m \simeq 3.6\ cm^{-1}$ or $\lambda = \lambda_m \simeq 1.75$.

As λ exceeds 1.75 cm the growth rate decays as λ increases. To achieve a higher growth rate, the capillary wavelength should exceed a particular value which was 1.75 cm in Larson's investigations. This value is not absolute and it varies according to the experimental conditions. The importance of capillary waves in wind-water interaction, initial wave generation and growth, and tendency of longer waves to break was presumed. However, explaining how this mechanism occurs remains primitive.

The most important question that is raised here is how the physical properties of the interface affect the size of the wave number of infinitesimal waves k_i.

It is assumed that the significant increase in critical wind speed for the contaminated surfaces occurred due to the expansion of λ_i (k_i) ceasing. It is assumed that the reduction in the magnitude of the surface tension causes such an effect. The growth rate of capillary waves remains insignificant until the ratio of k/k_m approaches 1, and this may require a higher wind speed in the case of contaminated water surfaces and low surface tension solutions (high elasticity solutions). The investigations below explain the correlation between the wave's growth rate, wavelength and the physical properties of the water surface.

For low-amplitude ripple propagated from a line source on deep water, hydrodynamic theory, for example Mansfield (1959) gives the equation:

$$a = a_\circ e^{-\Delta_c l} \quad \text{..... (2.12)}$$

$$\Delta_c = \frac{8\pi^2\mu_w}{\rho_w c_g \lambda^2} = \frac{16\pi^2\mu_w}{3\rho_w f \lambda^3} = \frac{8\pi\mu_w f}{3\sigma} \quad \text{.....(2.13)}$$

Where l and Δ_c is a distance from the line source and damping coefficient for a clean surface. The last two expressions are valid for water and for short wavelength ($\lambda < 0.5\ cm$) waves.

The last two expressions can be written in the form:

$$\sigma = \frac{\rho f^2 \lambda^3}{2\pi} \quad \text{..... (2.14)}$$

As shown in this equation, the value of the surface tension is a function of the cube of wavelength and the square of frequency. Brown (1935) found the frequency do diversity in surface tension value but it is not sufficiently large or regular to affect the surface tension value. In chapter one the parameters that may affect the value of the surface tension were discussed.

Experimentally, Davies and Vose (1963) observed the amplitude and damping coefficient of successive waves along a trough using particular measurements systems. To observe the relationship between the damping rate, wavelength and wave amplitude; the wave amplitude and wavelength were calculated using the previous equations based on Davies and Vose observations. The wave amplitude values are calculated based on $a_\circ$ as 1 cm. The following results in Table (2.7) show the observed and the calculated values. Figure (2.13) shows the damping rate as function of wavelength and wave amplitude.

Table (2.7) wavelength, wave amplitude, wave frequency and damping rate for Davies and Vose observations (1963)

λ (cm)	a (cm)	λ/a	Frequency (cycles sec^{-1}	Observed Δ_c cm^{-1}	Calculated Δ_c cm^{-1}
0.57	0.946	0.60	50	0.055	0.055
0.365	0.895	0.41	98	0.11	0.109
0.188	0.730	0.26	250	0.314	0.289
0.123	0.571	0.22	500	0.560	0.565
0.081	0.339	0.24	920	1.08	1.05

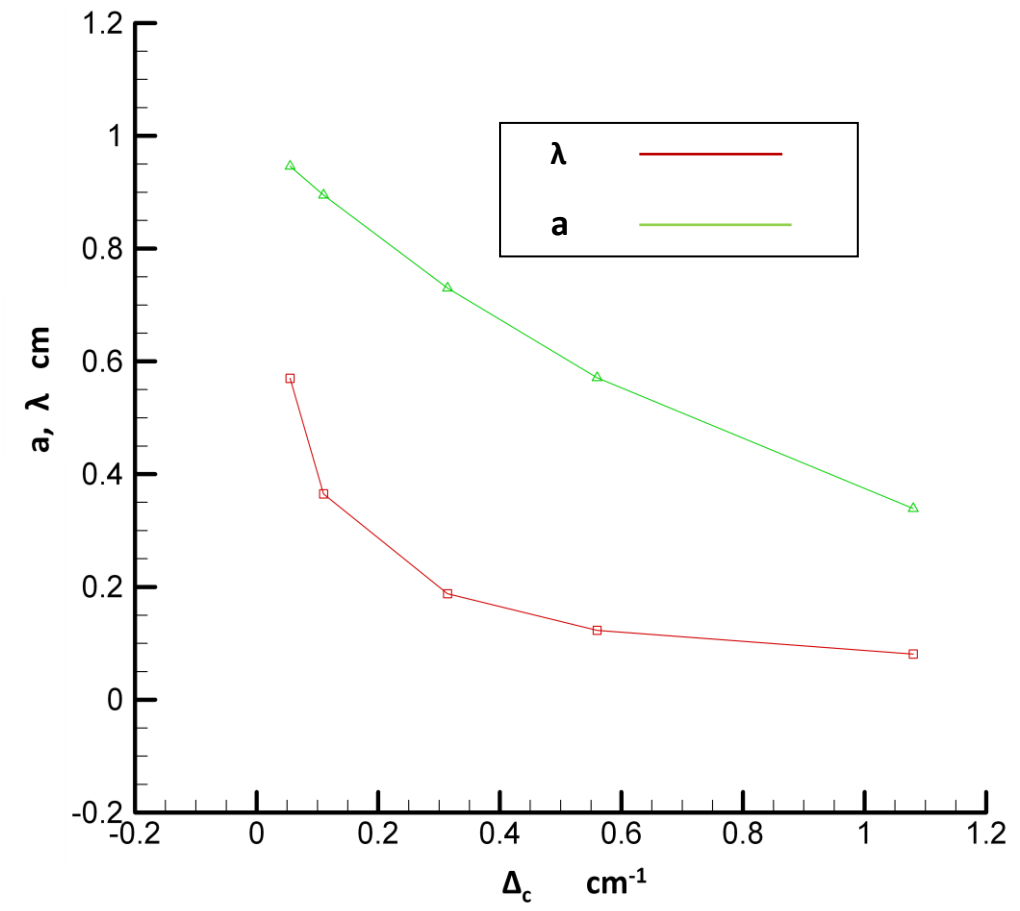

Figure (2.13): Correlation between damping rate, wave length and wave amplitude based on Davies and Vose observation.

Figure (2.13) shows that Δ_c is a function of λ^{-1}, a^{-1}, also Δ_c is a function of $(3\sigma)^{-1}$ as suggested in equation (2.13). As shown in chapter one; the presence of the active materials in the water causes a reduction in the magnitude of surface tension compared to the clean water; the effect of this reduction on wave growth rate was investigated experimentally and analytically. The mechanism of such reduction in growth rate is suggested as due to the expansion of the wavelength ceasing.

The wavelength and wave amplitude of infinitesimal waves should be considered together to illustrate the mechanism of initial wave growth and damping. Figure (2.14) shows the damping coefficient Δ_c as function of (λ/a). The damping coefficient is decaying exponentially as the ratio of λ/a is increasing and the highest magnitudes of Δ_c occur for the lesser values of (λ/a).

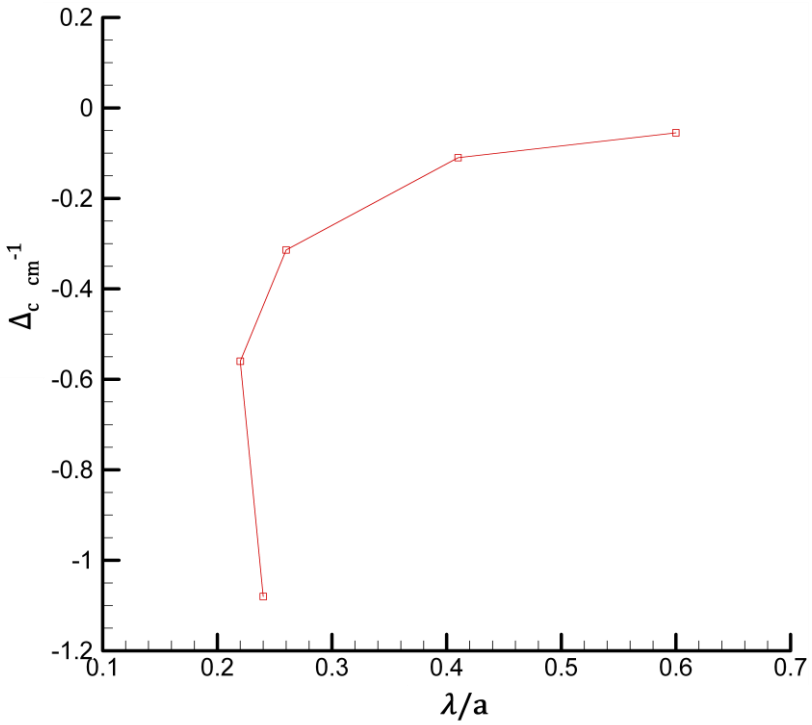

Figure (2.14): Correlation between Δ_c and λ/a for measurements of Davies and Vose

Another example to observe is the relationship between the surface tension and the wavelength as a function of time; Brown (1935) conducted an experiment using a solution of surfactant to observe such a relationship. The observation of Brown is shown in Figure (2.15).

Figure (2.15) shows the surface tension and wavelength falling as a function of time for 0.003 surfactant solution (reduced surface tension) at 20°C as observed by Brown (1935). The frequency of the ripple was 200 s^{-1}. The observations extended for 4 hours. A good correspondence occurs between decaying the trend of both wavelength and surface tension profiles with respect to time. The fall of both parameters was promoted by presence of surfactants. These observations illustrate the calming state of the water surface under the effect of wind action in the presence of such surfactants on the water surface. As shown in the Figure (2.14), as the magnitude of surface tension and wavelength falls, the damping rate increases**.**

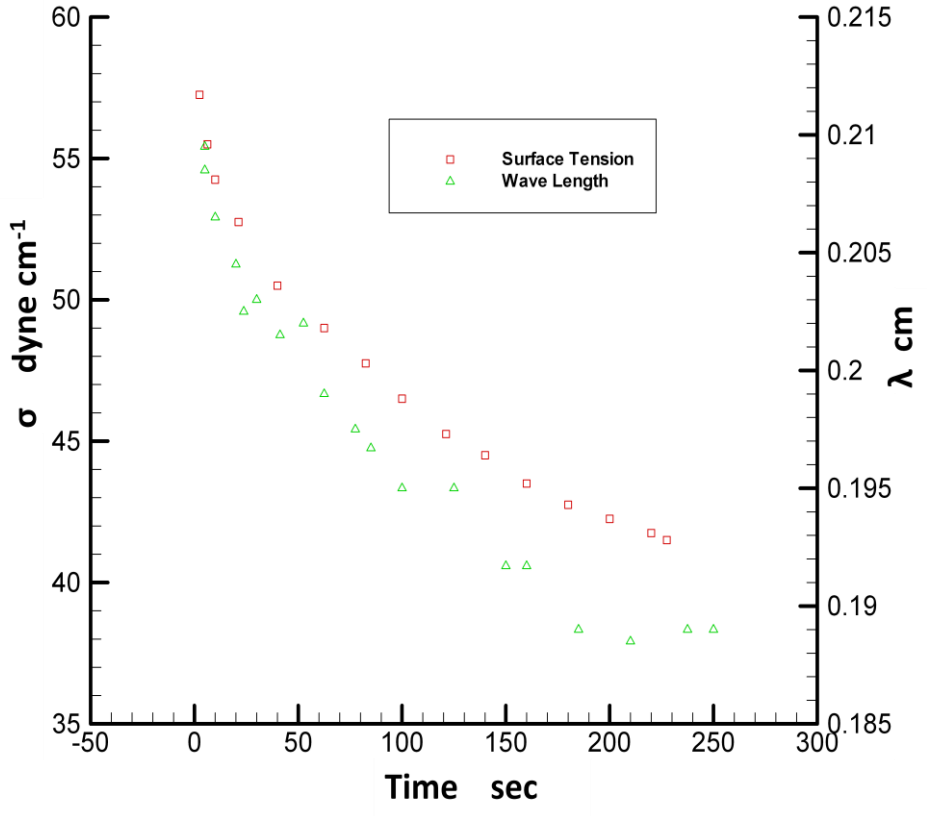

Figure (2.15): Correlation between the surface tension and wavelength as a function of time for a solution ceyl-pyridinium bromide (0.003 per cent)

Gottifredi and Jameson (1970) observed the wavelength in wind tunnel facilities using tap water, distilled water, SLS solution (low surface tension) and dilute glycerol solution ($\mu = 11.5\ cP$). The wind speed ranged from 2.5- 6 ms^{-1}. They observed that the first growing waves using still and tap water appeared markedly three-dimensional, while using the other solution the waves were more two dimensional and regular in appearance. The corresponding wavelength and wind speed that satisfied these conditions were as in Table (2.8).

According to Gottifredi and Jameson the pebbled appearance almost disappeared for SLS and glycerol solutions due in one case to the surface film and in the other to lower wave Reynolds number which is defined as $R_{ew} = c/k\nu_w$. From the definition; R_{ew} number is a function of wavelength, wave velocity and viscosity; in case of SLS solution the wavelength remained very small due to presence of the SLS solution (low surface tension, high elasticity and high surface resistance to structural distortion) and consequently R_{ew} is significantly low.

Table (2.8): The corresponding wave length for three liquids for a wind speed ranging from 2.5-6 ms^{-1}

Liquid type	Wavelength cm	Wind speed ms^{-1}
Tap water	1-3	3.5
Distilled water	1-3	2.5
SLS solution	1	6
Glycerol Solution	5-5.5	6

In the case of glycerol solution, the R_{ew} also remained low due to increased viscosity. In these two cases the growth rate of both solutions was less than the clean water case. The difference between the two cases can be described as: In case of using SLS solution the wave growth rate will remain low though at higher wind speeds; the presence SLS solution in the water causes a reduction in the wavelength and amplitude, thus the wave damping rate is very high. In glycerol solution, the growth rate was low at lower wind speeds, however, an increasing trend in the wave growth rate with higher wind speed is assumed and the waves will attain higher amplitudes before breaking. This is due to increase in the wavelengths of capillary waves which cause an increase in the exposed leeward wave's surface area to the wind (increase in the wind-wave interaction area).It is postulated that the growth rate is a function of the leeward surface area of the waves, A_w. If the wave is sinusoidal A_w is estimated as

$$A_w = \frac{a/2}{\sin(\theta)} \times w \approx \frac{\lambda \cos\theta}{4} \times w \quad \text{..... (2.15)}$$

Where a, θ and w are the wave amplitude, the angle between the undisturbed water surface and leeward wave surface (phase angle) and width of the leeward wave surface. In case of 2D waves as in low surface tension solutions w goes to zero and A_w remains very small.

In previous studies it is proved that the transfer of wind momentum and growth rate increases as the roughness of the surface increases. This is because the drag coefficient of rougher surfaces is higher than undisturbed surfaces. On the other hand the wind-wave interaction surface area is also increased as the surface becomes rougher. This causes an increase in the wind momentum flux and waves growth rate. It is suggested to parameterise the wind momentum flux equation by the factor

$A_{RU} = A_w/A_U$ where A_U is the area of undisturbed water surface. The momentum flux equation becomes in this form:

$$\tau = \rho C_D (U_z - U_\circ)^2 \, \Phi(A_{RU}) \quad \text{(2.16)}$$

Where Φ indicates function linking τ and A_{RU}. It is assumed that A_w is entirely in contact with the wind without separation.

As the factor A_{RU} increases, the τ increases and enhances the growth rate. The wavelength and the slope of the surface waves are the main parameters that affect the parameter A_{RU}. The waves with higher wavelength and lower steepness have a higher surface area than shorter and steeper waves.

If the separation between the wave surface and wind occurs it is important to introduce the parameter A_{wc} (the area at which the wind in direct contact with the surface area of a wave without separation). In this case τ is a function of the ratio A_w/A_{wc}, where the parameter A_{RU} becomes $A_{RU} = (A_w/A_{wc})/A_U$.

Miles (1967) derived a formula to predict the temporal damping of initial surface waves on the basis of characteristics of the surface film which can be expressed in terms of surface elasticity, surface viscosity and solubility of surface material. The formula is expressed in the form:

$$-\beta_t = \frac{1}{4} k \sqrt{2\nu_w \omega} \frac{\zeta^2}{(\zeta-1)^2+1}, \quad \text{(2.17)}$$

Where ζ is the non-dimensional value of surface elasticity defined as:

$$\zeta = (\tfrac{1}{2}\rho_w^2 \nu_w \omega^3)^{-1/2} k^2 \mathcal{X},$$

Where ω the angular frequency of the waves. The damping rate predicted by Miles model (1967) for four possible values of surface elasticity and pure water ($\sigma_0 = 72.5$ dyne cm^{-1}) was plotted versus wavelength by Kawai (1979b) and recalculated and plotted in Figure (2.16). *Kawai* concluded that the surface tension has no significant effect on the damping rate value.

This conclusion conflicts with earlier findings where the surface tension has a significant effect on the damping rate. This inconsistency can be explained as follows:

As shown in the above discussion, the reduction in the surface tension of a liquid is accompanied by a reduction in length of initial wavelets and a reduction in the growth rate. It is assumed that the wavelength is a function of surface elasticity and for a given wind speed the wavelength is smaller than those on pure water by a factor m.

$$\lambda_x = m\lambda_w \quad \text{.....} \quad (2.18)$$

Where λ_x, λ_w and m is the wavelength in the presence of a surface film, and wavelength in absence of surface film ($\mathcal{X} = 0$) respectively and the proportionality factor depends on $\mathcal{X}$ value. The factor m can be determined experimentally by measuring the temporal growth rate for several possible values of surface elasticity. The damping rates were predicted by Miles model is a function of k^3. It is assumed roughly for a given wind speed a reduction occurs in wavelength by the order 10%, 30% and 50% ($m = 0.1, 0.3$ and 0.5) if the surface elasticity attains the values of the order 10, 30, and 50 dyne cm^{-1} respectively. The corresponding reduction in the wavelength and the increase of damping rate due to increase in the elasticity on the basis of the above assumption is shown in Figure (2.16). In the light of this explanation, for a given wind speed the predicted damping rate in the presence of surface film ($\mathcal{X} > 0$) using Miles model will be higher than the corresponding damping rate in the absence of a surface film ($\mathcal{X} = 0$) and proportional with $\mathcal{X}$ magnitude. It is concluded that, the damping rate predicted by Miles (1967) is consistent with the observations and other theories that suggested the surface tension has a significant effect on damping rate. Kawai considered the magnitude of the surface tension through using equation (2.17), however, he did not consider the reduction in wavelength that occurs due to a reduction in the surface tension.

As shown in the Figure (2.16) and (2.17) the effect of the damping rate is significant only for very short waves. Figure (2.17) shows that at given conditions the wavelength attain higher magnitudes as the elasticity become negligible. This explanation explains the significant increase in critical wind speed in the presence of high elasticity surface film; the initial waves start to appear when the length of the initial wave becomes significant. This requires a higher wind speed in case of the presence of a higher elasticity surface.

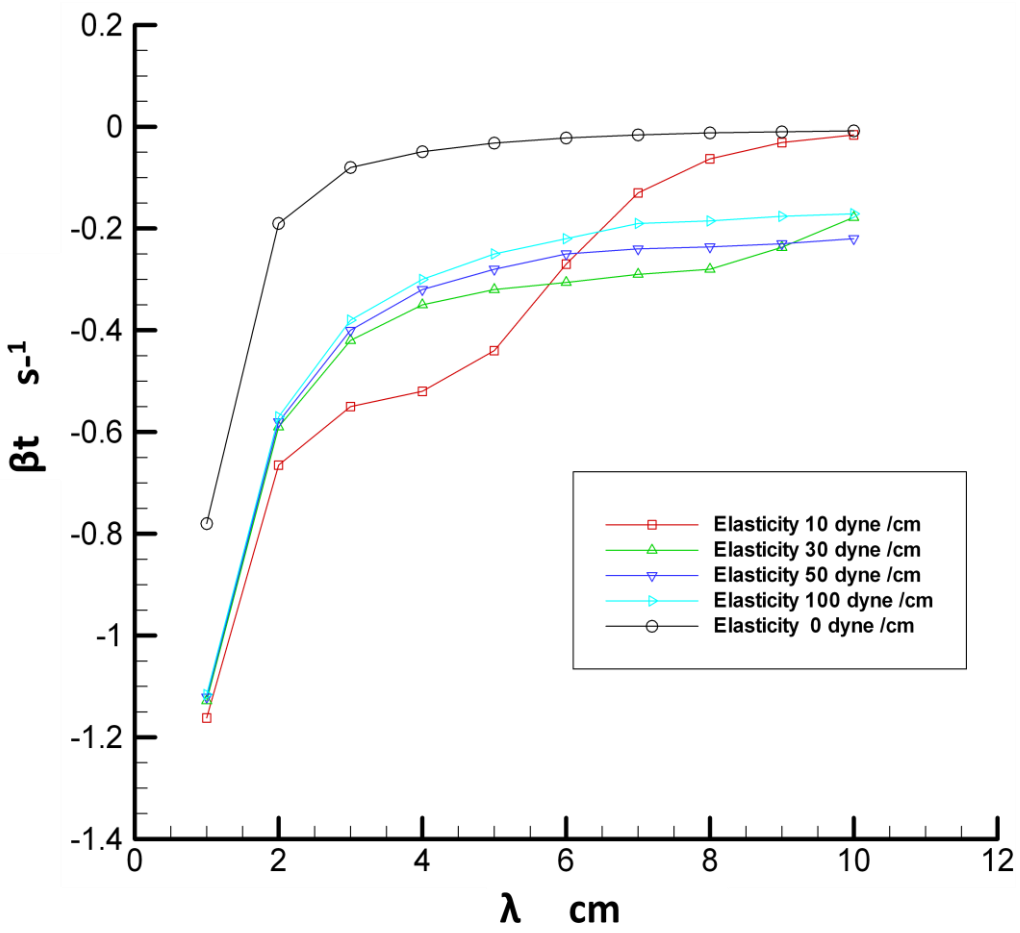

Figure (2.16): Correlation between damping rate and wavelength according to Miles (1967) for four possible values of surface elasticity and pure water

Gottifredi and Jameson (1968) studied the critical friction velocity as a function of wavelength for water solutions with different values of surface elasticity. The surface elasticity $\mathcal{X}$ had a considerable effect on short wavelengths even for a film of very low elasticity. To produce a particular wavelength by the action of wind, a significant increase in the corresponding friction velocity occurs as $\mathcal{X}$ is increased. For example, to produce a wave with $\lambda = 5$ cm, the corresponding friction velocity was 5.25, 9.75, 16.5, 23.25, 28.5 and 31.5 cm^{-1} for surface elasticity of the order 0,10,20,40 and 80 dyne cm^{-1} respectively. If $u_*/U_\infty = 0.05$ the wind velocity required to produce 5cm wavelength will increase from 105 cms^{-1} to 570 cms^{-1} if $\mathcal{X}$ is varied from 0 to 40 dyne cm^{-1}. The subsequent waves evolution depend on the characteristics of the initial wavelength, and in the presence of high elasticity surfaces the required wind speed to produce large wave is comparatively very high.

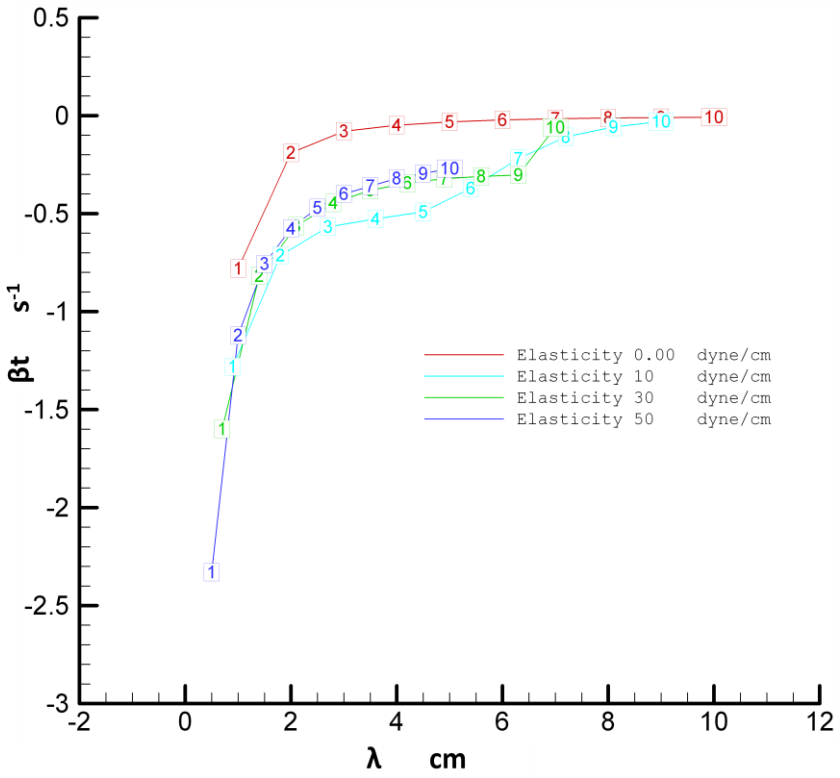

Figure (2.17): Show the increase in the damping rate due to increase the elasticity according to equation (2.18)

The effect of the parameters that affect the length of infinitesimal waves was discussed above. It is concluded that the parameters that expand or contract the initial wavelength should be considered to understand the wave's growth and damping. The surface tension and interface viscosity are suggested as the most important parameters that affect the expansion and contraction of the infinitesimal waves. The effect of the former was explored while the latter remains in need of much explanation and experimental investigations. The dimensionless number that balances the effect of the viscosity and surface tension is Ohnesorge number which is defined as $Oh = \frac{We}{Re} = \frac{\rho v}{\sigma} V = \frac{\mu}{\sigma} V$. The magnitude of Oh number indicates if the viscosity or the surface tension dominates the flow. The wavelength tends to expand if viscosity dominates the flow and tends to contract if surface tension dominates the flow

Experimentally Larson and Wright (1975) measured the attenuation of mechanical waves to approximate the kinematic viscosity. The frequency was accounted accurately and they used the dispersion relation of infinitesimal waves to calculate the wave number. The dispersion relation is given in the form:

$$\omega^2 = \left(\frac{980cm}{f^2}\right)k + (\frac{75cm^3}{f^2})k^3 \quad \text{.....} \quad (2.19)$$

Larson and Wright found that the wave length is a function of kinematic viscosity.

In the next section, the effect of viscosity on the characteristics of the wind generated surface waves will be explored.

2.3 Fetch length

To illustrate the growth of surface waves under action of gentle wind as fetch length increases based on the concept of interface kinematic viscosity; the kinematic viscosity through wind-water interaction process is divided into four categories:

- The kinematic viscosity of the air (outside the viscous sublayer).
- The kinematic viscosity of the water bulk.
- The kinematic viscosity through viscous sublayer.
- The kinematic viscosity of the interface.

The kinematic viscosity of the water bulk and air can be measured using particular measurement systems. The kinematic viscosity in the viscous sublayer was estimated in section (1.9) as the mean value of the air kinematic viscosity and water bulk. It was proved experimentally by Pokazeyev and Vornin (1982) that the wave growth depends on fetch length. In order to explain this phenomenon, it was assumed that the magnitude of kinematic viscosity of water surface (surface film) differs from the magnitudes of kinematic viscosity of water bulk and the contiguous layer of air, but correlates with them.

The following equation elucidates the above assumption. It is assumed the kinematic viscosity of the water surface can be formulated in the following form.

$$\nu_{ws} = \nu_w + \mathrm{f}(u_*, F, h, g) \quad \text{.....} \quad (2.20)$$

Where $\nu_{ws}, \nu_w, h, F \; and \; g,$ are the kinematic viscosity of the water surface, the kinematic viscosity of the water bulk, water depth, fetch and acceleration due gravity respectively.

To find out the relationship between the independent parameters in the second part of the equation (2.20) the dimensional analysis approach is applied.

$$\nu_{ws} = \mathrm{f}(u_*, F, h, g) \quad \text{..... (2.21)}$$

$$\nu_{ws} = C u_{*,}^{a} F^{b} h^{c} g^{d} \quad \text{..... (2.22)}$$

The fundamental quantities that are used in the dimensional analysis are length, mass and time. In order to increase the three fundamental quantities length, mass and time, the length dimension is resolved into three mutually perpendicular directions, which is distinguished by subscripts: $[L_x], [L_y], [L_z]$, Huntley (1952). The importance of this suggestion is to get a complete solution whilst it is difficult to obtain a complete solution if the dependent variables minus fundamental variables are more than or equal two. Another advantage is obtaining the direction of the length dimension as fetch or depth.

The corresponding dimensional equation of equation (2.22) is:

$$L_x^2 T^{-1} = (L_x T^{-1})^a (L_x)^b (L_z T^{-2})^d$$

The subscripts x and z indicate the increase in length dimension along the wind direction and depth of a water body.

From the corresponding dimensional equation, we get four simultaneous equations. The solutions of the simultaneous equations in terms of exponent **a,** are: $a = a,\ b = 2 - a,\ c = \frac{a}{2} - \frac{1}{2},\ d = \frac{1}{2} - \frac{a}{2}$ whence

$$\nu_{ws} = C\sqrt{\frac{g}{h}}\, F^2 \left[\frac{u_*}{F}\sqrt{\frac{h}{g}}\right]^a \quad \text{..... (2.23)}$$

The equation (2.23) can be written as

$$\nu_{ws} = \sqrt{\frac{g}{h}}\, F^2 \emptyset \left[\frac{u_*}{F}\sqrt{\frac{h}{g}}\right]^a \quad \text{..... (2.24)}$$

As shown in the equation (2.23), all the parameters inside the brackets are frequented out of the brackets except for u_*, so the exponent **a** can be estimated based on the value of u_*

The bound where ν_{ws} is fully dependent on u_*, hence $a = 1$ thus:

$$\nu_{ws} = CFu_* \quad \text{(2.25)}$$

From equation (2.25), ν_{ws} is function of F and u_*. The bound of $u_* < 2\,(\nu g)^{1/3}$ that was proposed by Donelan (1993) in the roughness estimation equation is suggested to apply in equation (2.24)

$$\nu_{ws} = CFu_*, \quad u_* < 2\,(\nu g)^{1/3}$$

By adding the bulk viscosity to the equation (2.25)

$$\nu_{ws} = \nu_{wb} + CFu_* \quad \text{(2.26)}$$

For the bound at which ν_{ws}, is independent from u_*, hence $a = 0$, whence

$$\nu_{ws} = C\sqrt{\frac{g}{h}}\,F^2, \;\; u_* > 2\,(\nu g)^{1/3} \quad \text{(2.27)}$$

By adding the bulk viscosity to equation (2.27) the equation becomes:

$$\nu_{ws} = \nu_{wb} + C\sqrt{\frac{g}{h}}\,F^2 \quad \text{(2.28)}$$

$$\nu_{ws} = \nu_{wb} + \emptyset\sqrt{\frac{g}{h}}\,F^2$$

From equation (2.28), whilst ν_{ws} is independent of u_*, it is directly proportional to $F^2 and \sqrt{g}$ and inversely proportional to $\sqrt{h}$. Since the frequency $f = \sqrt{\frac{g}{h}}$ the equation (2.28) can be written as:

$$\nu_{ws} = \nu_{wb} + \emptyset f\,F^2$$

In both equations (2.26) and (2.28), ν_{ws} is a function of the fetch. As ν_{ws} grows with fetch, it is supposed that it causes a reduction in Δ (the difference between the magnitudes of ν_{ws} and ν at particular fetch). The reduction in magnitude of Δ causes an increase in the homogeneity between the two contact layers of wind and water surface. A tight coupling is assumed to occur due to this action which causes a significant increase in wind- water interaction and in wind momentum flux to water bulk. This interpretation explains the wind growth with fetch and the difference between the characteristics of long travelled waves and short travelled waves. This interpretation is consistent with shear flow instability theory, (Miles 1962) that suggests; U_{cr} and U_{in} is fetch dependent and with observation of Kimmo and Kahma (1981) of exponential growth of a component of dimensionless spectrum with fetch.

At low and moderate wind speeds, increasing the magnitude of ν_{ws} affects the viscous sublayer thickness, surface roughness, surface film thickness, inception wind speed, critical wind speed (viscous damping rate), wavelength and initial wave growth rate. At higher friction speeds where the characteristic wave height is higher than the viscous layer, the surface waves are entirely visible and the surface film viscosity affects the transfer of wind momentum and wave growth rate due to wave-wave interaction.

Experimentally Larson measured the attenuation of mechanical waves to approximate the kinematic viscosity. The frequency was accounted accurately and they used the dispersion relation of infinitesimal waves (equation 2.19) to calculate the wave number. The wave number and the result shown in Table (2.9) and the correlation between the kinematic viscosity and the wavelength is shown in Figure (2.18)

Table (2.9): Wavelength, group velocity and kinematic viscosity of attenuation of mechanical waves as approximated by Larson and Wright (1975)

λ	k	C_g cm/s	ν (cm^2/s) $\times 10^{-2}$
2.08	3.02	21.3	1.28
2.03	3.08	21.5	1.23
0.159	3.41	22.5	1.24
1.7	3.69	23.5	1.29
1.48	4.23	25.2	1.22

1.25	5.0	27.6	1.11
0.97	6.44	31.6	1.18
0.82	6.72	34.8	1.24
0.72	8.67	37.3	1.03
0.66	9.4	39.2	1.01

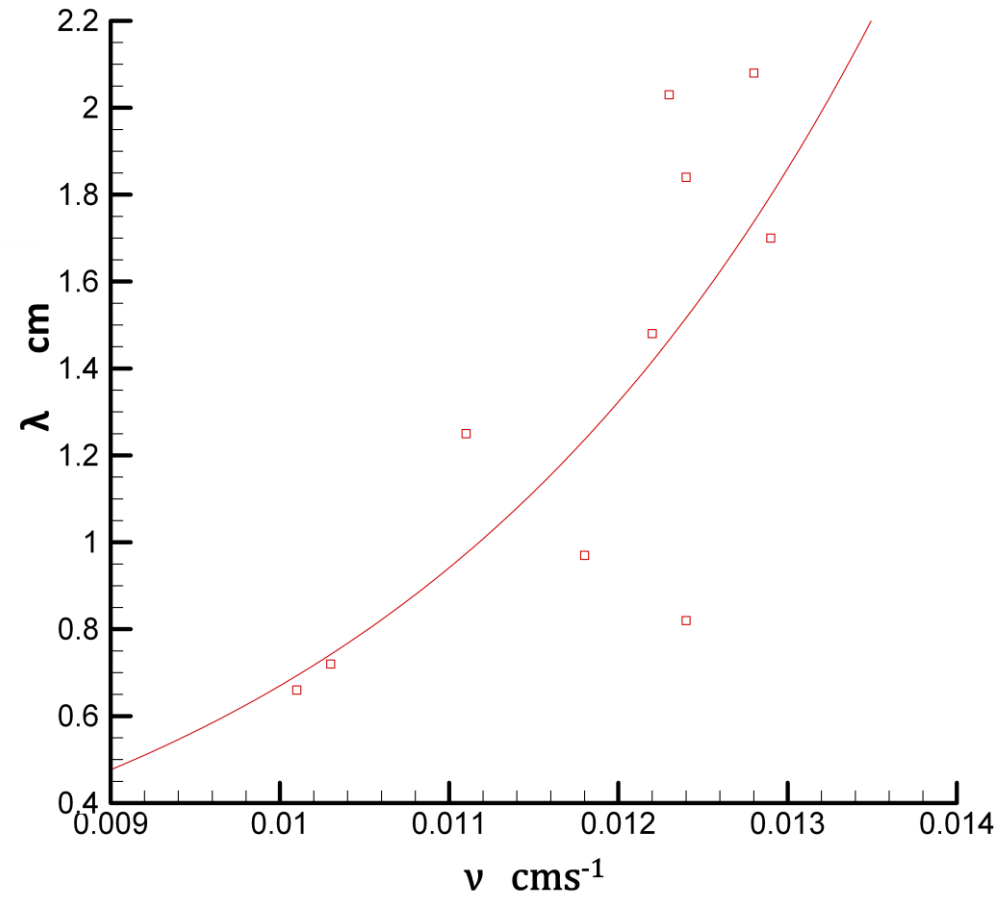

Figure (2.18): Correlation between wavelength and kinematic viscosity as measured by Larson and Wright (1975)

A shown in Figure (2.18), the kinematic viscosity of the water is a function of wavelength. These observations are justified as the wavelength increases, the magnitude of the kinematic viscosity increases and enhances the wind-wave interaction.

2.4 Wind -wave angle.

Instability theory assumed logarithmic boundary layer and the turbulence in the air is neglected. On this basis, Miles (1960) defined the growth rate γ being in the form $\gamma = (\rho_a/\rho_w)\ \beta\ \omega(\frac{U_r}{C_w}\cos\theta)^2$

The theory has proved successful in operational wave models such as Wamdai (1988) that suggested the atmospheric pressure input in the form

$$S_{in}(f,\theta) = \frac{\rho_a}{\rho_w}\beta\omega(\frac{u_*}{C}cos\theta)^2 F(f,\theta) \quad (2.29)$$

Where $S_{in}(f,\theta)$, the atmospheric input, $\beta = \beta(u_*\cos\theta, \Omega)$, $F(f,\theta)$ is directional frequency spectrum and $\Omega = \frac{gz_\circ}{U_r^2}$.

U_r is the reference speed which is defined by Miles (1959) as

$$U_z = U_r\ \log\left(\frac{z}{z_\circ}\right) = 2.5u_*\log(\frac{z}{z_\circ})$$

Snyder and Cox (1966) measured the actual growth rate to determine the exponential growth rate due to atmospheric input. They concluded that the atmospheric input is in the form

$$S_{in}(f,\theta) = \frac{\rho_a}{\rho_w}\beta\omega(\frac{U_{10}}{C}cos\theta - 1)F(f,\theta) \quad (2.30)$$

Hsiao and Shemdin (1983) conducted experiments at the coast of the Netherlands in the North Sea. They collected data in the range $1 < U_{10}/c < 7.4$. Shemdin (1983) found the data had a quadratic dependence on U_{10}/C and represented the atmospheric input source term as

$$S_{in}(f,\theta) = 0.12\frac{\rho_a}{\rho_w}\beta\omega(\frac{U_{10}}{C}cos\theta - 1)^2 F(f,\theta) \quad (2.31)$$

The results of these investigations have a similar magnitude to Mile-Janssen theory except Hsiao and Shemdin. The latter found that the data had a quadratic dependence on U_{10}/C and their results were significantly smaller than Snyder (1983). The resulting growth rate in instability depends upon the ratio of curvature of the wind

profile to its slope at a distance above the water surface for which $U = c$ (critical height).

Two points should be considered in the discussion of the equations (2.29, 2.30 and 2.31); the angle θ and the wind-water density ratio s:

θ in the above equation is the angle between the wind and wave. This angle changes according to the phase angle. Since the characteristics of the water surface are affected by several parameters as shown in chapter one and two; it is suggested to consider the angle α between the linear portion of wind velocity profile and water surface . It is assumed that this angle is a function of the parameter Δ; as Δ attains lower values, α attains lower values, then it will enhance the wind-water interaction, wind water coupling, wind momentum flux and wave growth rate. This can be summarised by α as a function of atmospheric input. The conditions of low air temperatures and long fetch are very appropriate in reducing α, however the higher air temperature and higher relative humidity are the appropriate conditions to increase α. In the light of this explanation; it is postulated that a significant increase should occur in the magnitude of the angle α in case of higher elasticity surfaces which cause a significant reduction in wind momentum flux. This is may occur due a reducing in strength of the wind-water coupling as the surface attain higher magnitudes. A good understanding of the parameters and conditions that may affect the magnitude of α helps in predicting sea state.

The other point that should be discussed is the parameter s. This parameter is part of the atmospheric input equation. The sensitivity of this parameter to conditions that affect the wave growth is insignificant. s tends to attain a constant value over a wide range of wind speeds, wave speeds and atmospheric conditions. The ratio ν/ν_{ws} is suggested to be introduced into the atmospheric input equation, since this ratio is affected by atmospheric conditions, fetch length and characteristics of the both water and air.

Considering the two points help to understand the observations and helps to predict the sea state over the whole range of wind and wave speeds.

2.5 Conclusion

The discussion of previous investigations has revealed that the wave growth rate is a function of, surface elasticity, bulk viscosity, wavelength (wave number), friction velocity, and wave frequency, fetch length, the parameter U_1 and relative wind speed u_*^n/U_z . The dependence of growth rate on the above parameter is varied according to the experimental condition and to the theory that is used to analyse the observations. The comparison between the observations show a scatter and disparity in some cases if the magnitude of one of the above parameters does not match the corresponding parameter in the other data

Capillary waves are very instrumental in wave formation, growth once formed and tendency of longer waves to decay. The action of capillary waves is to strengthen the coupling of wind-wave and to enhance the transfer of wind momentum to longer waves due to wave-wave interaction.

The action of the capillary waves is affected significantly by the physical properties of the water surface.

The key parameter that governs the formation and growth of the capillary waves is the length of these waves. The parameter that contract or expand the length of the capillary waves under action of low wind speed such as viscosity and surface tension should be considered in predicting the characteristics of the gravity waves. The lessening of the surface tension causes a contraction in the length of the capillary waves, whereas the increase of the viscosity causes an expansion in length of the capillary waves.

The damping rate of capillary waves was suggested in the form

$$\beta_d = -4k^2\nu_w = -4\left(\frac{2\pi}{\lambda}\right)^2 \nu_w$$

The damping rate is a function of the wavelength and water viscosity. If the effect of the elasticity (lessening of the surface tension) dominated the flow the wavelength tends to decrease and the damping rate increase, however, if the effect of increasing the viscosity dominated the flow, the damping rate will increase initially until the

wave length attains a particular value, then the damping rate tends to decrease or the growth rate tends to increase.

The difference in the mechanism of wave damping rate due to lessening of the surface tension or increasing the viscosity is; the former causes the gravity waves to attain less amplitude before breaking at a given wind speed due to decreasing the magnitude of λ/a, however, the latter will do the opposite due to an increase in the magnitude of λ/a at a given wind speed.

The Reynolds wave number which is defined as $R_{ew} = \frac{c}{k\nu_w}$ or $R_{ew} = \frac{c\,\lambda}{2\pi\nu_w}$ illustrates the importance of the wavelength; the R_{ew} attains -at a given wave velocity- a higher magnitude as the increase of the wave length exceeds the increase of the viscosity. It is suggested to use the parameter of ν_{ws} in the definition of the R_{ew} which seems more appropriate than using bulk viscosity since c and λ are related to the surface.

The damping due the viscous forces affects the growth of wave amplitude and the damping due to capillary forces affect the extension of wavelength.

Theoretically the growth rate reduces systematically as the elasticity increases.

As explained in this chapter, the wavelength of a surface wave is a function of surface elasticity, and for a given wind speed a wavelength of a water solution with ($\mathcal{X} > 0$), λ_x is smaller than λ_w by the factor m which depends on the magnitude of $\mathcal{X}$, where λ_w is the wavelength of pure water ($\mathcal{X} = 0$)

$$\lambda_x = m\lambda_w;\ m \leq 1$$

The wave attains the highest growth rate at a given friction velocity if the wavelength attain a particular length which defined as the critical wave length. It is obvious that this parameter is a function of the physical properties of water.

In order to explain the wave growth with fetch under the effect of a given wind speed the parameter ν_{ws} is introduced in this study. ν_{ws} is a function of fetch length for the whole range of the friction speeds. It is suggested that as the magnitude of ν_{ws} increases the difference between the kinematic viscosity of the air and the water decreases and enhances the homogeneity between than wind and water at the

interface. It is predicted that an increase in wind momentum flux will occur due to this action which will enhance the wave growth.

The wind-water interaction enhances as the interaction area increases. The interaction area increases as the surface becomes rougher and the characteristics of the capillary waves play a significant role in the size of the interaction area.

Chapter 3

Analysis and interpretation of velocity fields (I)

Introduction

The purpose of this research is to study the relationship between the hydrodynamics of the bulk flow under effect of low wind speed action and the surface wave generation mechanism. This can be achieved by analysing and interpreting the velocity fields of the bulk flow under effect of different wind speeds and observing the evolution of the surface. The corresponding parameters that affect the evolution of kinematics and dynamics of the bulk flow should be measured to explain the relationship between the wind speed and the bulk evolution. Understanding the correlation between the hydrodynamics of the bulk, wind shear stress and the characteristics of the resulting surface wave has a significant importance for:

- helping to predict the surface wave's growth under effect of wind action based on knowledge the characteristics of the bulk flow.
- helping to explain previous observations such as the significant increase in critical wind speed when a significant change in the surface elasticity occurs or when contaminates form a strong layer on the surface. In these two cases the transfer of the wind momentum was confined to the boundary adjacent to the surface. However, the surface velocity developed as part of a flow extending to the channel bed when a clean water surface was used.
- helping to explain the difference between the characteristics of surface wave at open oceans and limited fetch water bodies at a particular wind speed. The internal perturbations present naturally in the former are due to bulk surface temperature difference, density difference, etc, and they affect the growth of the surface wave.
- helping to improve the efficiency of wave energy systems when such systems are constructed in water bodies with limited fetch length and depth. This can be achieved by increasing the internal perturbations using mechanical means to increase the energy of the surface waves. It is assumed that the surface wave energy is a function of wind shear stress and density of the bulk perturbations.

Based on this assumption, the scouring effects can also be reduced significantly by damping the internal perturbations near the beach.

To analyse the kinematics and dynamics of the bulk flow under effect of wind action, a group of experiments were conducted using water channel-wind tunnel facilities as described in section (3.7). The velocity fields measured using the PIV system, were produced after being processed using commercial software. The velocity fields were analysed and interpreted by two methods:

1. Reading the velocity field images and movie sequences that were captured and recorded at different wind speeds. This includes observing the following parameters at different wind speeds: the evolution of eddy characteristics (size, strength), the direction of the flow with respect to wind direction at different depths from the surface and the velocity distribution through the bulk. This gives an approach to understanding the bulk evolution under effect of the wind action.
2. Converting the velocity field images to data using Tecplot software and a PIV commercial software package (LaVsion). The converted data are plotted against a position along the water channel in the direction of the wind. The most important parameters that can be extracted and converted to data from the velocity field images using the commercial software are flow velocity, velocity vector angle, vorticity, swirling strength, shear strength, and swirl and shear. After plotting these parameters against a position along the water channel, the above parameters were studied separately under the effect of wind action. In Chapter 4 the maximum value of each parameter at different wind speeds were determined and plotted against wind speed at three fetch lengths. This may help in analysing a large number of data that collected under different conditions of wind and water, thus revealing the relationship between the above parameters and the surface wave generation mechanism.

3.1 Why PIV and how does PIV work

Studying and analysing the dynamics and kinematics of water flow under action of wind requires in some cases measuring the average and instantaneous velocity

distribution across an extended area of the flow field. The average flow can be obtained by scanning a point velocity probe across the flow field; however, the instantaneous velocity cannot be obtained with such a technique. Other visualization techniques may reveal the instantaneous flow structure, but only qualitative or semi quantitative results can be achieved at best. The PIV technique can provide an accurate quantitative measure of the instantaneous flow velocity across a plane area of the flow field. PIV is an optical and non-intrusive based system that is related to both flow visualization and the optical point technique.

As described briefly by LaVision (2005); to measure the instantaneous flow in fluids such as water using PIV, the flow should be seeded with solid tiny naturally buoyant particles called tracers. A light sheet formed by passing a double pulse laser beam with small time separation through an optical arrangement works to illuminate the particles. The particle displacement is measured locally across the whole field of an image recorded in the time between the laser pulses as a single image exposed twice or as a pair of single exposures. The image is scaled by the magnification factor and then divided by the known pulse separation time. A camera positioned typically perpendicular to the plane of the light sheet is shuttered to capture the light scattered from the particles. The choice of the two pulses' delay to obtain adequate displacement of the particle image on the CCD depends on the flow velocity and camera lens magnification factor.

For evaluation of the particle images it is assumed that the tracer follows the flow with the local flow velocity between the two illuminations. The digital PIV recording is divided into a small subarea – a so called 'interrogation window'. Using a statistical correlation technique one local displacement vector is determined for each interrogation window. For this reason the size of the interrogation cell is selected so that all particles within this area have moved homogeneously in the same direction and same distance. For good results the number of particles within one interrogation cell should be at least ten.

The evaluation of the particle images depends on the way these images have been recorded by the camera used. One possibility is to record the scatter light of both illuminations in one frame in what is called 'single frame double exposure'. These pictures can be evaluated by auto correlation techniques. The other possibility is to

record the scattered light from the first illumination in one frame and the scattered light from the second illumination in another frame. This is called ‘double frame double exposure’ which is used in the current experiments. These double frame images can be evaluated by cross correlation. Figure (3.1) illustrates the configuration of the PIV mechanism.

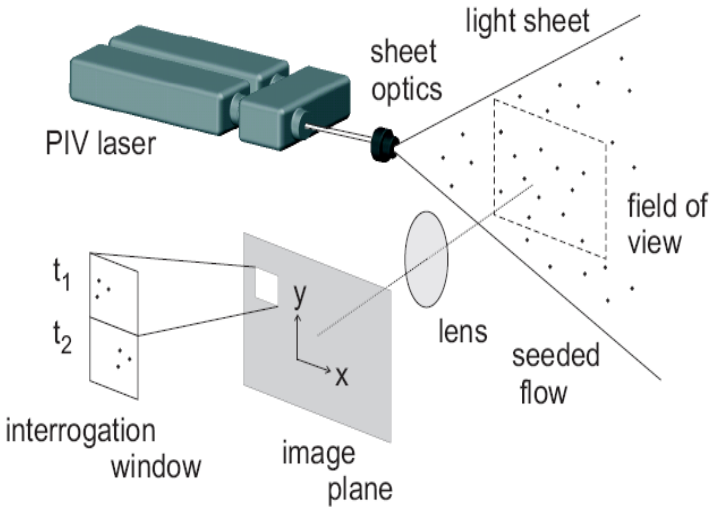

Fig (3.1) illustrates the main components and functions of the PIV system (Extracted from Lavision)

3.2.1 Autocorrelation (single frame / double exposure)

Statistical methods are used to determine the local displacement vector for each interrogation window. In autocorrelation techniques the scattered light from the first and second exposure of the particles is recorded in one image. The complete image is subdivided into so called interrogation windows and each window is evaluated by auto correlation.

The auto correlation function is characterized by two identical correlation peaks rotationally symmetrical about the highest central peak indicating zero displacement. This is a consequence of the fact that one cannot detect the sign of the displacement because it is not known which particle is illuminated by the first and second laser pulse. Thus the information from auto correlation is ambiguous and not conclusive if the prior information about the observed flow is not known. Also the detection of very small displacements can be a problem as in this case the correlation peaks are very

close to the central peak. Compared to cross-correlation the auto-correlation peaks are significantly smaller. High noise increases the possibility that the displacement correlation peak makes the background disappear.

3.2.2 Cross correlation (double frame double exposure)

This technique is used in the current measurements to determine the local displacement vector for each interrogation window. The scattered light from the first and second exposure of the particles is recorded in two different images. The complete image is subdivided in interrogation windows and each window is evaluated by cross correlation.

For cross-correlation a fast double shuttered CCD camera is typically used to record images with ‘double frame double exposure’. The minimum time between the two pulses is limited by the time necessary for the frame transfer of the camera. As the second transfer cannot be shuttered, the two images have two different background intensities and a suitable filter in front of the camera lens should be used. But compared to autocorrelation a higher and unambiguous correlation (peak) can be achieved.

3.3 Main features of PIV techniques

The PIV technique allows capture of the whole velocity field instantaneously, which offers a new insight in fluid mechanics especially in unsteady flow. The PIV technique has features distinct from other techniques of flow measurement velocity systems. The understanding of these features helps the user to exploit the PIV technique to produce accurate velocity field images and hence extract information out of these images. Raffel et al (1998) outlined briefly the PIV features as follows:

- **Nonintrusive velocity measurements**. There are various techniques to measure flow velocity - for instance Pitot tube and hotwire. Both of these techniques employ a probe and work intrusively. The PIV, being an optical technique, works non-intrusively. This feature of a PIV system makes the flow

measurements possible in some applications where intrusive techniques would not be suitable. For instance, it can be used in high wind flows with shocks and in boundary layers close to a wall. In the boundary layer the flow may be disturbed by the presence of probes. Using such intrusive techniques would make the flow measurement difficult and inaccurate.

- **Indirect velocity measurements**. As explained above the PIV technique uses tracers to measure the flow velocity. The PIV measures the flow velocity indirectly by measuring the velocity of tracer particles within the flow. The properties of the tracers that have been added to the flow before the experiments depend on the physical properties of the fluid and application conditions.
- **Whole field technique**. The unique feature of PIV and the Doppler global velocimetry (DGV) technique is the ability to record images of large parts of flow fields in a variety of applications. However, other techniques for velocity measurement only allow the measurement of the velocity of the flow at a single point. Also due to the possibility of high spatial resolution in PIV, PIV allows for detection of the spatial structure even in unsteady flow fields. The temporal resolution at PIV is low due to technical restrictions, however.
- **Velocity Lag**.

  It is important to check carefully whether the tracer particles will faithfully follow the motion of the fluid elements. This depends on the objective of the investigations; however, small particles will follow the flow better. Also the other parameters such as particles density and effect of the buoyancy should be considered.
- **Illuminations**. The scatter light efficiency is better for larger tracer particles; however the larger size of tracer particle contradicts the demand to have as small a particle as possible in order that they follow the flow faithfully. In most applications a compromise has to be found. In liquid flows, larger particles can usually be accepted as opposed to gases. The tracers that are used in the current experiments are hollow glass spheres with an average diameter of 9-13μm.
- **Duration of the illumination pulse**. The duration of the illumination light pulse must be short enough so that the motion of the particles is 'frozen'

during the pulse exposure in order to avoid blurring of the image. The duration of the illumination pulse in the current measurements was 10μs. The duration of the illumination pulses depends on the technical specification of the camera and on the application.

- **Time delay between the illumination pulses**. The time delay between the illumination pulses must be long enough to be able to determine the displacement between the images of the tracer particles with sufficient resolution and short enough to avoid particles with an out of plane velocity component leaving the light sheet between the subsequent illuminations.
- **Distribution of tracer particles in the flow**. In order to obtain optimal evaluation for PIV recording, a homogeneous distribution of medium density is desired.
- **Size of the interrogation window**. The digital (PIV) recording is divided in small subareas – so-called 'interrogation window'. The size of the 'interrogation window' at evaluation must be small enough so that the velocity gradient has no significant influence on the result. Furthermore, it determines the number of the independent velocity vectors and therefore the maximum spatial resolution of the velocity map which can be obtained at the given spatial resolution of the sensor employed for recording. In current measurements the digital (PIV) recording is divided in 64×64 interrogation windows. Figure (3.1) illustrates the term of the interrogation window

In addition to the above PIV technique aspects, (Hyun et al 2003) added that the PIV method still suffers limitations in the dynamic range of velocity measurement. Also the quality of data is affected by the size of the seed particles, image quality and size, camera frame rate and processing software.

3.4 Experimental facility.

The experiments were conducted using the PIV system as a measurement system in a water channel of 9 m length, 1.22 m width, and 0.53m depth, fitted to a wind tunnel section transitioning smoothly over the water surface, in the Fluid Mechanics Laboratory at the University of Hertfordshire. The actual water depth was 0.45m. The

fan speed was set at six positions to change the wind speed. The wind speed was measured at a height of 1.22 m over the water surface where the fluctuations in the measured data are less. At this height the effects of the water surface and the roof of the wind tunnel is less than other heights. Hot wire (H.W) anemometry was used for measuring the wind speed. Measurements using the Hot wire techniques at the given location are given in Table (3.1). The hollow glass sphere tracers with diameters of 9-13μm were added to the water before conducting the experiments to illuminate when the laser sheet passing through the flow.

The 15Hz PIV system includes: one 2M pixel camera, high resolution 2048×2048, with the ability to control exposure time, triggering the image acquisition, and trigger schemes together with 50 mJ double pulses YAGPIV laser. Commercial software (DaVis) was used to analyze the data. DaVis is a CCD image acquisition and processing program developed by LaVision. DaVis is specially developed for LaVision's camera system and to control a great variety of other devices including lasers. DaVis possesses the versatility to control and evaluate a wide range of imaging (e.g. PIV and PTV Particle Image and Tracking Velocimetry).

Table (3.1) shows the wind speed measurements using Hot Wire at six positions of the fan motor input frequency.

Fan Frequency Input (Hz	0	10	20	30	40	50
$U_{1.2}$ ms^{-1}	0	1.07	1.92	2.73	3.6	4.5

The double laser beam used to illuminate the spheres was sited under the water channel and the camera placed perpendicular to the laser sheet. In order to allow the laser sheet to traverse the water from the bottom to the surface and to capture instantaneous images, parts of the bottom and channel sides are made from glass. The PIV measurement zones were located at three fetch lengths from the upstream leading edge of the water channel. Fig (3.2) shows the facilities of the experiments. In this chapter all the measurements were obtained at first fetch (F1). However, the effect of the fetch length will be considered in Chapter 4.

Water channel and wind tunnel

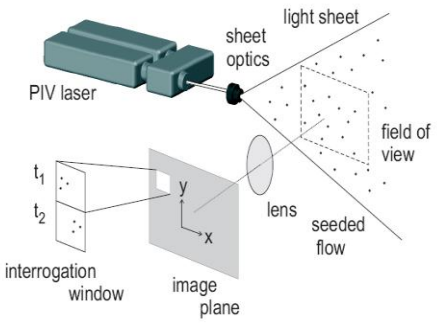

Digital camera

Fig (3.2), the experiment setup; water channel, wind tunnel, PIV laser and Digital camera

3.5.1 PIV Calibration

To achieve highly accurate results, the equipment and measurement systems were calibrated and adjusted. The camera image was calibrated using a calibrated block as the reference point. The calibration block is an L shape block made from Perspex, and it is used to calibrate the camera image by drawing lines on the side facing the camera lens and to calibrate the straightness of the laser sheet (the laser sheet is perpendicular to the wind direction). The clearness of the captured images is controlled by adjusting the camera lens position. The exposure time and repetition rate should be determined before capturing images according to the magnification factor of the camera. For current measurements, the exposure time was 10μs and the repetition rate was 10 Hz. These values are recommended by the manufacturer based on experimental tests in similar conditions to the current tests.

The straightness of the laser sheet was adjusted precisely with the same calibrated block by aligning the laser sheet with the calibration block edge in order to ensure that

the laser sheet was perpendicular to the windward direction. The thickness of the laser sheet should not be more than 2 mm. Fig (3.3) shows the calibration block image. The dimension of the calibrated images can be seen.

To obtain accurate velocity fields images the tracers should follow the flow faithfully in all directions when the flow is driven by the action of the wind. Since the diameters of the tracers are very small and the density of the traces is very close to the density of the water it is assumed that the tracer's particles will faithfully follow the motion of fluid particles. The traces particle images at different wind speeds show the distribution of the traces through the bulk and give the ability to inspect the quality of distribution of the traces in the bulk. The tracer's particle image at 'still' water is shown in Figure (3.4). It can be predicted that the traces will follow the flow faithfully if the distribution of the traces particles through the bulk flow is homogeneous. Actually the tracer's materials and size still challenge the users using the PIV system as a nonintrusive measurement system.

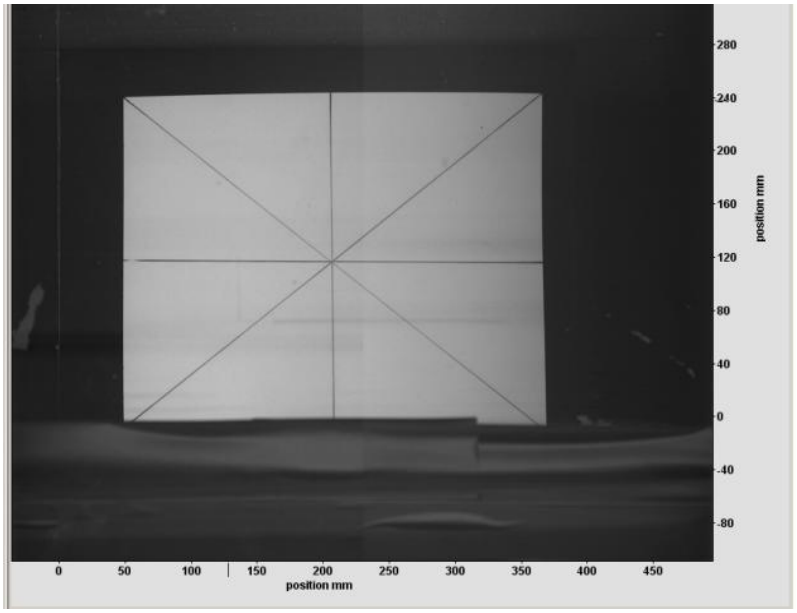

Fig (3.3) Calibrating block image. The crossing lines were drawn to view a clear image

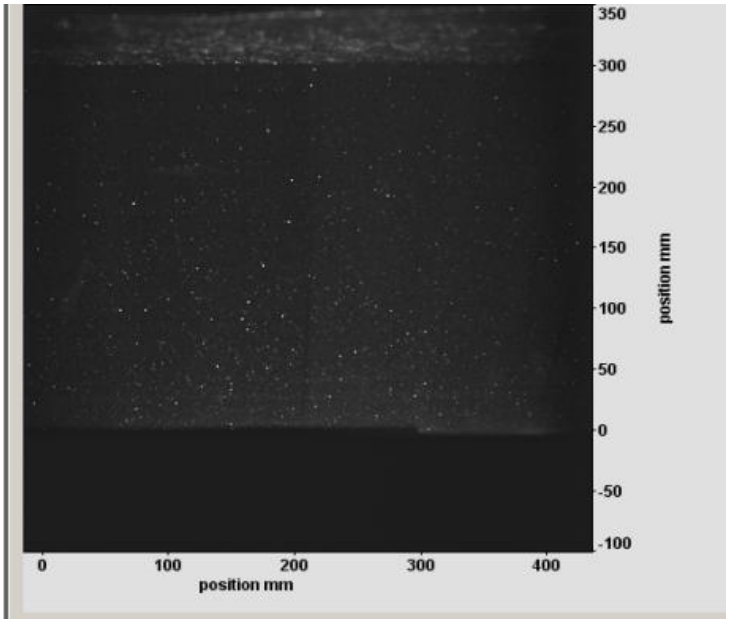

Fig (3.4): The tracer particle image. The distribution of the traces through the bulk can be observed

3.5.2 Accuracy and Repeatability

The accuracy and repeatability are two important criteria used to judge the quality of experimental work measurements. An experimentalist gets confident in analysing collected data if the collected data of an experimental work shows a sufficient accuracy and repeatability.

The repeatability is the variation in measurements taken by a single person or instrument on the same item and under the same conditions. A measurement may be said to be repeatable when this variation is smaller than some agreed limit criteria. However, the accuracy is the quality of measurements being near to the true value or the degree of closeness of a measured or calculated quantity to its actual (true) value.

The repeatability can be measured straightforwardly as long as it is possible to repeat the same conditions of the measurements. However in other cases such as the current measurements, repeating the same conditions is very difficult; the flow attains different orders of background perturbations. In such cases the quality of the repeatability criteria of the measurements can be valued rather than the quantity.

On the other hand, the actual values of the bulk flow parameters under the effect of wind action are not available. Until now the scientists try to find precise measurement systems to measure the flow parameters under the effect of wind action. The new measurement systems were modified to reduce, or eliminate in the best cases, the errors that may occur in using classical systems. A nonintrusive PIV system was used in the current measurements to achieve high accuracy measurements. However, a possible source of error may occur in the current measurements since the flow parameters were measured indirectly. Hollow glass spheres were added to the water before conducting the experiments to be illuminated when the laser sheet passes the water channel.

In the current measurements the repeatability was tested by repeating the experiments under as similar conditions as possible. Good results were achieved in most cases.

To achieve high accuracy measurements the following criteria were considered:

1. Location of the measurement zone.

Two main faults were found in the wind tunnel and water channel design that were used in the current measurements. These faults could cause significant errors if they are not considered when conducting the experiments. The first one is due to the level of difference between the water surface and the output of the wind tunnel. This may cause a flow separation at the upstream edge of the water channel. The second is due to the length of the water channel. Since the water channel is not long enough, the retuned flow may affect the directions of the forthcoming flow. To avoid the effect of these faults on the accuracy of the measurements, the measuring zones were selected beyond these zones where the error was expected to occur.

1. Features of the measurement system used in the experiments.

The PIV system that was used for the current measurements has features which are not available in other systems that can be used in the current experimental conditions. The features of the PIV system were discussed in section 3.3.

2. Conducting the experiments.

The PIV system, including laser system and camera system, was calibrated before running the experiments according to the system manufacturer recommendations.

Also the size and distribution of the seeds in the water were considered and tested before conducting the experiments.

Since the actual values of the flow parameters under action of the wind are not available, the accuracy of the current measurements can be deduced from the following observations:

1. The logical trends of the flow parameters when the wind increases gradually.

The flow velocity increases as the wind increases and the higher magnitudes of the flow velocity occur at the maximum wind speed applied in the experiments. The other parameters showed different trends. However, all the parameters showed significant trends when $U_{1.2} > 2.73$ ms^{-1}.

2. The consistency between the current findings and the previous findings.

It was observed in experiments conducted using wind tunnel facilities that the surface waves became visible as the flow transition from laminar to turbulent occurred. The flow transition occurred at $U_{\infty} \approx 3$ms^{-1}. In the current experiments the waves became visible at a wind speed of the order 2.73 ms^{-1}. The flow transition from laminar to turbulent was deduced at this speed from the following:

The behaviour of the velocity vector angle as the wind attains different magnitudes. This point will be discussed later in detail in this chapter and in Chapter 4.

A significant increase occurred in the magnitudes of the flow parameters as the flow transition to turbulent was completed and when the wind attained higher magnitudes.

The previous studies showed that the contaminants on the water surface can form a strong layer on the surface and impede the transfer of wind momentum to the bulk. This action caused a significant increase in the magnitude of the critical wind speed. To test the effect of the contaminates on the transfer of wind momentum to the water bulk (thus the laminar-turbulent flow transition and wave generation), a simple experiment was conducted in the current water channel. A small amount of dye was injected in the middle of the water channel for contaminated water surface and for clean water surface. The fan was run at the maximum speed. In the both cases the waves became visible after the flow transition to turbulent occurred. The laminar-

turbulent flow transition occurred on the contaminated surface after the wind shear stress pushed the film downwind of the channel.

The current measurements using the PIV system were conducted in three zones along the water channel. The measurements that were conducted near the sudden expansion of the cross section of the wind tunnel showed significant increase in the flow parameters compared to the measurements that were conducted at the other two zones. Higher air turbulence is expected to occur due to changing the cross section of the wind tunnel suddenly. It is known from previous studies that the air turbulence is important in wave generation, wave growth rate and on the bulk flow parameters. This subject will be discussed in section 4.5.

The above observations and the features of the PIV give the experimental analyst a great deal of confidence in the accuracy of the PIV system as a nonintrusive system to measure the flow parameters under the action of the wind. The above observations describe the quality of the PIV measurements accuracy while the quantity is still a difficult question waiting answer.

3.6 Velocity flow field

PIV is an optical technique to measure instantaneously a 2D velocity field (also 3D arrangements are possible). The system has a capability to measure the entire flow in a plane with either two or three velocity components. A principal advantage of PIV is its capability to provide information about the instantaneous flow field, Hyun et al (2003). Several images should be captured and processed to provide an instantaneous velocity field.

One of the important parameters that should be considered in studying the kinematics and dynamics of the flow field under the action of steady wind is the background perturbation that may occur in the bulk before blowing the air over the water surface. The background perturbation may occur in the water body from previous experimental runs, any source of vibration from the surrounding field of the experiment, or due to the convection currents through the bulk. Two sets of velocity

fields below illustrate the effects of wind-induced shear into the bulk as the bulk attains different orders of the background perturbations.

The first sets of velocity fields were measured with low background perturbations (the velocity fields at still water attain minimal value). Figure (3.5) shows the average of the velocity field images for 19 second movie for 'still' water (the wind tunnel fan speed is zero). The average velocity is very low for the entire velocity field. The direction of the velocity vectors is controlled by a weak vortex in the middle of the flow field. Dark regions can be seen in the upper part and in the middle of the image. Occurrence of dark regions between the velocity field layers indicates a change in the flow direction. The dark regions are characterized by a very low flow velocity. Under still water conditions, the tracers move as shown through movie sequences in an oscillatory motion. However, the translational movement is insignificant. The angles, α**,** that the velocity vectors made with respect to the horizontal axis X were measured; X is defined as parallel to the water surface and positive in the direction of the wind (the direction of increasing the fetch). The correlation between α and X will be shown later in this part while the correlation between α and $U_{1.2}$ will be shown in Chapter 4; $U_{1.2}$ is the wind speed that was measured at height of 1.2 m from the water surface. Figures (3.5a-h) show the velocity field images captured from the 19 second movie at equal intervals in between. Figure (3.5) show the average image of the 19 sec movie

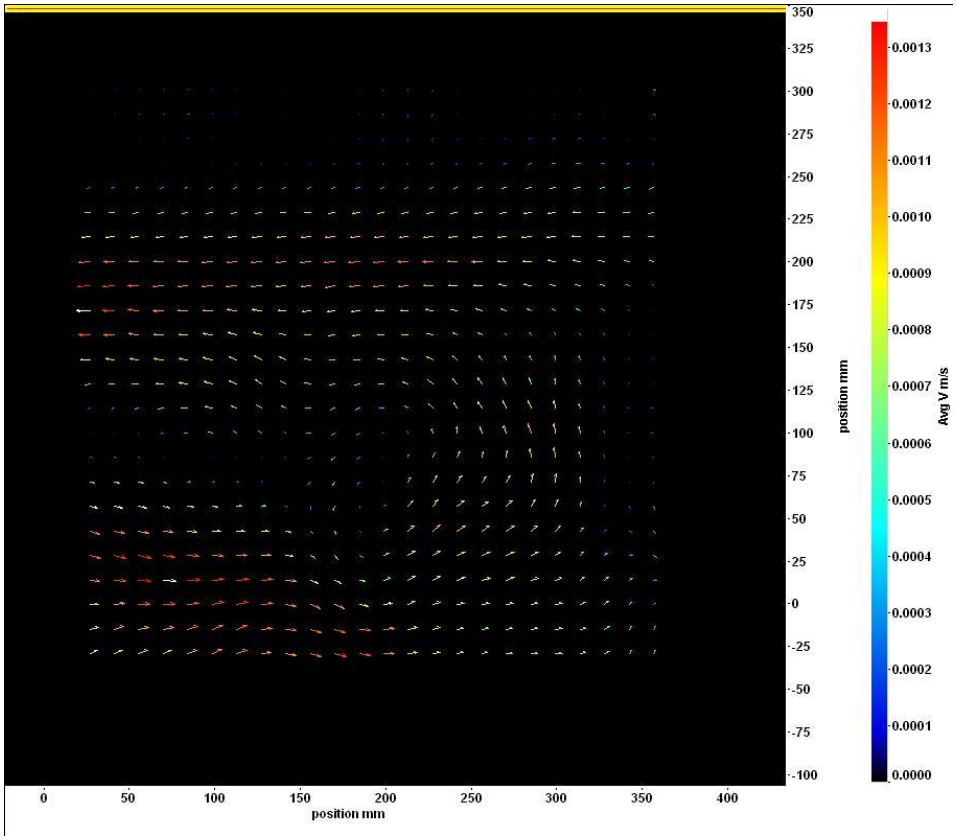

Fig 3.5: Average velocity field at still water conditions (zero fan speed)

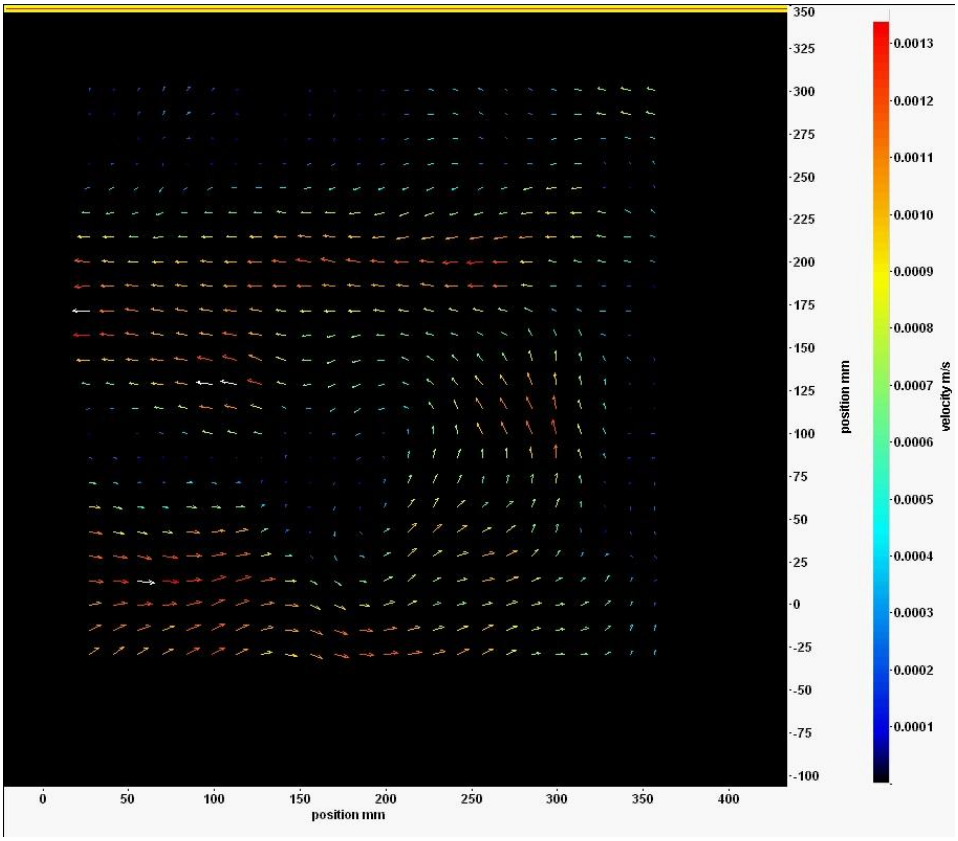

Figure (3.5a): After zero seconds from the beginning of the movie

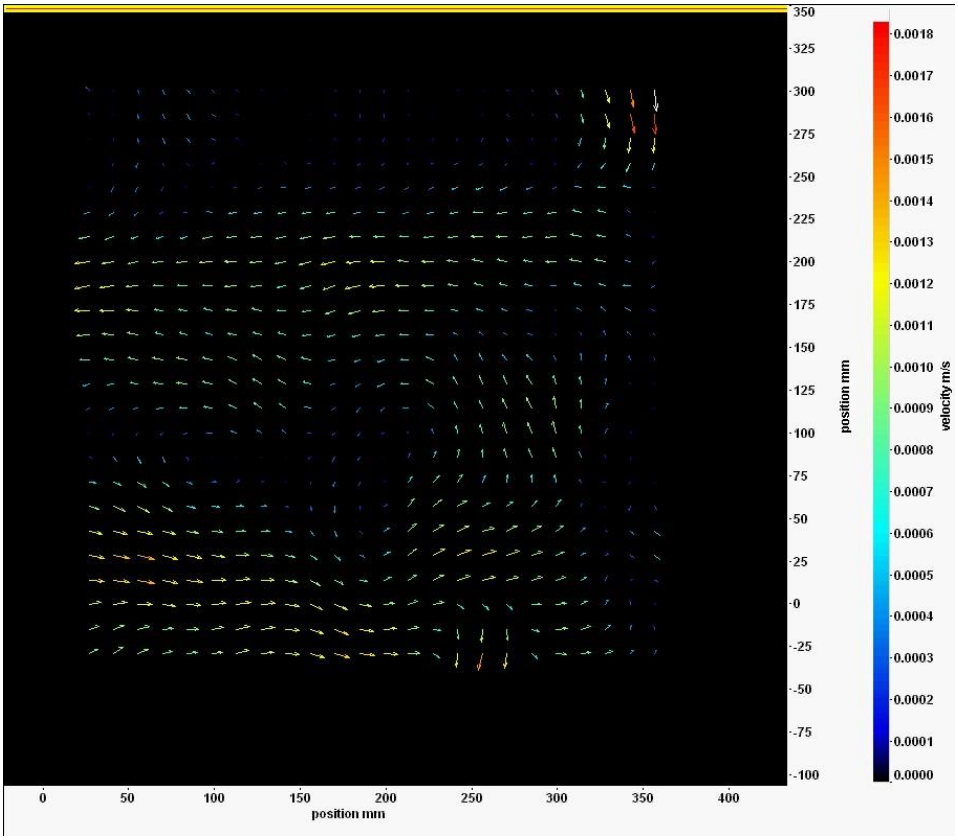

Figure (3.5b): After 2.71 seconds from the beginning of the movie

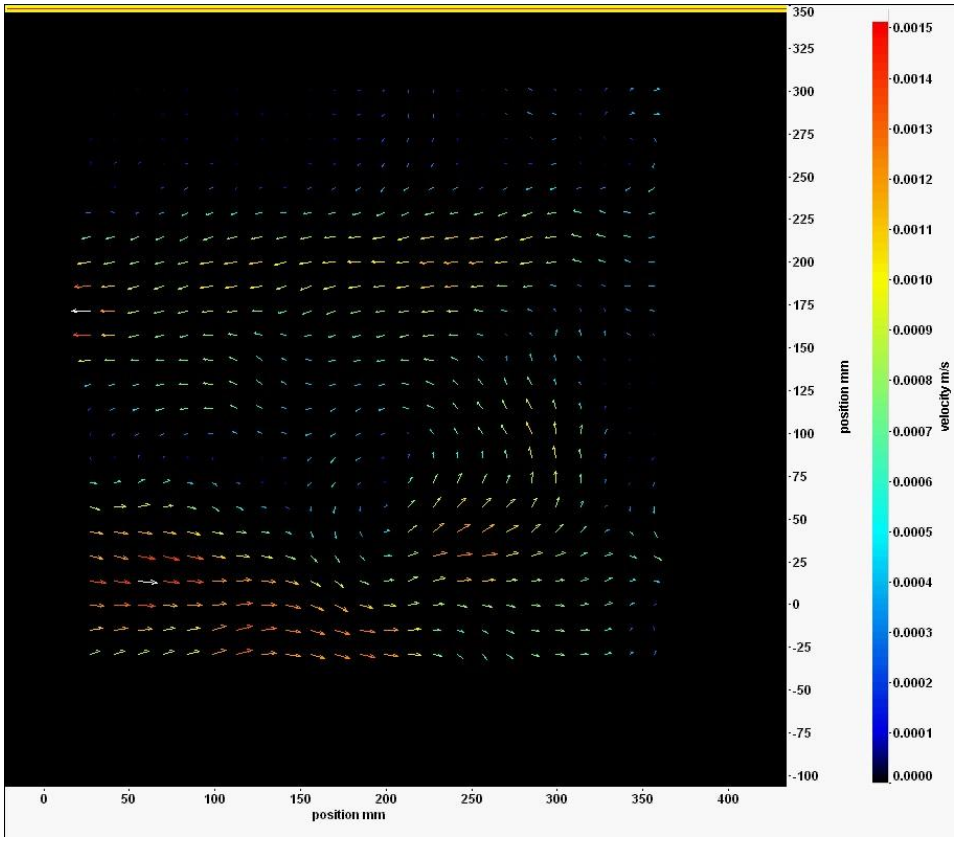

Figure (3.5c): After 5.42 seconds from the beginning of the movie

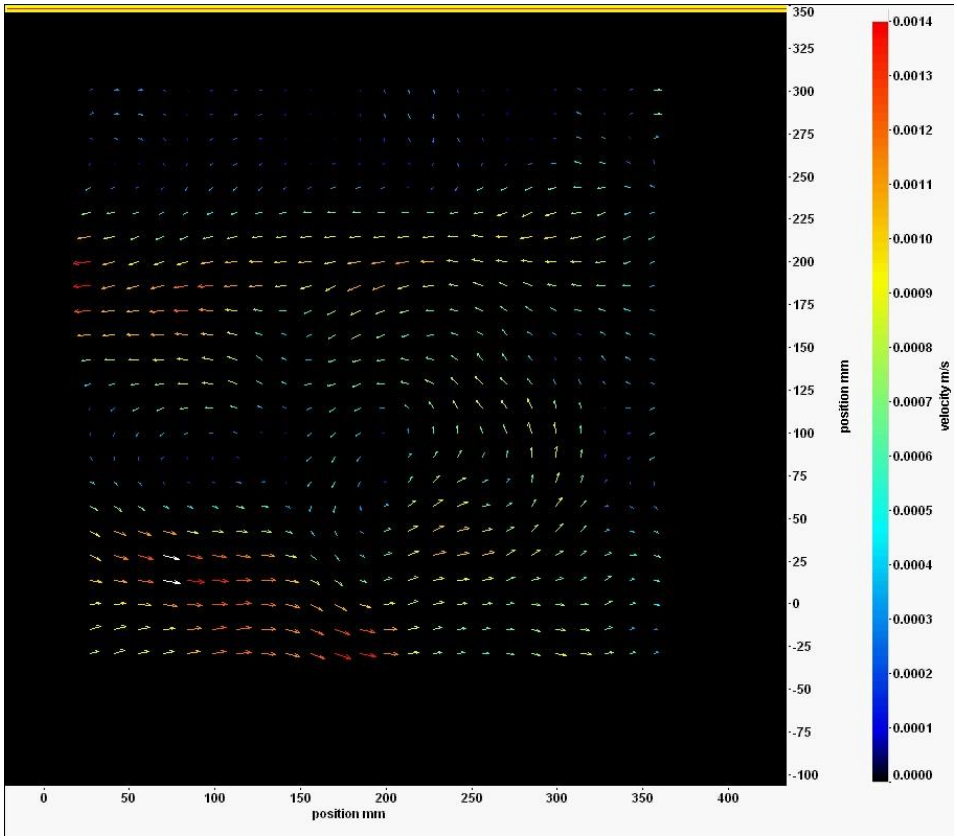

Figure (3.5d): after 8.14 second from the beginning of the movie

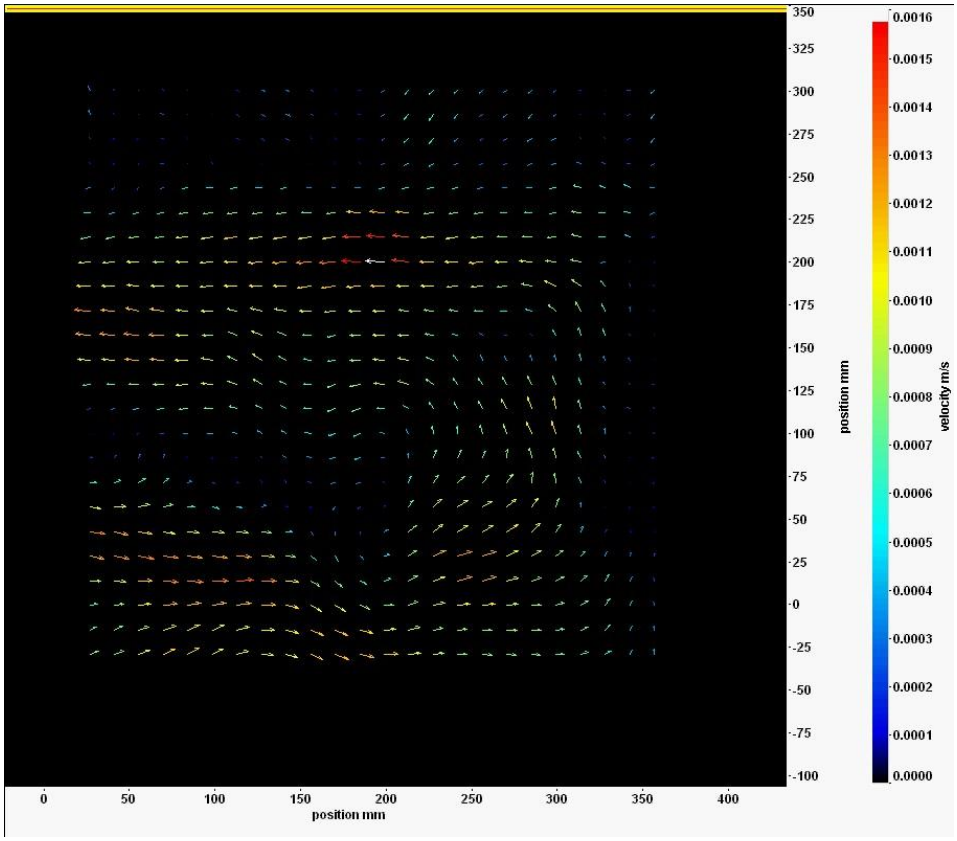

Figure (3.5e): After 10.85 seconds from the beginning of the movie

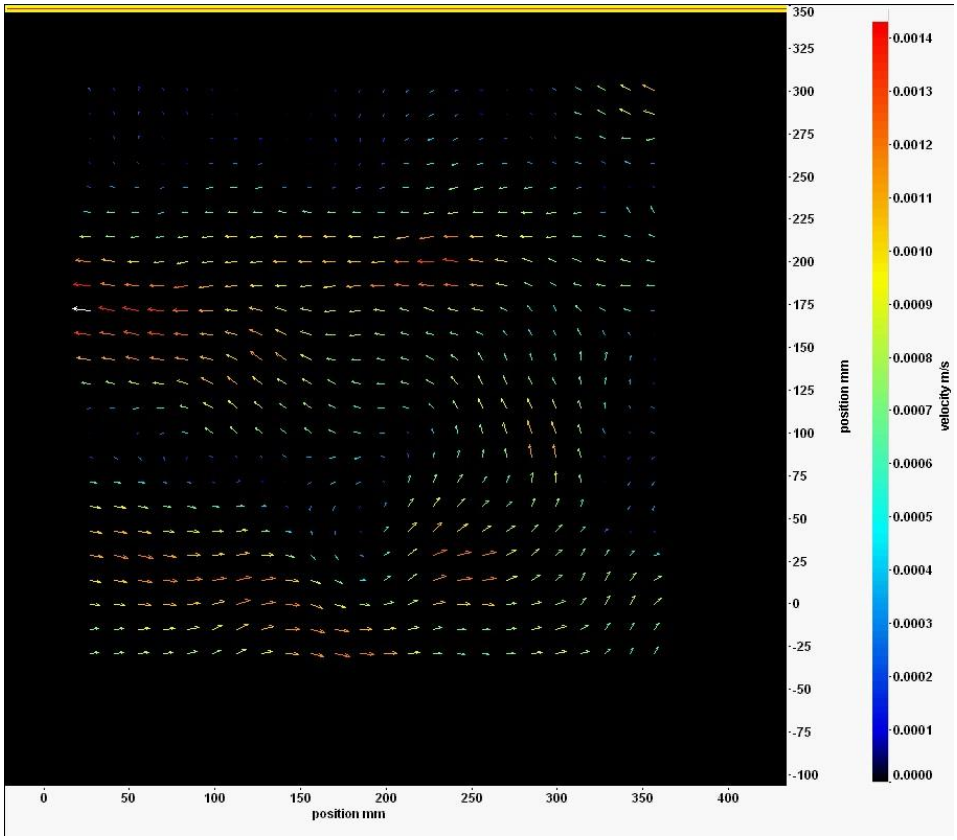

Figure (3.5f): After 13.57 seconds from the beginning of the movie

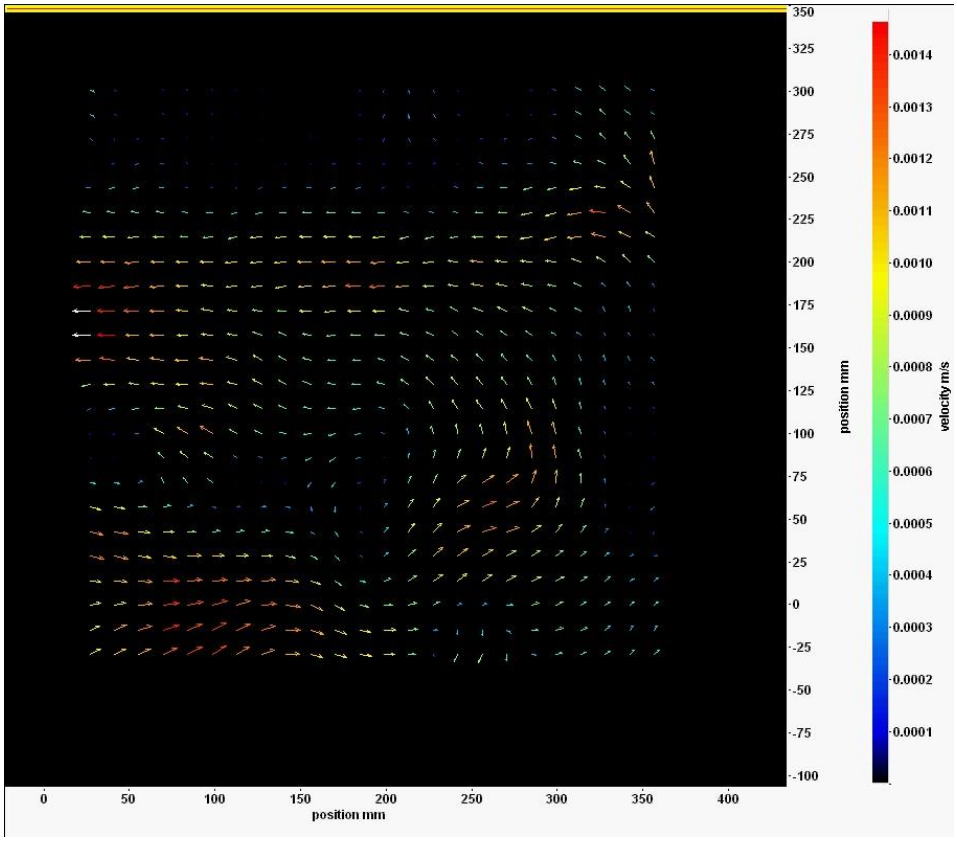

Figure (3.5g): After 16.28 seconds from the beginning of the movie

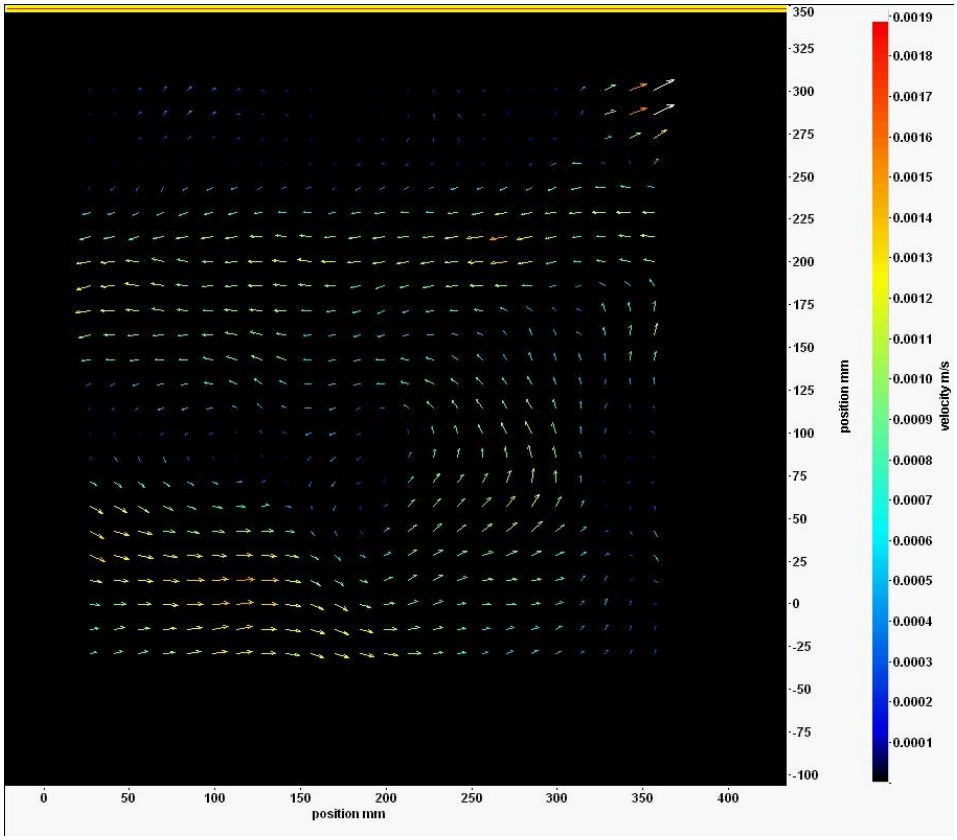

Figure (3.5h): After 19 seconds from the beginning of the movie

The effect of the wind is now considered. In comparison with the zero wind speed at a wind speed of 1.07 ms^{-1}, the entire velocity field shows an increase in the magnitude of the velocity. Also the velocity field shows change in flow directions with respect to the wind direction and dark (calm) regions occur between any two layers with opposite flow directions as shown in figure (3.6). A sequence of movies at this speed showing the flow at dark regions indicates a change in the flow directions with respect to the wind direction. Also, the generation of eddies started in these regions. Figures (3.6a-h) show the velocity field images captured from the 19 second movie at equal intervals in between.

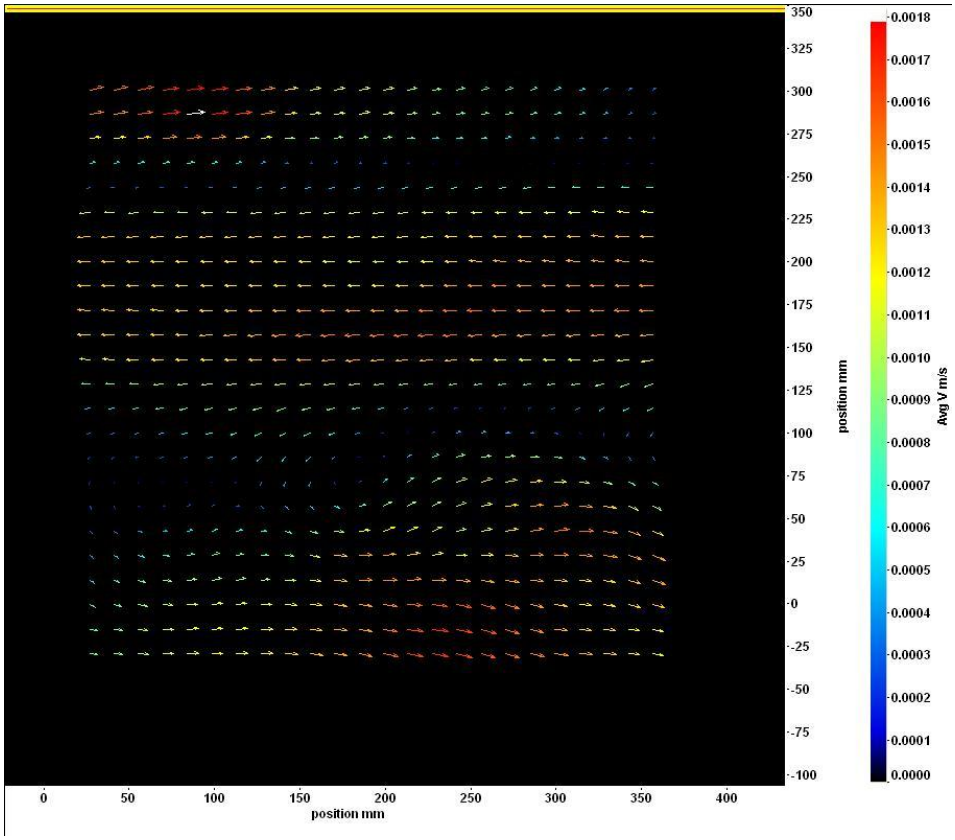

Fig 3.6: Average velocity field at wind speed of the order 1.07 ms^{-1}

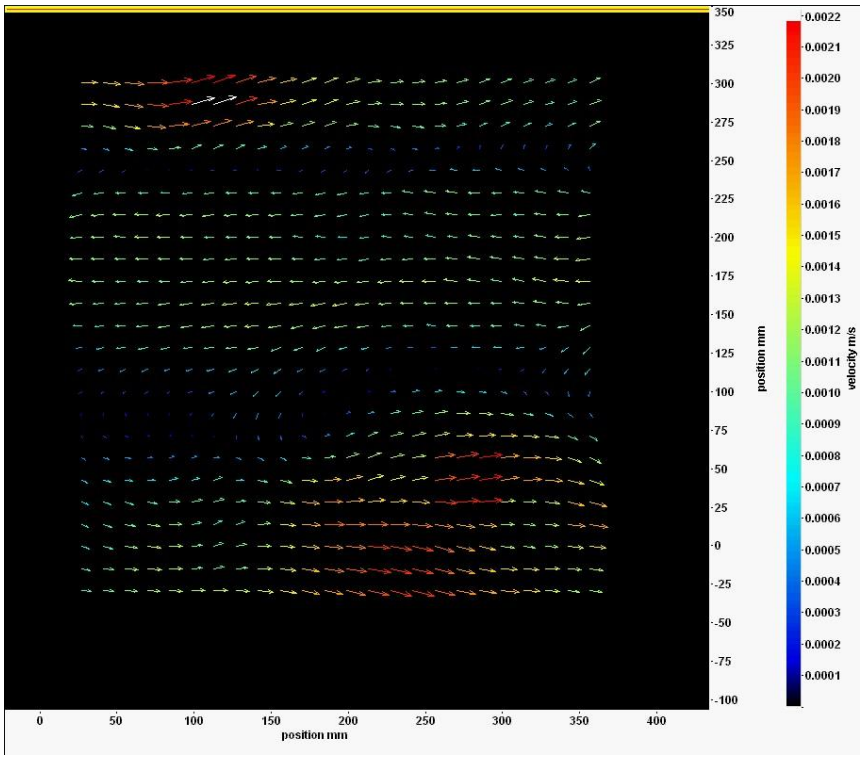

Fig (3.6a): After zero seconds from the beginning of the movie

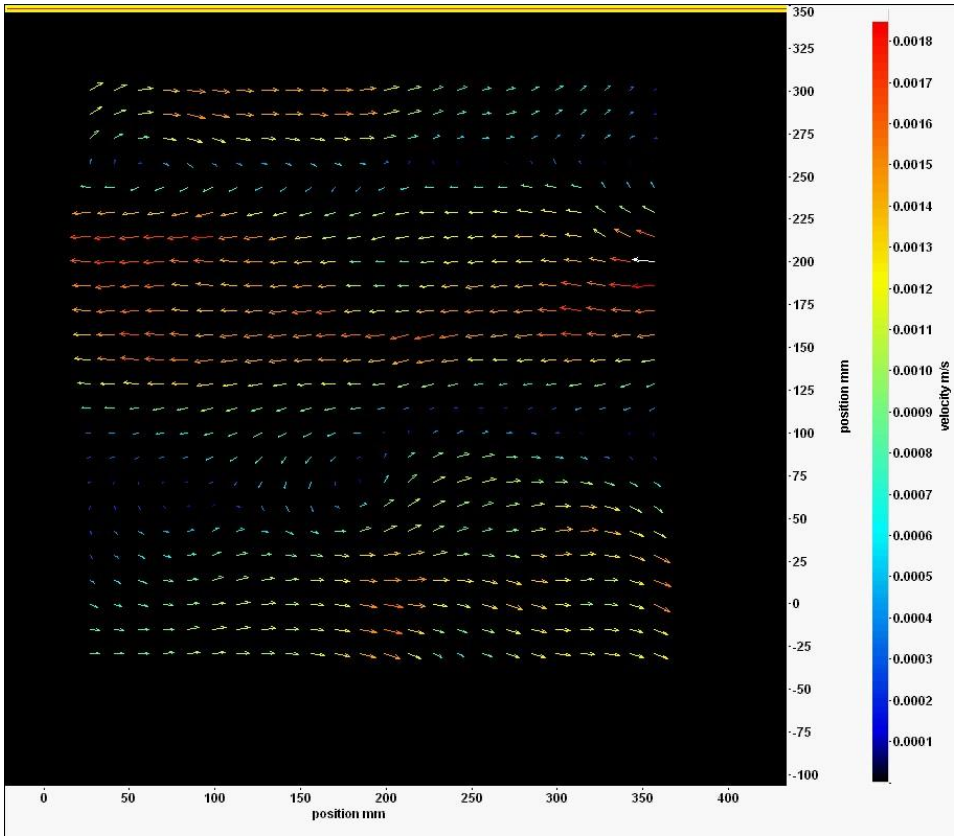

Fig (3.6b): After 2.71 seconds from the beginning of the movie

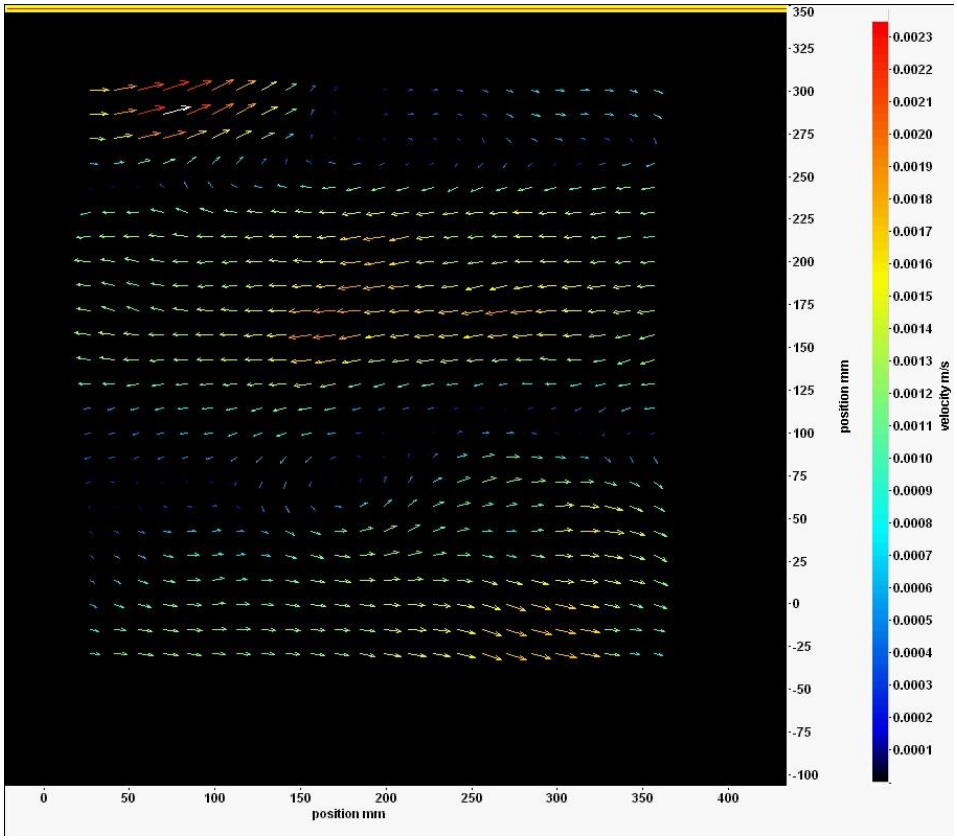

Figure (3.6c): After 5.14 seconds from the beginning of the movie

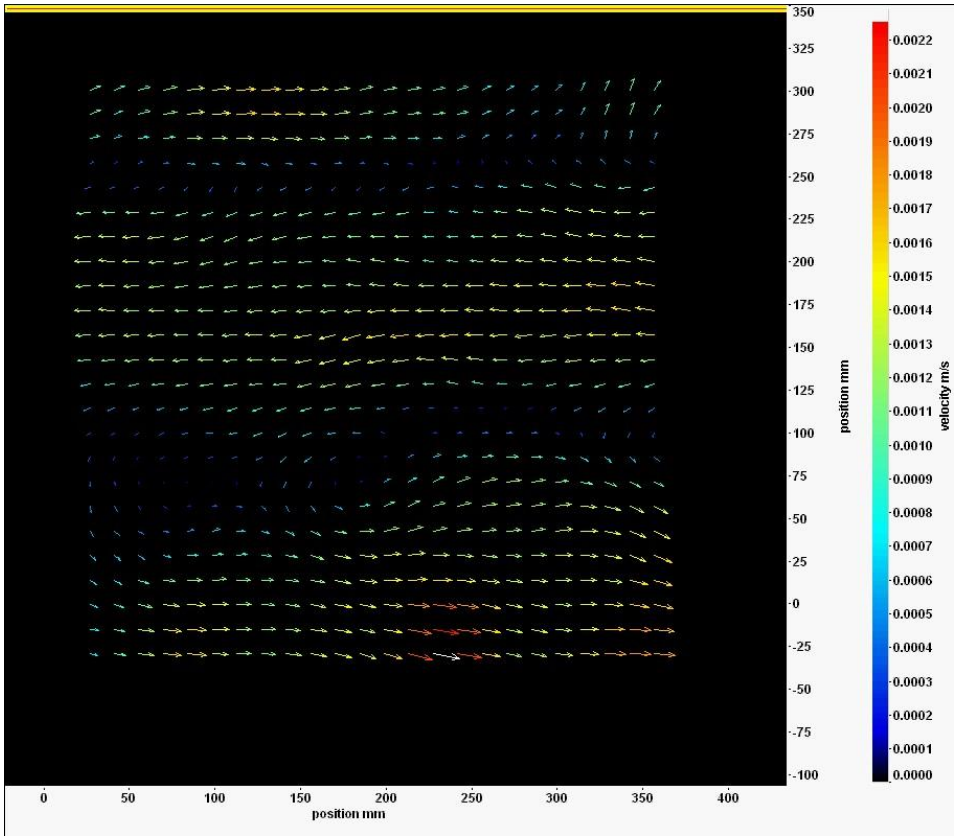

Fig (3.6d): After 8.13 seconds from the beginning of the movie

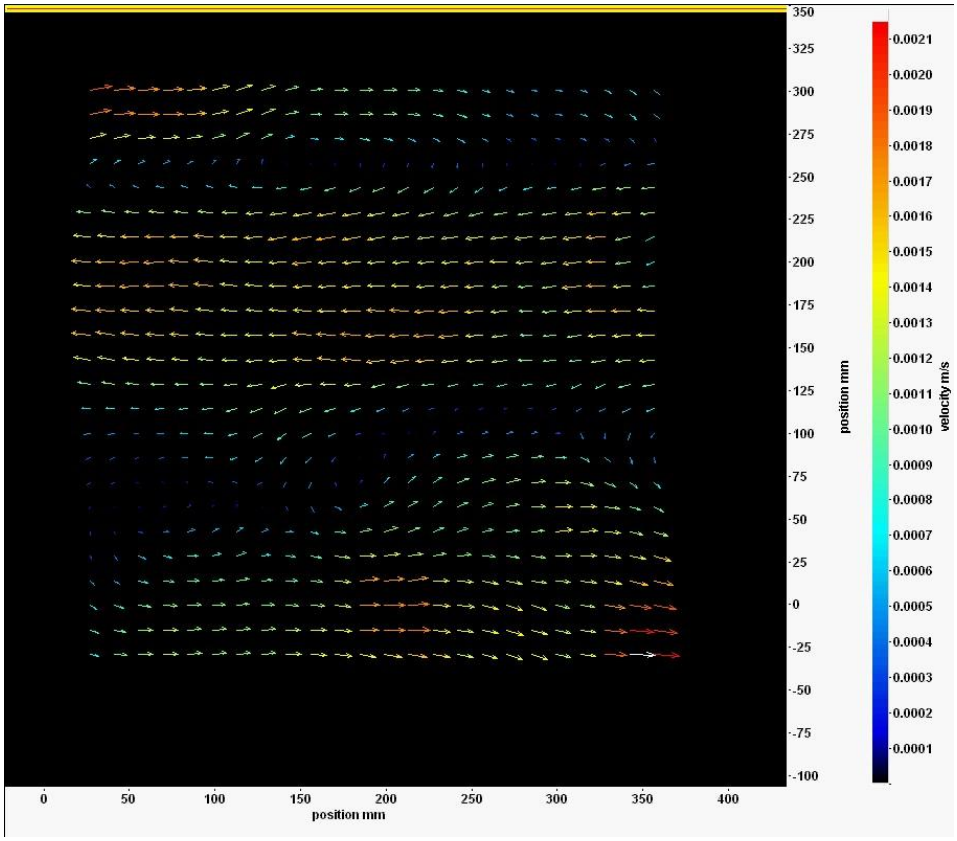

Fig (3.6 e): After 10.85 seconds from the beginning of the movie

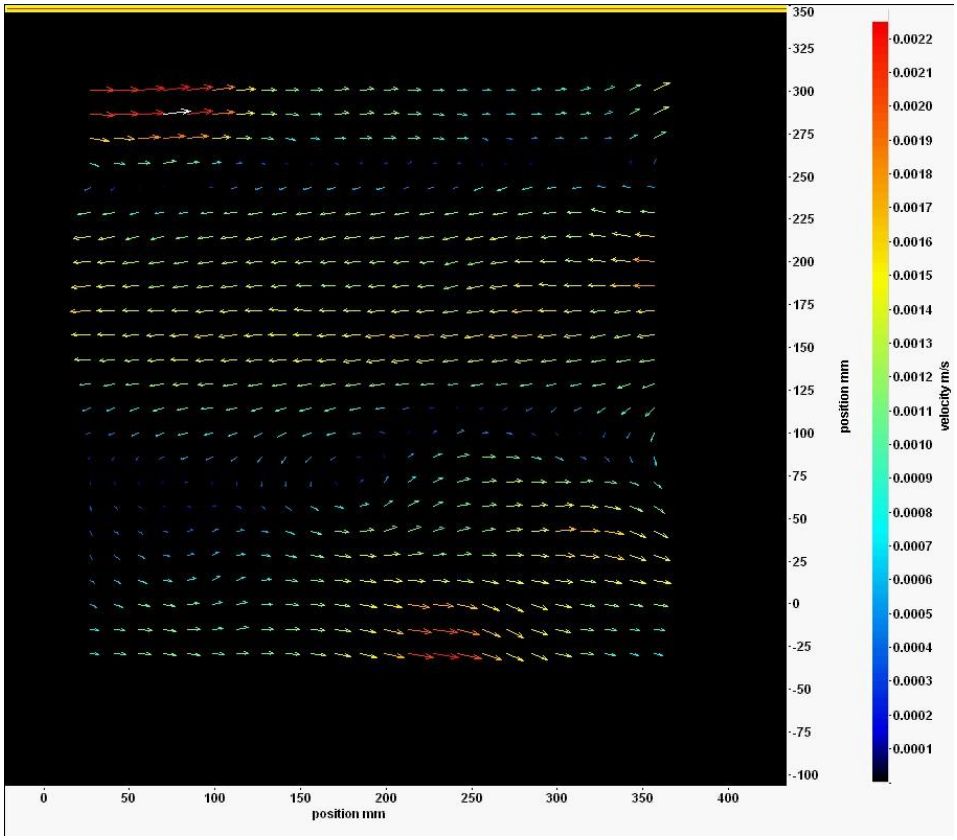

Fig (3.6f): After 13.57 seconds from the beginning of the movie

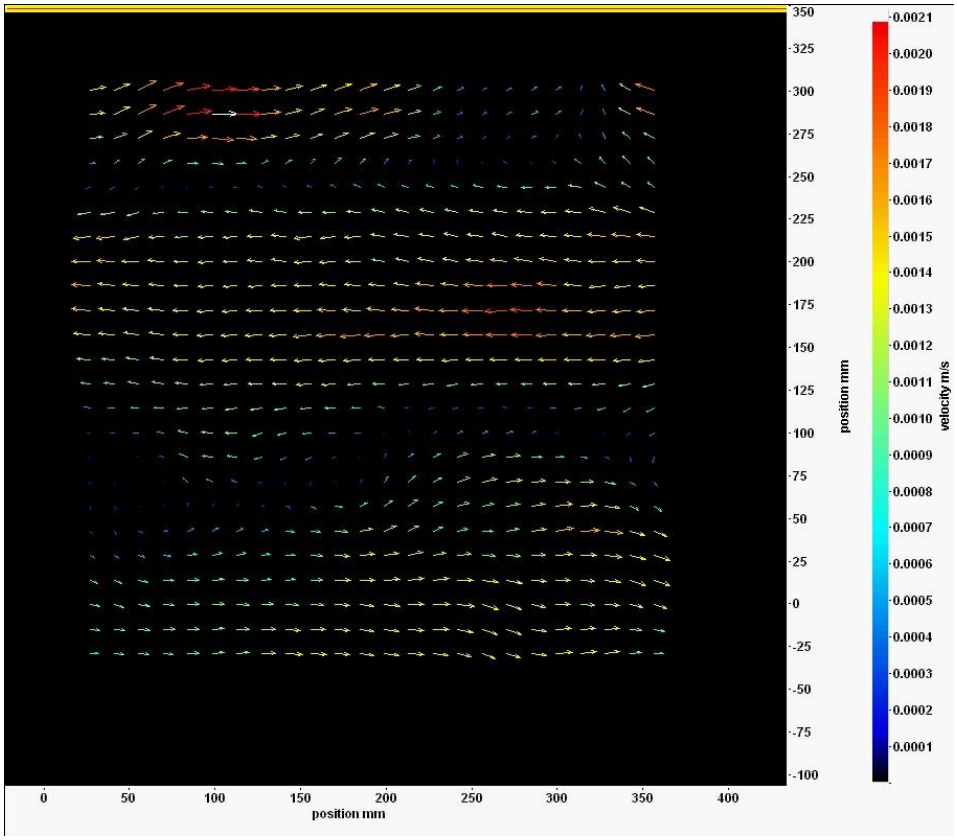

Fig (3.6f): After 16.28 seconds from the beginning of the movie

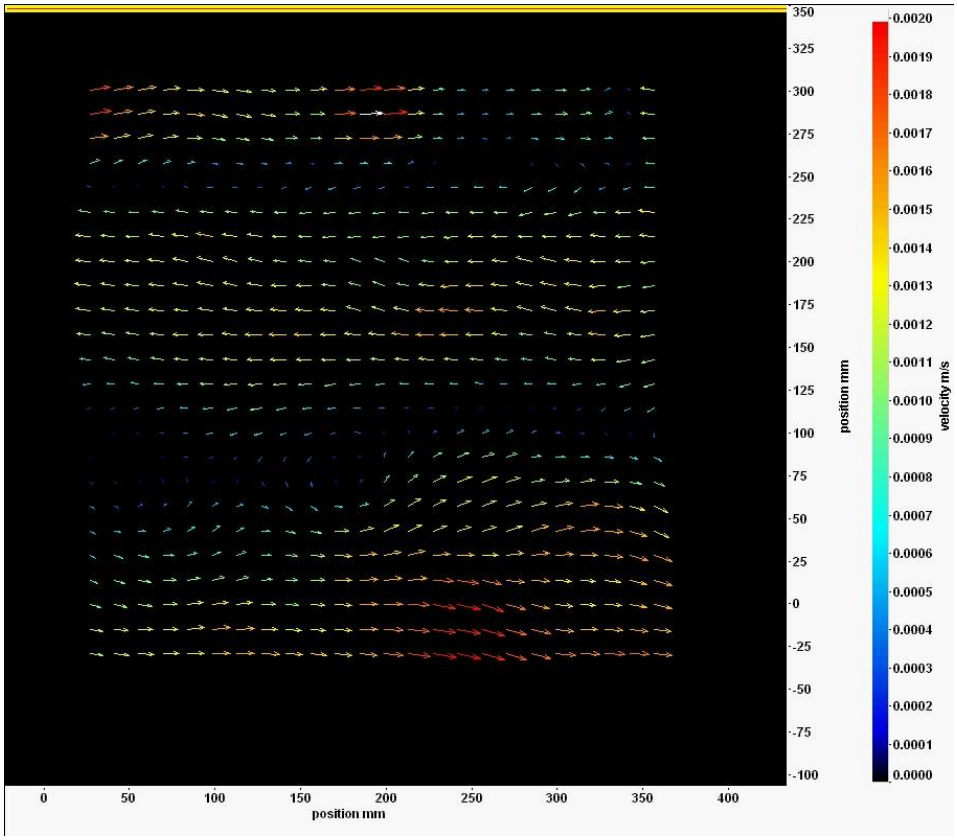

Fig (3.6h): After 19 seconds from the beginning of the movie

The main features of the Figures (3.6a-h) are: the flow structure, flow direction and the position of the dark regions did not change significantly. This indicates that flow-flow interaction (the interaction between the flow layers at different depths from the surface) is insignificant when the wind speed is in the order of 1.07 $ms^{-1.}$ or less.

On the other hand, the existence of *calm regions* on the water surface, which are characterized by low drift speed, immediately prior to the visible waves have been noted by Plate et al (1969) and Caulliez et al (1998). These two studies were conducted at a range of low wind speeds under lab conditions. The existence of *calm regions* on the water surface indicates a transforming of the surface from undisturbed to disturbed. In the flow field, the existence of dark regions may indicate transformation of the flow direction and therefore eddy generation. Another interpretation of the existence of dark regions 'at this speed' may be that there is a conversion of the tracer's movement from oscillatory motion around a reference point to translational motion. This interpretation was inferred from observing the relationship between the velocity vector angle and wind speed as shown in Chapter 4.

Existence of calm regions in the both cases of water surface and bulk flow indicates a significant change in the flow and surface state.

At a wind speed of 1.92 ms^{-1}, stronger eddies appear at different depths from the surface. Movie sequences at this speed show that the increase of the flow velocity expands to the entire flow field and the direction of the flow is controlled by the direction of the largest eddy where the velocity vectors switch around the centre of the eddies . Figure (3.7) shows the average of the velocity field at wind speed of 1.92 ms^{-1}. However, Figures (3.7a-h) show the velocity field images captured from the 19 second movie at equal intervals in between. The flow-flow interaction increased as the wind speed increased and the flow direction at a particular zone changed continuously. The distribution of the eddy centres indicates that the effects of wind induced shear and flow-flow interaction are distributed to the entire flow.

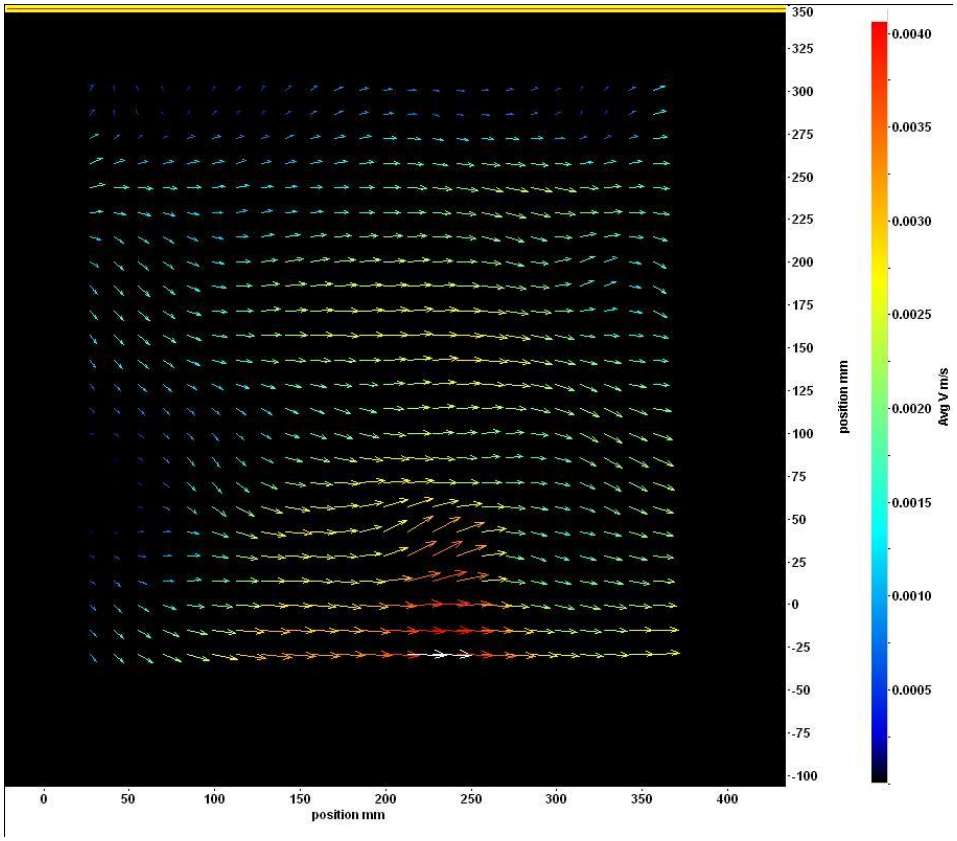

Fig (3.7): Average velocity field at wind speed of the order 1.92 ms^{-1}

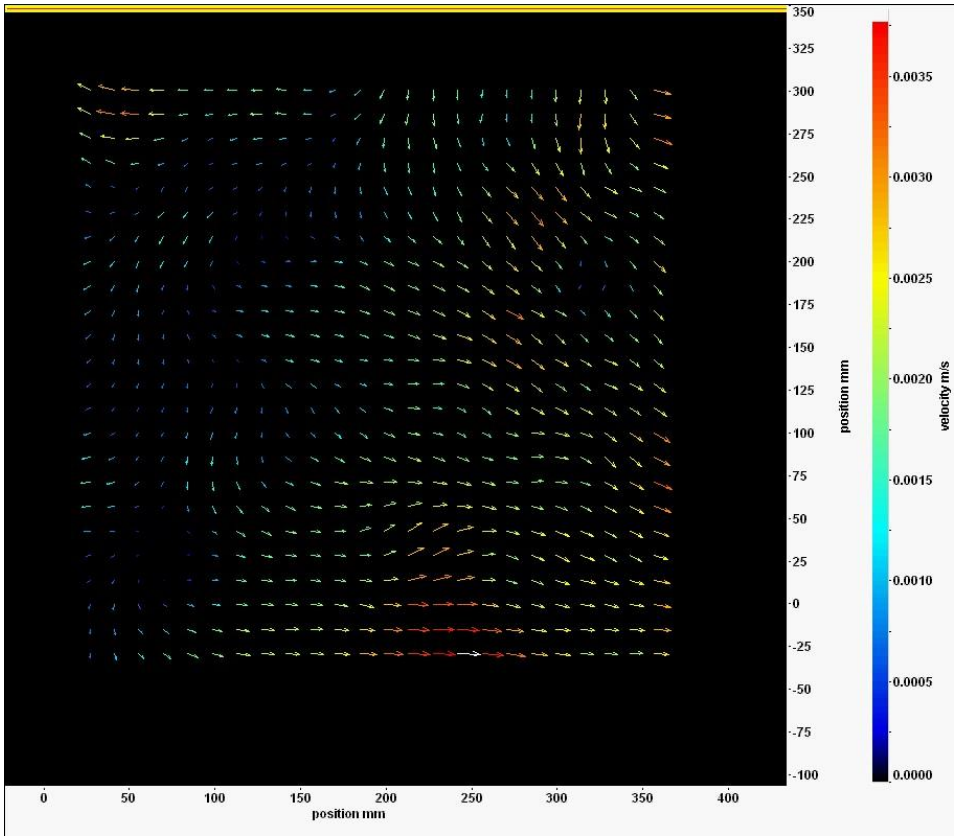

Figure (3.7a): After zero seconds from the beginning of the movie

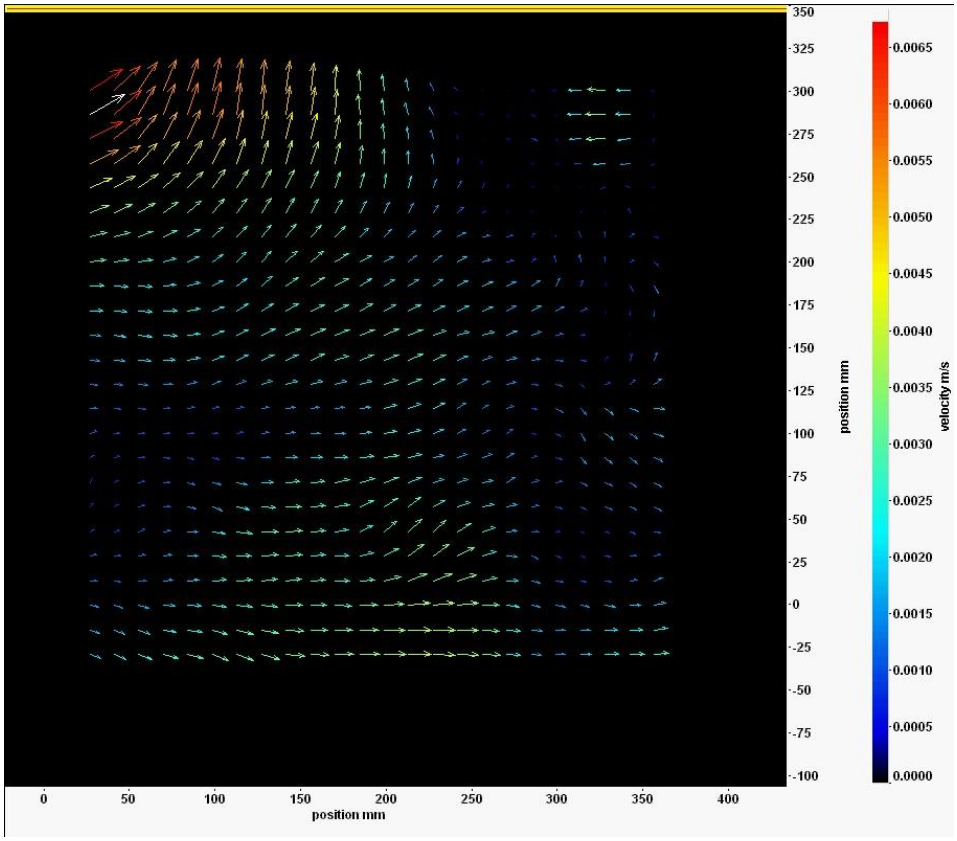

Figure (3.7b): After 2.71 seconds from the beginning of the movie

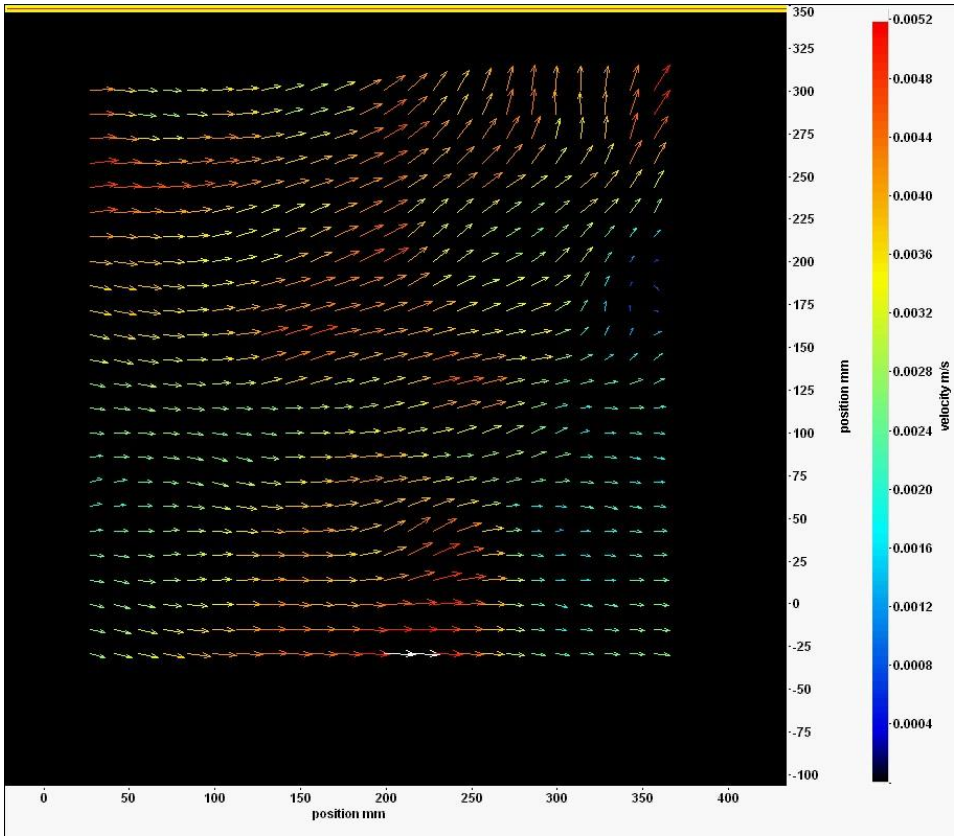

Figure (3.7c): After 5.42 seconds from the beginning of the movie

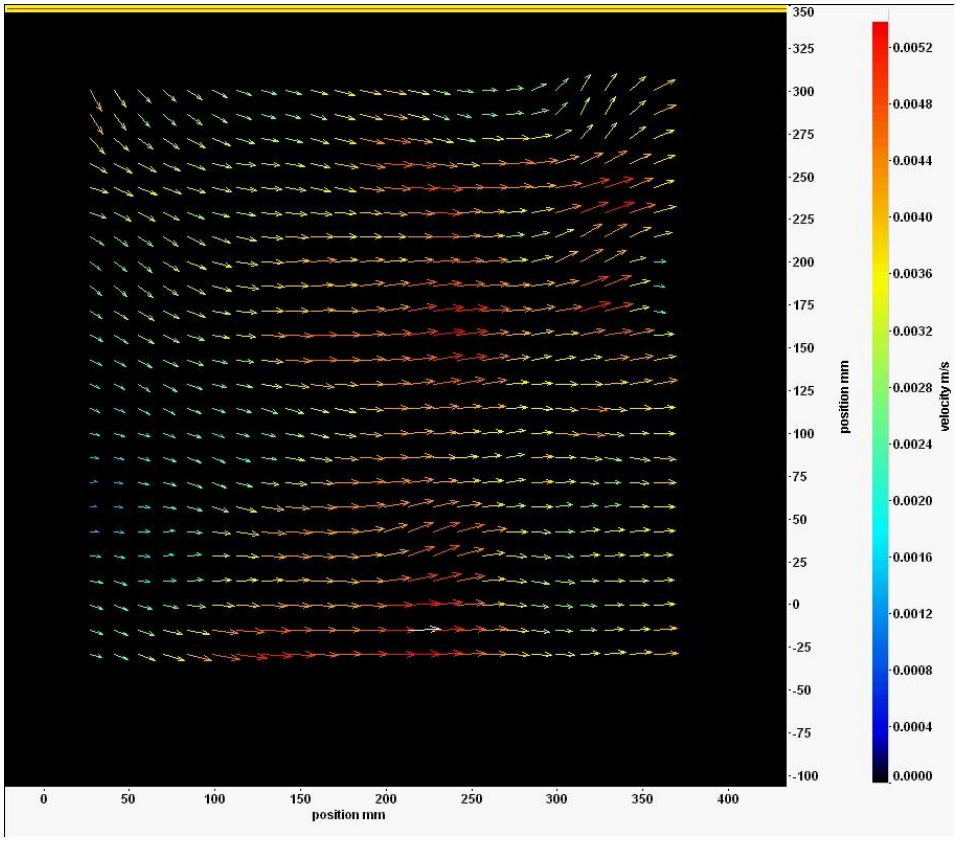

Figure (3.7d): After 8.14 seconds from the beginning of the movie

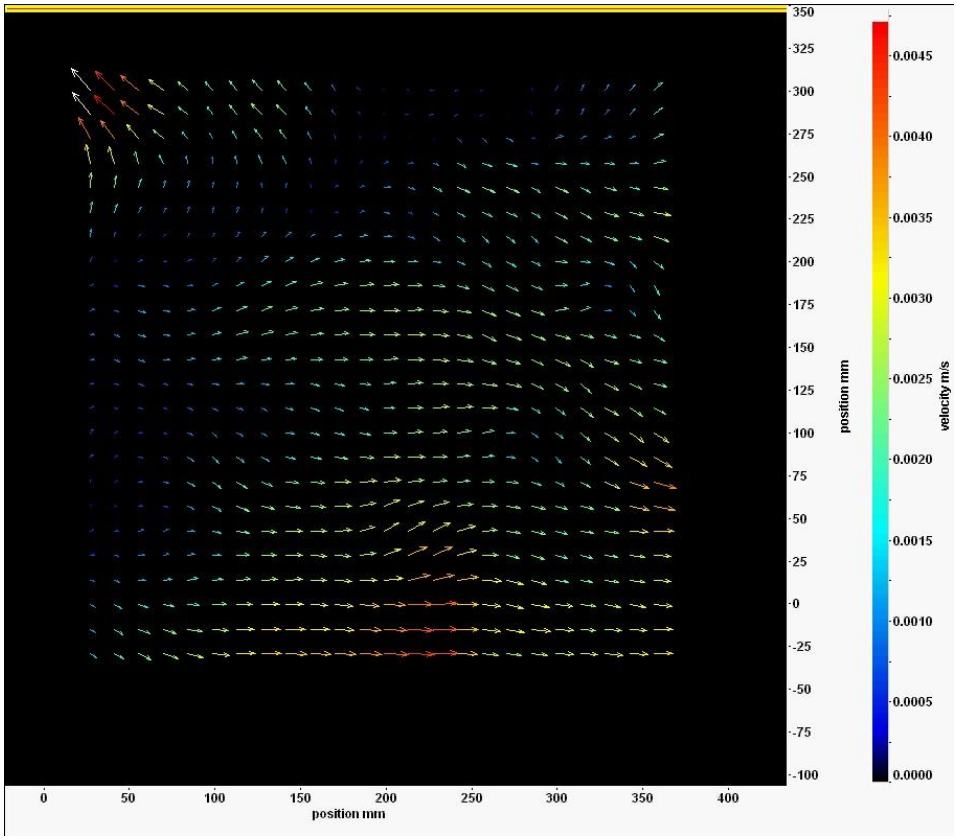

Figure (3.7e): After 10.85 seconds from the beginning of the movie

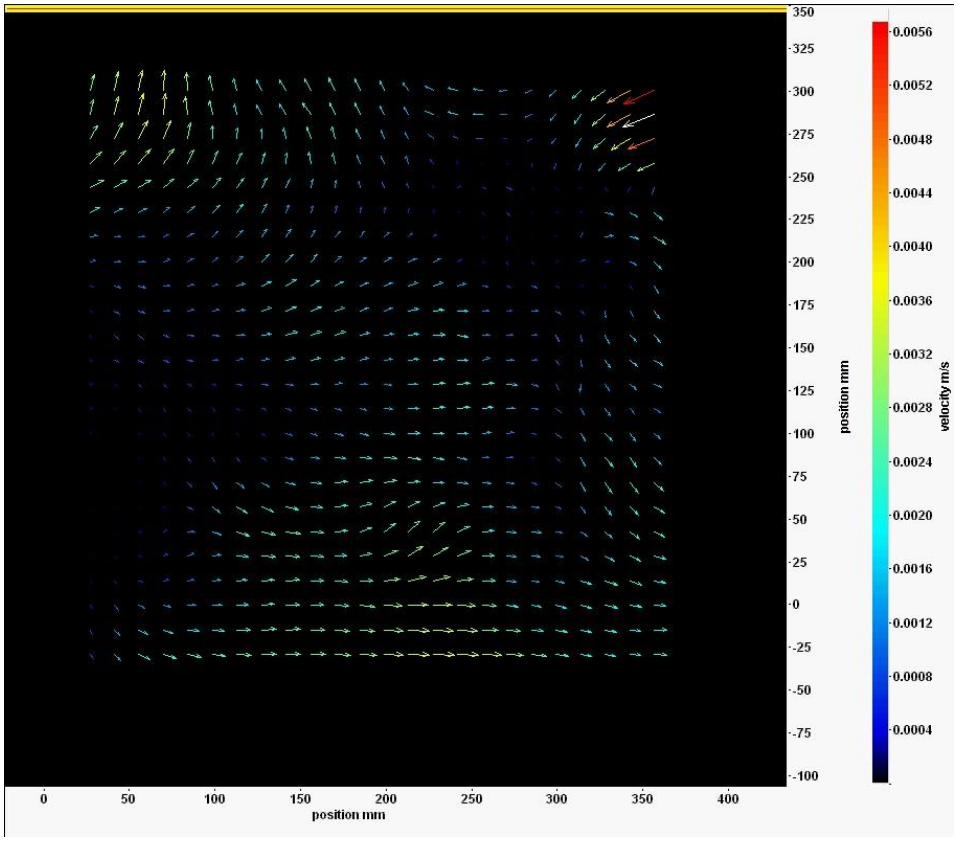

Figure (3.7f): After 13.57 seconds from the beginning of the movie

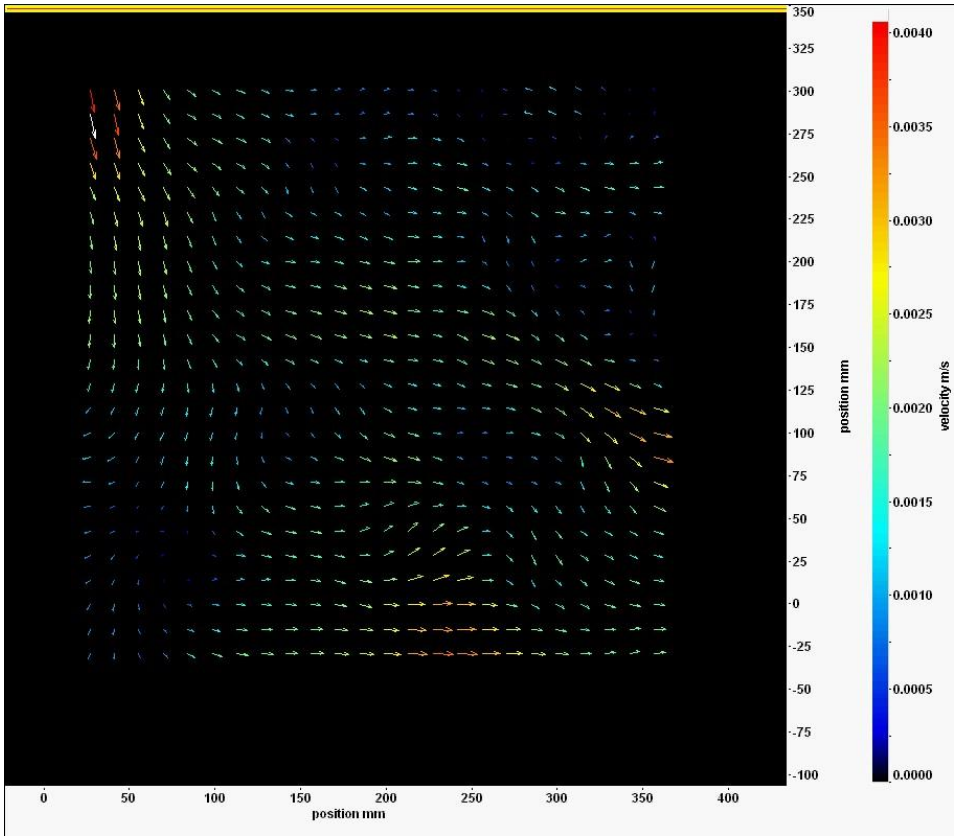

Figure (3.7g): After 16.83 seconds from the beginning of the movie

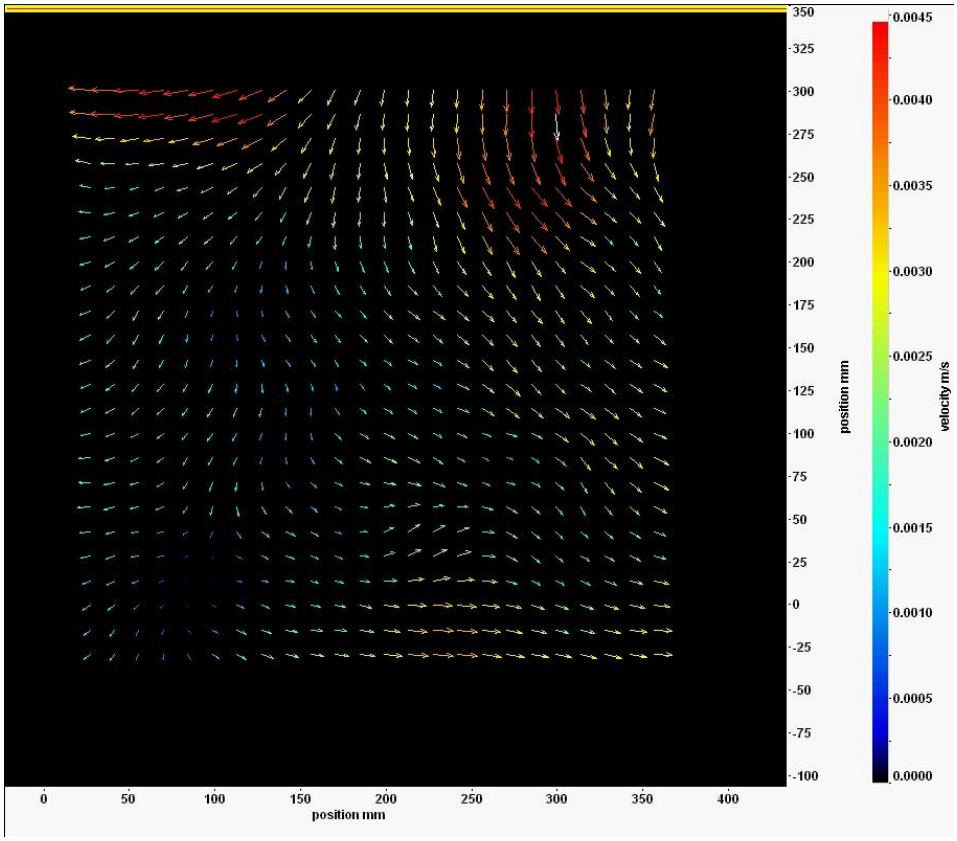

Figure (3.7h): After 19 seconds from the beginning of the movie

At a speed of the order 2.73 ms^{-1}, the surface waves started to be visible to the naked eye. The onset of the visible waves were observed by Ataktürk and Katsaros (1999) at Lake Washington at a wind speed of the order 3 ms^{-1}, Kahma and Donelan (1989) 3.1 ms^{-1} Keulegan (1951) 3.3 ms^{-1}; Kunishi (1957) 2.4 ms^{-1} under laboratory conditions. Other studies have shown less than these magnitudes, as shown in section 1.8. The relationship between the wind speed and evolution of the bulk flow is obvious. When the wind speed reaches the magnitude of the order2.73 ms^{-1} the flow becomes turbulent and Reynolds number attains a higher value as shown in table (3.2). The Reynolds number was defined in equation 3.1. The relationship between the evolution of vortices' size and speed, entire flow velocity and surface wave generation can be observed. The generation of the surface wave at this speed emphasizes the importance of the dynamics and kinematics of the water flow on the generation and growth of the surface waves. Figure (3.8) shows the average velocity field at a wind speed of 2.73 ms^{-1}. Figures (3.8a-h) Figures show the velocity field images captured from the 19 second movie at equal intervals in between.

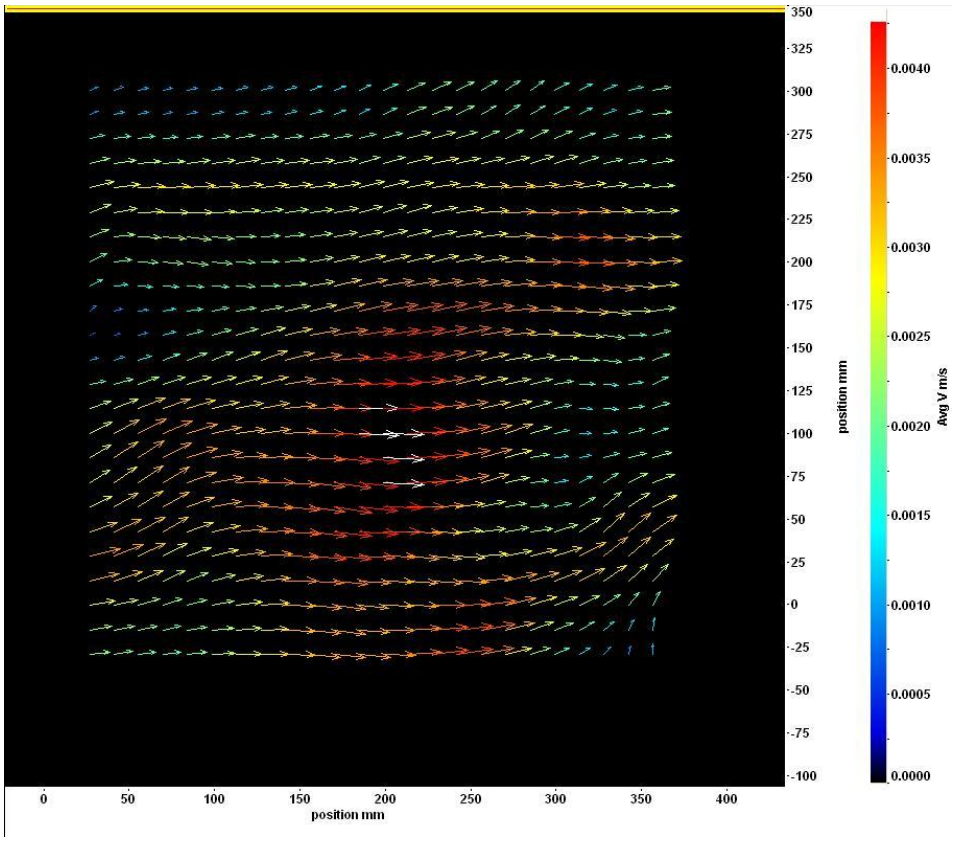

Fig (3.8): Average velocity field at wind speed of the order 2.73 ms^{-1}

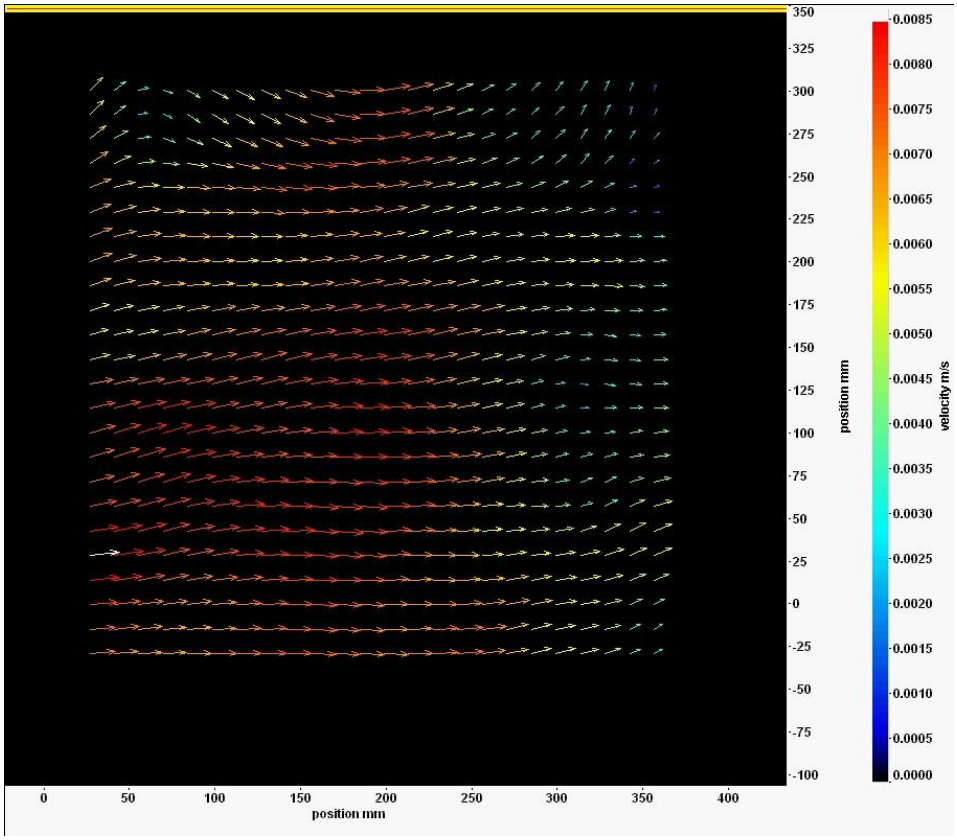

Figure (3.7a): After 0 seconds from the beginning of the movie

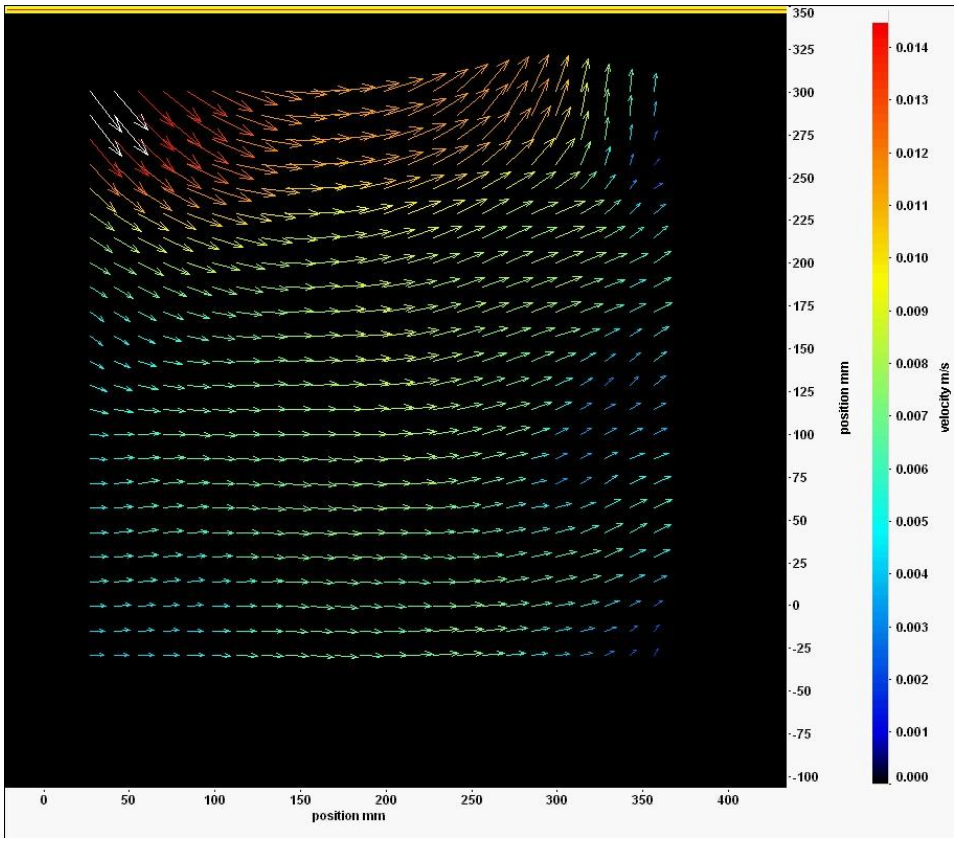

Figure (3.7b): After 2.71 seconds from the beginning of the movie

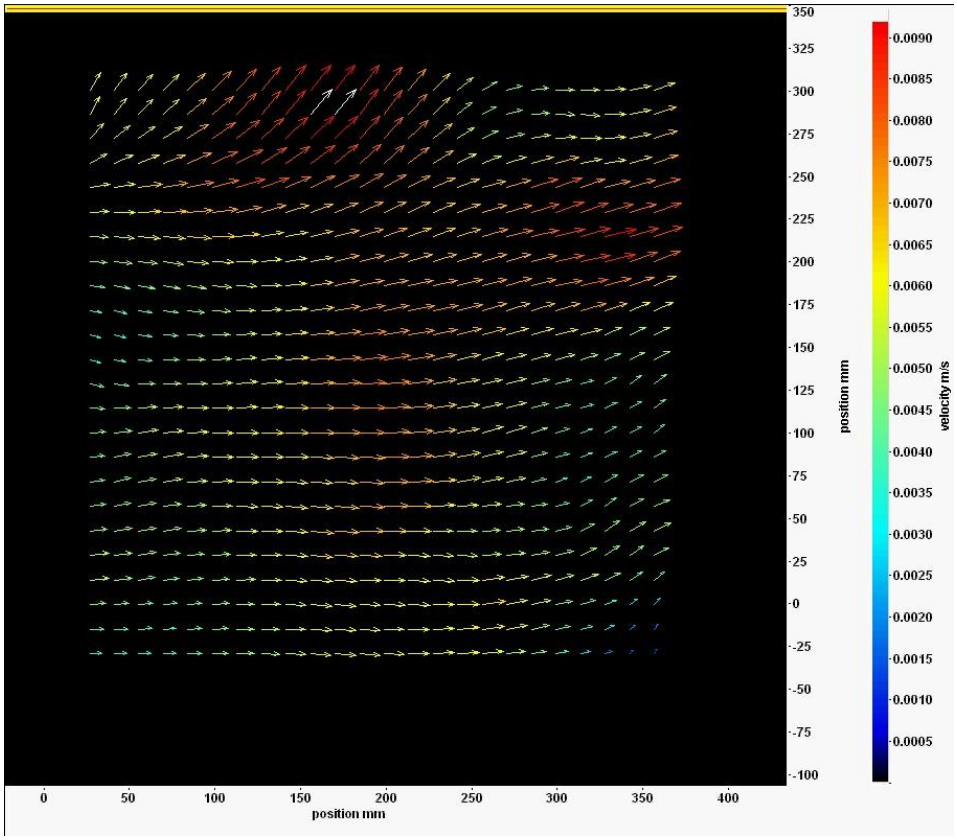

Figure (3.7c): After 5.42 seconds from the beginning of the movie

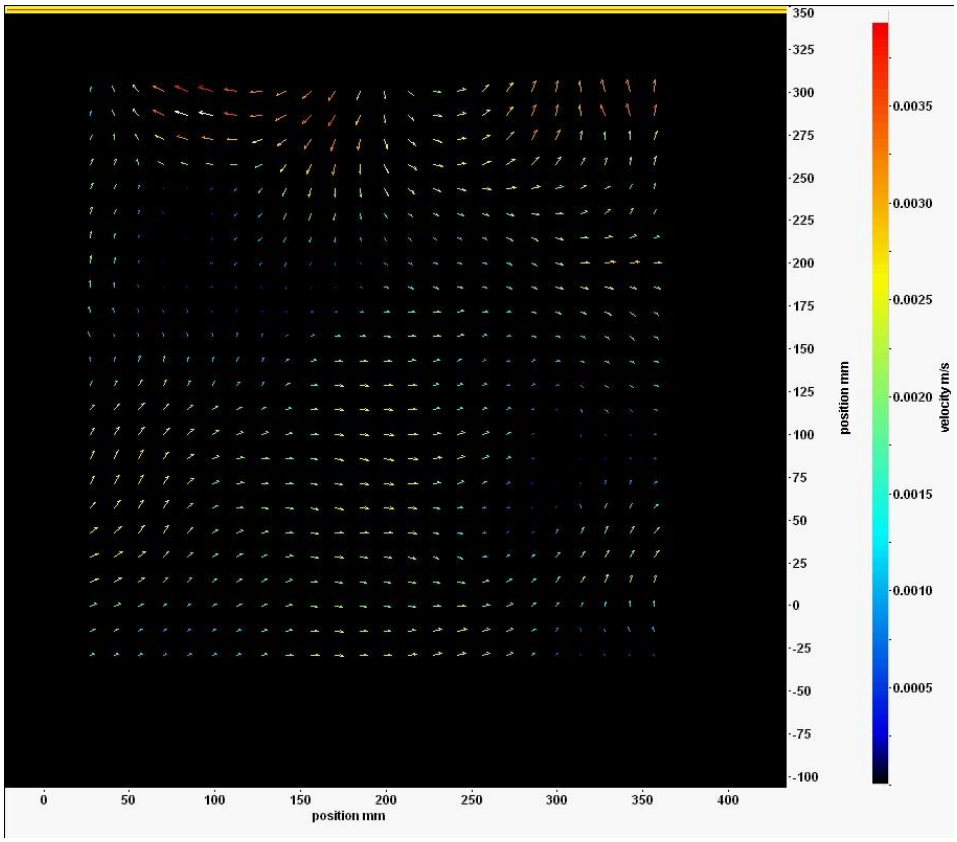

Figure (3.7d): After 8.14 seconds from the beginning of the movie

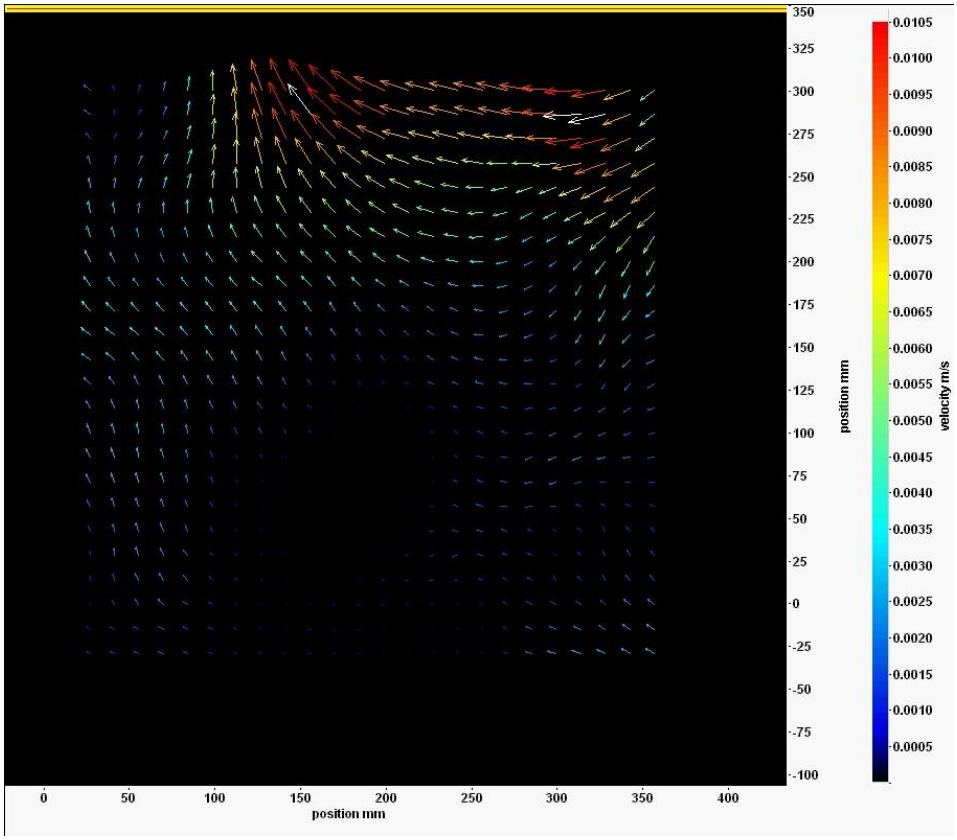

Figure (3.7e): After 10.85 seconds from the beginning of the movie

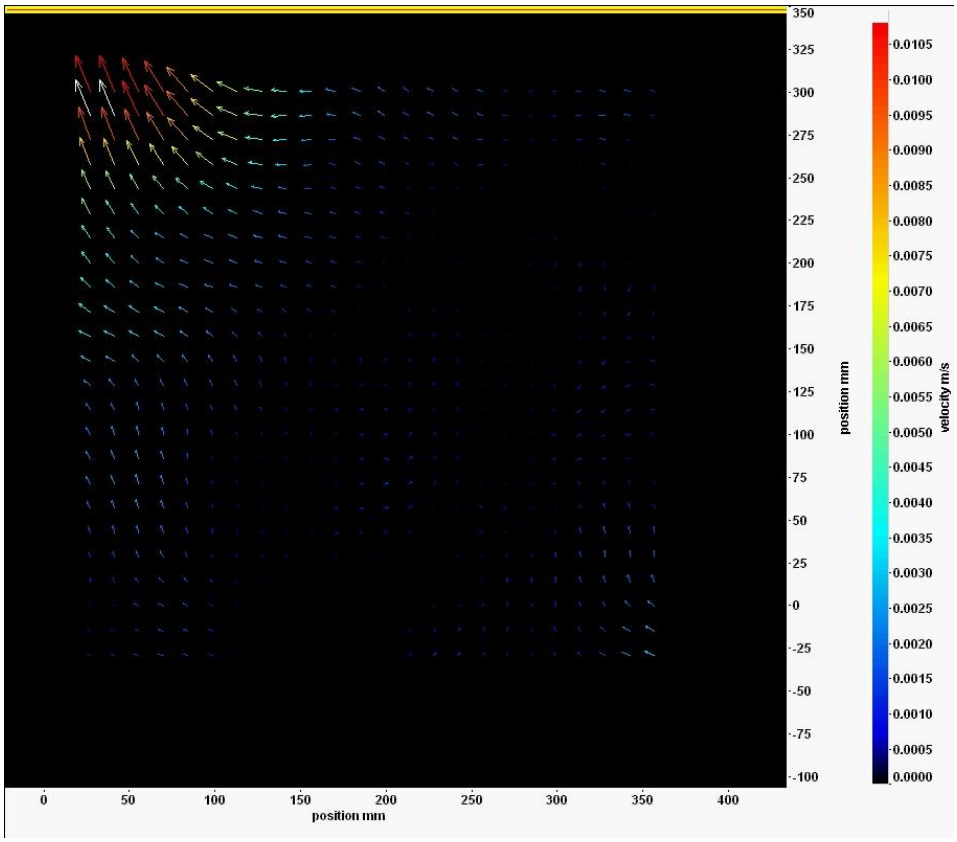

Figure (3.7f): After 13.57 seconds from the beginning of the movie

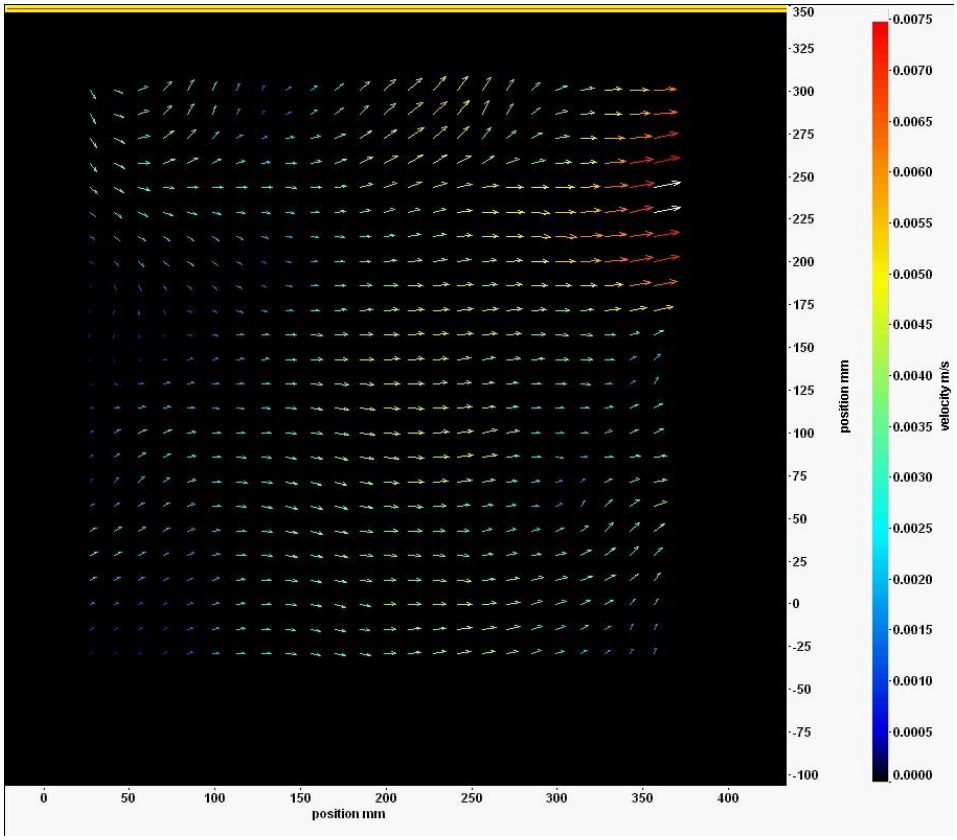

Figure (3.8g): After 16.22 seconds from the beginning of the movie

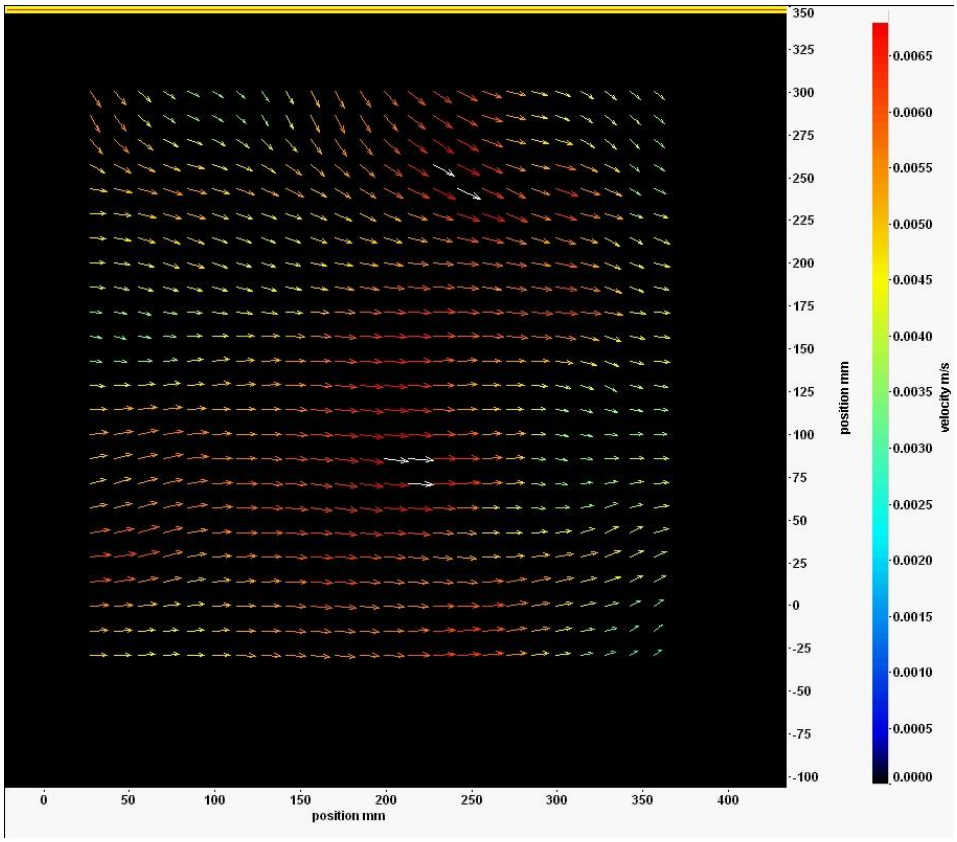

Figure (3.8h): After 19 seconds from the beginning of the movie

The appearance of the dark regions prior the transformation of the flow direction is very clear in the above figures particularly in Figures (3.8e-g). This action causes a significant increase in the density of the flow perturbations and therefore the wave growth rate. The flow regime can be predicted as a turbulent flow in such cases through tracing the movie sequence of bulk evolution rather than calculating Reynolds number; the flow–flow interaction becomes significant. Also the fluctuation of the flow near the surface that support the wave generation is observed through the movie sequence.

As the wind speed attains the order of 3.6 ms^{-1}, the size of the eddies increase, but their number decreases as shown in the movie sequence. Figure (3.9) shows that, the small eddies merges into large ones. At the same time an increase in surface wave amplitude and speed can be observed. The movie sequence shows that most of the eddy motion is directed towards the surface which causes additional evolution in wave growth. The Reynolds number rises to 2428 at the current wind speed. It is assumed that the waves attain energy from the wind flow and from eddies that propagate towards the surface; in the absence of one of these sources, the waves become weak and tend to attenuate. This may explain the increase of the attenuation rate of the waves that are generated in a particular way on a soapy water surface in Keulegan's (1951) investigations as shown in Chapter 1. It is assumed that the detergent solution in a particular mechanism affected the wind momentum flux. Therefore, the induced perturbation was reduced and the eddies evolution ceased. In such a case the waves have lost a main source of energy to survive. The same justification is assumed for the significant increase in critical wind speed for contaminated surfaces. Figure (3.9) shows the average velocity field at a wind speed of 3.6 ms^{-1}. Figures (3.9a-h) show the velocity field images captured from the 19 second movie at equal intervals in between.

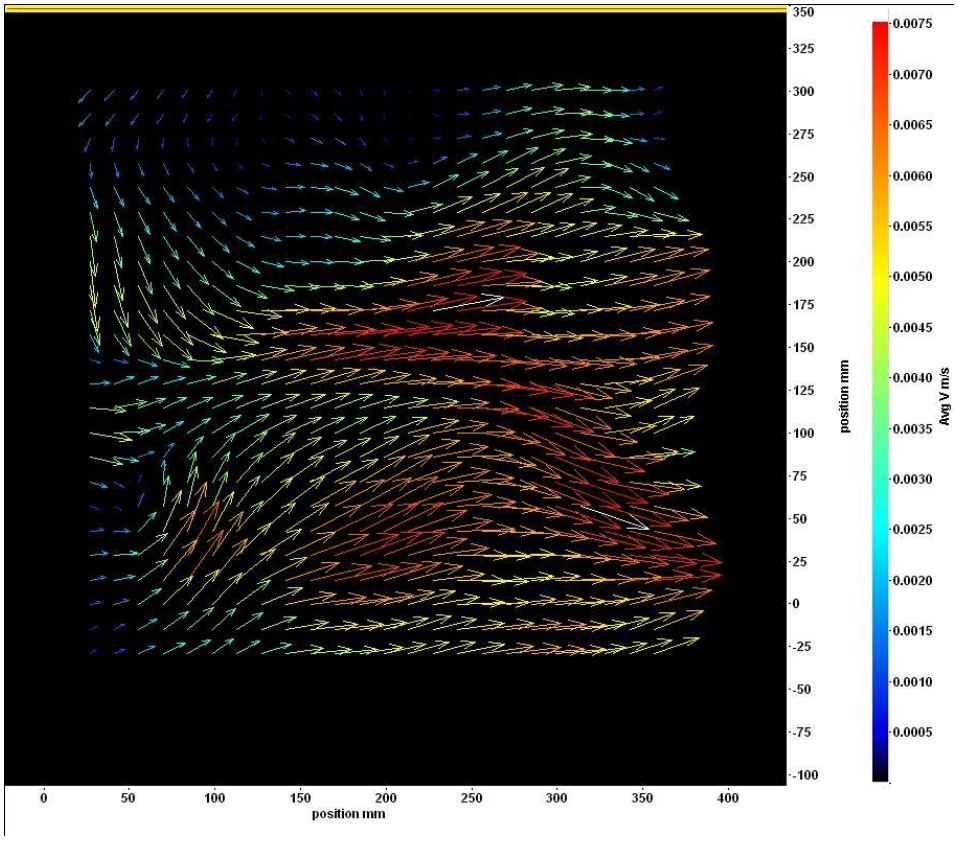

Figure (3.9): Average velocity field at wind speed of the order 3.6 ms^{-1}

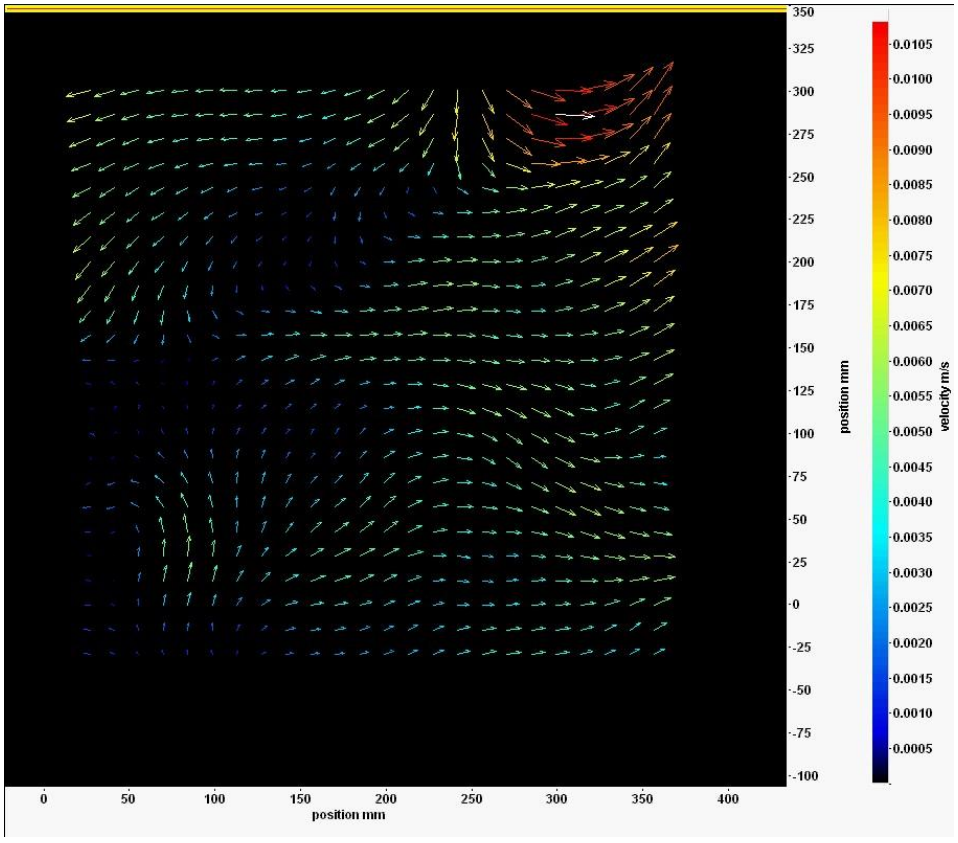

Figure (3.9a): After zero second from the beginning of the movie

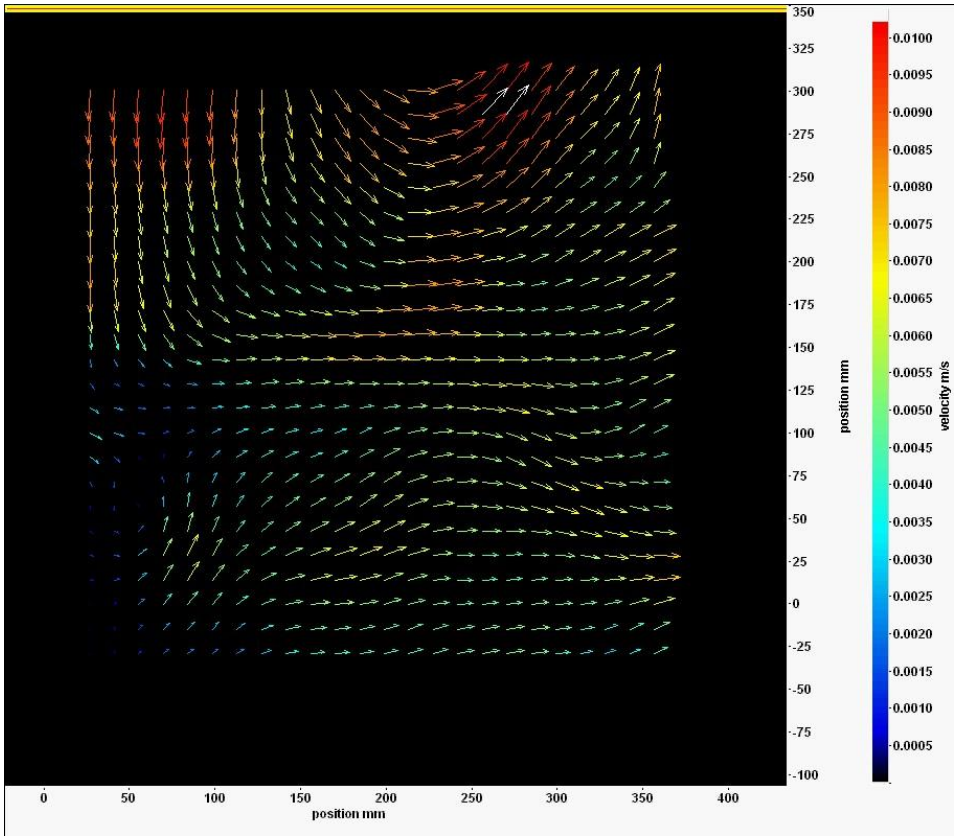

Figure (3.9b): After 2.71 seconds from the beginning of the movie

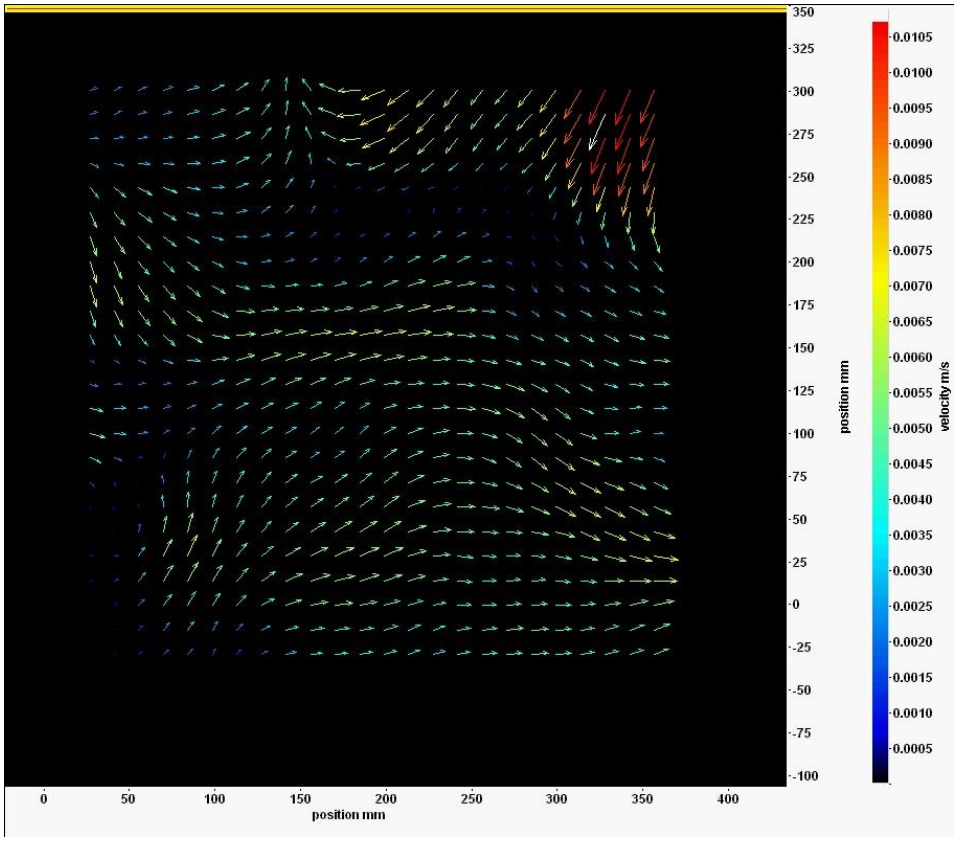

Figure (3.9c): After 5.42 seconds from the beginning of the movie

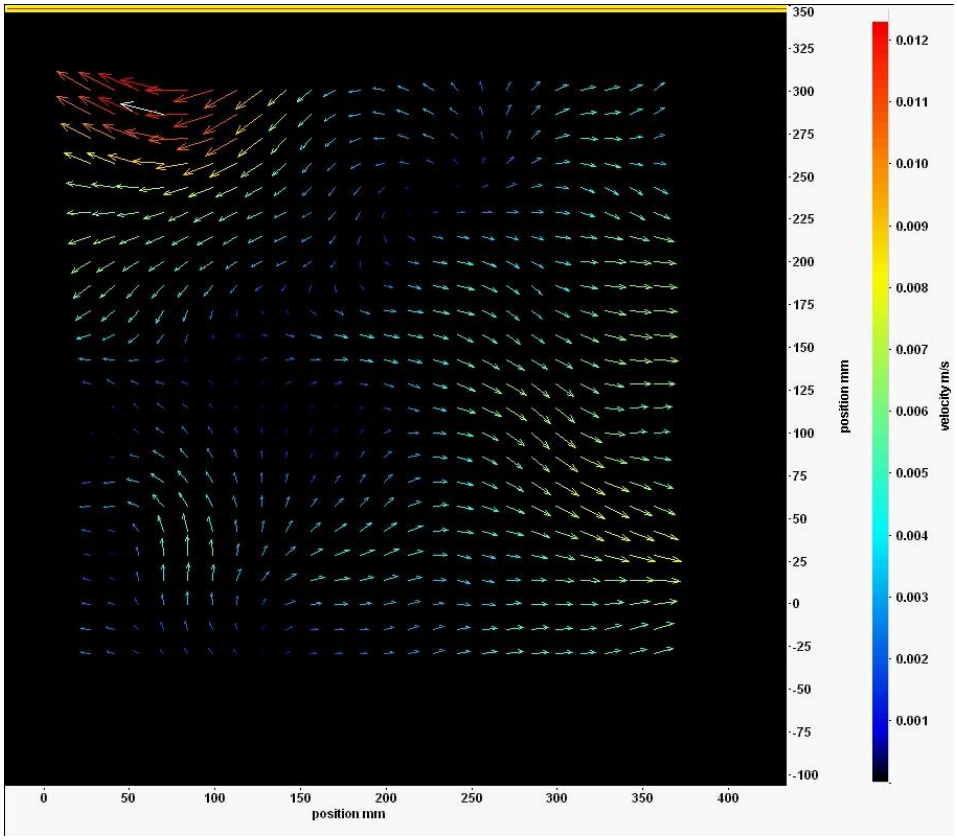

Figure (3.9d): After 8.14 seconds from the beginning of the movie

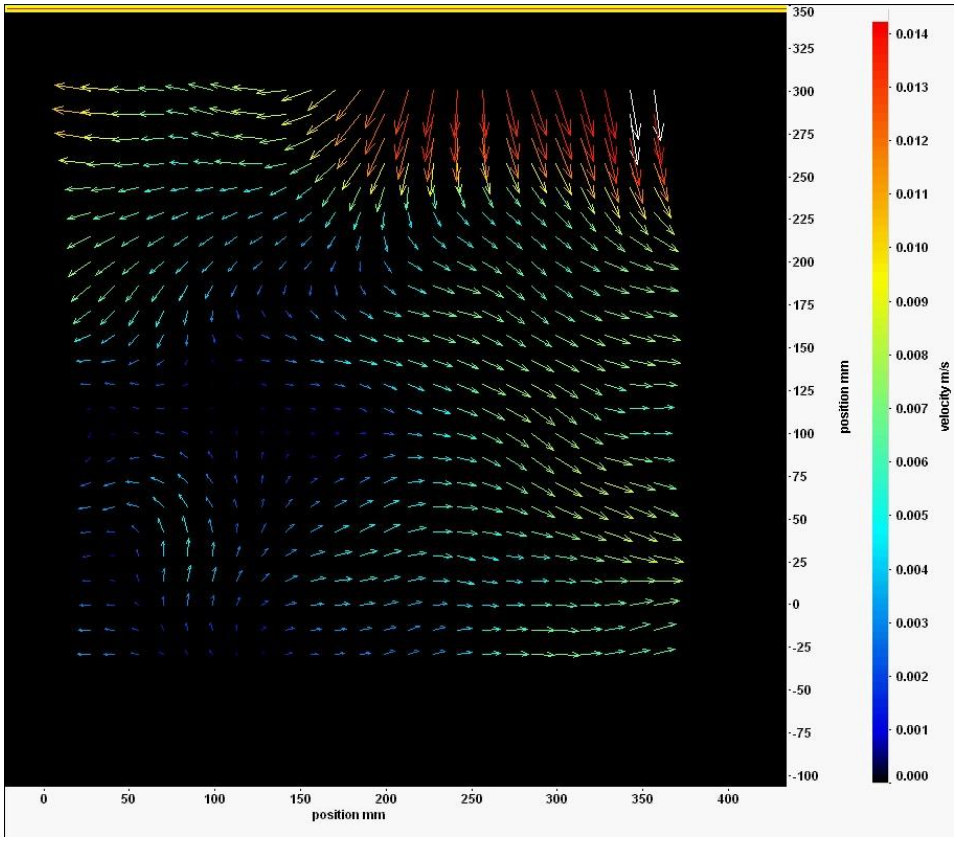

Figure (3.9e): After 10.85 seconds from the beginning of the movie

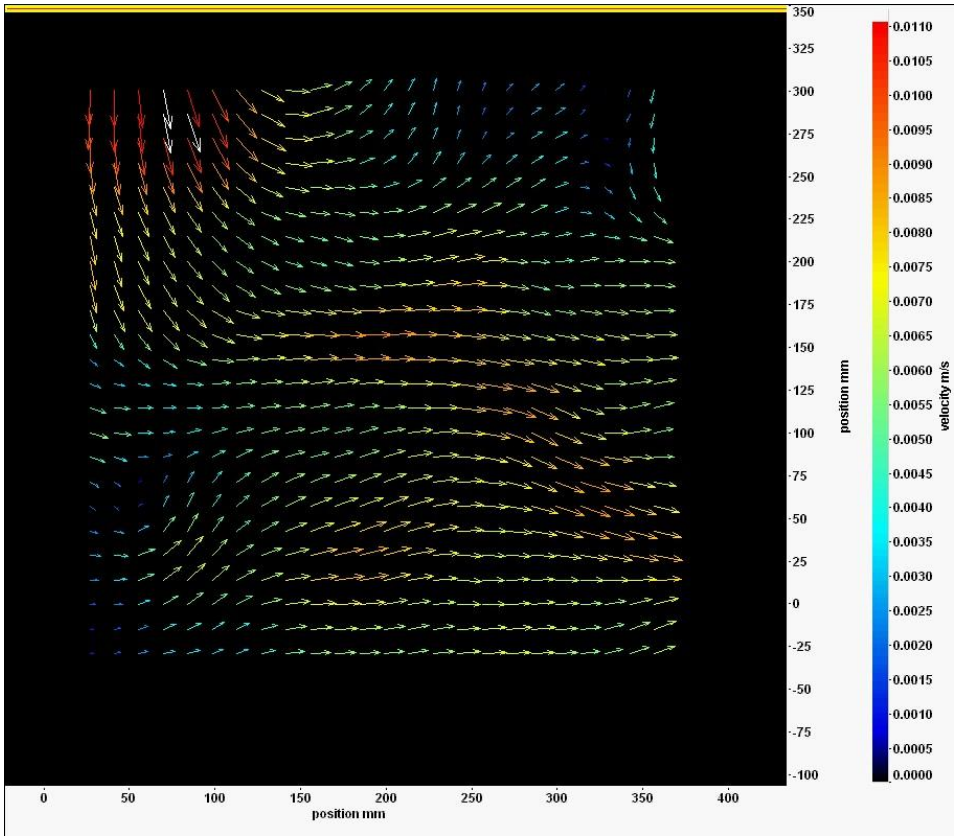

Figure (3.9f): After 13.57 seconds from the beginning of the movie

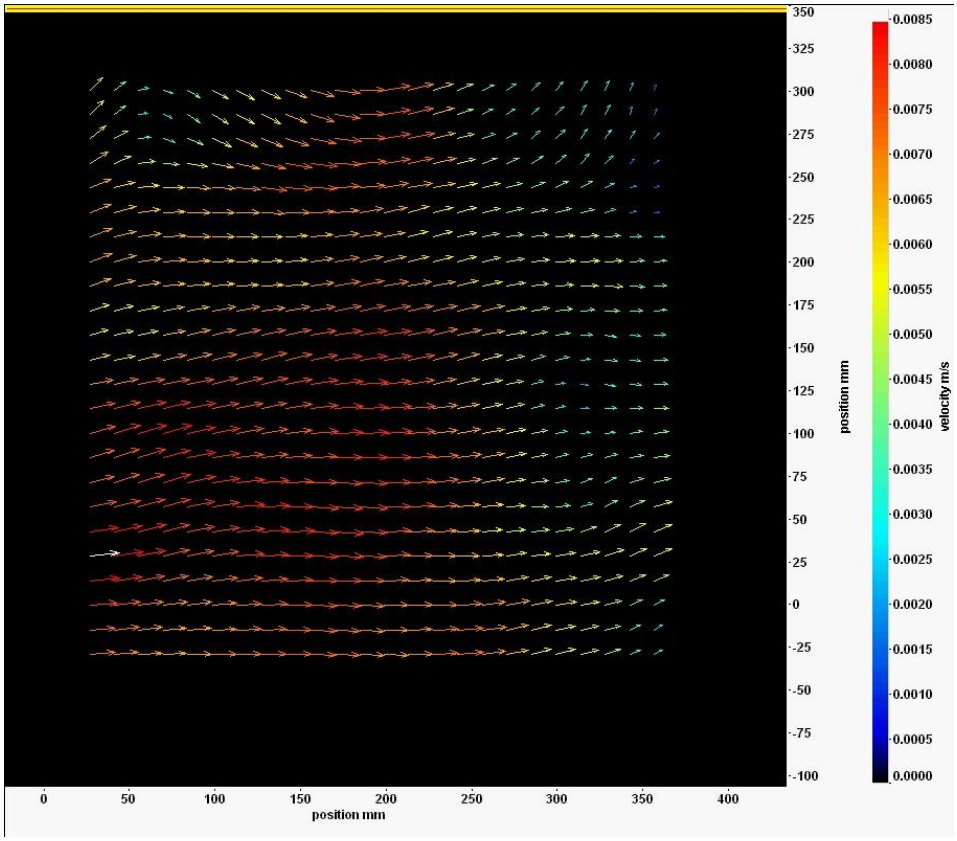

Figure (3.9g): After 16.28 seconds from the beginning of the movie

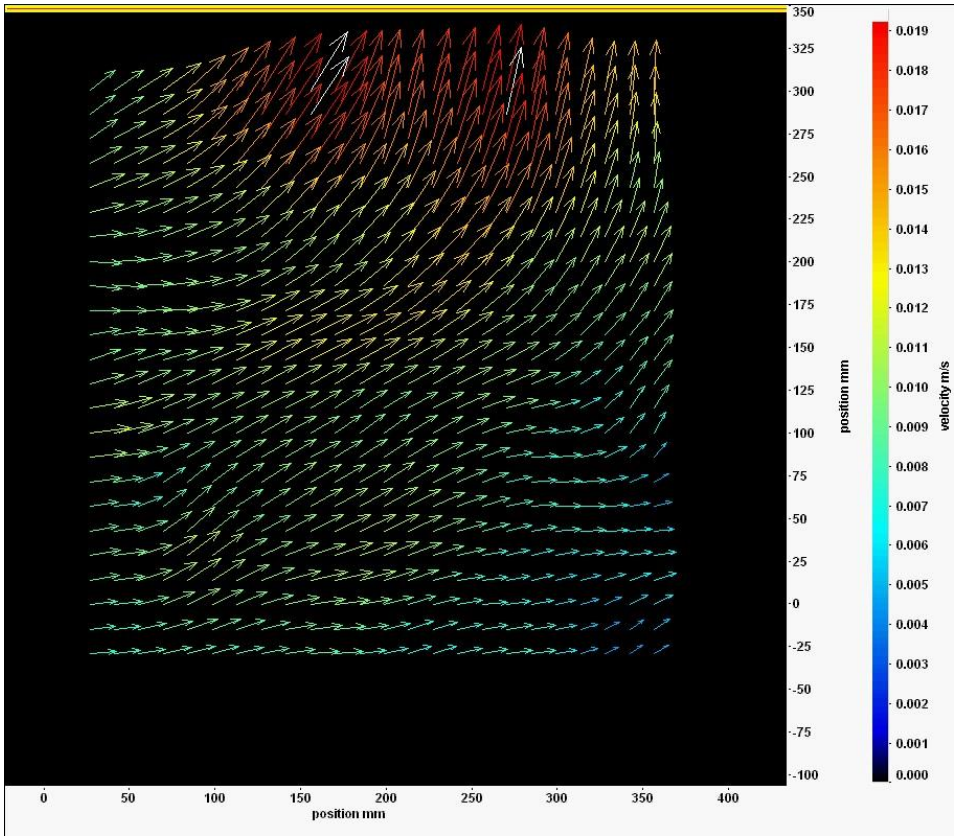

Figure (3.9h): After 19 seconds from the beginning of the movie

At a wind speed of the order 4.5 ms^{-1}, a notable and visible augmentation in wave velocity and amplitude can be seen. The waves become appreciable from the upstream leading edge of the channel and propagate in the wind's direction. In the flow side there is a significant increase in the flow velocity and in the flow turbulence near the surface. The flow fluctuation near the surface provides the surface waves with the energy which makes the waves growth faster under action of the wind. Also, the bulk flow becomes perpendicular to the wind direction in the upper half of the channel as observed through tracing the figures (3.10a-h). The sequence of instantaneous images below presents explains the bulk flow evolution when the wind speed attains higher magnitudes. Figure (2.10) shows the average flow velocity for the 19 second movie when the wind speed of the order 4.5 ms^{-1}.

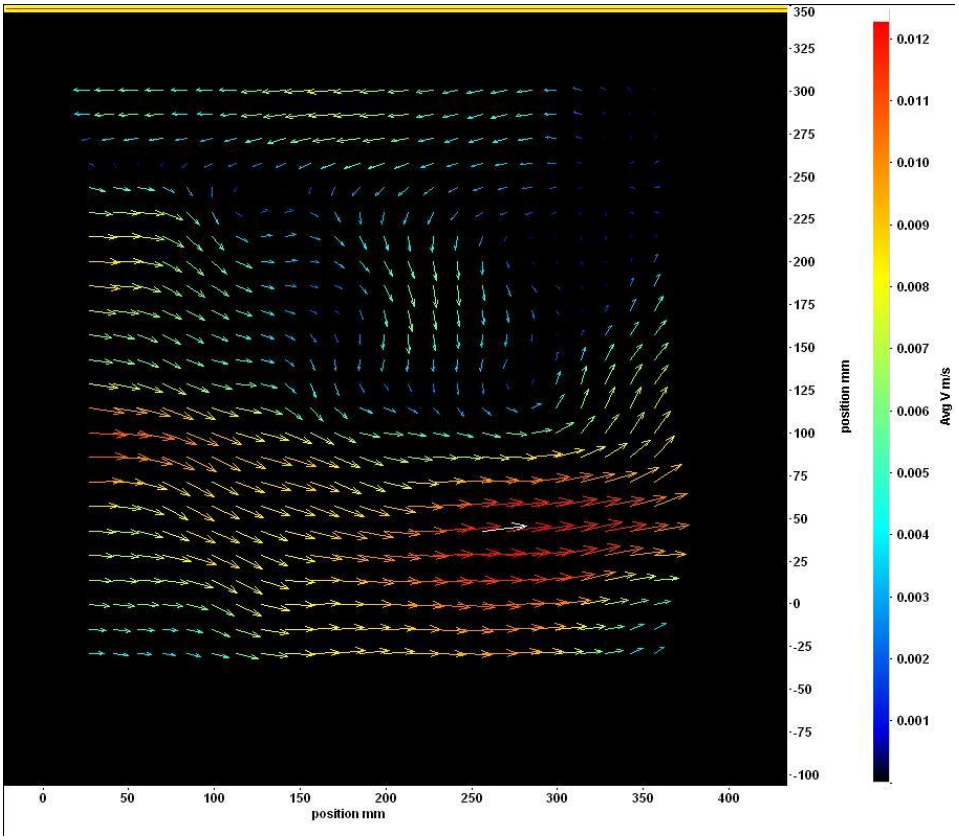

Figure (3.10): Average velocity field at wind speed of the order 4.5 ms^{-1}

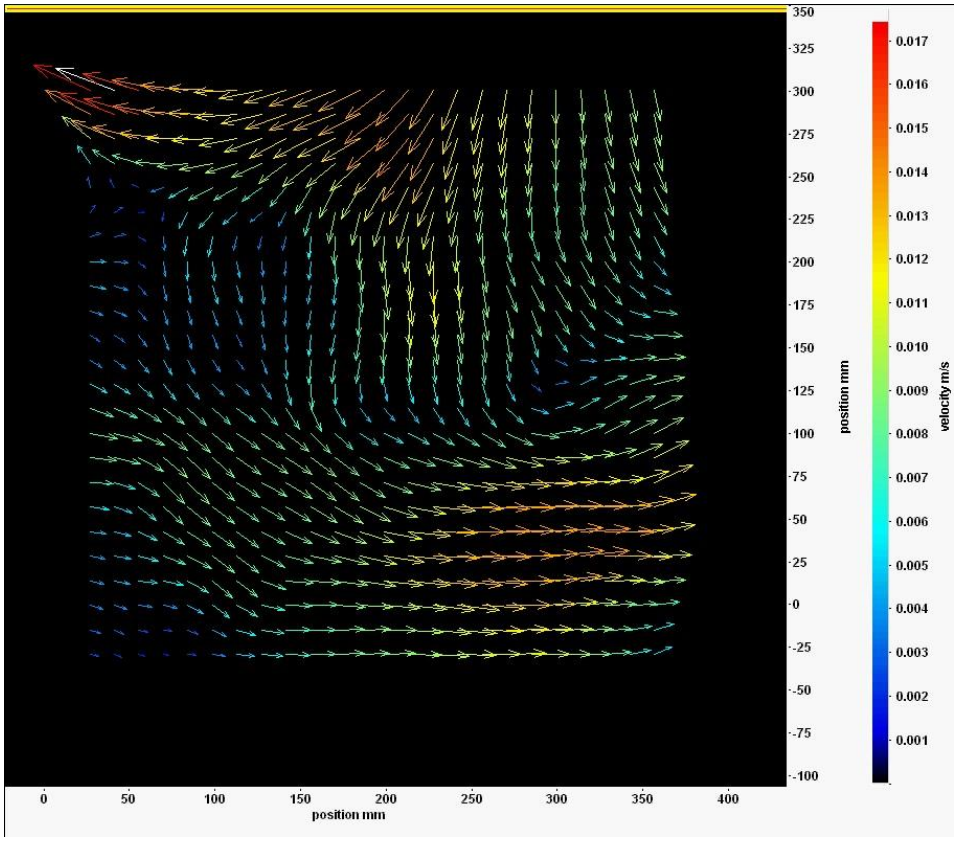

Figure (3.10a): After zero seconds from the beginning of the movie

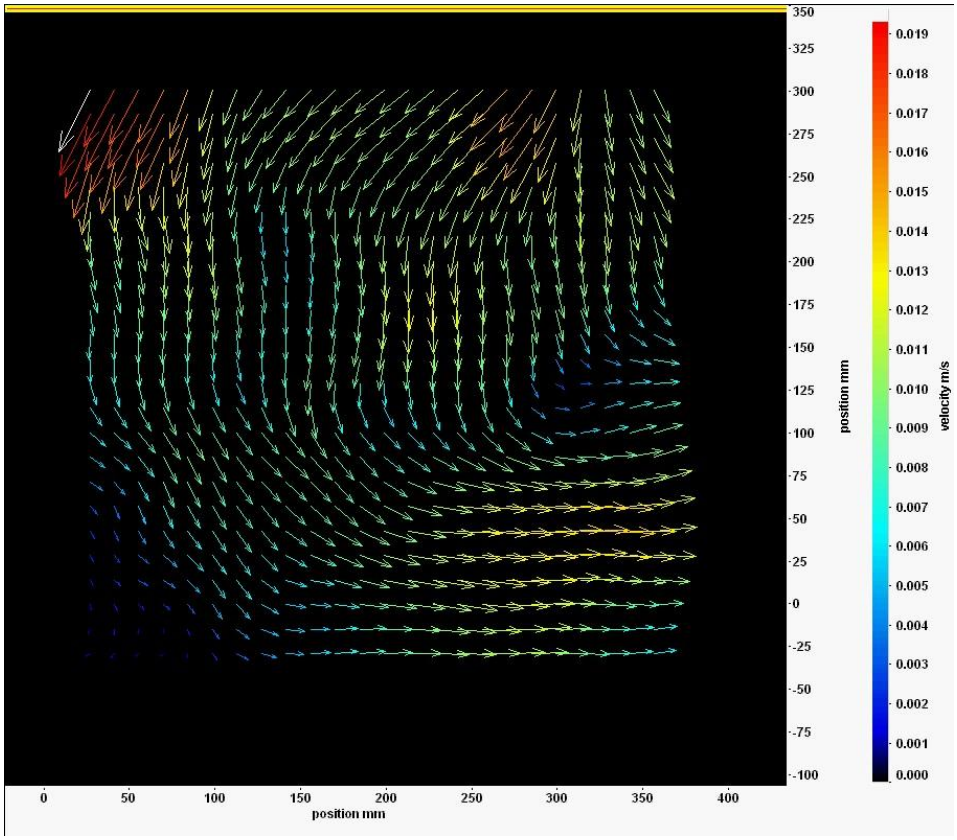

Figure (3.10b): After 2.71 seconds from the beginning of the movie

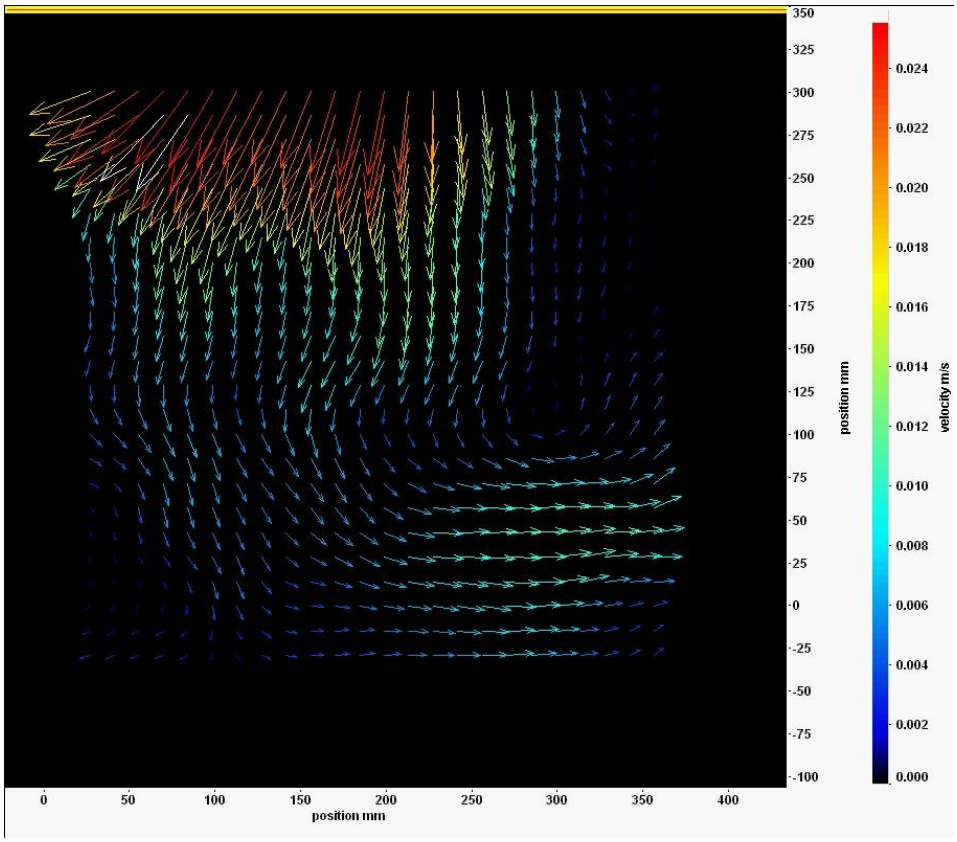

Figure (3.10c): After 5.42 seconds from the beginning of the movie

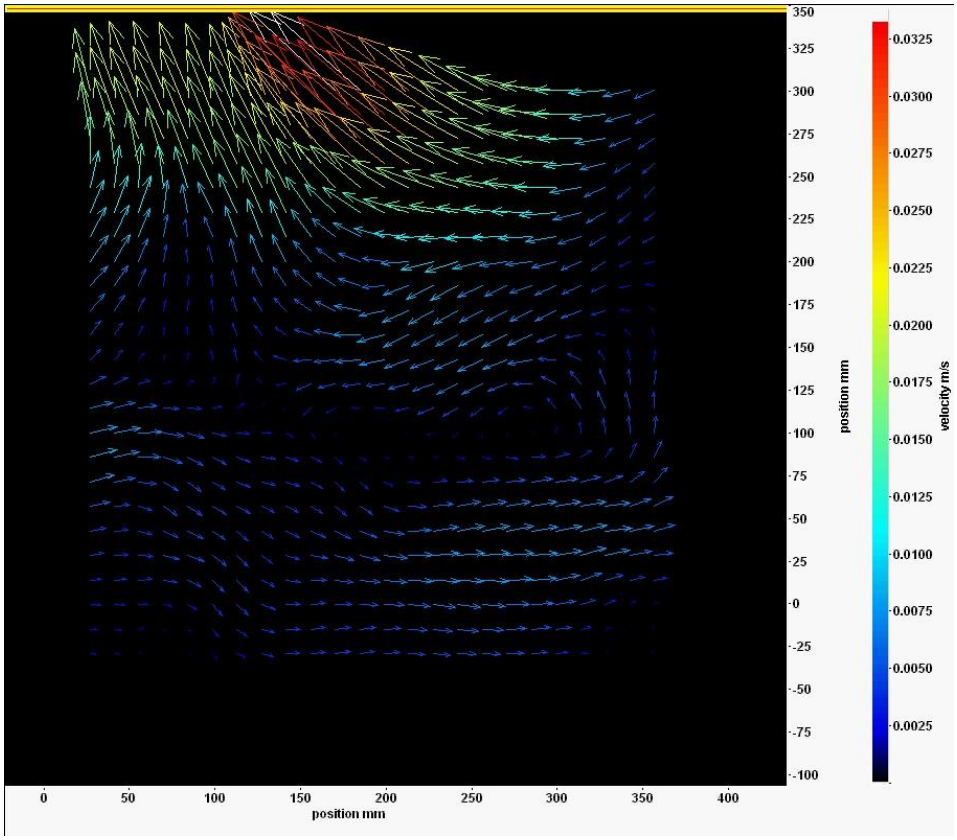

Figure (3.10d): After 8.14 seconds from the beginning of the movie

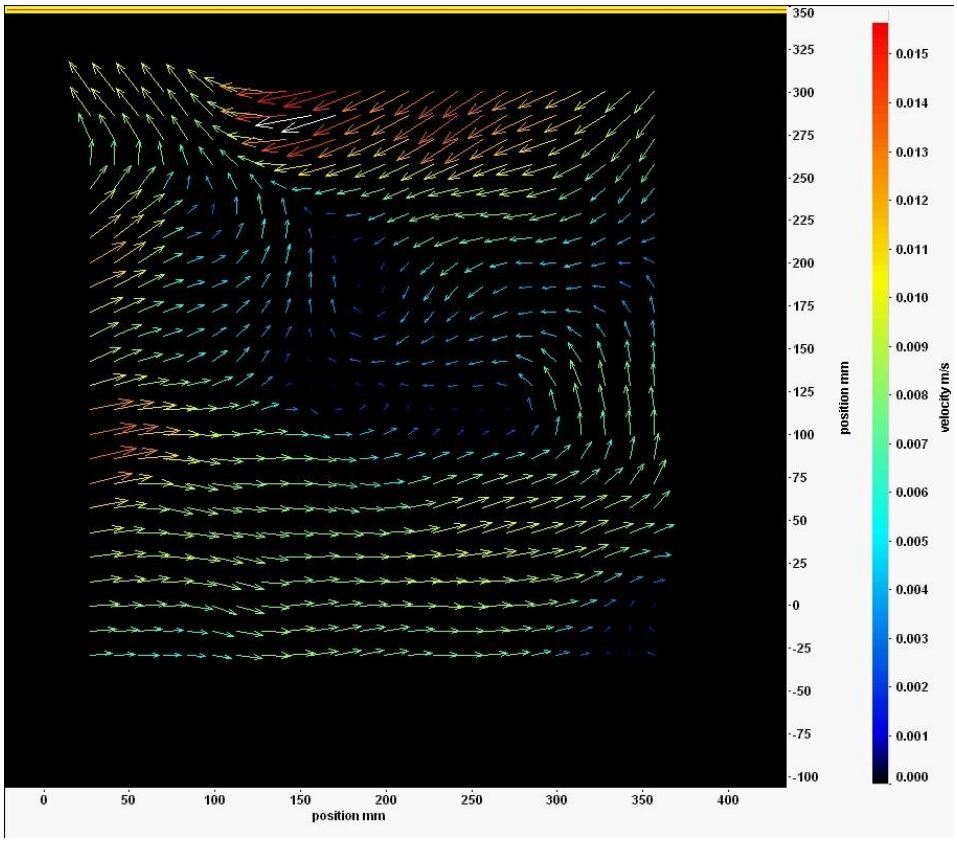

Figure (3.10e): After 10.85 seconds from the beginning of the movie

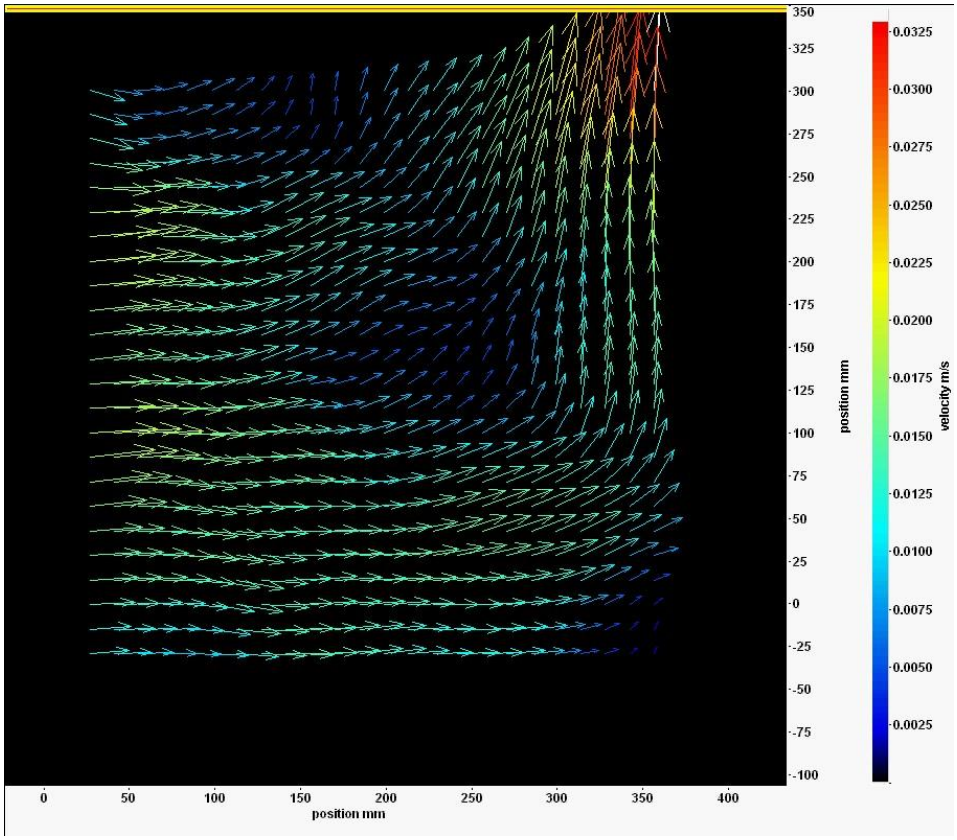

Figure (3.10f): After 13.57 seconds from the beginning of the movie

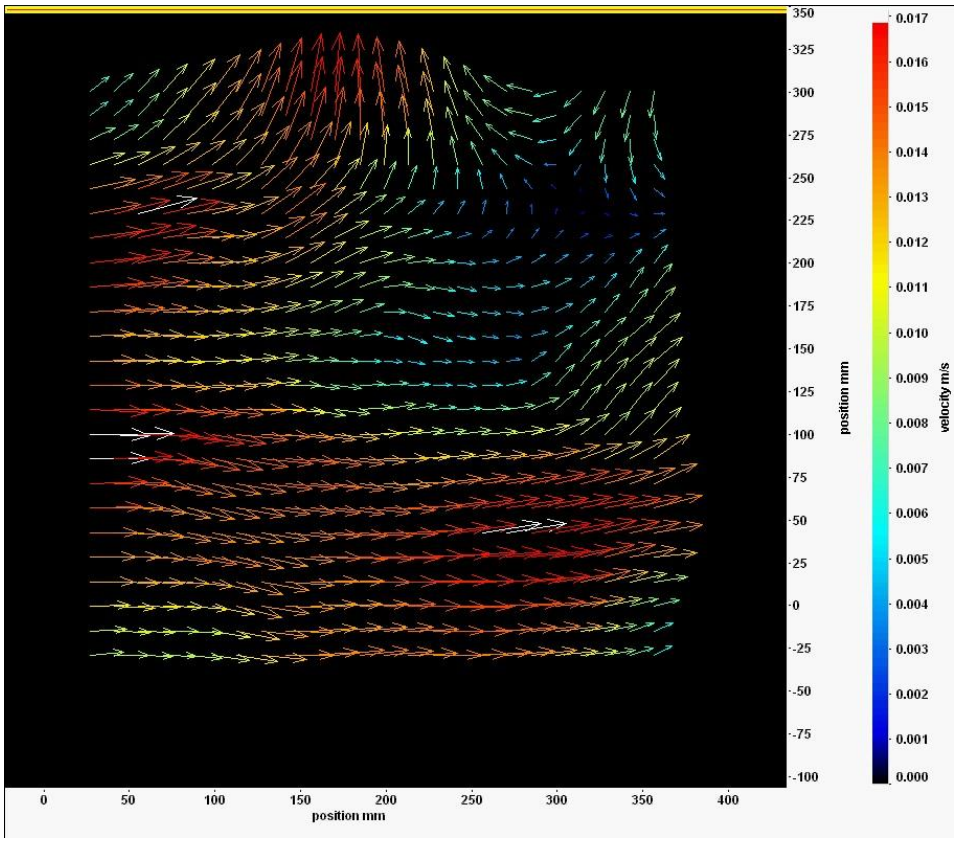

Figure (3.10g): After 16.28 seconds from the beginning of the movie

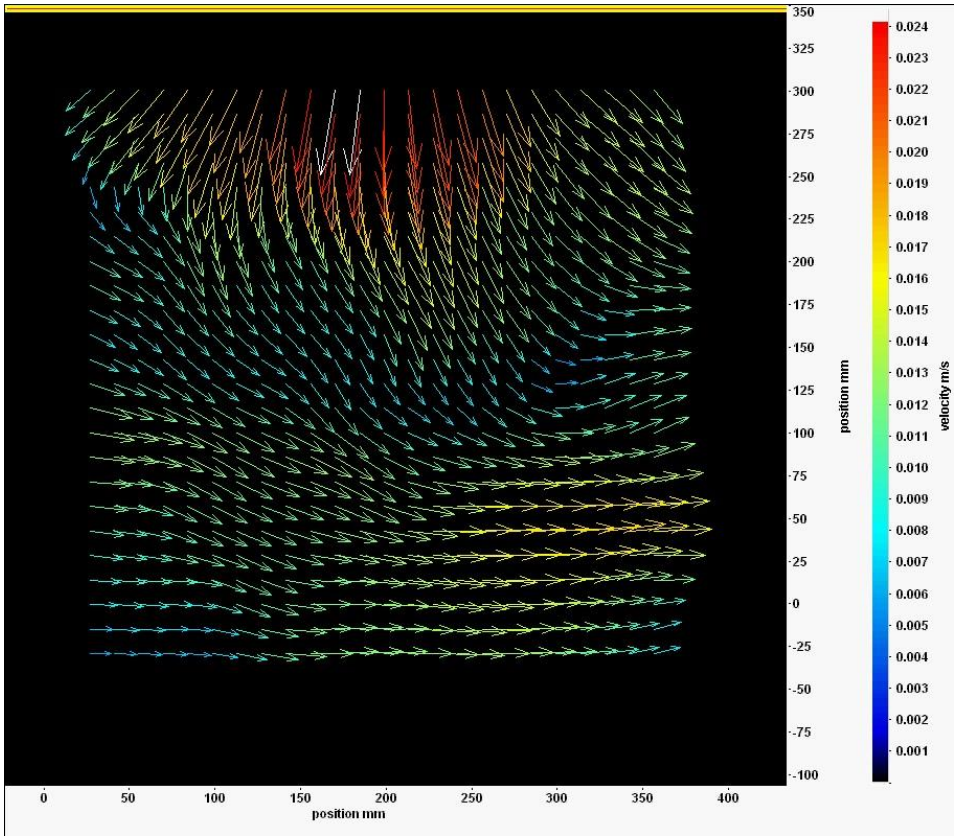

Figure (3.10h): After 19 seconds from the beginning of the movie

Figures (3.6) to (3.10) show the wind induced perturbations in the flow field in stages. The first stage shows the water particles moving in an oscillatory manner. The second stage shows the tracers motion converting from oscillatory to translational movement forming calm regions at different depths from the surface. The third stage is characterized by eddies forming at different locations from the surface and with an increase in flow velocity. Surface waves with small amplitude are generated at this stage. Further increases in wind speed show the flow characterized by augmentation in eddy size and speed and, the flow fluctuations near the surface becoming significant which cause an increase in the wave's velocity and growth rate.

The second set of velocity fields was obtained with background perturbations in a magnitude higher than the first set. The aim of this action is to examine the effect of the density of the background perturbations on wave evolution under the effect of the wind action. The initial flow velocity was higher than the corresponding velocity for the first set. Such condition of increasing initial flow velocity can be achieved by mixing the water by a mechanical means before running the wind tunnel fan or by starting a new experiment after a previous one without giving sufficient time to the

flow to attain still water conditions. The following velocity fields show the evolution of such flow under the effect of the same conditions as in the first set. As shown in figure (3.11), the average flow velocity at 'still' water conditions attained the value of the order 0.007 ms^{-1} which corresponds to the first set at a wind speed of the order 2.73 ms^{-1} and the flow direction followed the normal direction of the wind. The flow velocity of the entire flow is approximately homogeneous. The movie sequence shows that the velocity vectors oscillate with larger angles with respect to the X axis than the first set. The water particles at the upper half of the flow which are much closer to the surface oscillate in larger angles than the lower half. This indicates interaction between the water particles and air particles even if the effect of the wind shear is negligible. Figures (3.11a-h) show the velocity field images captured from the 19 second movie at equal intervals in between.

.

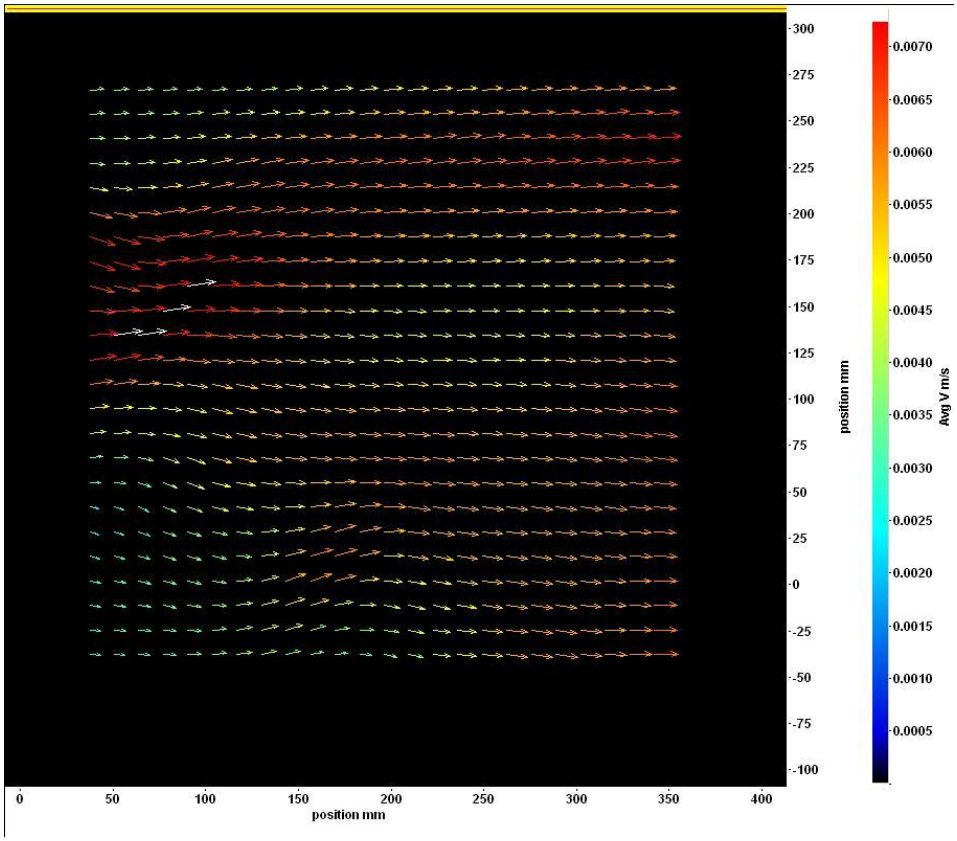

Fig (3.11): Average velocity field at still water conditions (zero fan speed).

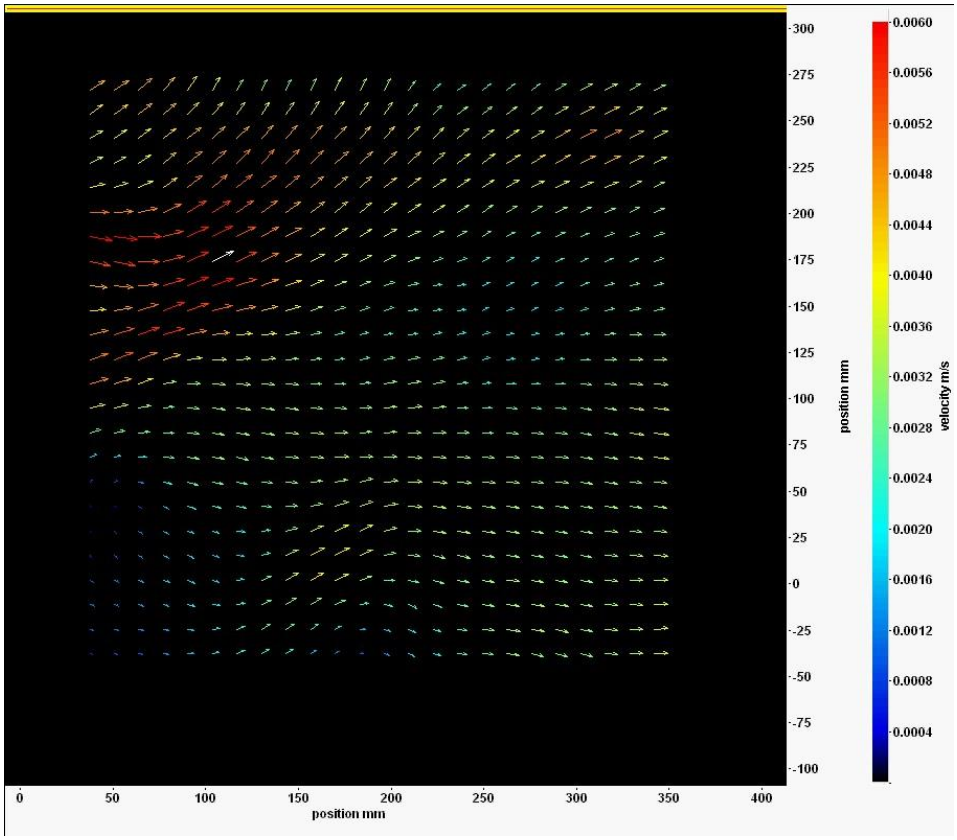

Figure (3.11a): After zero seconds from the beginning of the movie

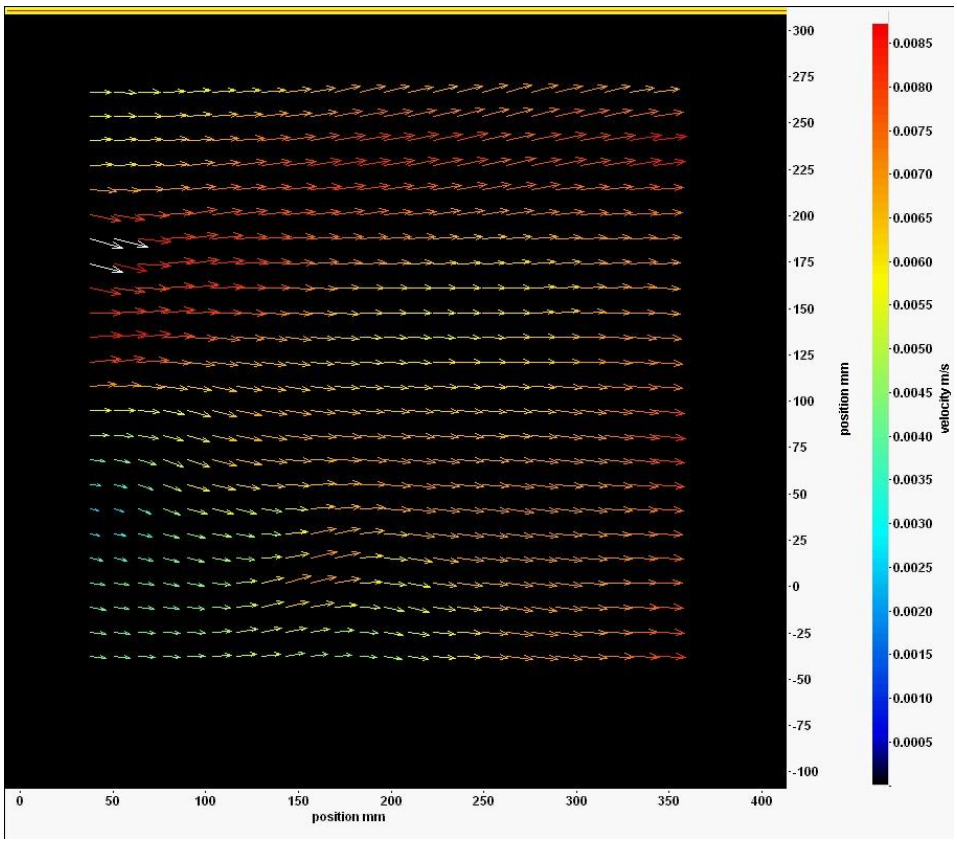

Figure (3.11b): After 2.71 seconds from the beginning of the movie

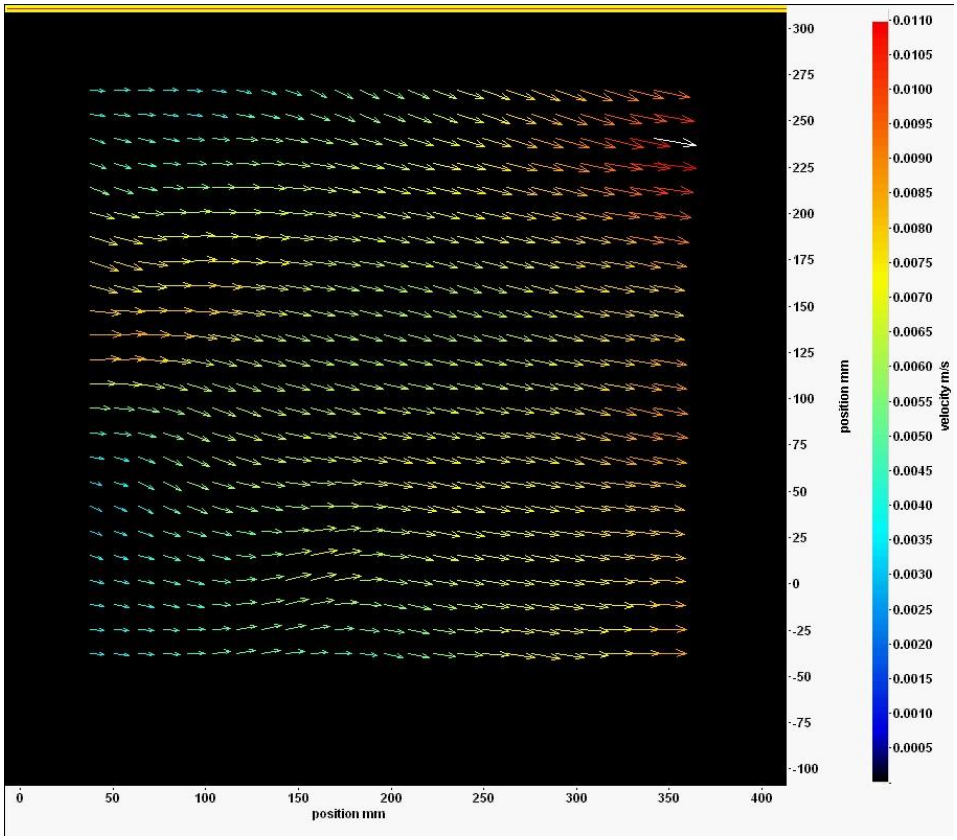

Figure (3.11c): After 5.42 seconds from the beginning of the movie

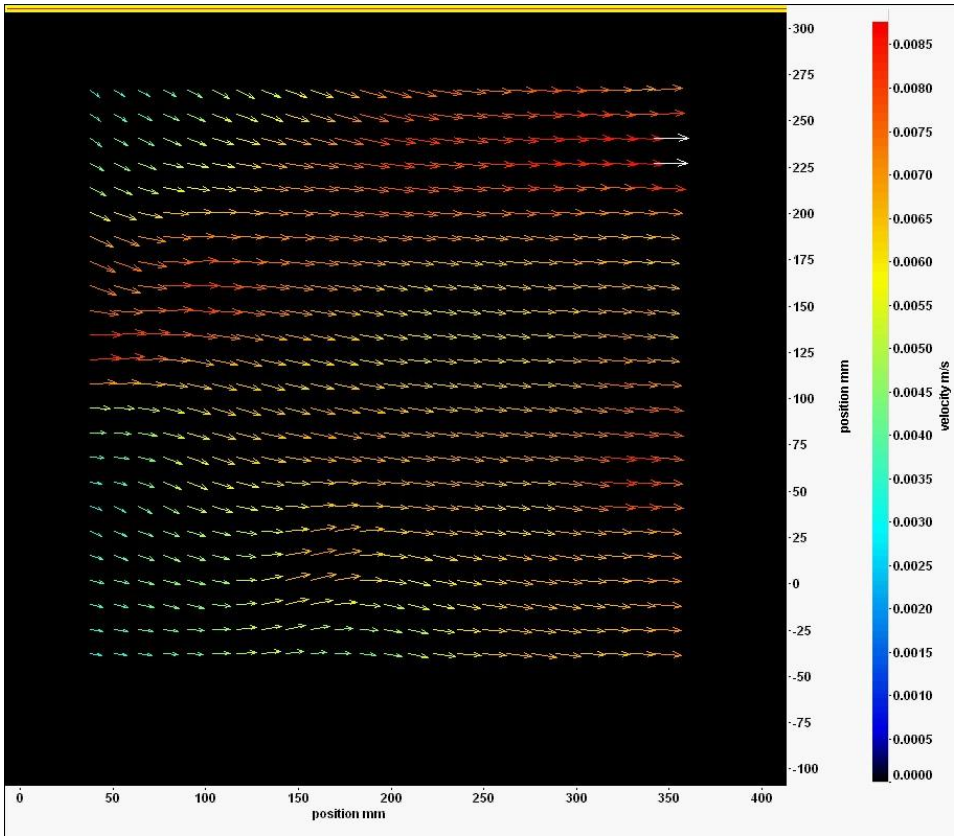

Figure (3.11d): After 8.13 seconds from the beginning of the movie

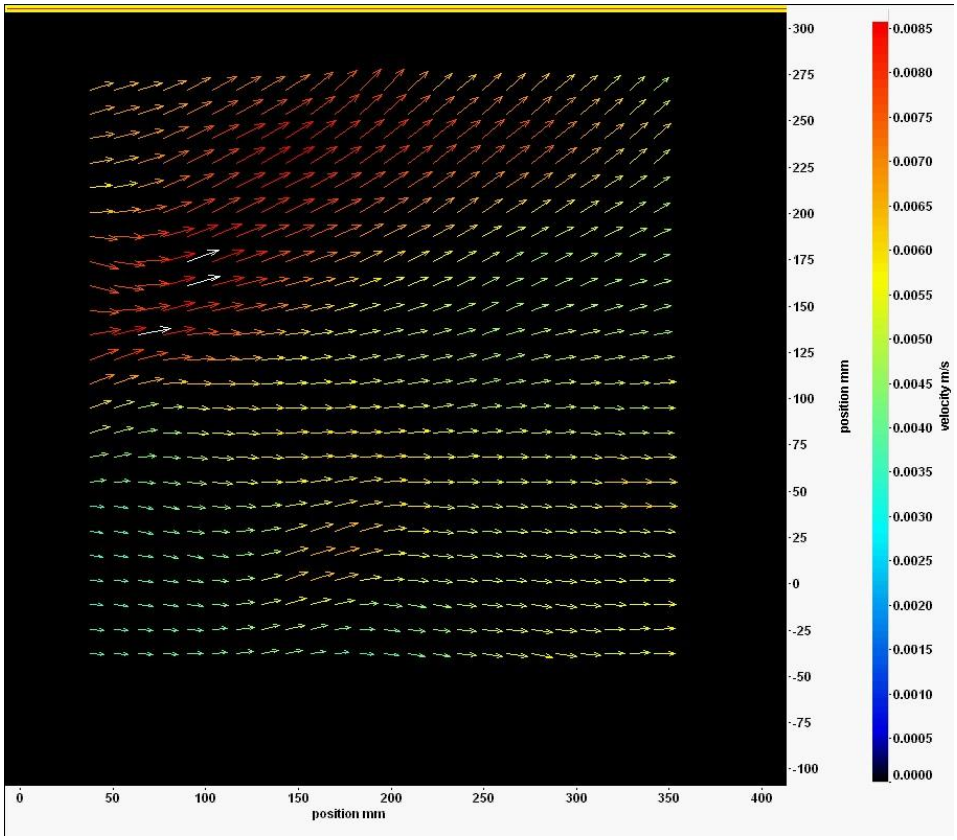

Figure (3.11e): After 10.85 seconds from the beginning of the movie

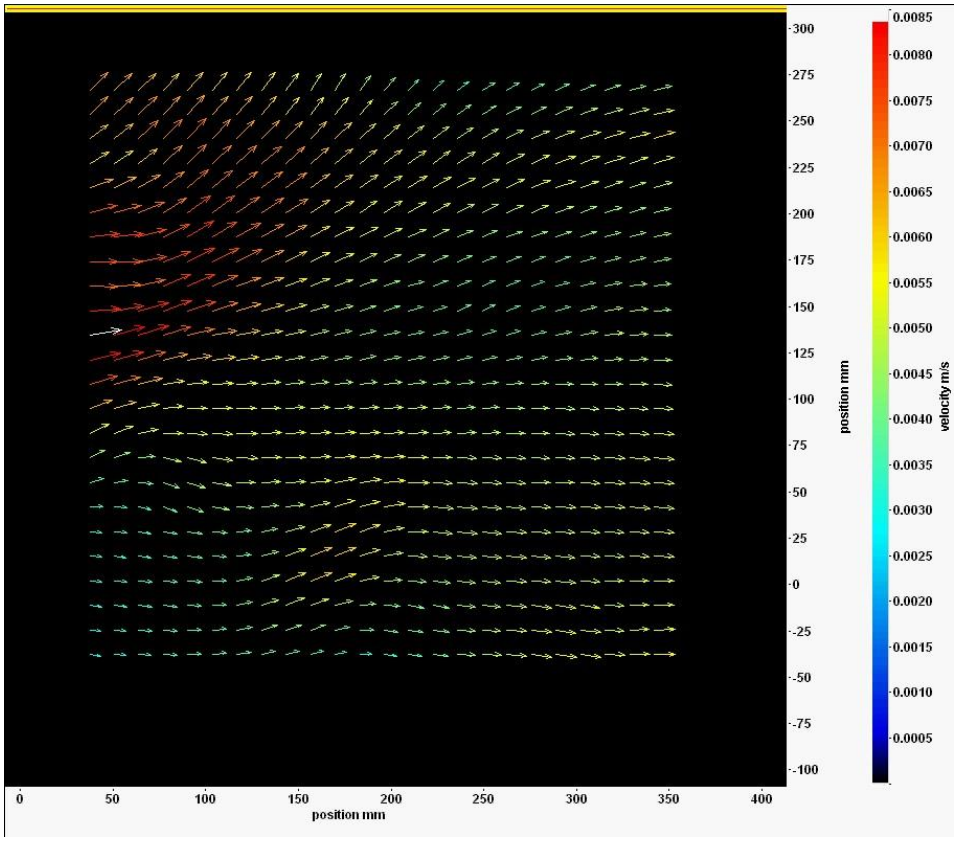

Figure (3.11f): After 13.57 seconds from the beginning of the movie

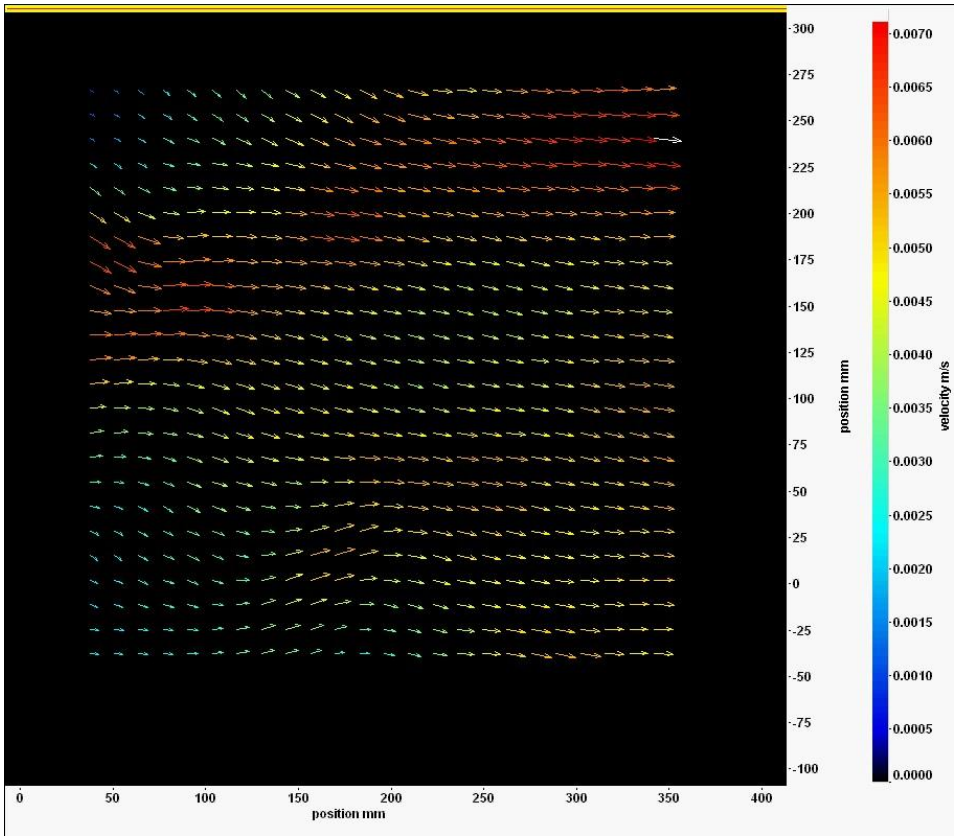

Figure (3.11g): After 16.28 seconds from the beginning of the movie

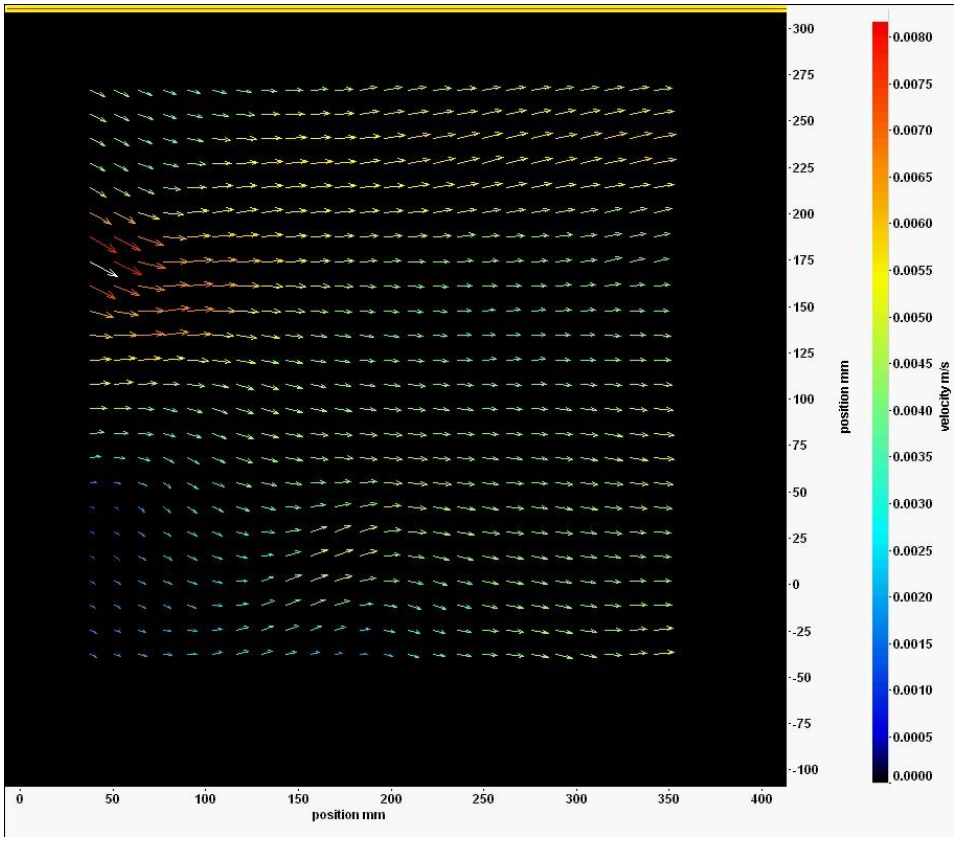

Figure (3.11h): Velocity fields after 19 seconds from the beginning of the movie

The effect of the wind is now considered. Between zero wind speed and a wind speed of the order of 1.07 ms^{-1}, significant changes occur, as shown in Figure (3.12); the bulk flows in the direction opposed to the wind direction and the higher flow velocity is restricted to the upper layer of the image. The difference between the wind direction and bulk flow direction can be observed also in the first set. This gives an indication to how the bulk responds to the action of the wind as the wind speed increases. The presence of the dark regions, characterized by very low velocity, is very obvious now. However, the average flow velocity and the size of dark regions are higher than the corresponding regions in the first set of velocity fields.

Based on the results of the first set, the flow direction and location of new eddies generation can be predicted at higher speeds. Based on previous runs a change in bulk flow direction will occur where the dark regions appear, also eddies generating starts at these regions. The possibility of generating eddies increases as the wind speed attains higher magnitudes with a significant change in the bulk flow direction.

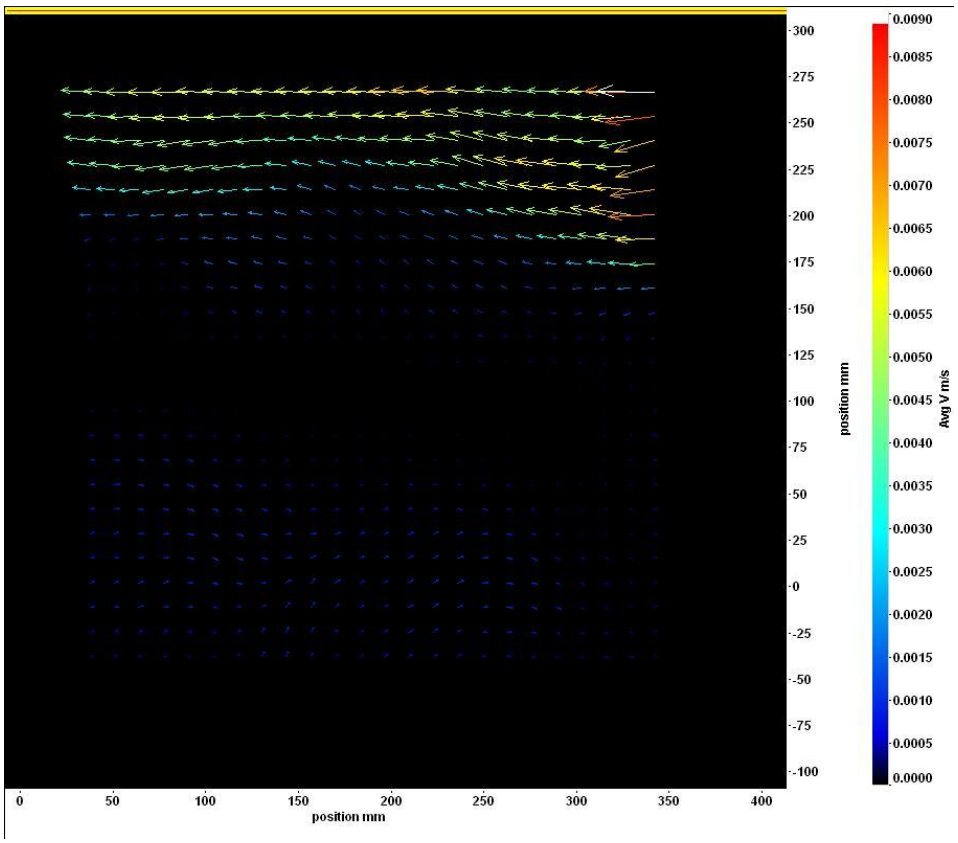

Figure (3.12): Average velocity field at wind speed of the order 1.07 ms^{-1}

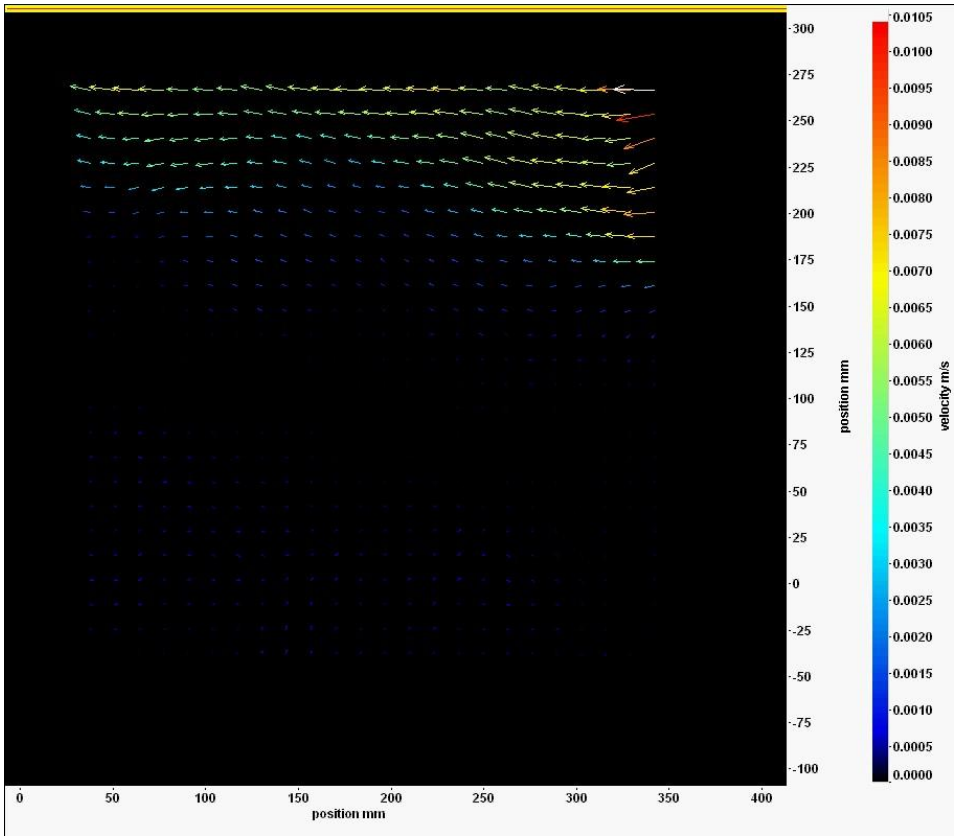

Figure (3.12a): After zero seconds from the beginning of the movie

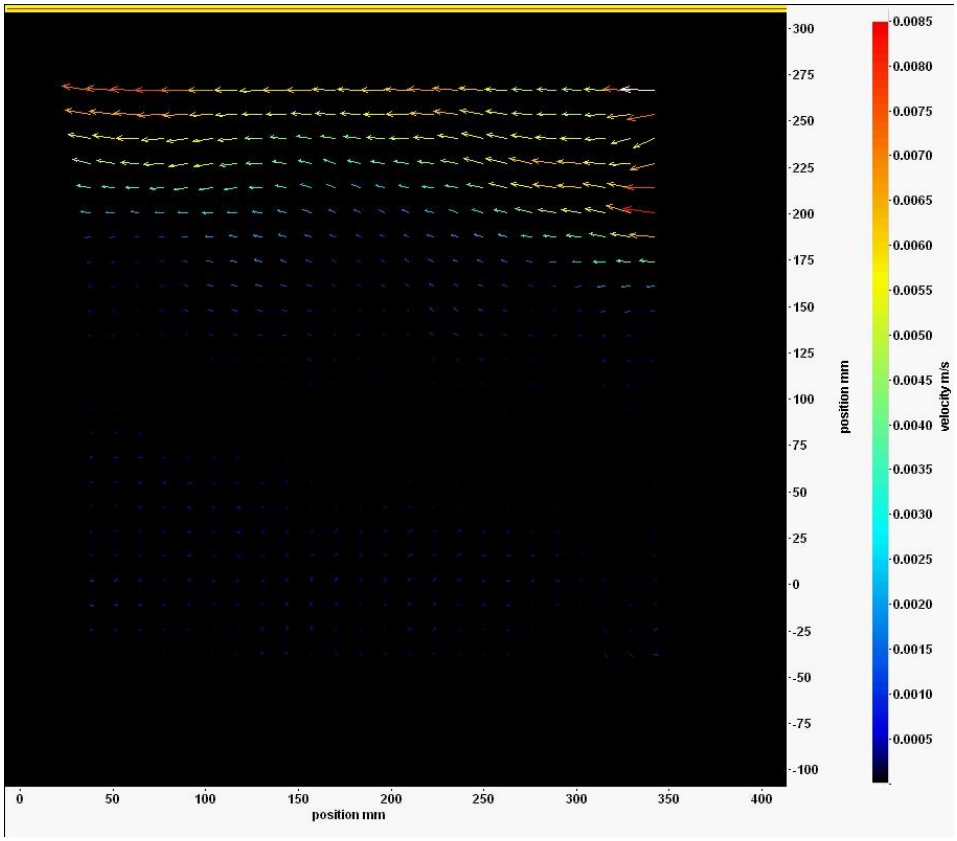

Figure (3.12b): After 2.71 seconds from the beginning of the movie

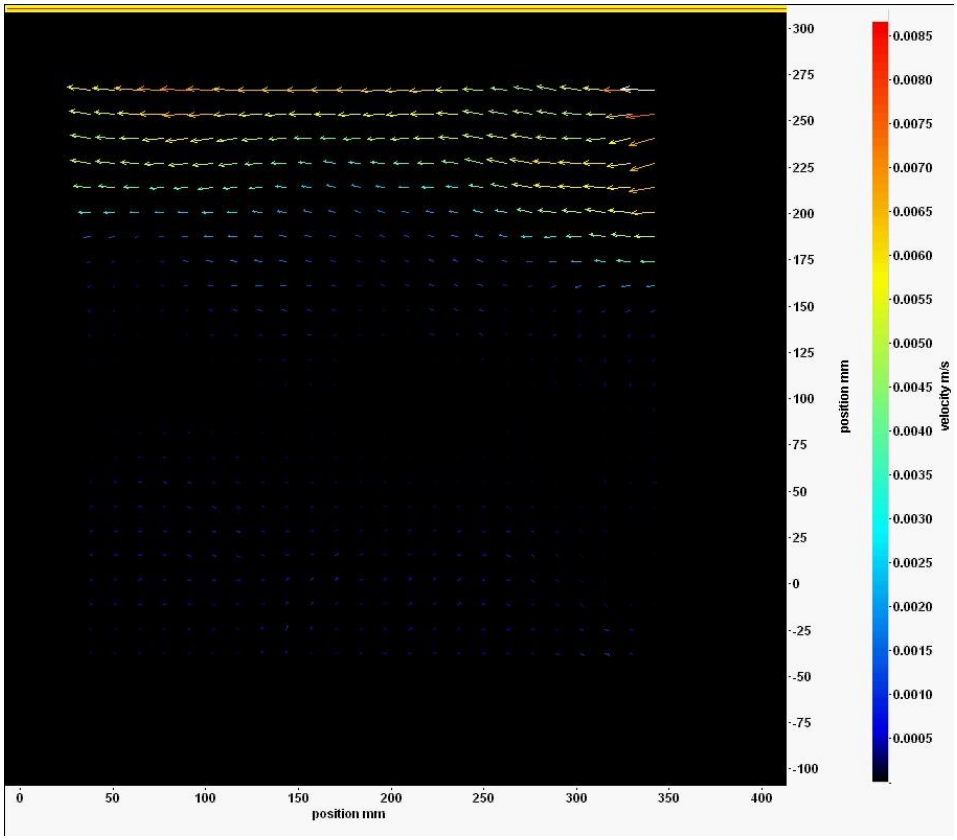

Figure (3.12c): After 5.42 seconds from the beginning of the movie

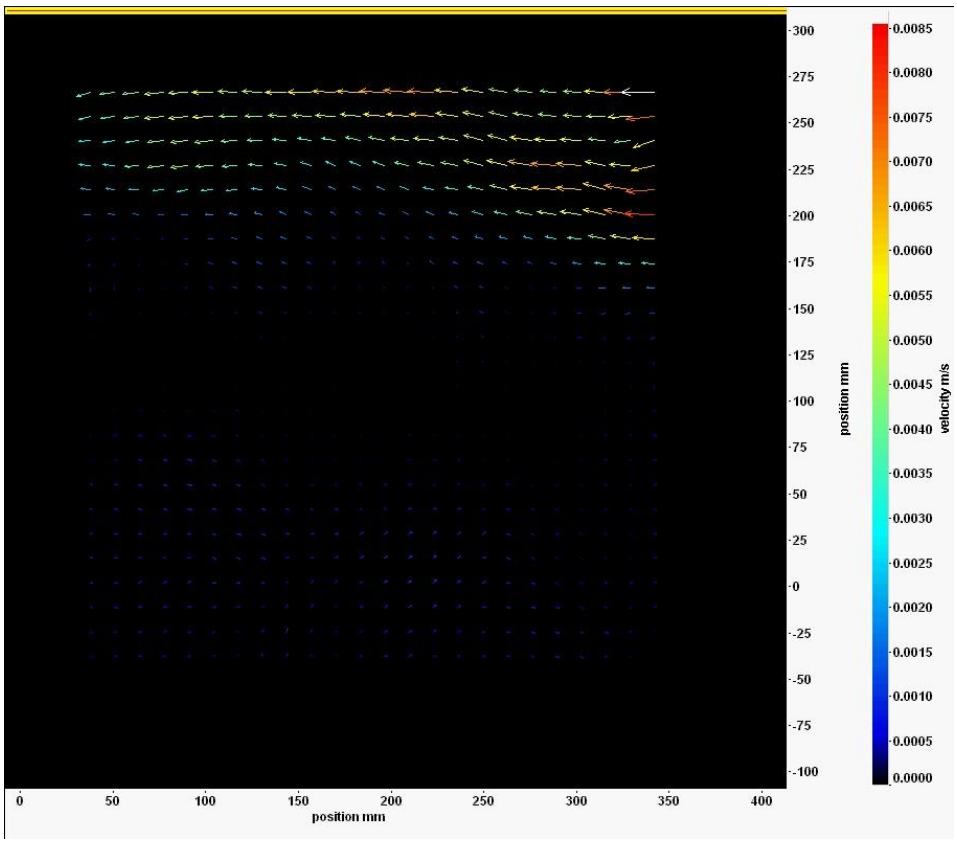

Figure (3.12d): After 8.14 seconds from the beginning of the movie

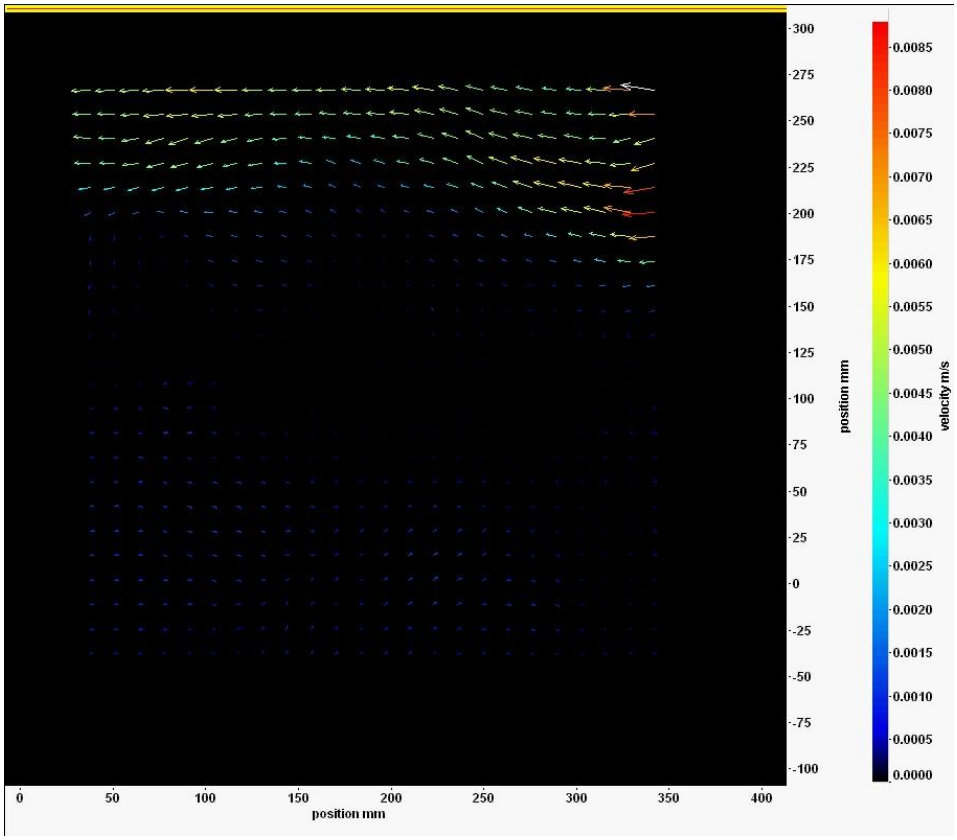

Figure (3.12e): After 10.85 seconds from the beginning of the movie

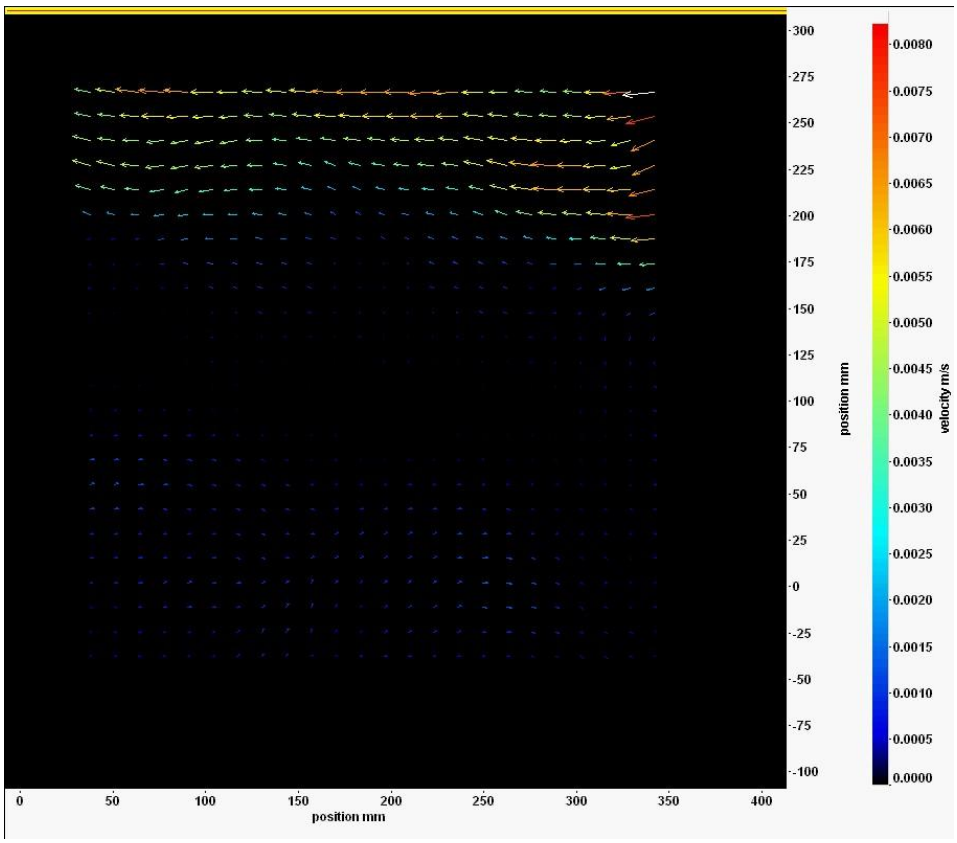

Figure (3.12f): After 13.57 seconds from the beginning of the movie

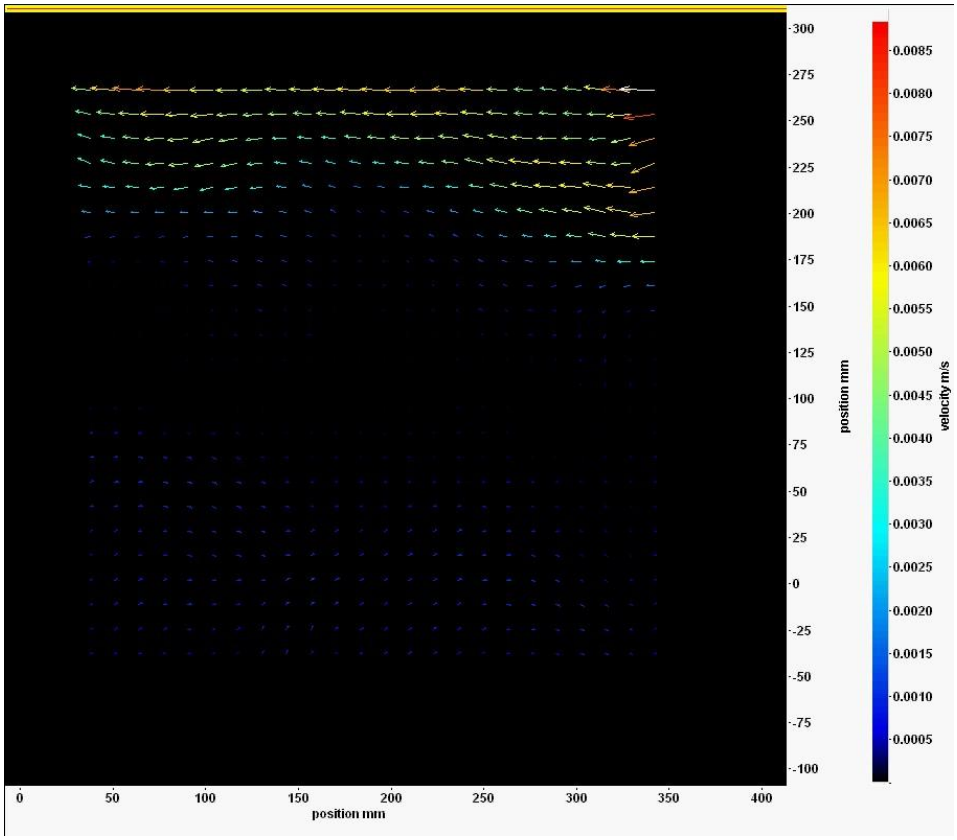

Figure (3.12g): After 16.28 seconds from the beginning of the movie

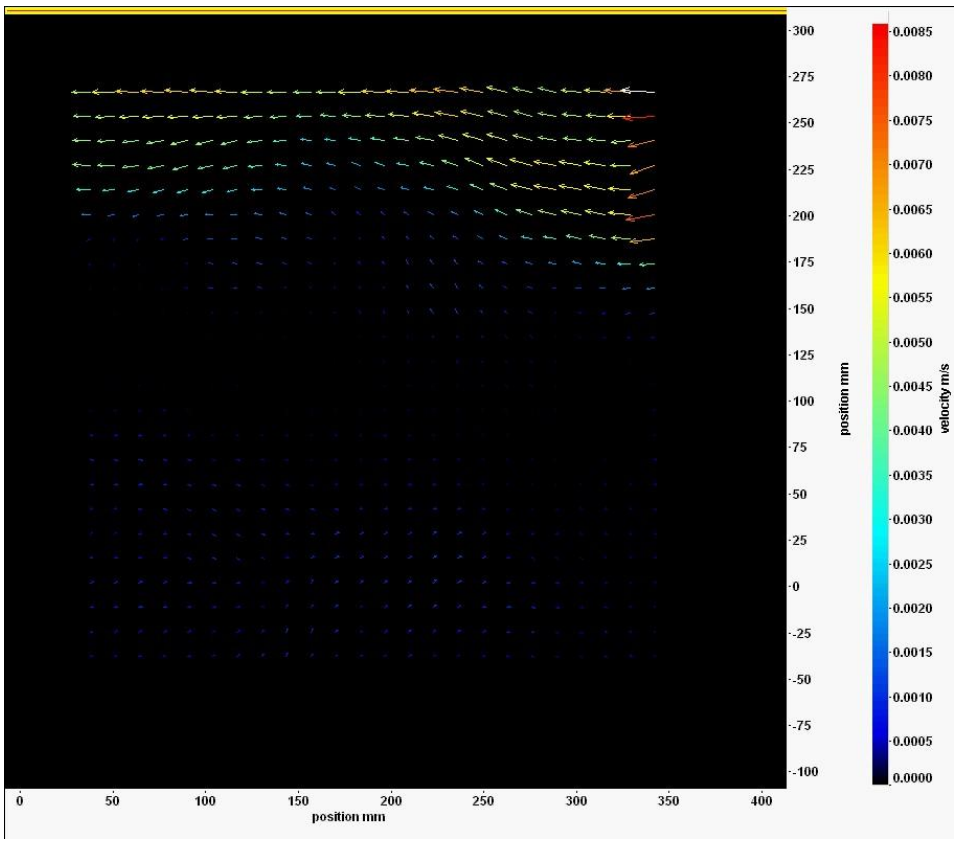

Figure (3.12h): After 19 seconds from the beginning of the movie

As predicted from the previous figures, at a wind speed of the order 1.92 ms^{-1} a significant change in flow direction occurs and the eddies become visible where the dark regions were occurred. The movie sequence below shows the change in the flow direction and eddy formation. The main eddy starts from the top right corner and accelerates the flow below; the bulk flow is directed by the direction of the largest eddy rotation. Figures (3.13b and 3.13f) explain the mechanism of the transfer of rotational movement from the centre of an eddy to the surrounding flow. This reveals the importance of the location of the eddy centres in the flow direction. Figures (3.13a-h) show that the flow direction changes continuously. This is because the induced shear and the strength of the eddies at the current wind speed are not sufficient to direct the flow in a particular direction. In general the flow velocity attains lower magnitudes as the water depth increase. The higher flow speed is concentrated near the surface.

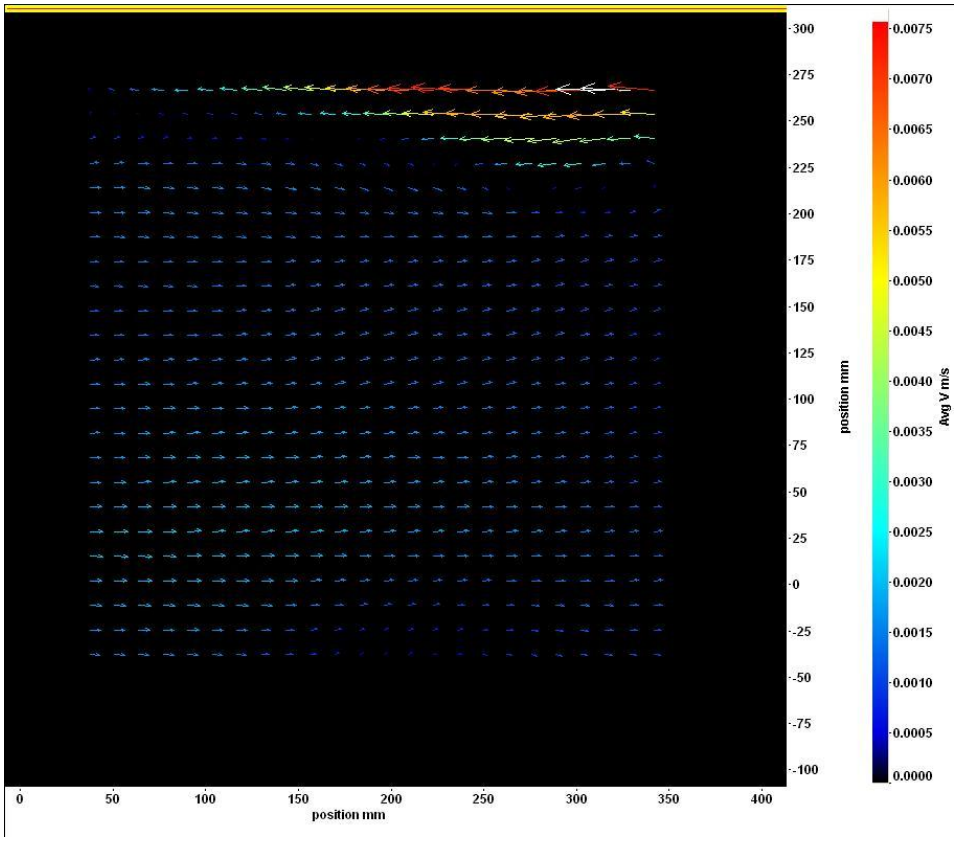

Fig (3.13): Average velocity field at wind speed of the order 1.92 ms^{-1}

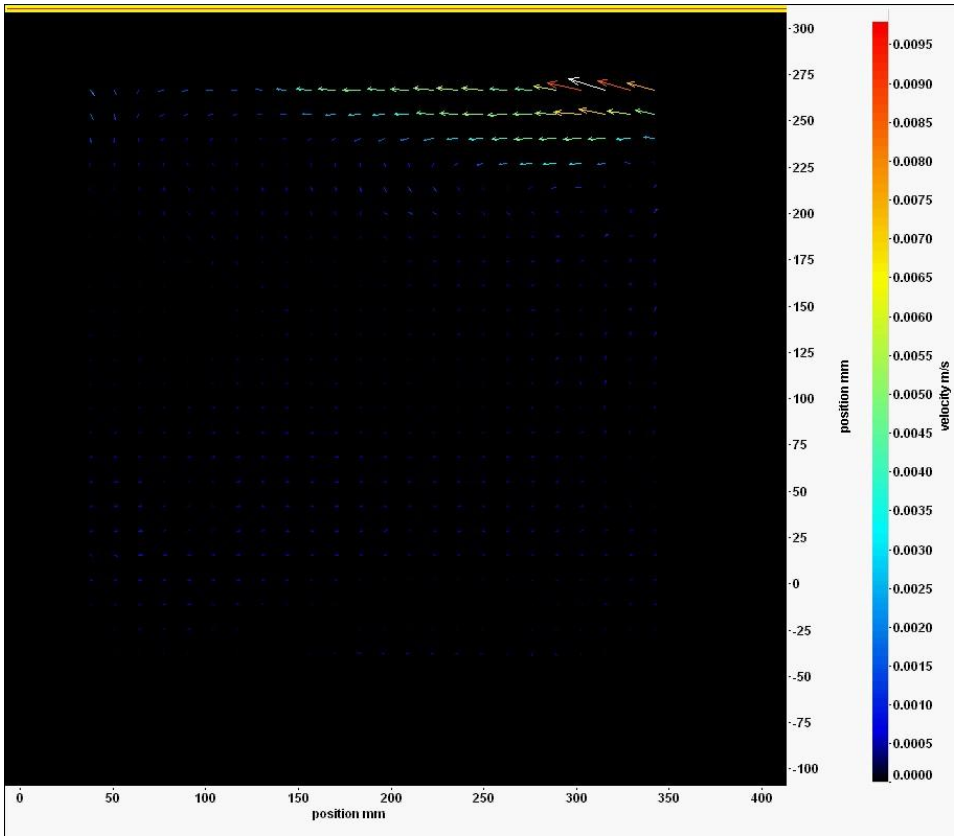

Figure (3.13a): After zero seconds from the beginning of the movie

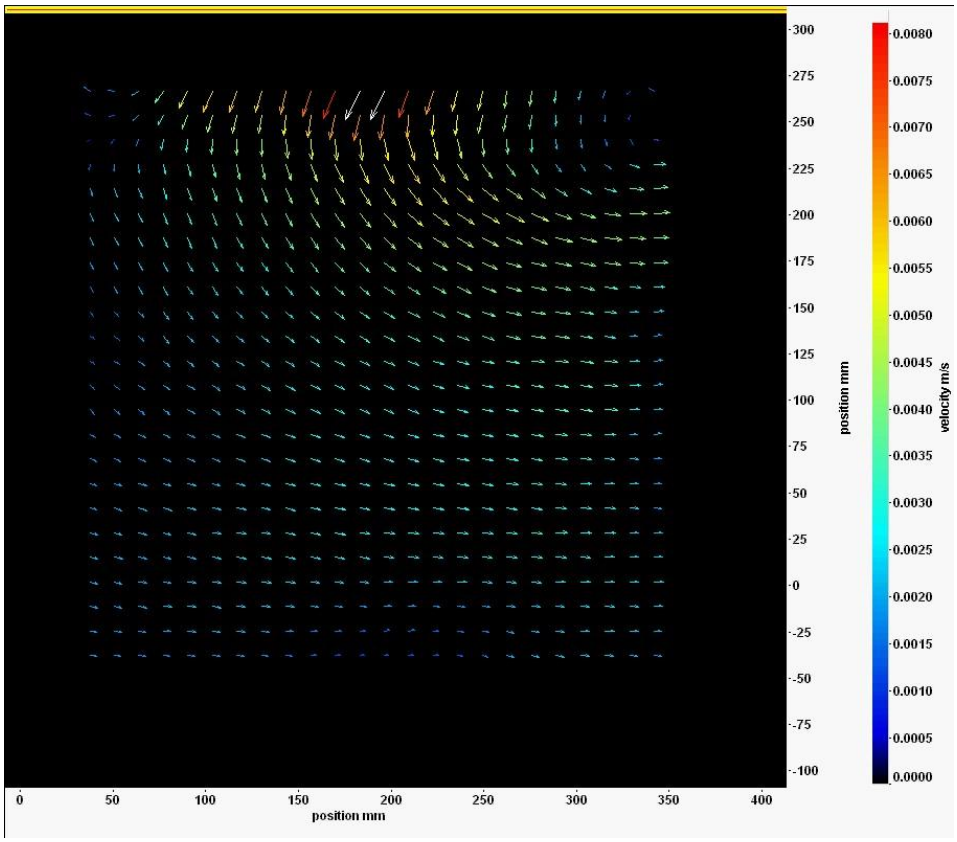

Figure (3.13b): After 2.71 seconds from the beginning of the movie

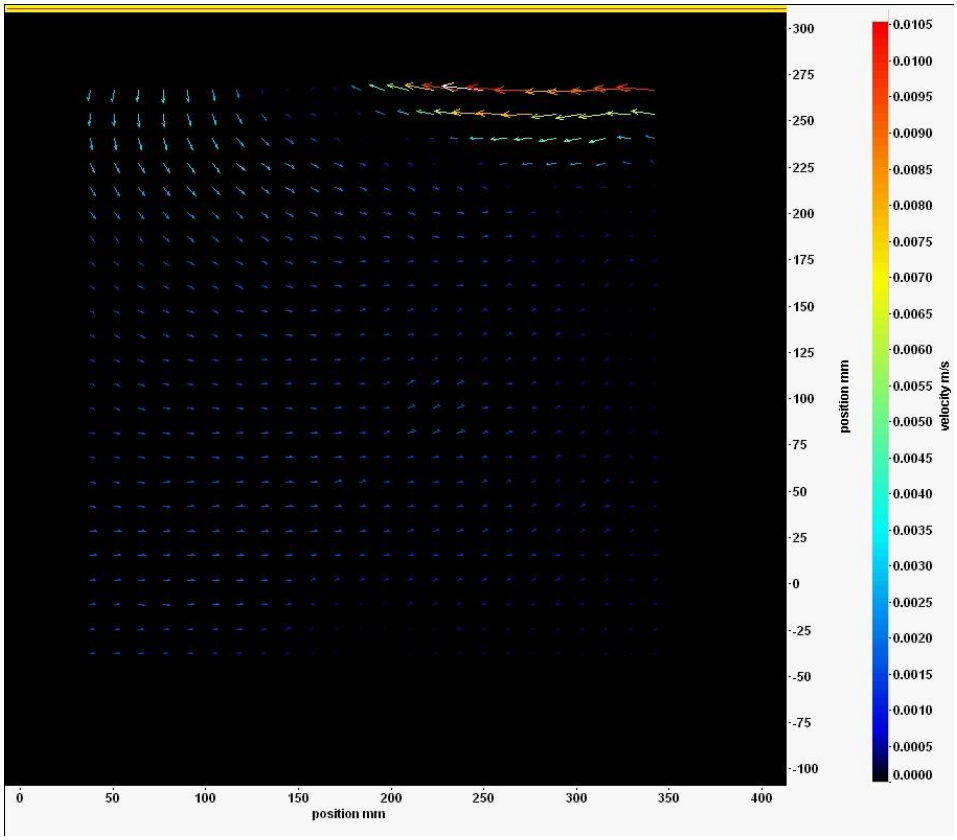

Figure (3.13c): After 5.42 seconds from the beginning of the movie

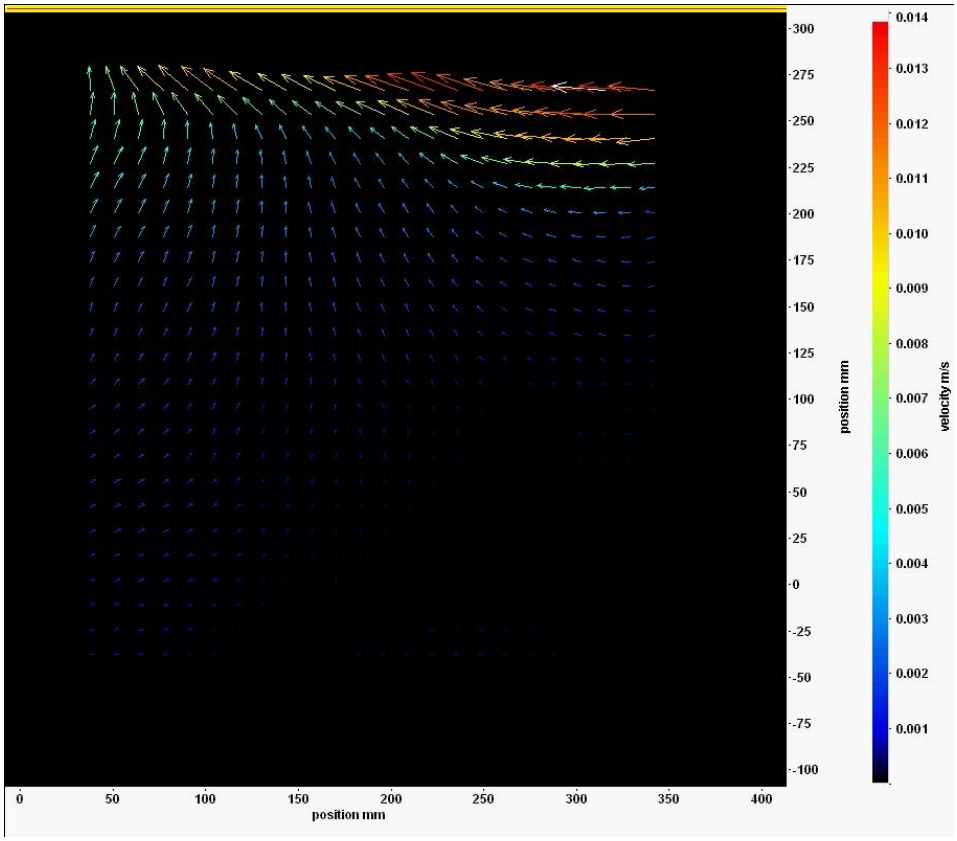

Figure (3.13d): After 8.14 seconds from the beginning of the movie

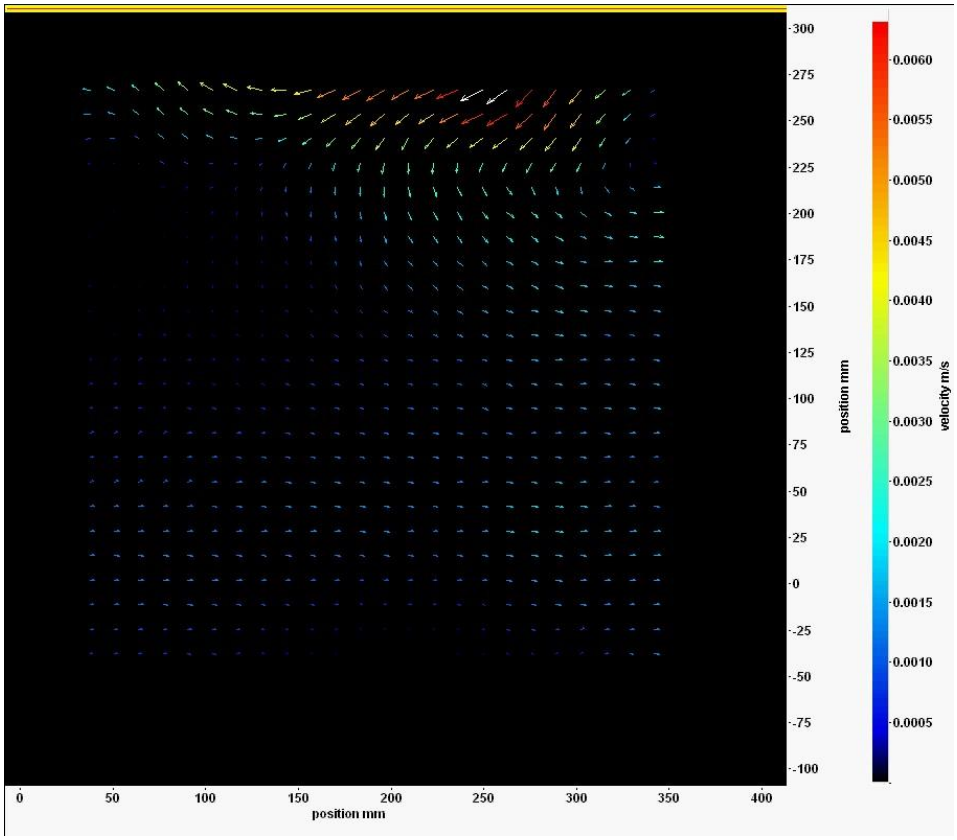

Figure (3.13e): After 10.85 seconds from the beginning of the movie

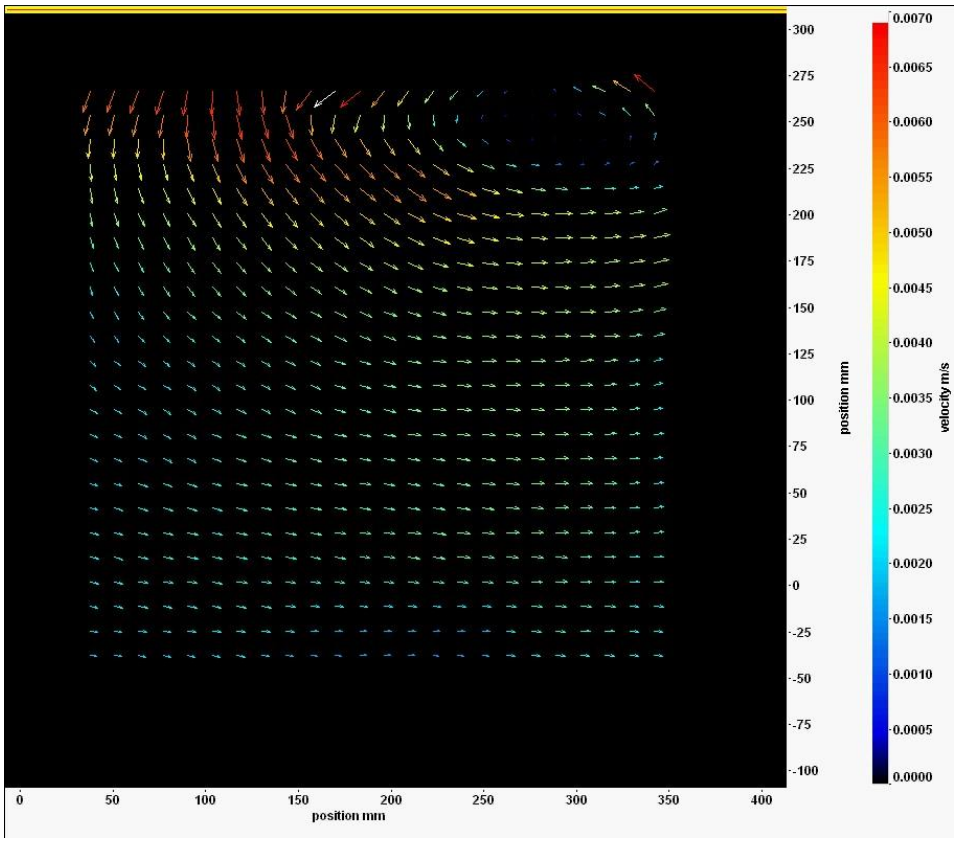

Figure (3.13f): After 13.57 seconds from the beginning of the movie

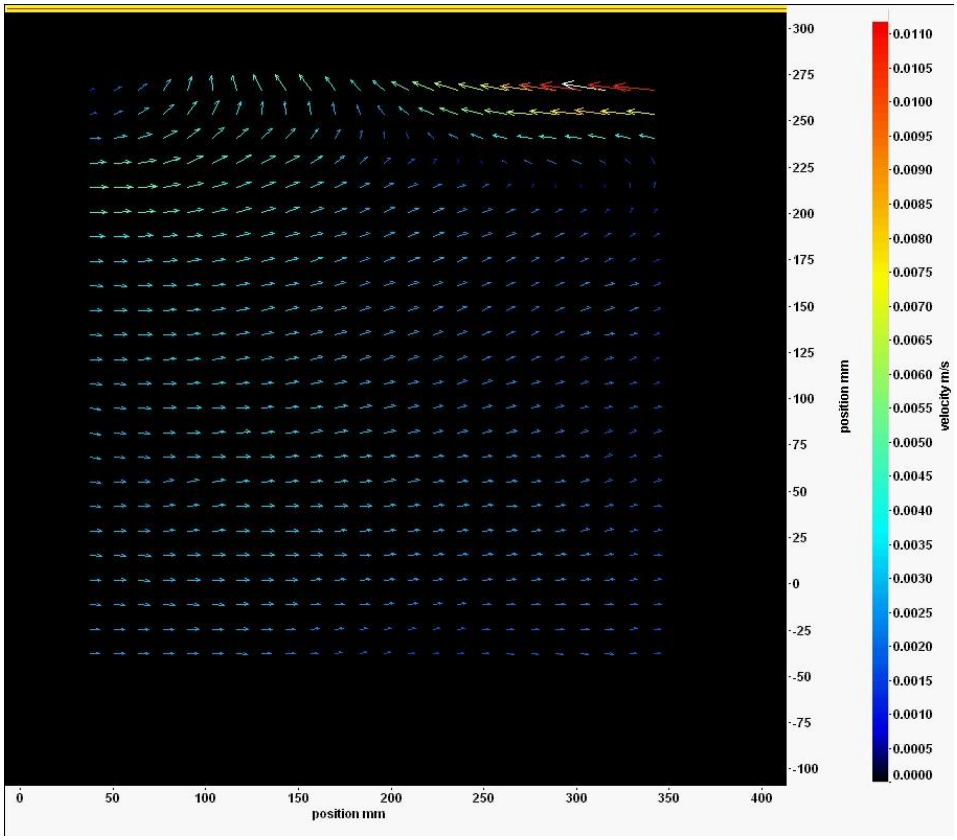

Figure (3.13g): After 16.28 seconds from the beginning of the movie

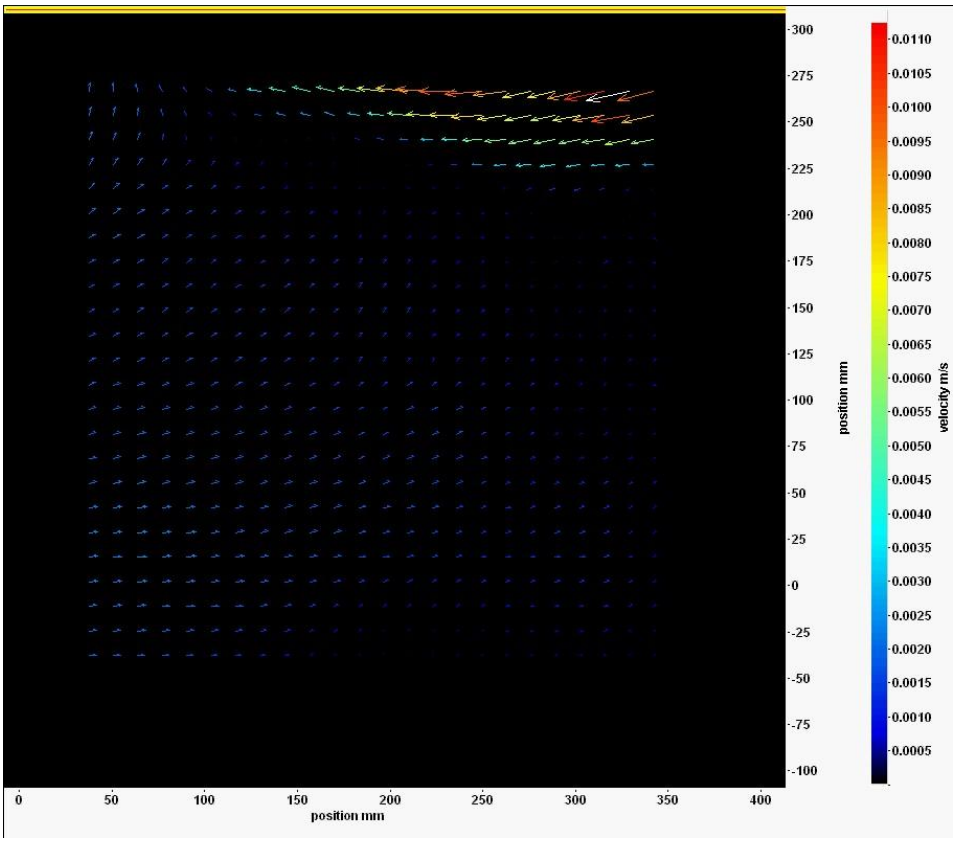

Figure (3.13h): After 19 seconds from the beginning of the movie

As the wind speed attains the magnitude of the order 2.73 ms^{-1} the magnitude of wind induced shear becomes sufficient to direct the flow in the direction of the induced shear or in the direction of the strongest eddy. Figure 3.14 shows the average velocity field for the 19 second movie. As shown in Figure (3.14) the higher velocity magnitudes are concentrated in the upper half of the image. The entire flow follows the direction of the wind, however. In the upper half of the bulk flow the velocity vectors oscillate with large angles with respect to the X axis compared with the lower half.

Figures (3.14a-h) show a movie sequence for the flow evolution. The direction of the entire flow is the same as in the corresponding wind speed in the first set. However, the maximum average velocity is somewhat greater.

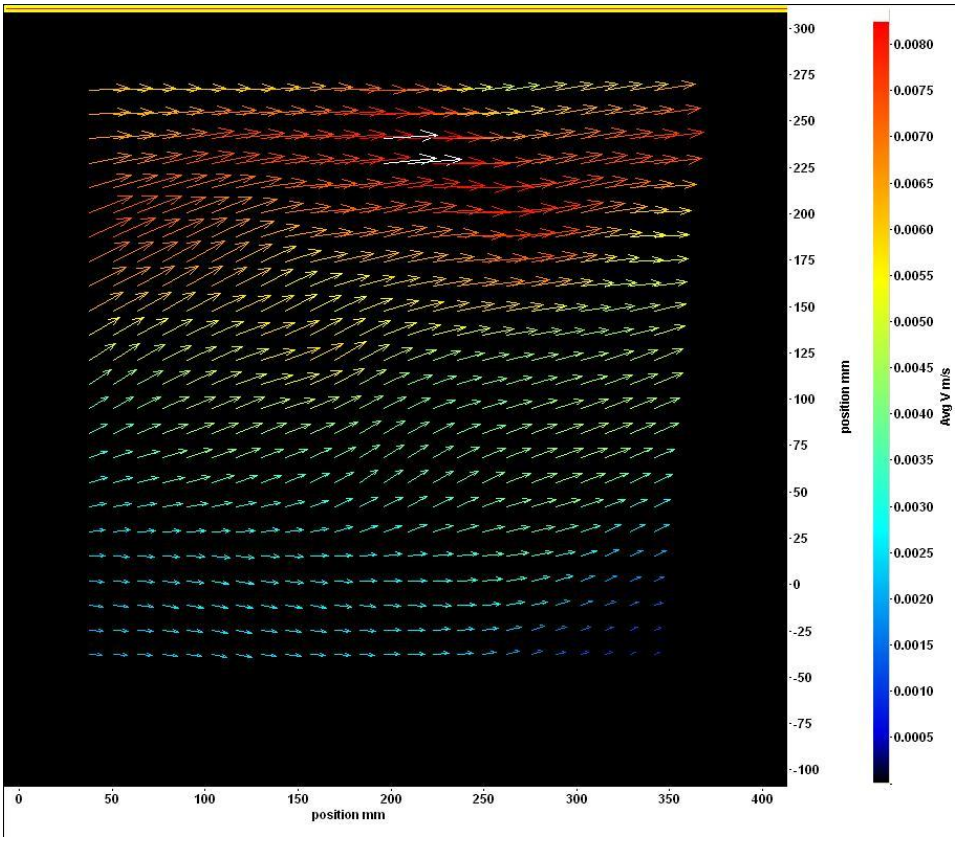

Figure (3.14): Average velocity field at wind speed of the order 2.73 ms^{-1}

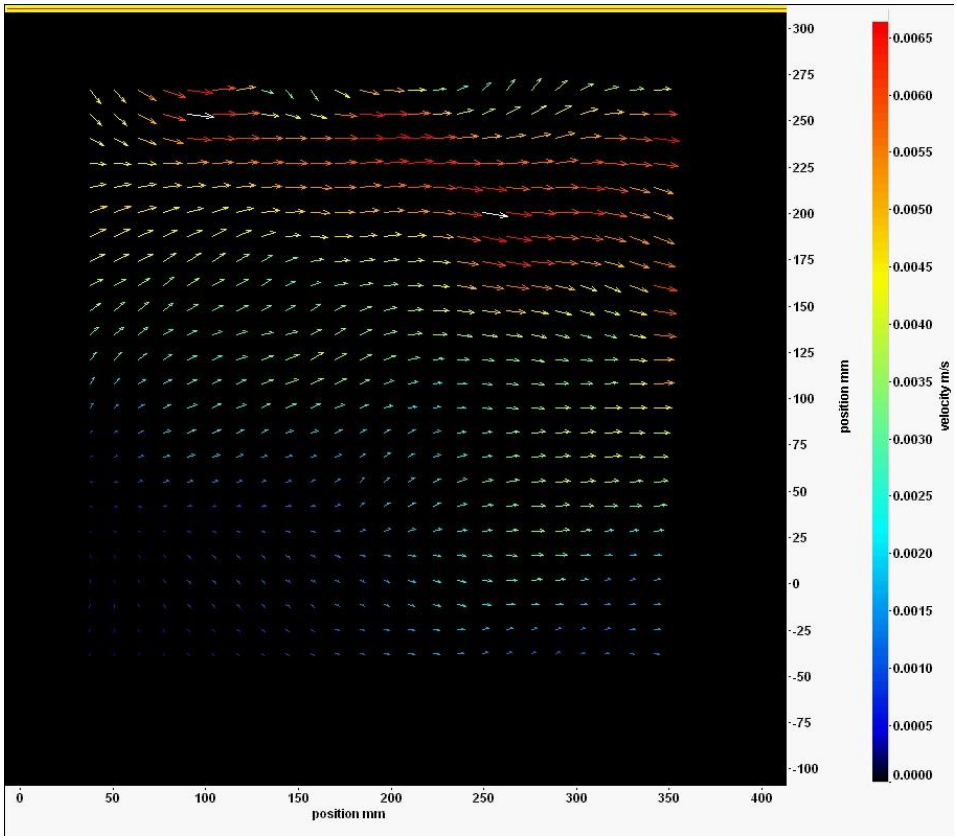

Figure (3.14a): After zero seconds from the beginning of the movie

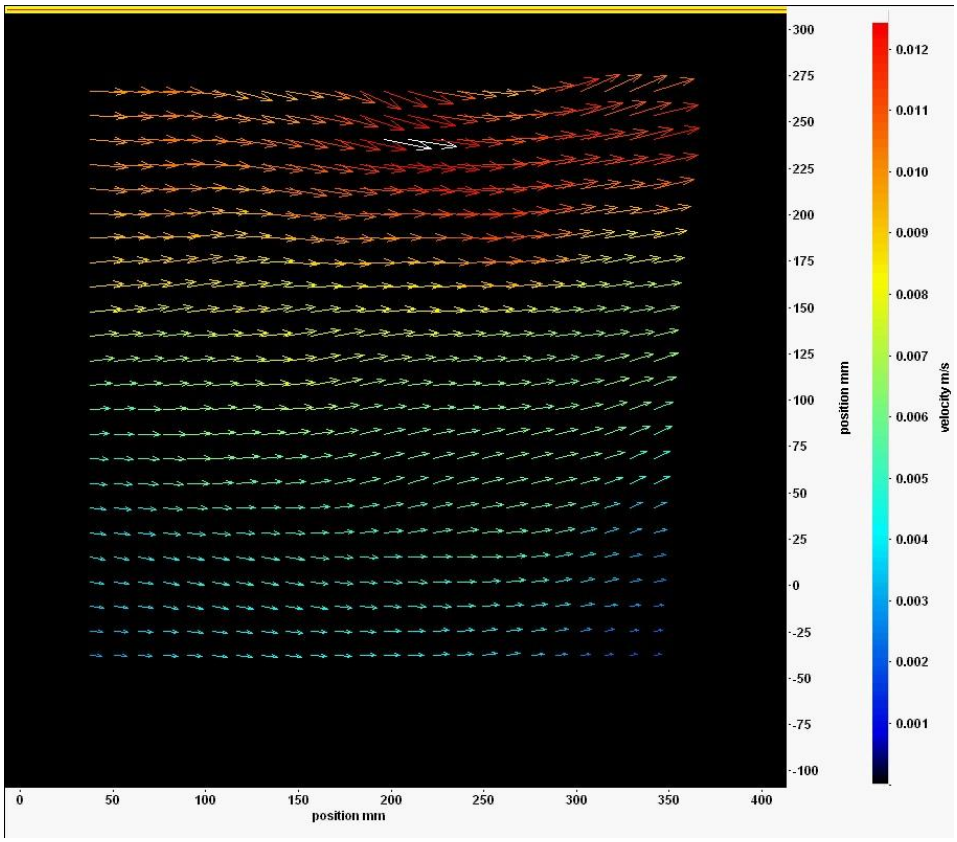

(3.14b): After 2.17 seconds from the beginning of the movie

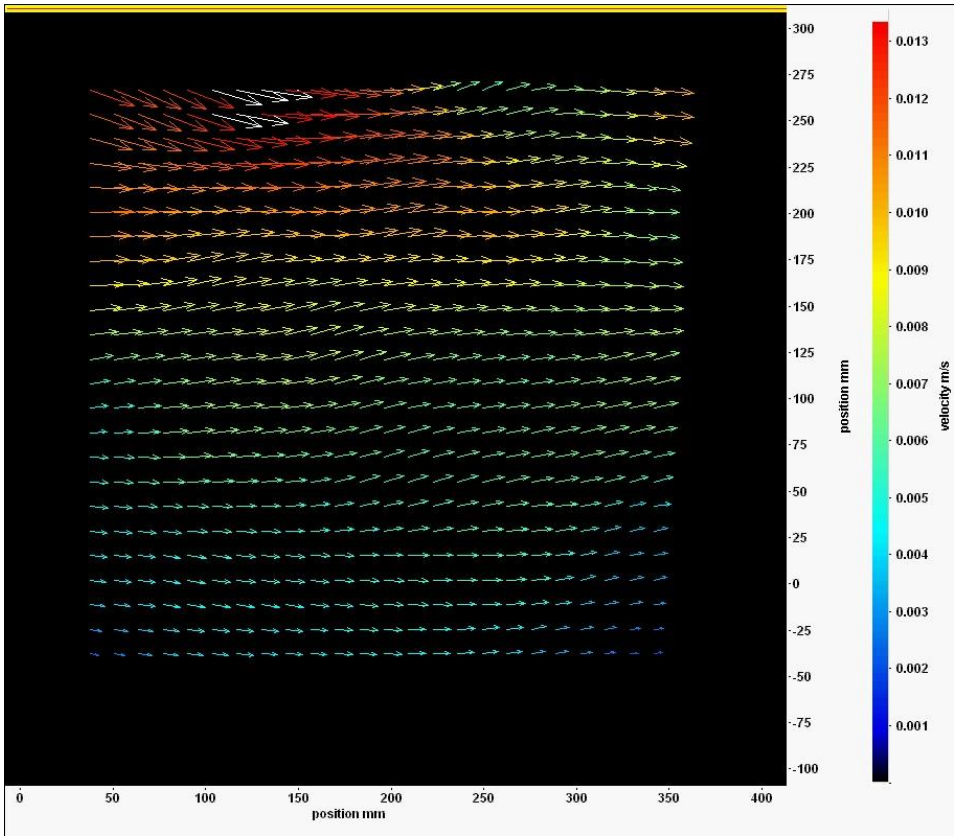

Figure (3.14c): After 5.42 seconds from the beginning of the movie

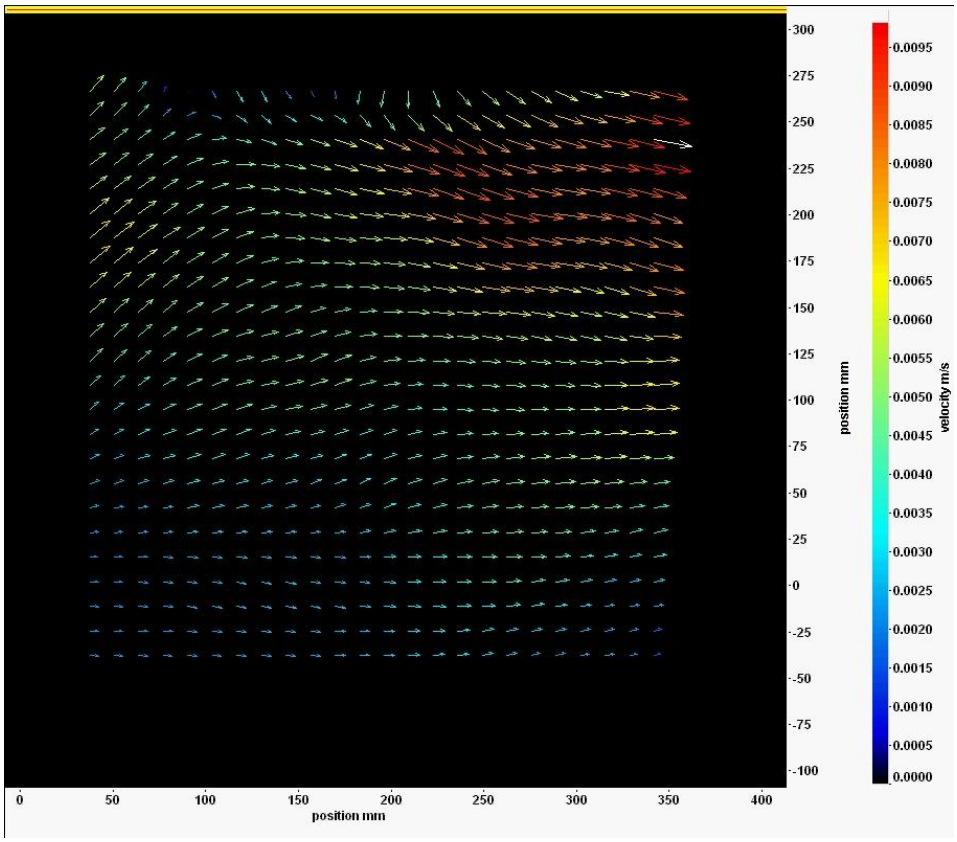

Figure (3.14d): After 8.14 seconds from the beginning of the movie

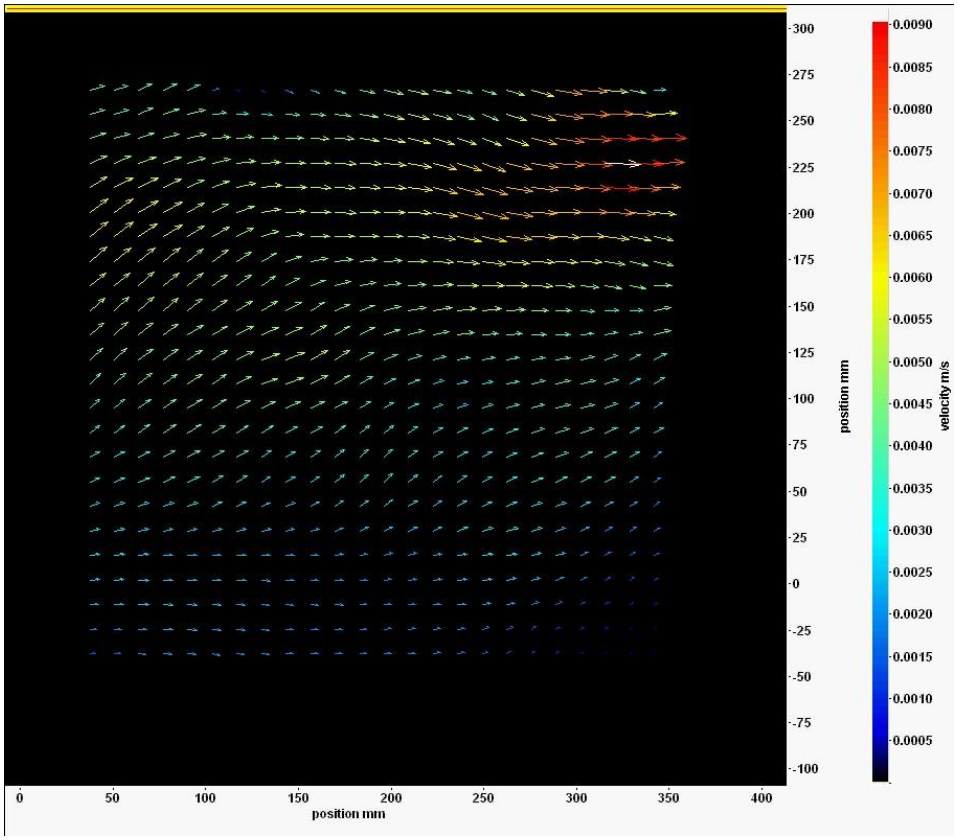

Figure (3.14e): After 10.85 seconds from the beginning of the movie

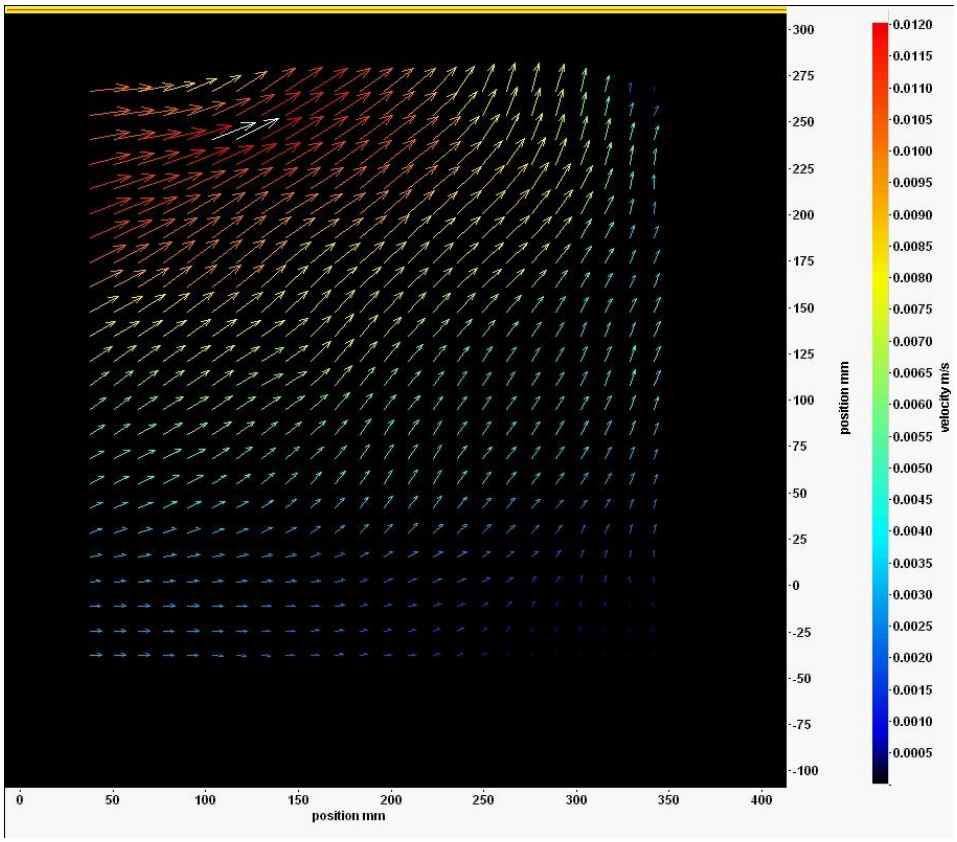

Figure (3.14f): After 13.57 seconds from the beginning of the movie

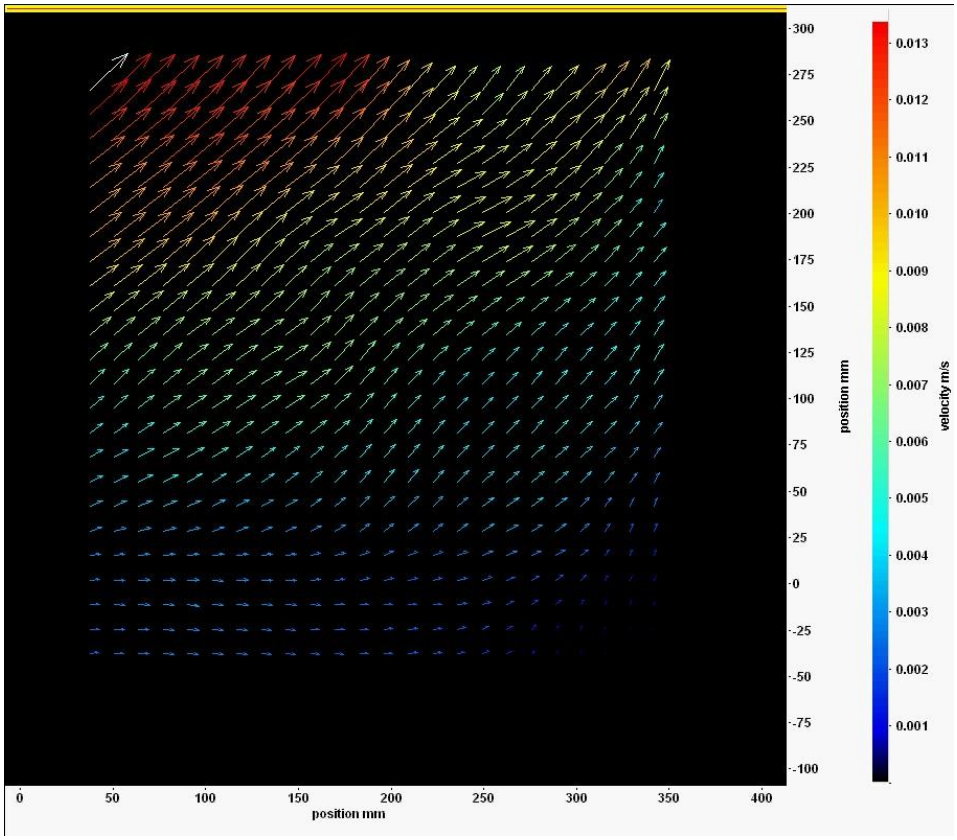

Figure (3.14g): After 16.28 seconds from the beginning of the movie

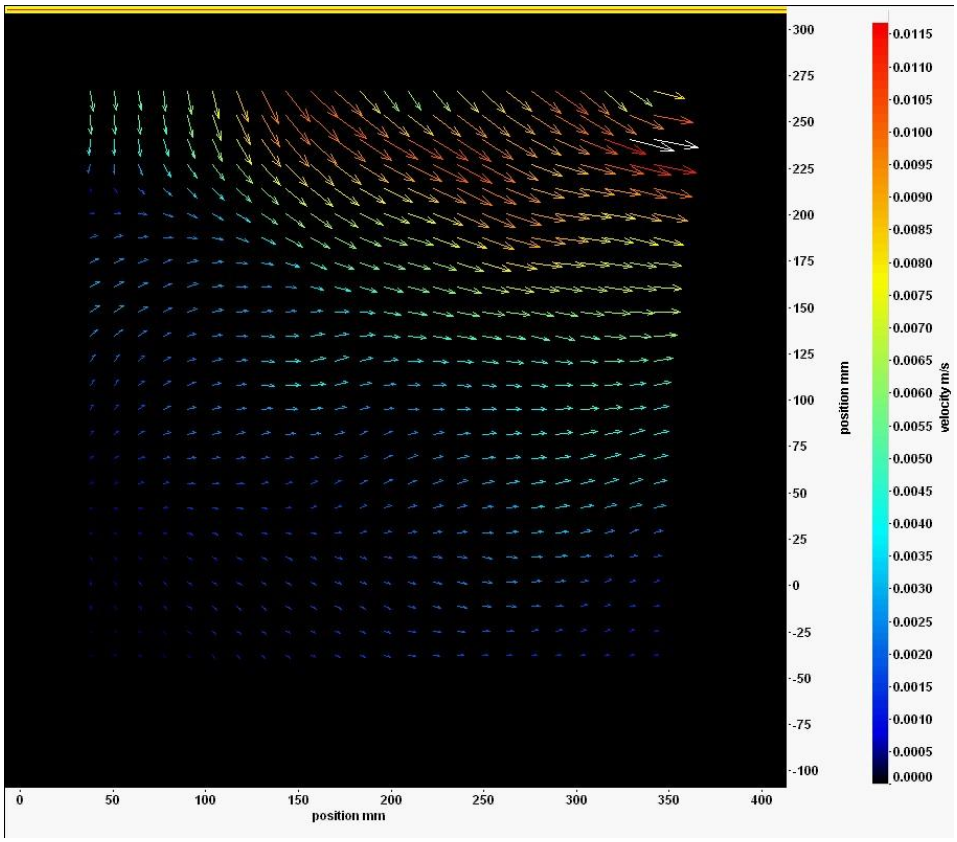

Figure (3.14h): After 19 seconds from the beginning of the movie

As the wind speed attains the magnitude of the order 3.6 ms^{-1} an increase in the velocity field occurs and new eddies at different locations in the flow field can be seen. Figure (3.15) shows the average velocity field for the 19 second movie. Figure (3.15) shows that the eddy formation starts from the surface; a significant increase in the bulk flow velocity occurs below the eddies due to the eddies' rotation. This mechanism causes a significant increase in the density of the bulk perturbation and in the bulk energy. Tracing the movie sequence at the current speed gives added insight to this mechanism. The effect of the wind induced shear starts from the upper part of the bulk flow, Figure (3.15a); a significant increase in the bulk flow velocity from the surface to the channel bottom is observed in Figures (3.15b and c); the formation of a number of eddies near the surface at different locations in the bulk flow can be observed in Figures (3.15d-g); a vertical motion of the flow particles due to the transfer the wind momentum and wind induced shear is shown in Figure (3.15h). Through the above sequence, the flow attains different directions with respect to the wind direction. Under the influence of the wind action, the strongest and largest eddies govern the flow direction.

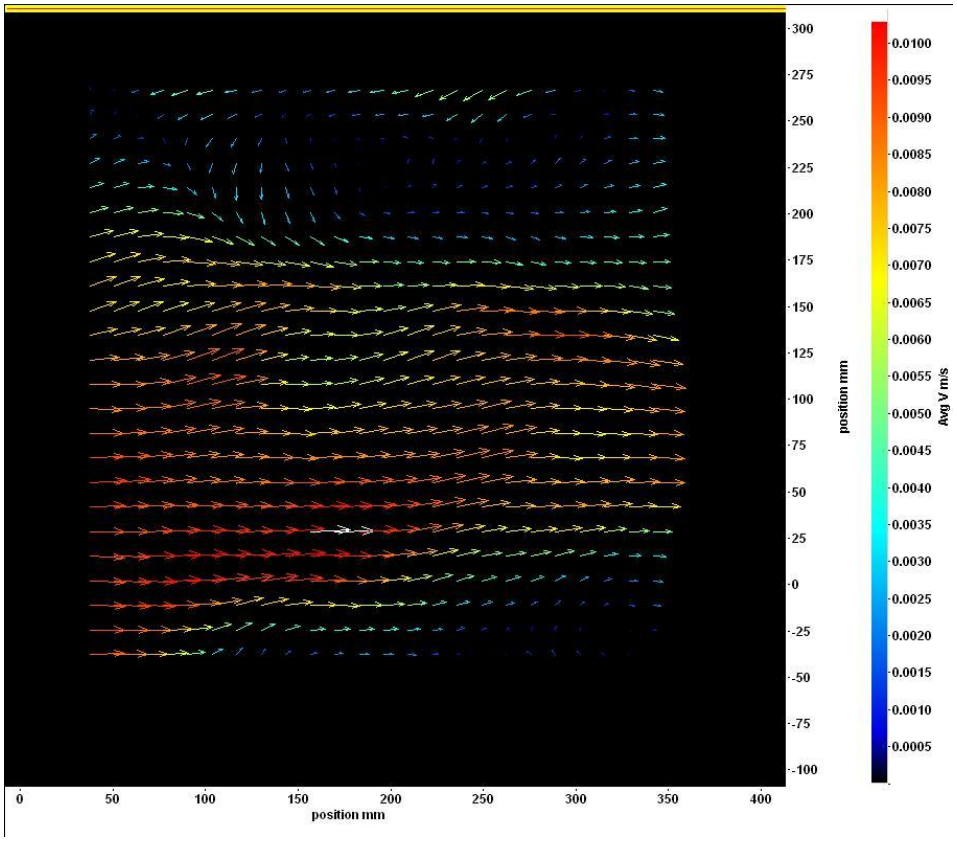

Fig (3.15): Average velocity field at wind speed of the order of 3.6ms^{-1}

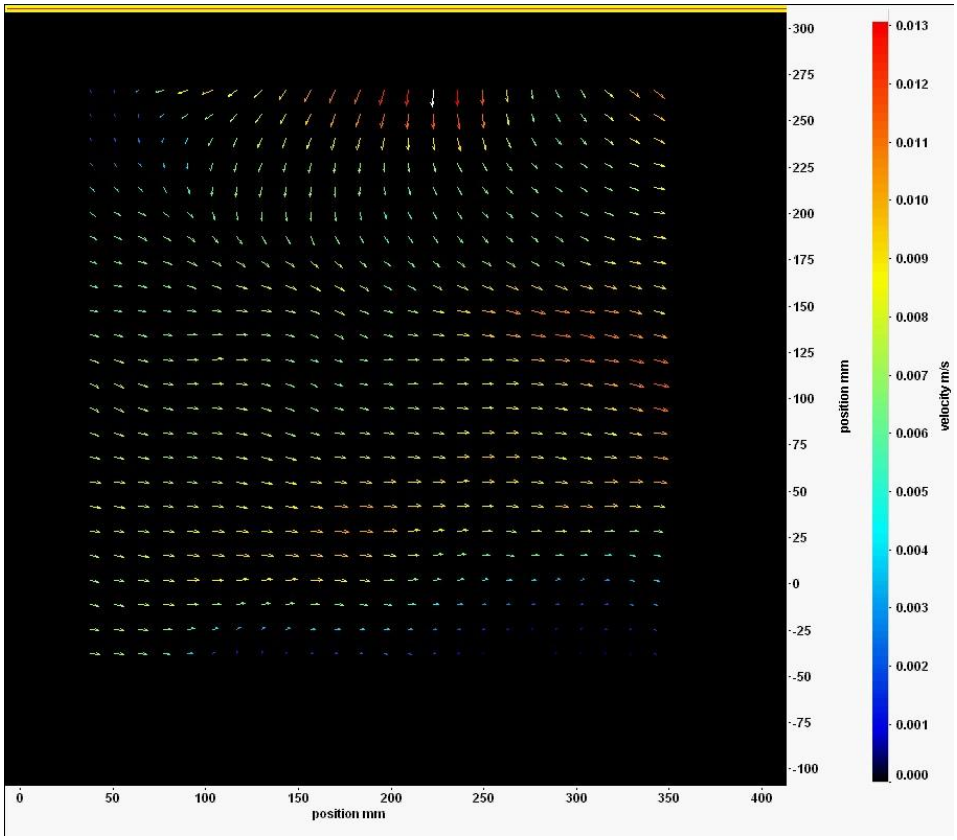

Figure (3.15a): After zero seconds from the beginning of the movie

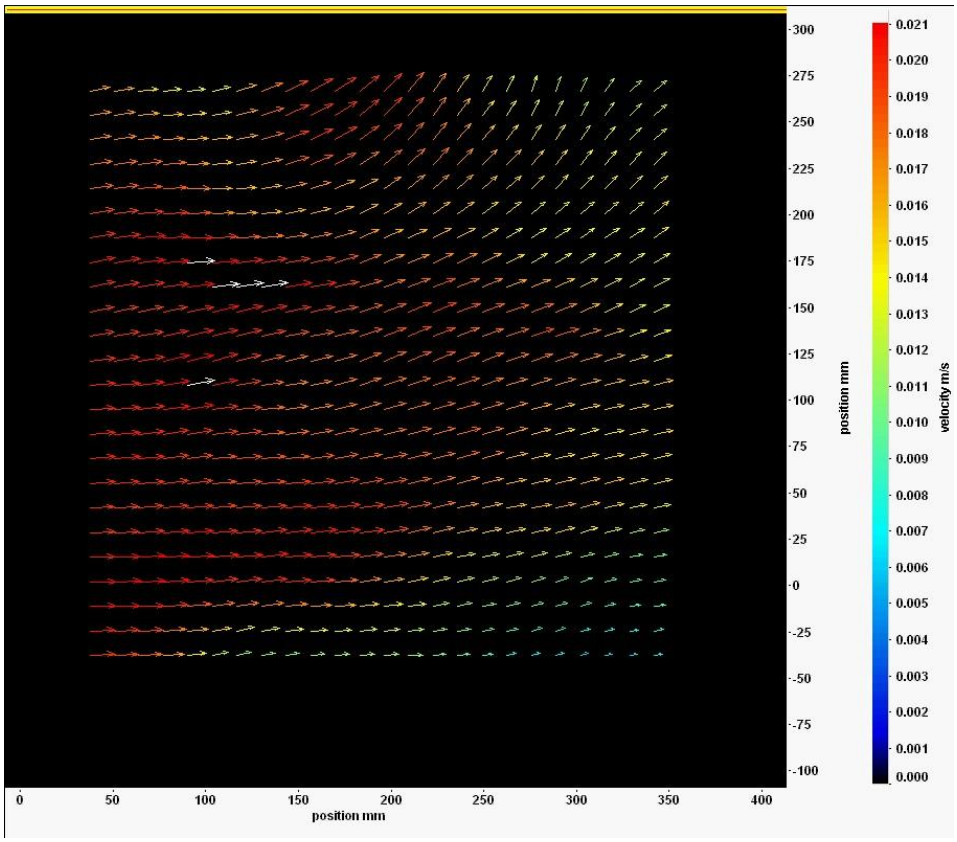

Figure (3.15b): After 2.71 seconds from the beginning of the movie

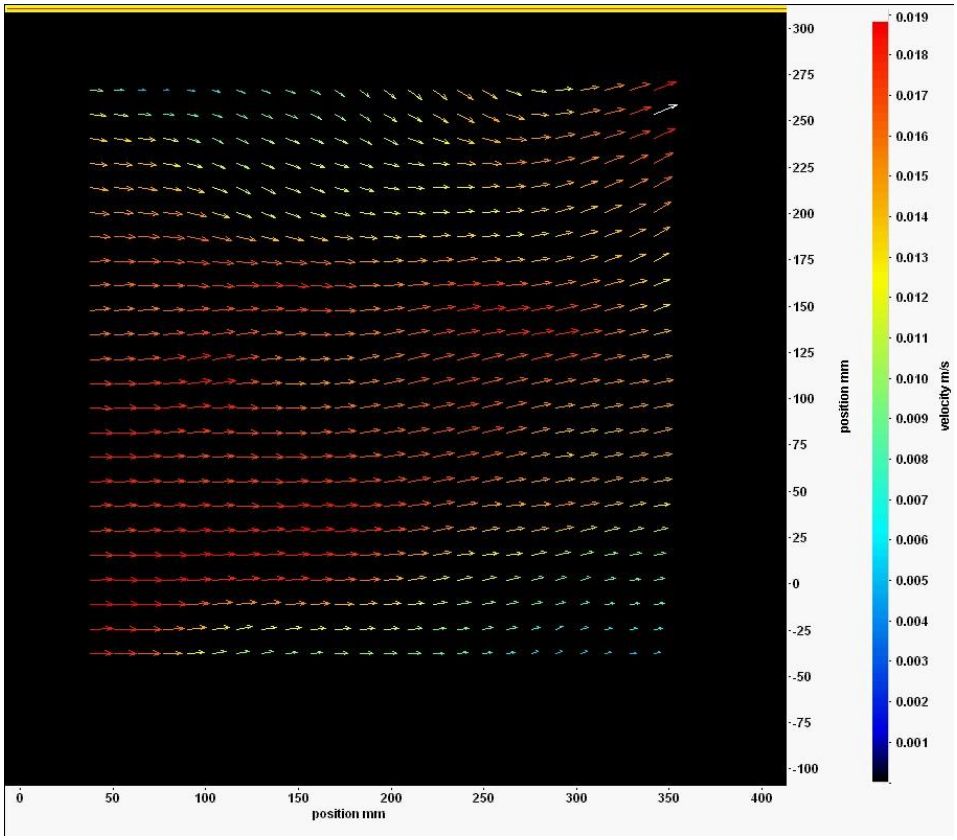

Figure (3.15c): After 5.42 seconds from the beginning of the movie

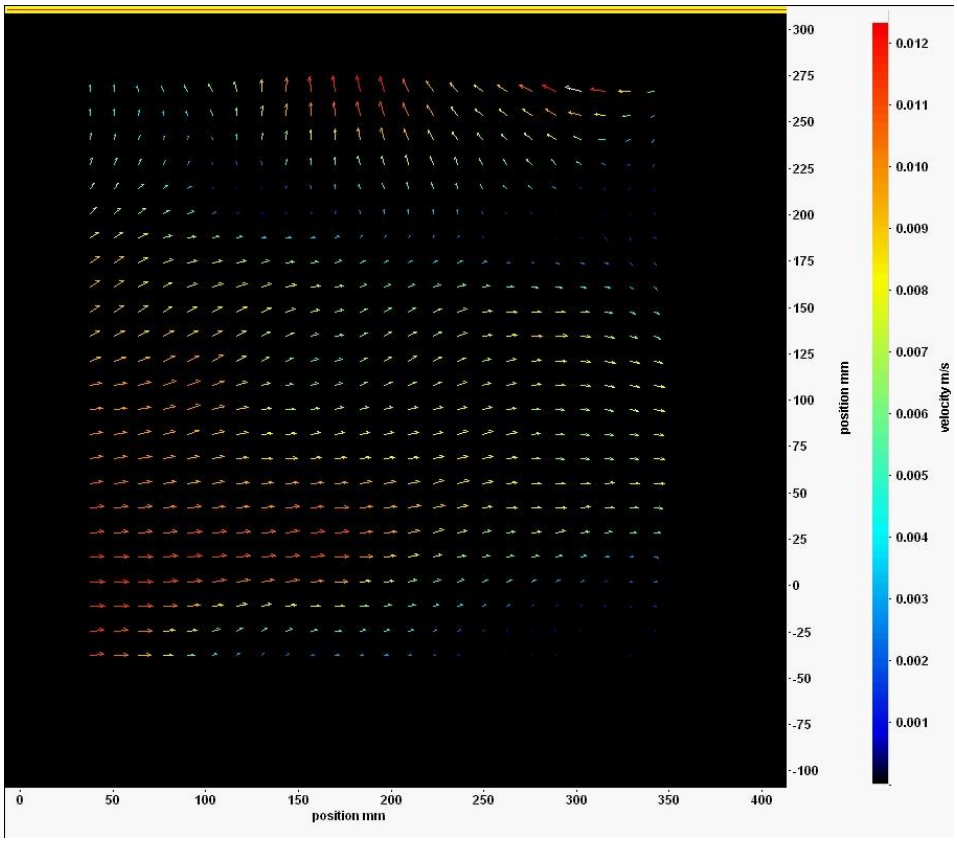

Figure (3.15d): After 8.14 seconds from the beginning of the movie

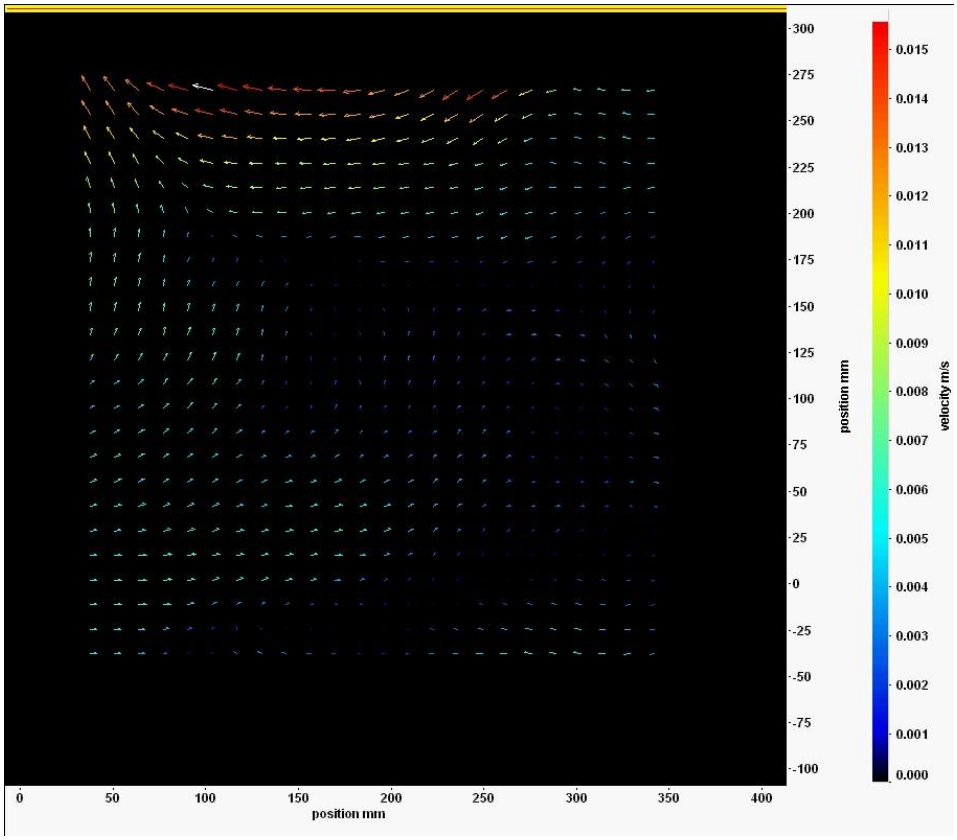

Figure (3.15e): After 10.85 seconds from the beginning of the movie

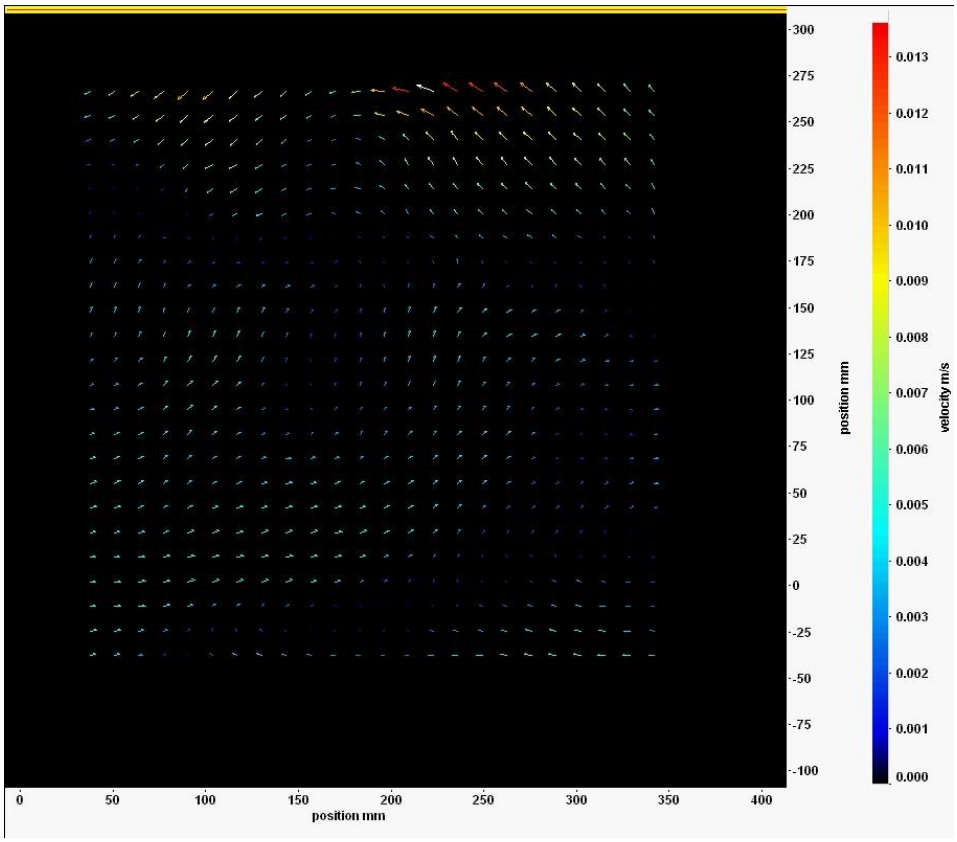

Figure (3.15f): After 13.57 seconds from the beginning of the movie

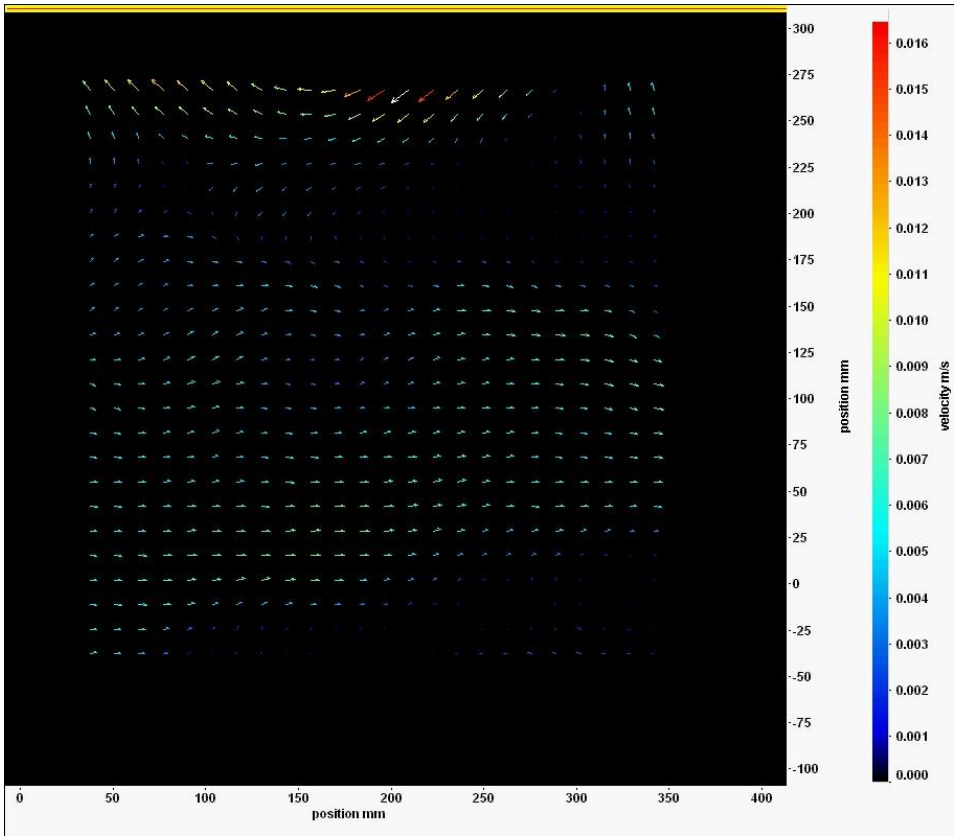

Figure (3.15g): After 16.28 seconds from the beginning of the movie

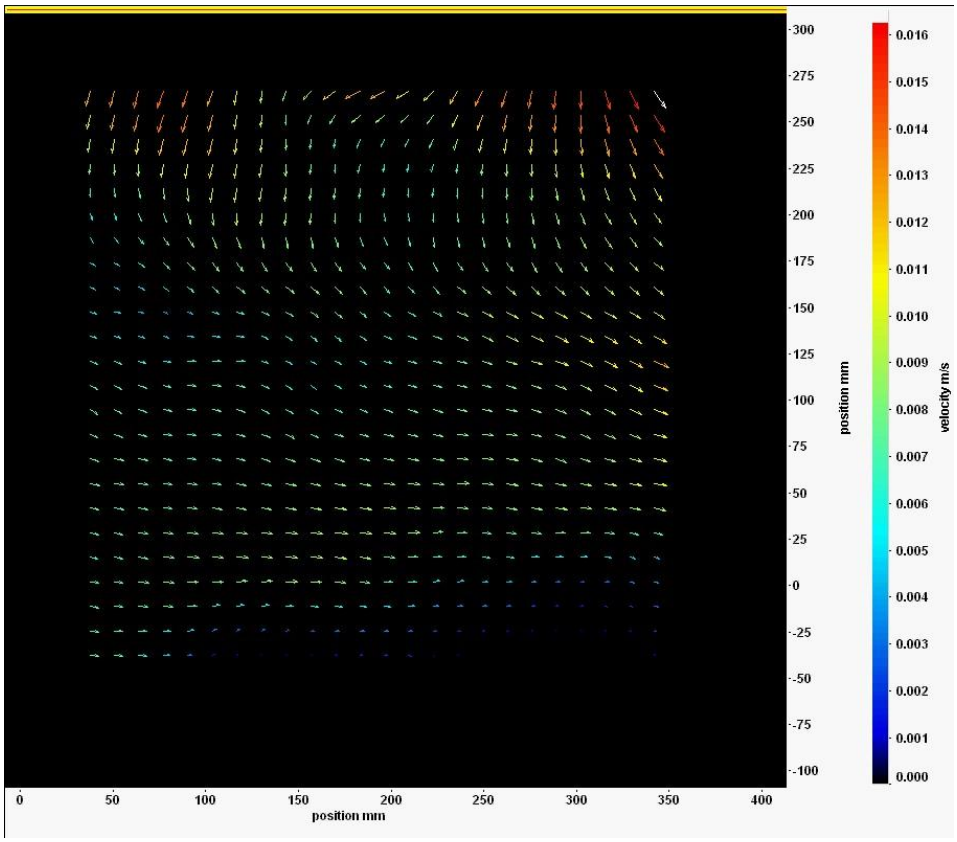

Figure (3.15h): After 19 seconds from the beginning of the movie

A significant increase in the average bulk flow velocity is observed as the wind speed attained the magnitude of the order 4.5 ms^{-1} in comparison with the first set at the corresponding speed. Figure (3.16) shows the average flow velocity at the current speed; two distinct flow directions can be observed. In the upper part of the flow, the flow follows the direction of the upper eddies; however, the lower part follows the direction of a large eddy located near the bottom. These flows in the bulk cause a significant increase in the turbulence fluctuations particularly at higher flow velocity. The movie sequence for the bulk evolution at the current wind speed is made up of images obtained at different times. Figures (3.16a-h) outline the bulk flow evolution sequence.

A significant increase in the flow velocity, particularly near the surface, and formation of an eddy in the middle of the flow is observed in Figure (3.16a). The flow obtains two distinct directions as new eddy formations start near the surface as shown in Figures (3.13b-c). Figure (3.16d) shows a similar view of an average flow velocity, Figure (3.16), but with a higher flow velocity. The two distinct flow directions which are separated by a line of eddies are obvious in the upper parts in Figure (3.16) and (3.16d).

A significant increase in the flow velocity and turbulence particularly near the surface with a significant change in the flow direction can be observed in Figures (3.16e-h).

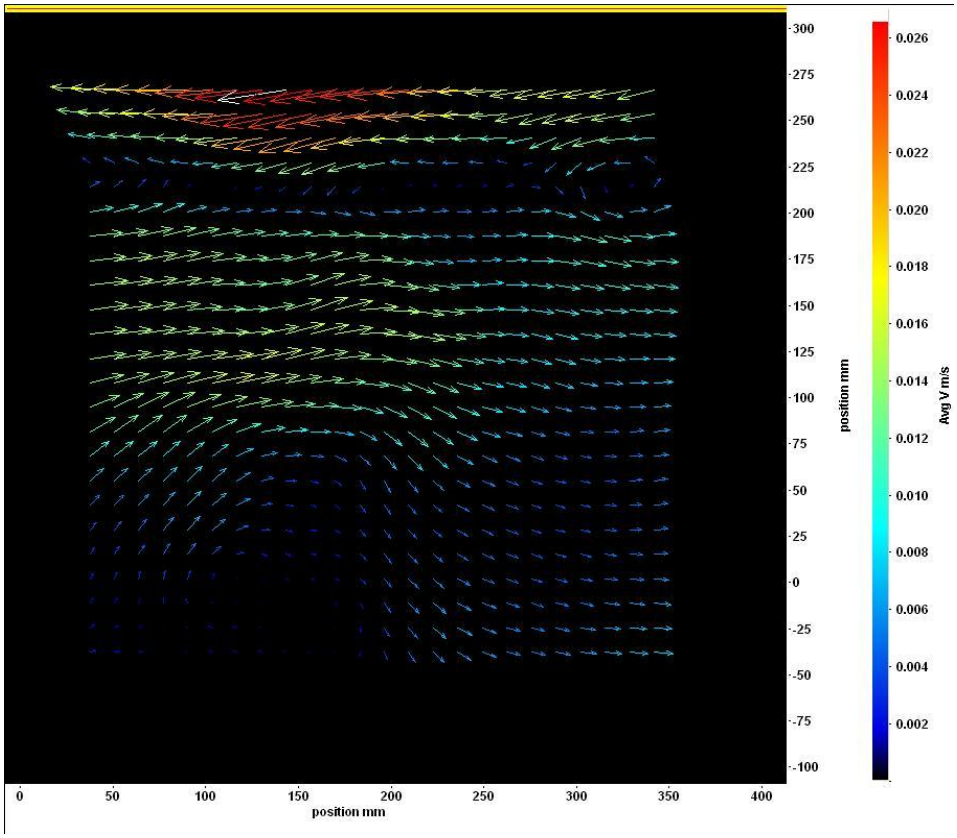

Figure (3.16): Average flow velocity field at wind speed of the order 4.5 ms^{-1}

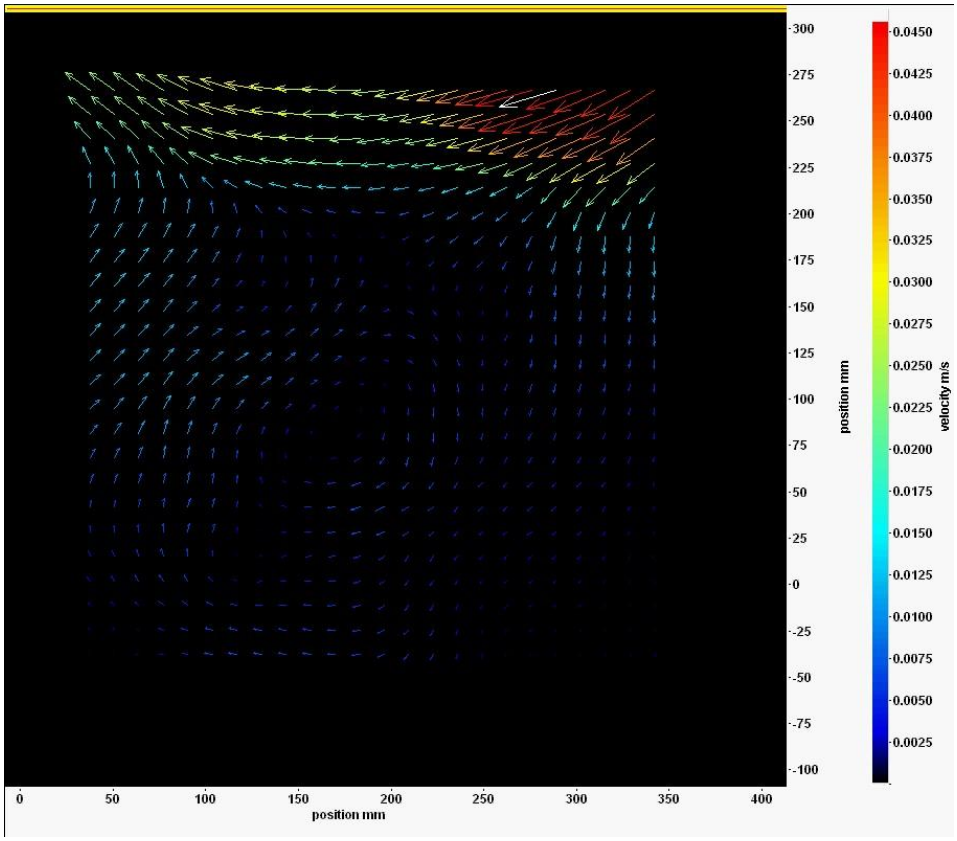

Figure (3.16a): After zero seconds from the beginning of the movie

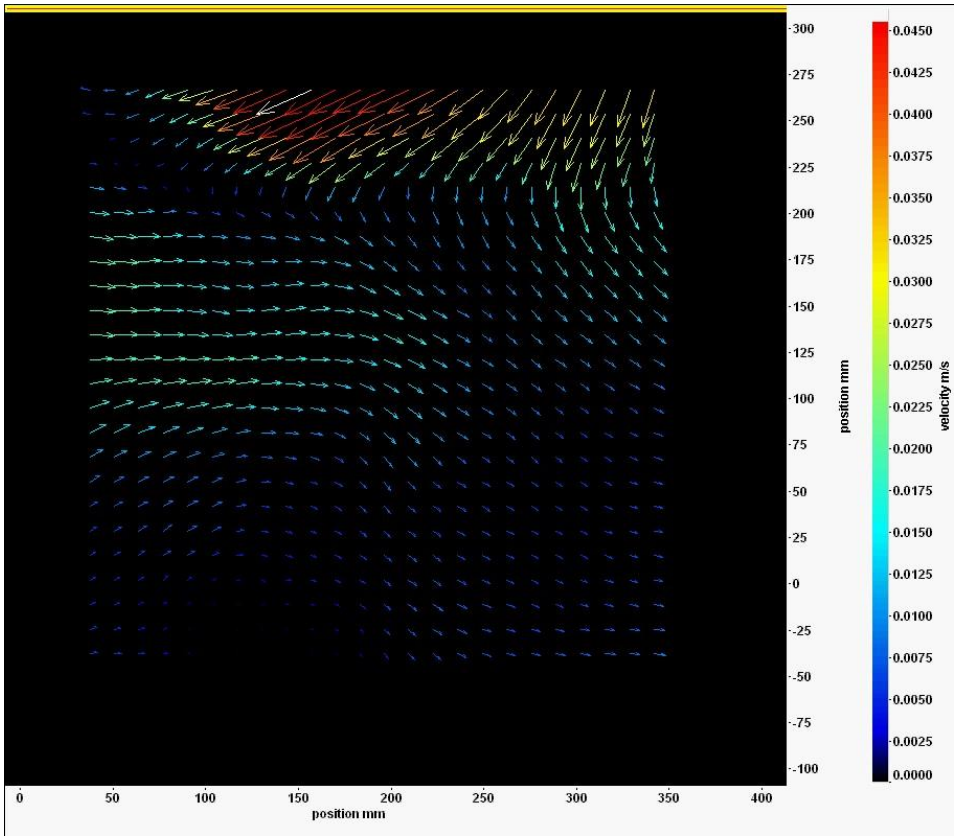

Figure (3.16b): After 2.17 seconds from the beginning of the movie

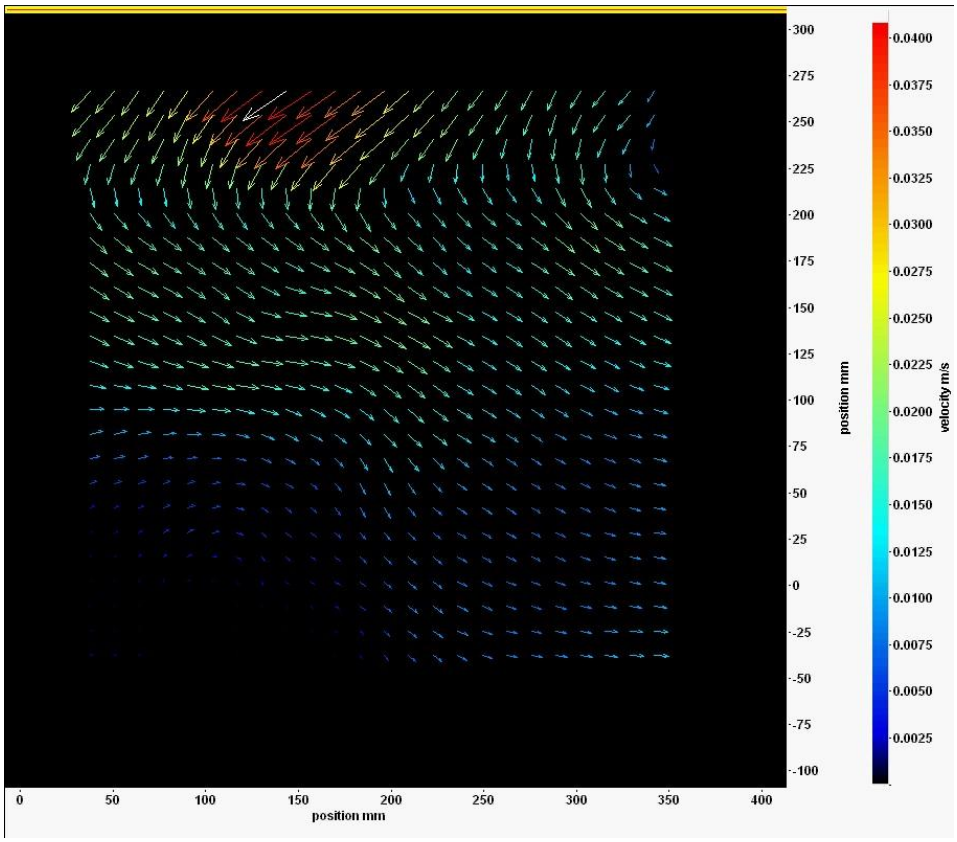

Figure (3.16c): After 5.42 seconds from the beginning of the movie

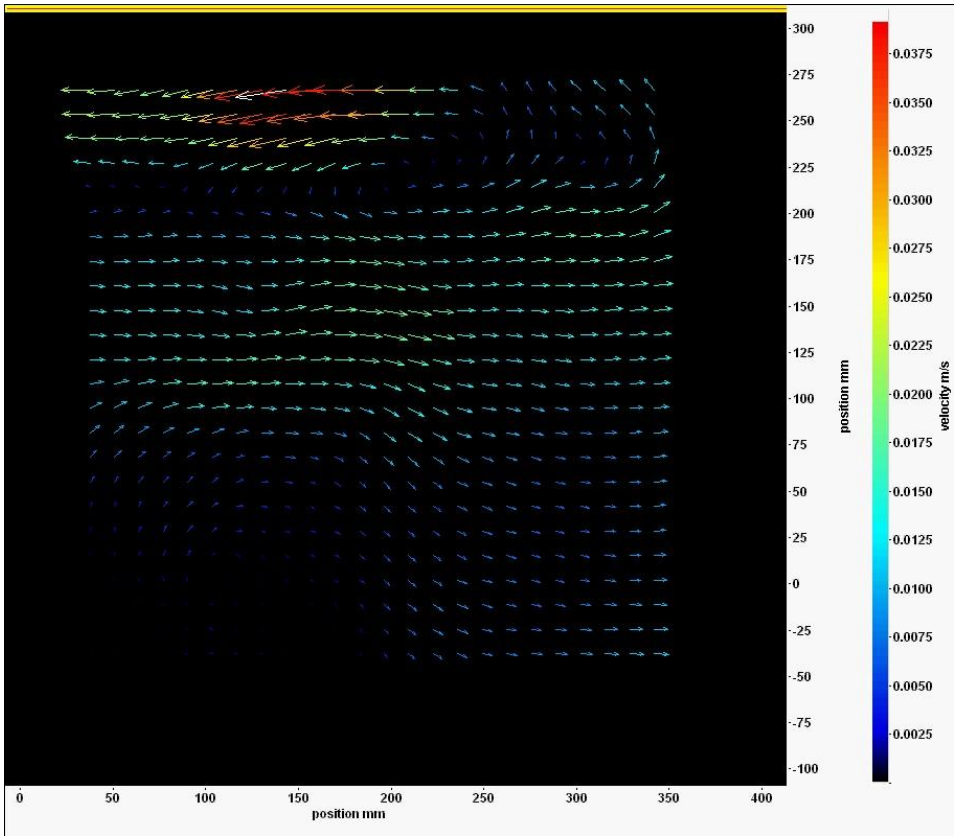

Figure (3.16d): After 8.14 seconds from the beginning of the movie

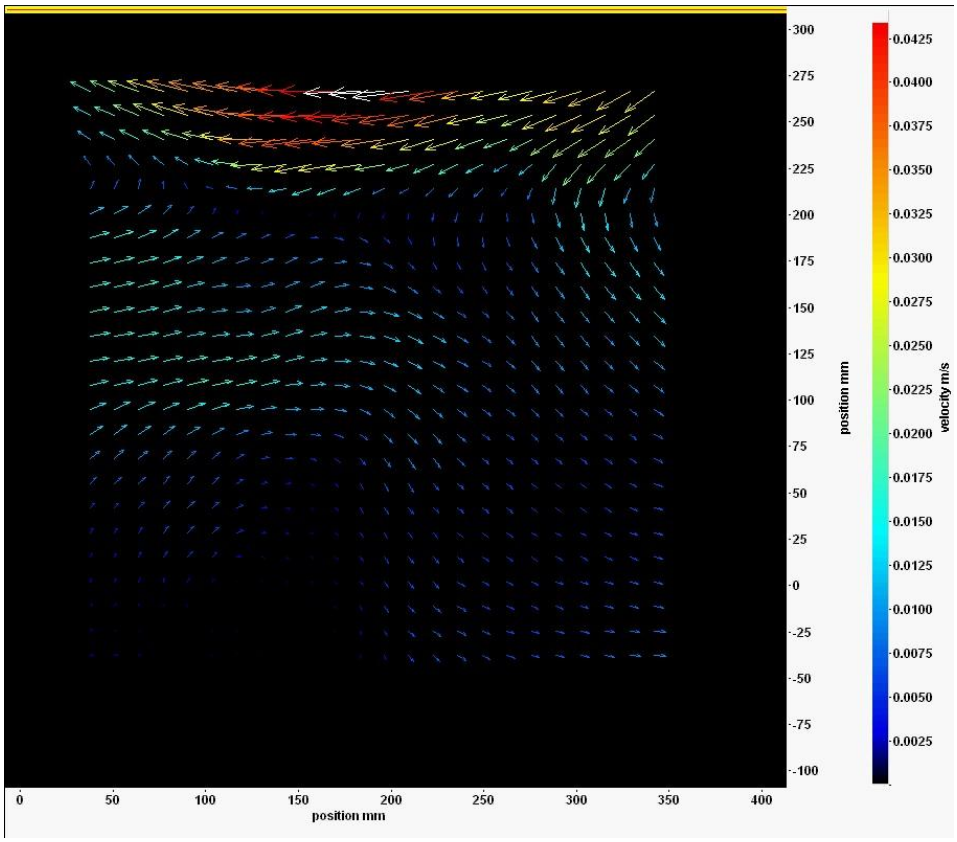

Figure (3.16e): After 10.85 seconds from the beginning of the movie

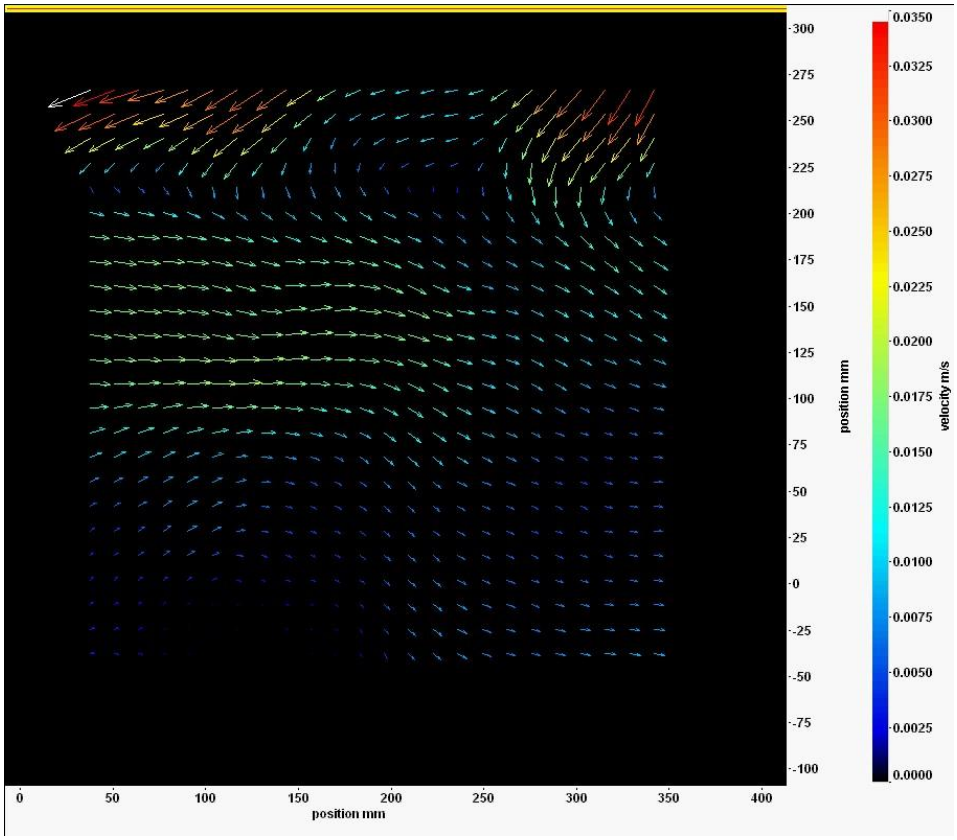

Figure (3.16f): After 13.57 seconds from the beginning of the movie

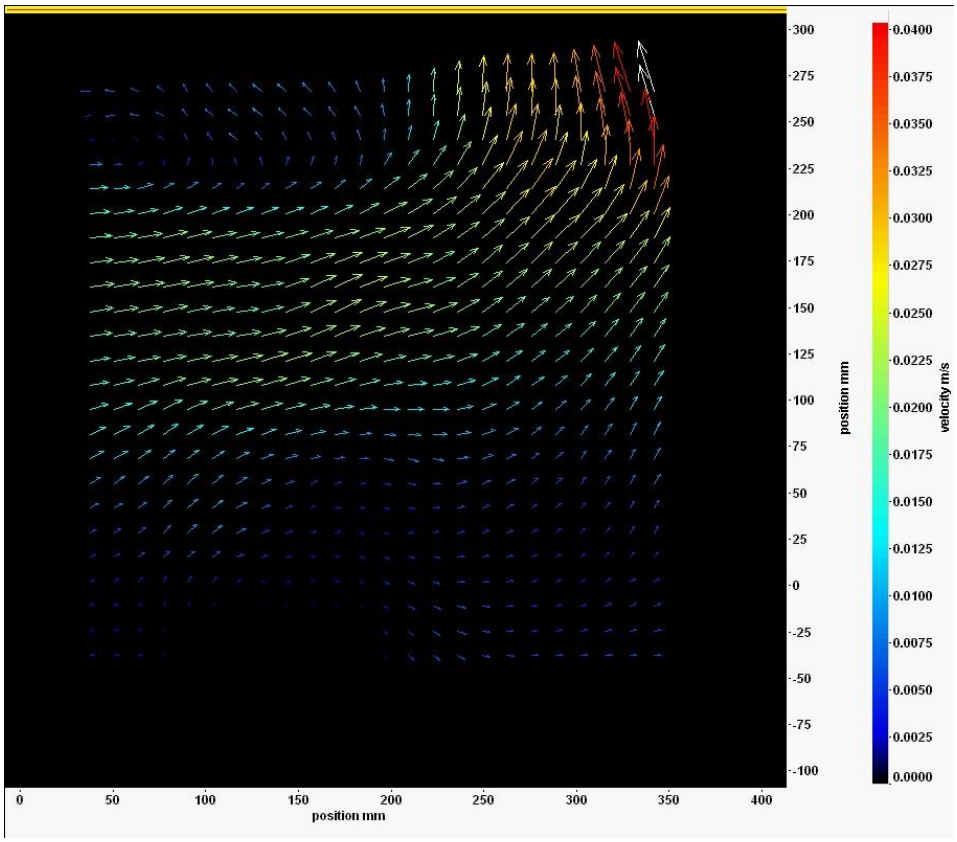

Figure (3.16g): After 16.28 seconds from the beginning of the movie

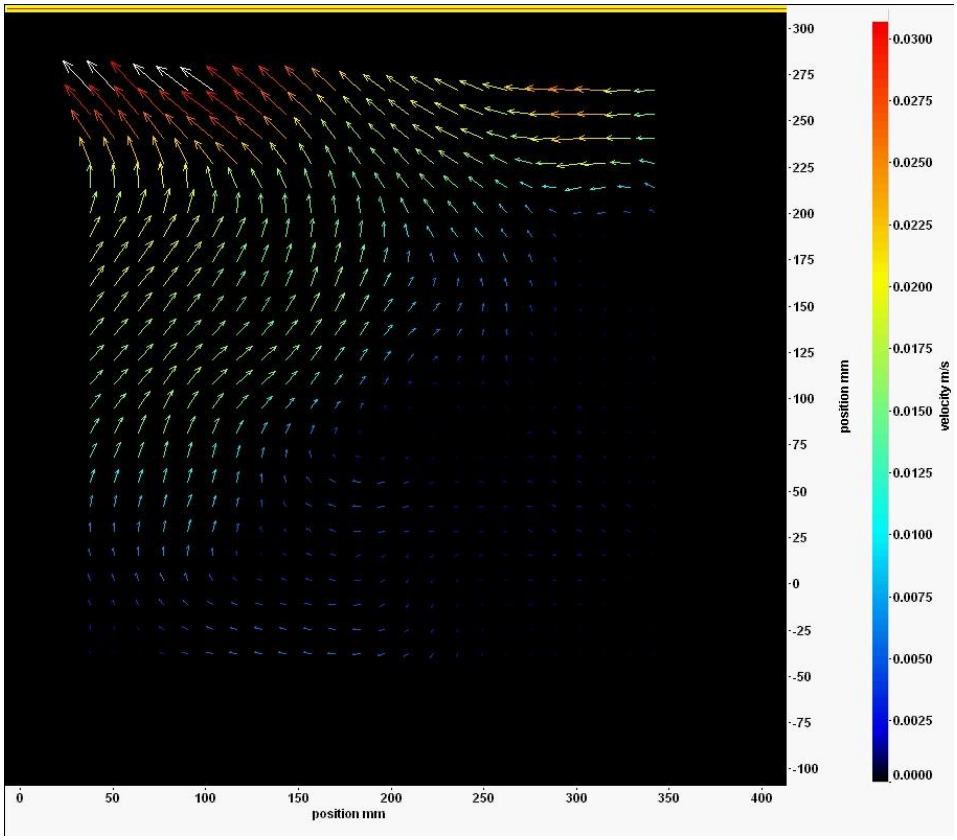

Figure (3.16h): After 19 seconds from the beginning of the movie

Both velocity fields in the first set, as shown in Figures (3.5-3.10), and the second set, as shown in Figures (3.11-3.16), are related to two different experiments. The experiments were conducted under the same conditions (wind speed, water depth, fetch length, etc) except the density of the background perturbations were different; the initial flow velocity was used to characterise the initial background perturbations.

The dimensionless number that can be used to judge the effect of the background perturbations on the bulk flow evolution is Reynolds number. Since the water depth, water density and dynamic viscosity of the water are approximately constant, the only parameter that affects the magnitude of the Reynolds number is the mean flow velocity. Reynolds number for the two sets is estimated based on the mean flow velocity using equation (3.1) and the results are tabulated in Table (3.3). The magnitude of the water density, water depth and dynamic viscosity in equation (3.1) was considered as 1000 kgm^{-3}, 45 cm and 0.001 $P_a s$ respectively. The Reynolds number (Re) determines the ratio of the inertia forces to viscous forces and scales the flow regime. The magnitude of Reynolds number that determines the flow regime depends on the definition of the Reynolds number parameters and the field of

application. For instance U_m in equation (3.1) may be defined as mean flow velocity, friction velocity, etc. and h_w may be defined as pipe diameter for the flow in the pipes or channel depth for the flow in the open channels, etc. In the current results, Reynolds equation parameters of ρ_w, h_w, U_m *and* μ_w are defined as water density, water depth in the channel, mean flow velocity and dynamic viscosity of water bulk respectively. The mean flow velocity was estimated for the two sets by dividing the average velocity field images into five equal parts from the bottom to the top; the average velocity in each part was estimated using the scale on the right side of each flow velocity image. Then the mean value was calculated manually.

$$Re = \frac{\rho_w h_w U_m}{\mu_w} \quad \text{..... (3.1)}$$

Table (3.3) shows the values of Reynolds number for the first and the second sets

Wind speed ms^{-1}	Reynolds Number (set one)	Reynolds Number (set two)
0	450	2360
1.07	540	821
1.92	951	1129
2.73	1406	2090
3.6	2428	3300
4.5	2880	4266

As shown in Table (3.3) the magnitudes of the Re number for the first set increase gradually as the wind speed increases and the maximal magnitude occurs as the wind attains the maximal speed.

Broadly the magnitudes of the Re number in the second set followed the same trend as the first set as the wind speed increased from 1.07 to 4.5 ms^{-1}. However, when the wind speed was approximately zero the magnitude of the Re number for the second set was approximately five times the corresponding magnitude for the first set. As shown in Table (3.3) the magnitudes of the Re number for the second set are higher than the corresponding magnitudes for the first set. These results show the importance of the background perturbation of the bulk flow on Reynolds number and in the flow regime, which significantly affects the growth of the wave energy. Based on this

analysis the trend of the surface wave energy growth at a particular wind speed can be predicted, based on the knowledge of the bulk perturbations density. As the flow attaining higher magnitudes of background perturbations in absence of the wind action, a higher wave growth is expected as the wind attains different orders. The duration of every run in the two sets was 19 sec and the other conditions such as the water level, ambient temperature, water density, viscosity.etc, during the experiments were unchanged. The other experiments observations showed a consistence with the above observations. It should be noted that it is not possible to repeat the same experiment with the same background perturbations. The water bulk attains different magnitudes of background perturbations based on the initial condition of the experiment.

To give a better understanding of the wind-wave generation phenomenon as the bulk attains different magnitudes of background perturbations, the term of *kinetic-energy densities* proposed by Helmholtz (1888) is used here. Darrigol (2005) reported 'Helmholtz had seen stratified and whirling clouds that directly suggested the analogy between atmospheric and sea waves. By similarity argument, he showed that the scale of the waves varied as the square of wind velocity, and that similar waveforms occurred when the ratio of kinetic-energy densities of two media was the same in the reference system for which the waves are stationary'. According to Darrigol these rules imply that the typical atmospheric waves in the atmosphere are much larger than waves on the ocean, since the ratio density is much smaller in the atmospheric case. For example, waves of one meter in length in the ocean correspond to waves of about two kilometres in length between two layers in the atmosphere under the same wind (relative velocity) and with a temperature difference of 10° C. The ratio of kinetic energy density of water and air, ζ, for the two sets of the above experiments were calculated based on the equation (3.2). Table (3.4) shows the magnitudes of U_m and ζ for the two sets as $U_{1.2}$ vary from 1.07 to 4.5 ms^{-1}.

$$\zeta = \frac{\rho_w V^2}{\rho_a U_{1.2}^2} \quad \text{..... (3.2)}$$

Where ρ_w, ρ_a are water density and air density respectively.

Table (3.4): The ratio of kinetic-energy density of water and air for the two sets of the current experiments with different background perturbations.

$U_{1.2}$ ms^{-1}	V ms^{-1} (set 1)	V ms^{-1} (set 2)	ζ (set 1) %	ζ_2 (set 2) %	ζ_1/ζ_2
1.07	1.2 x 10^{-3}	1.83 x 10^{-3}	0.105	0.243	0.43
1.92	2.11 x 10^{-3}	2.51 x 10^{-3}	0.10	0.142	0.7
2.73	3.12 x 10^{-3}	4.65 x 10^{-3}	0.108	0.242	0.45
3.6	5.4 x 10^{-3}	7.33 x 10^{-3}	0.187	0.35	0.53
4.5	6.4 x 10^{-3}	9.48 x 10^{-3}	0.168	0.37	0.45

The magnitude of ζ for the two sets exhibits a significant increase at wind speed of the order of 3.6 and 4.5 ms^{-1}. However, the minimum magnitude of ζ occurs at the wind speed of the order 1.92 ms^{-1} for the first and the second set. The reduction in magnitude of ζ at this speed is justified due to the transition in the flow direction with respect to the wind direction which may reduce the flow velocity and thus the magnitude of the *kinetic-energy density*. A significant increase in magnitude of ζ occurs as the flow regime transition from laminar to turbulence is completed. According to the data in Table (3.3) and (3.4) the flow transition is completed at wind speeds of the order 2.73 and 1.92 ms^{-1} for the set one and set two respectively. Broadly, the magnitudes of ζ for the second set are higher than for the first set and the ratio of ζ_1/ζ_2 is approximately 0.5 except for wind speed of 1.92 ms^{-1}. The above estimation of the magnitude of ζ water verifies the importance of the background perturbation on the kinematics and dynamics of the flow and consequently the surface wave formation and evolution under effect of the wind action. The higher magnitudes of ζ indicate an increase in bulk perturbations due to wind momentum flux. The density of the bulk perturbation and therefore the growth of surface energy can be predicted based on the knowledge of ζ. As the magnitude of ζ increases, the bulk perturbations increase and make the flow and the surface much more appropriate for the generation and growth of the eddies and waves.

These results may justify the discrepancy in the estimation of the magnitude of critical wind speed (the minimum wind speed required to generate visible waves) between real field observations and laboratory observations. Based on the above discussion the magnitudes of critical wind speed at real fields should be lesser than the laboratory observations due to the presence of natural background perturbations. The latter occur due to interface lamina formation, bulk-surface temperature difference, bulk-surface

density difference and the extent of the water body. This conclusion is consistent with the observations shown in Chapter 1.

It is proposed that the effect of the background perturbation on the growth rate of surface wave energy should be considered for generating energy from the surface wave, particularly in limited fetch water bodies and under the effect of moderate wind speed. The gained energy from the waves can be raised significantly by introducing perturbations into the flow field by mechanical means. This action increases the vorticity and the wave growth rate so that the energy produced by the wave energy can be increased. Also considering the effect of the background perturbation on growth rate of surface is important for reducing the scouring on water reservoir banks and beaches. The resulting scouring due to propagating the surface waves over the banks and beaches depends on the magnitude of the wave's energy. The waves transfer their energy to the banks and cause scouring when the waves propagate over the banks frequently for a long time. It is suggested that damping the motion inside the bulk near the beaches will attenuate the wave power thereby reducing the scouring effect on the banks and the beaches.

3.7 Boundary layer thickness 'water side' δ_w

The boundary layer thickness is defined as the distance from the wall where the velocity differs by one percent from the external velocity. This definition is applicable when the air flows over a solid plate. However when the air blows over a water surface, two boundary layers can be defined: the first according to the above definition (wind side) and the second is related to the water side. The latter is defined based on the ratio between $U_\circ$ and V_z, where, V_z, is the bulk flow velocity at a depth z from the surface. Phongikaroon and Judd (2006) proposed that the boundary layer thickness is determined where the velocity drops to 10% of its surface value ($V_z = 0.1U_\circ$). Phongikaroon and Judd measured the velocity field in a water tank of a dimension ($35\ cm \times 10.4\ cm \times 10.4\ cm$) constructed and fitted to a wind tunnel. The wind speed was 5.1 ms^{-1} and the PIV measuring zone was located at 8.1 mm from the upstream leading edge of the water tank. They estimated the δ_w from the velocity field images using the PIV system under the effect of the above conditions. According

to their definition δ_w was 19 cm from the water surface where the bulk flow velocity was dropped to $0.1U_\circ$. Since the velocity profile in the bulk changes continuously due to the generation and propagation of the bulk vorticies, it is suggested estimating the δ_w based on the magnitude of V_{RMS} (root mean square of the bulk velocity) since V_{RMS} showed less fluctuation than V under effect of wind action. From the results of the V_{RMS}, δ_w can be determined by visual inspection. V_{RMS} is calculated for the given number of vector fields using the equation:

$$V_{RMS} = \sqrt{1/n \sum_{i=1}^{n} (V_i - V_{avg})^2} \quad \text{(3.3)}$$

V is calculated for the given number of vector fields according to the equation $V = 1/n \sum_{i=1}^{n} V_i$ where n is the number of the captured images . Figures (3.17-19) show the V_{RMS} for velocity fields at three different wind speeds and Figures (3.17a-3.19a) visualize the V_{RMS} field images. Figures (3.17-19) and (3.17a-3.19a) show the occurrence of the boundary layer in the water channel under the effect of wind action. The boundary layer thickness can be determined from visual inspection for the V_{RMS} field's images and visualization images. The drop in the velocity is readily apparent in these figures. The exact definition of the boundary layer thickness suggested by Phongikaroon et al cannot be applied to the current experiments due to differences between the facilities of the current experiments and their experiments. These differences involve the structure of the experimental field, the location of the PIV measuring zone with respect to the leading edge of the wind tunnel and the applied wind speed. Also, Phongikaroon used the PIV velocity field in the water tank to determine the boundary layer thickness while the current study used the RMS of the velocity fields. Also, due to restrictions of the water channel structure that were used in the current experiments, velocity measurement close to the surface was not possible. The maximal height of the velocity fields was 10 cm beneath the surface.

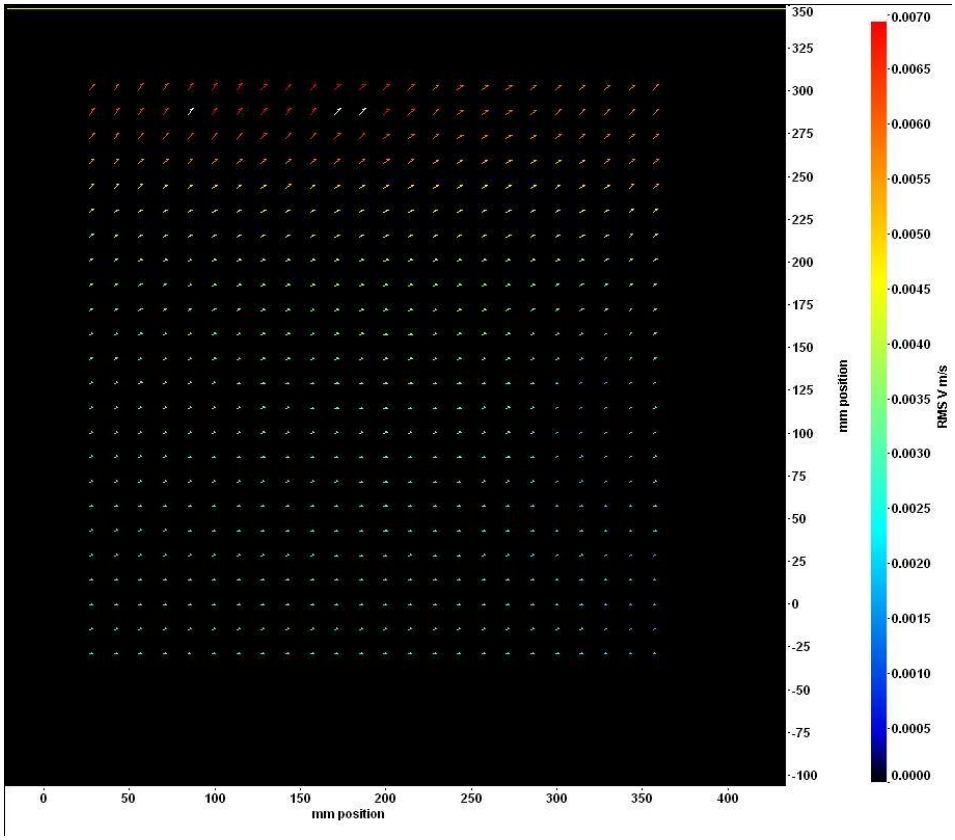

Figure (3.17): V_{RMS} of velocity field at a wind speed of the order 2.73 ms^{-1}

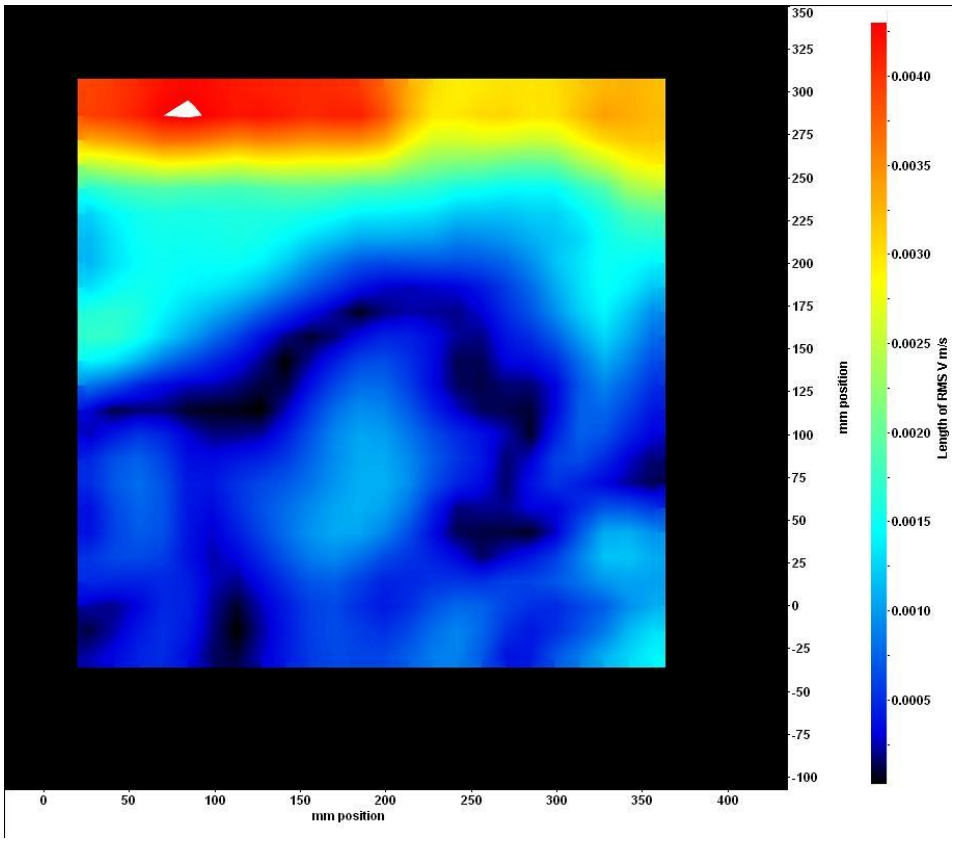

Figure (3.17a): visualization image based on the magnitude V_{RMS} at a wind speed of 2.73 ms^{-1}

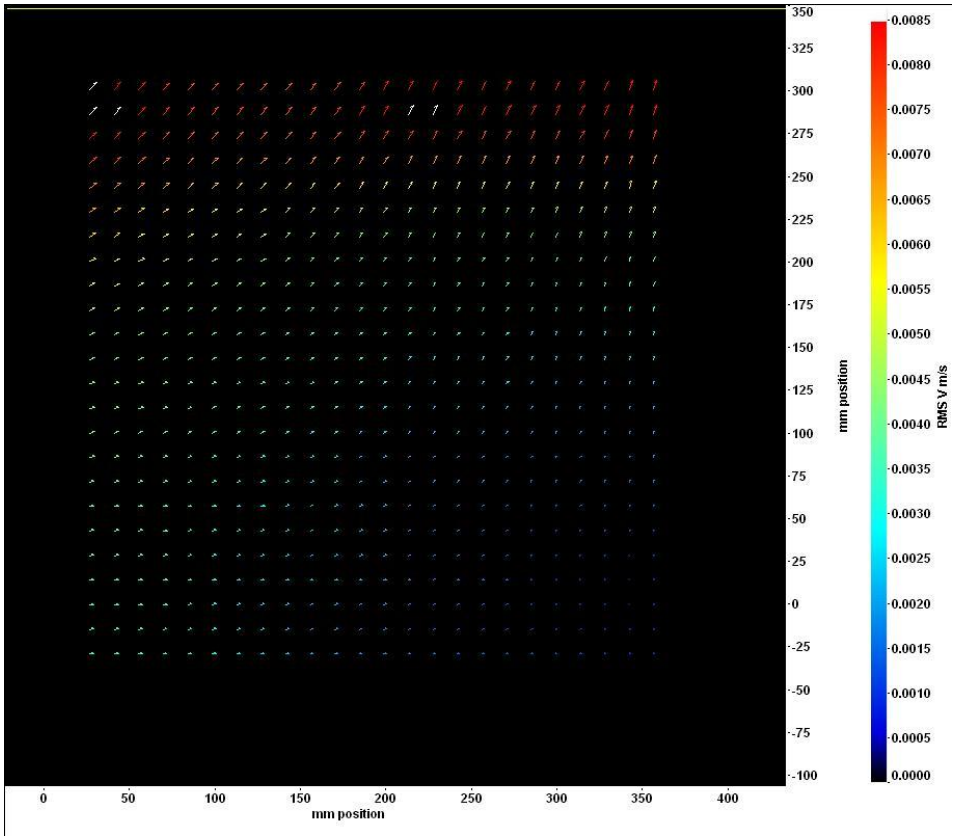

Figure (3.18): V_{RMS} of velocity field at a wind speed of the order 3.6 ms^{-1}

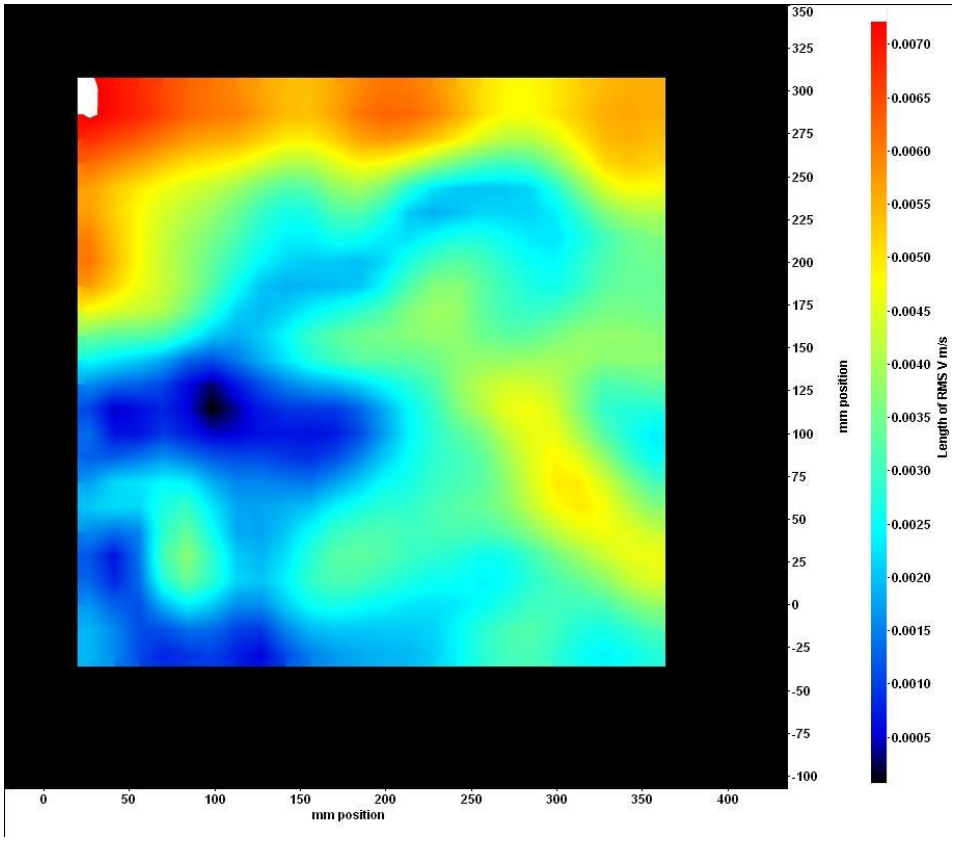

Figure (3.18a): Visualization image based on the magnitude V_{RMS} at a wind speed of the order 3.6 ms^{-1}

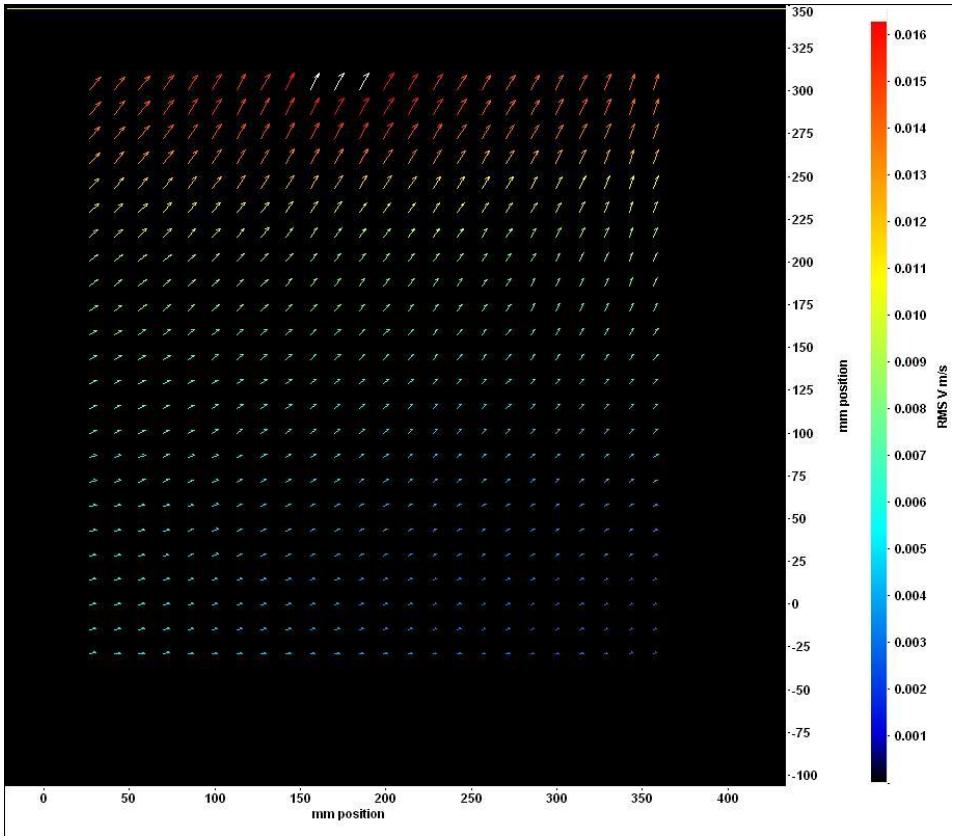

Figure (3.19): V_{RMS} of velocity field at a wind speed of the order 4.5 ms^{-1}

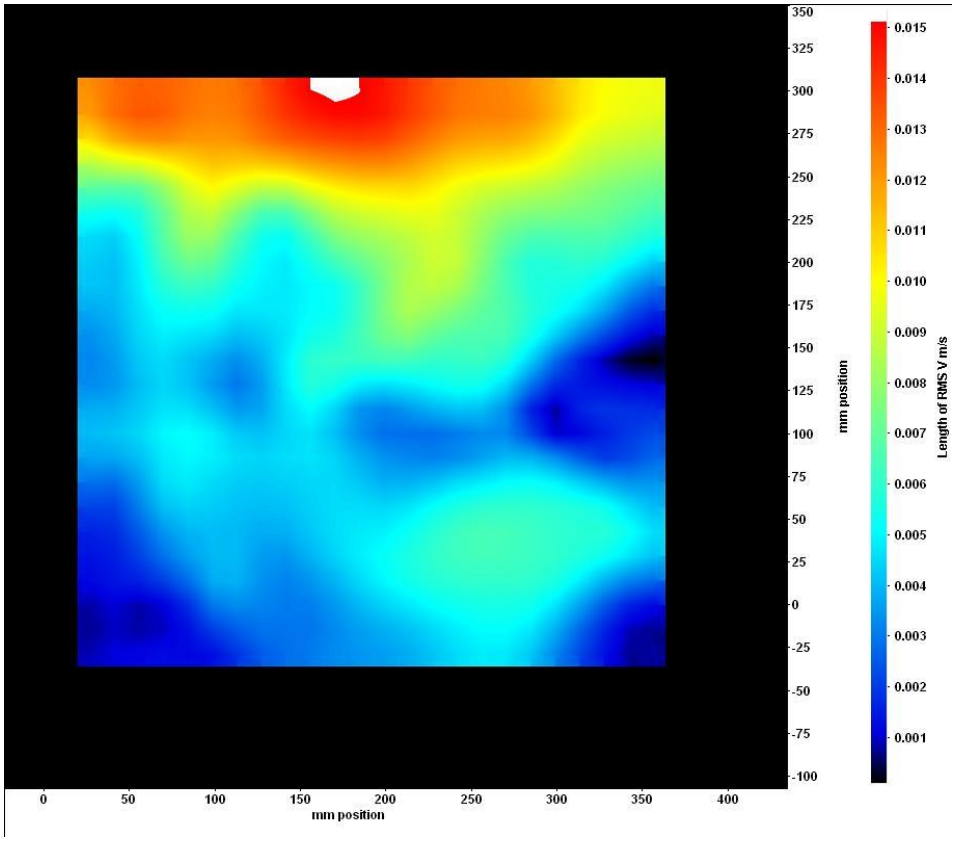

Figure (3.19 a): Visualization image based on the magnitude V_{RMS} at a wind speed of the order 4.5 ms^{-1}

In order to determine the δ_w based on the ratio between the bulk flow velocity and surface velocity following the suggestion of Phongikaron and Judd, the surface velocity is estimated. The empirical formula of Fitzgerald (1963) as $U_\circ = 0.03U_\infty$ is used to determine the surface velocity. The correlation between the surface velocity and the parameters that affect its value was discussed in section (1.5).

As shown in figure (3.17 and 3.17a), at a speed of 2.73 ms^{-1} the surface velocity is in the order of 0.082 ms^{-1}. At a depth of approximately 19 cm from the surface the V_{RMS} drops to 0.0035 ms^{-1} which is equivalent to $0.043U_\circ$. At a wind speed of 3.6 ms^{-1} the surface velocity is of the order of 0.108 ms^{-1} and the V_{RMS} is of the order of 0.005 ms^{-1} at approximately 19 cm from the surface, which is equivalent to $0.046U_\circ$. Finally at a wind speed of 4.5 ms^{-1}, the surface velocity is of the order of 0.135 ms^{-1} and the V_{RMS} is of the order 0.011 ms^{-1} at approximately 19 cm from the surface which is equivalent to $0.0814U_\circ$. It was noted that the V_{RMS} drop occurred at the same depth from the water surface. However, at a wind speed of 4.5 ms^{-1}, the percentage drop of field velocity with respect to surface velocity was higher than as wind speed was in the order of 2.73 ms^{-1} and 3.6 ms^{-1}. The thickness of the boundary layer that was estimated based on the V_{RMS} in the current measurements is identical to Phongikaroon (2006) estimation and the velocity drop at this depth approached the 10% of its surface velocity at higher wind speed. It can be concluded that the boundary layer thickness is approximately constant with wind speed in the current measurements. However, the drop of the bulk velocity at the boundary layer edge with respect to its surface velocity is a function of the wind velocity. This gives an indication of the correlation between wind velocity and bulk velocity which does not seem as linear. In the light of the above observations, it is suggested to define the boundary layer thickness as the water depth from the surface where a significant drop in the magnitude of V_{RMS} occurs with respect to the surface velocity. The ratio between and $U_\circ$ is proposed is a function of wind speed.

3.8 The hydrodynamics of the flow

The momentum flux from the wind to water was estimated based on the difference between wind speed and surface speed using a drag coefficient as a correlation factor

as shown in equation (1.23). The correlation between the rate of momentum flux and the induced perturbation can be inferred from the evolution of the bulk flow parameters such as instantaneous velocity (flow velocity) *V*, Vorticity, *Rot (z)* Swirling strength S_w, Shear strength τ_s, and Velocity vector angle, α. These parameters attain higher values as the flow perturbations increase due to the increase in the transfer of the wind momentum. The correlation between these parameters and wind speed will be discussed below and in Chapter 4.

To explore the kinematics and dynamics of the flow under the effect of the wind action that blows steadily over the water surface at different speeds, the following properties of the flow that are extracted from the PIV measurements will be discussed and analysed.

- Average of instantaneous flow velocity fields, V
- Velocity vector angle, α
- Vorticity, *Rot (z)*
- Swirling strength, S_w
- Shear strength, τ_s
- Swirl and shear, $S_w and \tau_s$

To show more clearly the effects of the wind speed on the evolution of the bulk flow, the velocity field images were imported using Tecplot software to generate plots. The PIV measuring zone was located at (1.52) m from the upstream leading edge of the water channel F1, and the wind tunnel fan was set at six positions to generate wind with six different speeds. The following figures and analyses are related to the data collected at F1 (the same conditions of the first set of the velocity field that discussed in section (3.6)

3.8.1 Average of instantaneous flow velocity fields

The velocity fields were recorded at six different wind speeds for 19 seconds each. The average of the velocity, ($\boldsymbol{V}$) , of each recording was calculated as $\boldsymbol{V} = 1/n \sum_{i=1}^{n} V_i$ Figure (3.20) shows the relationship between the flow velocity and the position along the water channel at different wind speeds. It should be noted that each curve in the following figures was plotted based on more than 2000 data points which made it difficult to show the data points in the following figures.

The PIV measure was located at F1 and instantaneous flow velocity V_i s calculated according to the equation.

$$V_i = \sqrt{Vx_i{}^2 + Vy_i{}^2} \quad \text{.....} \quad (3.4)$$

As shown in Figure (3.20) the average flow velocity increases steadily when the wind speed increases from zero to 2.73 ms^{-1}. However, at wind speeds of 3.6 and 4.5m/s, the increase of flow velocity reaches a peak followed by rapid decay. This is in contrast with the lower wind speeds where a plateau may be seen. The maximal flow velocity occurs at the maximal wind speed whereas at low wind speeds the flow velocity is comparatively very low. This pattern reveals the evolution of the flow under the action of steady wind, which may help in understanding the relationship between the wind speed, surface wave generation and flow evolution. It is not possible to generate surface wind waves without introducing perturbations through the flow. These results confirm the prediction of an analytical model by Teixeira and Belcher (2006) that the key stage in surface wave initiation may be immediately following laminar-turbulent transition of the flow, when the turbulence is not too anisotropic. They concluded that the turbulence in the water may be much more important for the initiation of surface waves than previously expected because the associated pressure fluctuations are much more efficient. Also these results are consistent with the experimental results of Caulliez et al (1998) that were conducted in a laboratory, which supports the idea of an 'explosive wave' - as they called it - after the transition of the flow to turbulence of shear currents induced by the wind. Explosive waves describe the abrupt growth of the initial surface wave under the action of wind. The corresponding values of Reynolds number that scale the bulk flow regime for the results of Figure (3.20) are shown in Table (3.2). The appearance of the visible wave starts at a wind speed of 2.73 ms^{-1} and the corresponding Reynolds number at this speed indicates that the flow transition to turbulent occurs at this speed.

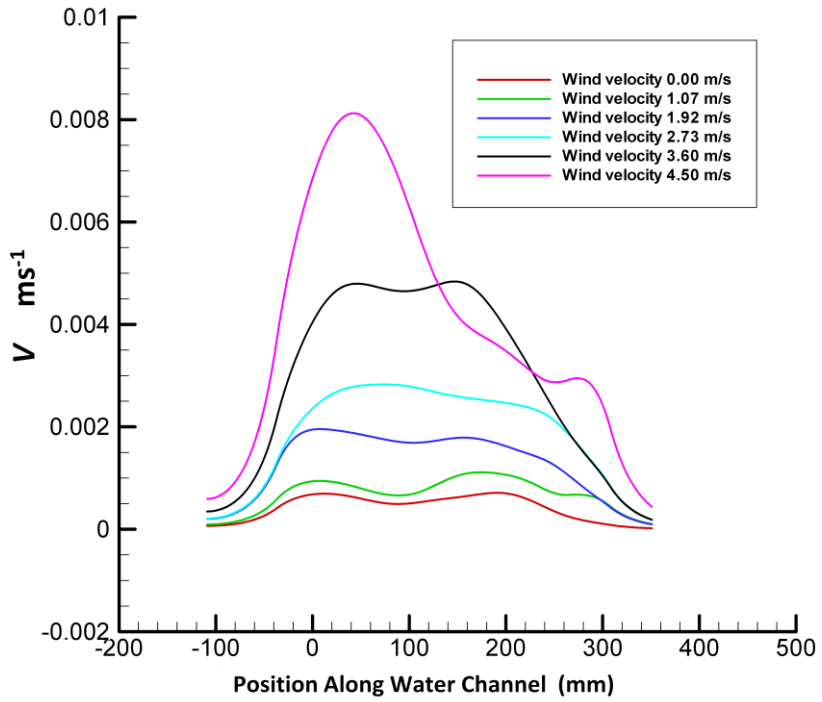

Figure (3.20): Correlation between the positions along the water channel and the average flow velocity at different wind speed.

3.8.2 Velocity vector angle (α)

Another parameter that can be extracted from the velocity fields and helps in understanding the kinematics and dynamics of the flow under the action of wind is the velocity vector angle **α**. The velocity vector angle describes the angular movement of the tracers though the bulk with respect to the axis X in the direction of the wind. The tracers showed and angular movements with respect to the axis X as the water depth increase from the surface to the bottom of the channel. The PIV velocity fields revealed that the tracers have two movements: translational (linear) and angular. In the first one the tracers propagate in different directions making a distance with respect to a reference point. In the second the tracer's particles oscillate in an angular manner making an angle with respect to the **X** axis. The angle **α** is positive in the direction of the wind and in the direction of the water surface. Figure (3.21a) shows the correlation between the velocity vectors angles and the wind speed. The maximal velocity vector angles occur where the wind speed attains the minimal and maximal magnitudes. Initially, the magnitude of velocity vector angle decays when the wind speed increases and the least magnitude occurs at a wind speed of the order 2.73 ms^{-1}. Then the velocity vector angle grows to higher values at higher wind speeds. This

sequence could be understood as a change in the movement of water particles from random movement in all directions at lower wind speeds to a confined movement following the direction of wind induced shear at higher wind speeds, or as the flow regime transition from laminar to turbulent. The purpose of analysing the velocity vector angle is to find a relationship between the flow regime (laminar, transitional and turbulent) and the magnitude of the velocity vector angle, and therefore a relationship between velocity vectors angles and the initiation of surface waves. An explosive growth of surface waves occurred after transition of the flow to turbulence. This phenomenon was observed experimentally and was proved analytically. Based on such investigations, the parameter that used to scale the flow regime transition, from laminar to turbulent, can be used to scale the transition of the water surface flow from undisturbed surface to fully developed wave. Since the velocity vector angle is a function of wind and flow velocity, it is suggested that this parameter is used to scale such a transition. A visible surface wave was observed at F1 (1.52 m from upstream edge of the water channel) at a wind speed of 2.73 ms^{-1}. The shear current induced by the wind is insignificant when the wind speed is less than of 2.73 ms^{-1}. It is supposed that the laminar -turbulent transition occurs in the flow - in the current measurements - as the magnitude of velocity vector angle attains the minimum magnitude. At this angle the water particle movements translate from random behaviour to directed movement by the induced wind shear and eddies. In these conditions the surface waves start to be visible. The other experiments conducted in similar conditions to the current experiments showed that the laminar-turbulent transition occurred when the waves became visible, and this occurred as the wind speed approached 3 ms^{-1}. The previous and current observations of wind speed where the waves become visible were taken as reference points to estimate when the laminar-turbulent flow transition occurred.

Figure (3.21b) illustrates the relationship between the velocity vector angle (α) and the water height (h_w). The water height was measured from the bottom of the channel and was divided into seven parts from the bottom of the channel up to depth close to the water surface. Each part represents the flow at a particular depth in the water channel. The velocity vector was estimated at each part, and in this way the behaviour of $\boldsymbol{\alpha}$ at different depths from the bottom of the channel could be estimated.

The difference between the min-max velocity vector angles at each part for six different wind speeds was recorded and plotted against the water height. At the first section near the bottom (0-30mm) the magnitude of, α, fluctuates between 13°- 45° for all wind speeds except for the wind speed of 3.6 ms^{-1} which was 98°. Broadly, α, is a function of wind speed and water height. For example, at the wind speed of the order 0 and 1.07 ms^{-1} ,α ,grows as the h_w increases and the maximun α magnitude occurs at h_w of the order 230 mm and 280 mm (approximately at middle depth of the water channel) for the two speeds respectively then α decays to different magnitudes. At speed of 1.92 and 2.73 ms^{-1} α attains low magnitudes and fluctuates over a small range as h_w increases. The magnitude of α fluctuations increase at a speed of the order 3.6 ms^{-1}. However, at a speed of 4.5 ms^{-1} α shows exponential growth with respect to h_w. The correlation between the maximum fluctuations in magnitude of α and the wind speed is shown in Figure (3.21c). The minimum fluctuations in magnitude of α occur at the wind speeds of 1.92 and 2.73 ms^{-1} which gives another confirmation for the results presented in Figure (3.21a). The most important feature of the above findings was repeatability when the experiments were conducted in different conditions.

The other interpretation of the behaviour of α may be attributable to the wind-water interaction mechanism. It is suggested that the wind particles attract and repel the water particles due to the electrostatic charges that accumulate on both of them. The repulsion and attraction processes may cause an angular motion for the water particles under the 'still' water conditions and at very low wind speed action. Under the effect of higher wind speed action, the wind induced shear gradually exceeds the repulsion and attraction forces. The water particles follow the direction of the induced shear and which causes a reduction in α magnitudes. At a higher wind speed the magnitudes of α increase due to the induced shear, eddies formation and propagation. This interpretation may help in understanding the wave generation mechanism when the surfactants or contaminants on the water surface disrupt the wave initiation and growth under the action of low wind speed. The surfactants and contaminants initiate a lamina (barrier) between the air and the water surface and eliminate the attraction and repulsion forces between the charged particles in the air and water bulk. In this case the contaminants shield the water from the effect of wind action which makes the two flows of water and wind independent from each other. In this case the wave

generated by the effect of the mechanical action only whereas the other actions (thermal and chemical) are put out of action. A higher wind is required to producing and growth surface waves.

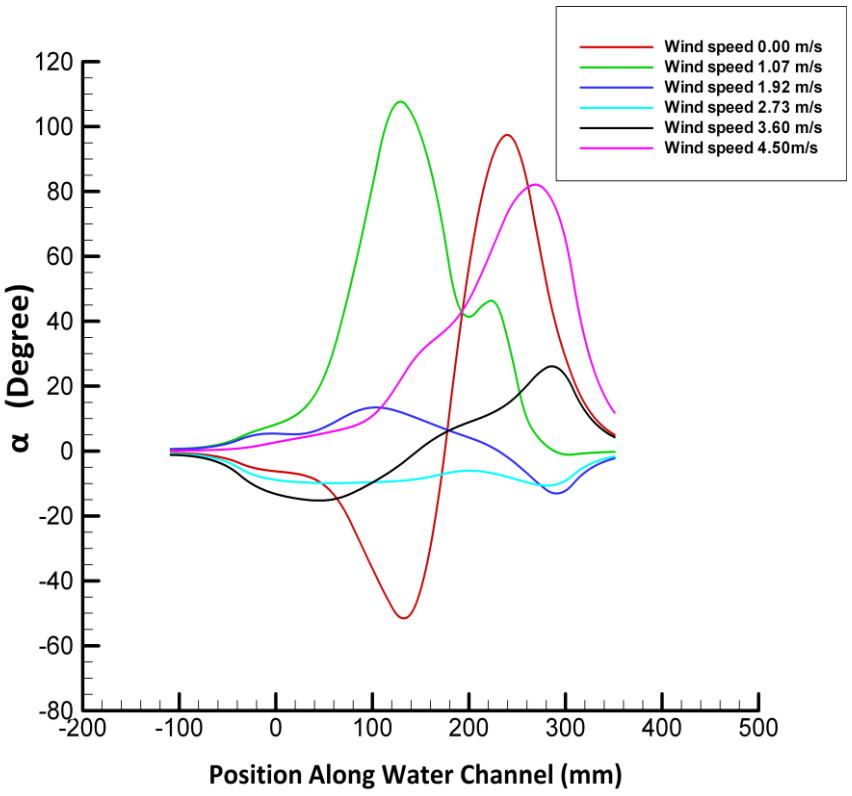

Figure (3.21a): Correlation between the position along water channel and velocity vector angle at different wind speeds

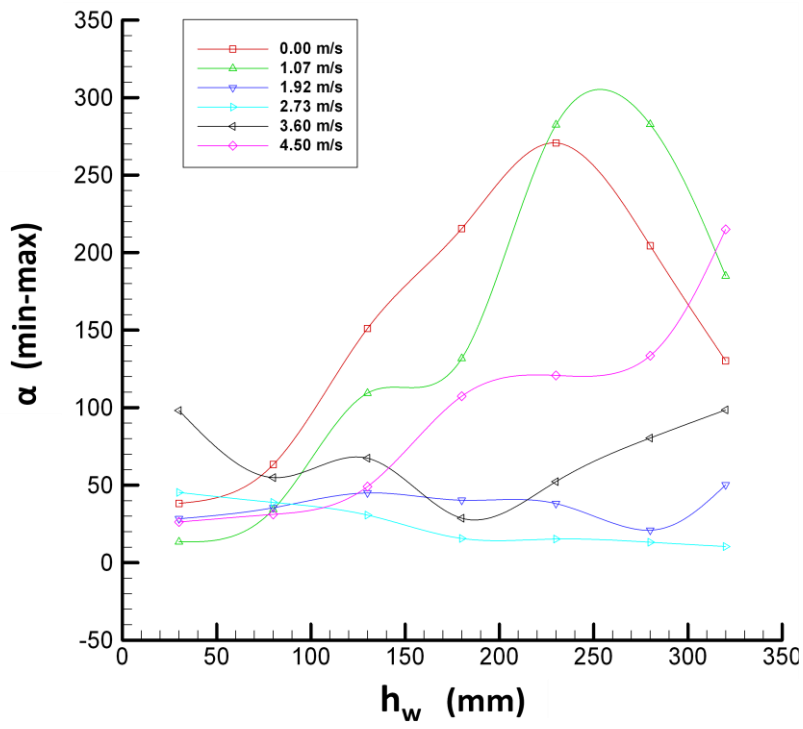

Figure (3.21b): Correlation between the maximum difference of the angle α and water depth with wind speed

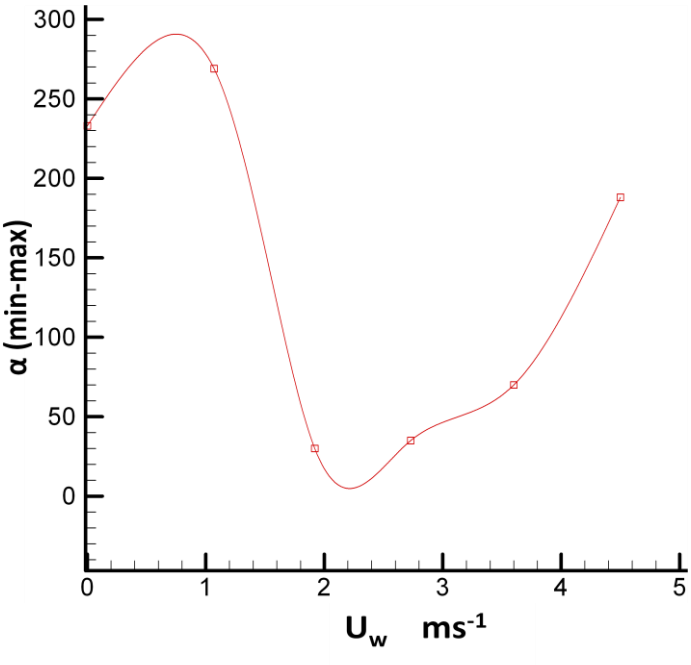

Figure (3.21c): Correlation between the maximum difference of the angle α with wind speed

3.8.3 Vorticity

The vorticity analysis is generally used to identify location of eddies and to calculate the eddy characteristics (size, strength, etc). The possibility of forming stronger, larger and faster eddies increases as the vorticity attains higher magnitudes. It has been surprisingly challenging for the fluid dynamics community to arrive at a consensus definition of an eddy, Adrian (2000).The definition offered by Kline and Robinson (1989) 'a n eddy exists when an instantaneous stream line mapped into a plane normal to the force exhibits a roughly circular or spiral pattern, when viewed in a reference frame moving with the centre of the vortex core'. According to Adrian (2000), a key condition in this definition is that the velocity field must be viewed in a frame that moves at the same velocity as the core of the vortex. A second condition is that the vorticity is concentrated in a core.

Unfortunately**,** vorticity not only identifies the vortex core but also any shearing motion present in the flow, Adrian (2000). Vorticity is defined as

$Rot(z) = \nabla \times V$.

The symbol ∇ can be used to describe the curl (rotational motion at points in a fluid). The vector product operation can be visualised as a pseudo-determinant:

$$\nabla \times V = \begin{vmatrix} i & j & k \\ \frac{\partial}{\partial x} & \frac{\partial}{\partial y} & \frac{\partial}{\partial z} \\ u & v & k \end{vmatrix} x \quad y \quad z$$

The vorticity Rot- z in current measurements determines the two dimensional vorticity in the xy-plane. The rotation of the vectors fields is calculated according to the equation (3.5). Vorticity is calculated by simple central differences in the measured velocity components.

$$Rot\ (z) = Exy - Eyx$$
$$Rot\ (z) = \frac{\partial u}{\partial y} - \frac{\partial v}{\partial x} \quad \text{..... (3.5)}$$

Fig (3.22) shows the relationship between the vorticity versus position along the water channel at different wind speeds. The vorticity has positive and negative values

depending on the direction of rotation - positive for clockwise rotation (following the direction of the wind). When the wind speed increased from approximately zero to 1.07ms^{-1} the direction of rotation did not change and the vorticity attained a less values. The vorticity increased when the wind speed increased if the main eddies kept the same direction of rotation and decreased if the direction of rotation changed. A significant increase in vorticity occurred at wind speeds of the order 3.6 ms^{-1} and 4.5 ms^{-1} where a significant increase occurred in Reynolds number and in the ratio of the water-wind kinetic energy density.

The relationship between the existing eddies and surface wave was observed by Volino & Smith (1999); the wave became visible to the naked eye as the vorticity magnitude became significant. However, insight into the wind-waves generation and evolution mechanism can be obtained from observing the evolution of the vorticity; the existence of large and strong scale eddies may indicate the existence of high energy waves. So the parameters that affect the vortices' formation and evolution may affect the formation and evolution of the waves in the same way. For instance, in shallow water, the friction induced by the water body bottom confines the evolution of the vortices' size and speed which in turn confines wave evolution; only low amplitude waves with limited wavelengths can be generated on shallow water surfaces even if the wind speed is significantly high. This is an example of one of the factors constraining the growth of the wave's amplitude in shallow or short fetch water bodies. The correlation between the statistics of surface waves (amplitude, wave length, steepness, etc) and vortex statistics (size, strength, etc) should be considered under high wind speed in a water channel with different depths in further experiments. It is hypothesised that analysis of eddy characteristics could provide a guide to predicting the surface wave's statistics and vice versa.

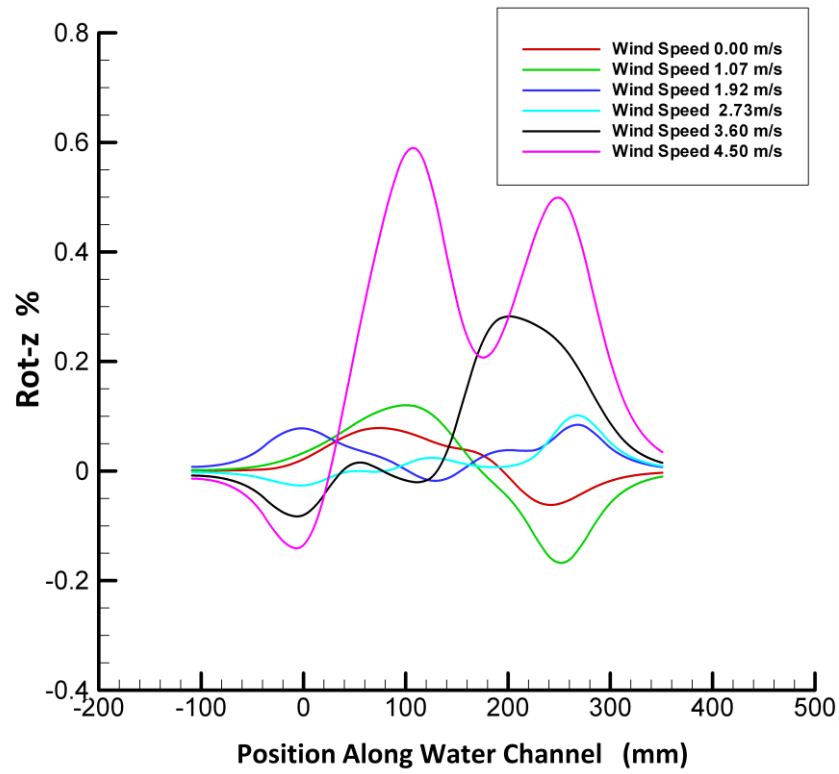

Figure (3.22): Correlation between the position along water channel and vorticity at different wind speeds

3.8.4 Swirling Strength

Swirling strength is a parameter indicating a location around which the streamlines are closed, which is typically the location of the eddy core. According to Adrian et al (2000) Swirling strength is noted at all locations where a eddy was identified, and the swirling strength is more useful as a means of identifying eddies and calculating reliable vortex statistics than vorticity. This is because the vorticity is much nosier than the swirling strength and tends to identify local shear layers present in the field. The swirling strength in Figure (3.23) is determined by computing the eigenvalues of the velocity gradient centre. The critical point analysis of the local velocity gradient tensor and its corresponding eigenvalues have been proposed by several groups such as Zhou et al(1996,1999) in order to extract the underlining structure from velocity fields. In three dimensions, the local velocity gradient tensor will have one real eigenvalue (λ_r) and pair of complex conjugate eigenvalues ($\lambda_{cr\pm i\lambda_{ci}}$) when discriminant of its characteristics equation is positive. According to Chong et al

(1990), when this is true the particles trajectories about the eigenvector corresponding to (λ_r) exhibit a swirling, spiral motion. λ_{ci}^{-1} represents the period required for a particle to swirl once about the λ_r axis. Thus $\lambda_{ci} > 0$ corresponds to shorter, more circular ellipse (eddies). Zhou et al (1996,1999) showed that the strength of any local swirling motion is quantified by λ_{ci}, which they defined as the swirling strength of the vortex. Adrian et al (2000) reported, in two dimensions, that the local velocity gradient tensor will have two real eigenvalues or a pair of complex conjugate eigenvalues. Therefore, eddies are easily identified when $\lambda_{ci} > 0$. The algorithm of (3.6) is used in the current measurements to calculate the swirling strength from the velocity field.

$$\max(0, -(ExyEyx - ExxEyy/2 + (ExxExx + EyyEyy)/4)). \quad \ldots\ldots (3.6)$$

$Exx = \frac{\partial u}{\partial x}$, $Eyy = \frac{\partial v}{\partial y}$, then

$$\max\left(0, -\left(\frac{\partial u}{\partial y}\frac{\partial v}{\partial x} - \frac{\partial u}{\partial x}\frac{\partial v}{\partial y}/2 + \left(\frac{\partial u}{\partial x}\frac{\partial u}{\partial x} + \frac{\partial v}{\partial y}\frac{\partial v}{\partial y}\right)/4\right)\right)$$

i.e. only the positive part of the swirling strength λ_{ci}. The rest is set to zero to display swirl only.

In practice, high levels of swirling strength indicates the location of a vortex or eddy core. As shown in Figure (3.23), the swirling strength values at wind speeds less than 3.6 m/s are insignificant. A noticeable increase in the swirling strength values occurs at wind speeds of 3.6 ms^{-1} and 4.5 ms^{-1}. These results do not match very well with Adrian's observations particularly at low wind speeds where the swirling is insignificant compared to the vorticity as shown in Figures (3.22 & 3.23). It is important to consider how the bulk flow is driven; for example Adrian analysed the PIV velocity fields that were measured in the radial plane of a fully developed turbulent pipe flow, whereas the current measurements were conducted in a semi open water channel under the action of wind. The difference between the characteristics of the flow when the flow is driven by the action of wind or by mechanical means such as a circulation pump was observed in particular experiments conducted in two channels. In the first one, the flow was driven by the action of the wind and in the second the flow was driven by the action of the circulation pump. To find the difference between the two flows a small amount of dye was injected into both channels from the surface. When the flow was driven by wind action the dye followed

the wind shear that was concentrated near the surface, whereas the dye was distributed across the channel from the surface to the bottom when the flow was driven by a circulating pump. This also may explain the difference between the characteristics of the surface waves that are generated by a mechanical vibrator and by those generated by the action of the wind. Pierson et al (2003) have exposed two types of surface wave in opposition to the wind: one generated by mechanical vibrator and the other generated by wind action. They reported that the waves generated by mechanical vibrator collapsed faster than the other. The difference between the two cases may refer to the type of motion that was generated in the flow field by the action of the vibrator and under the action of the wind. The latter introduces motion into the entire area of the flow field whereas the former introduces a local motion depending on the location of the vibrator.

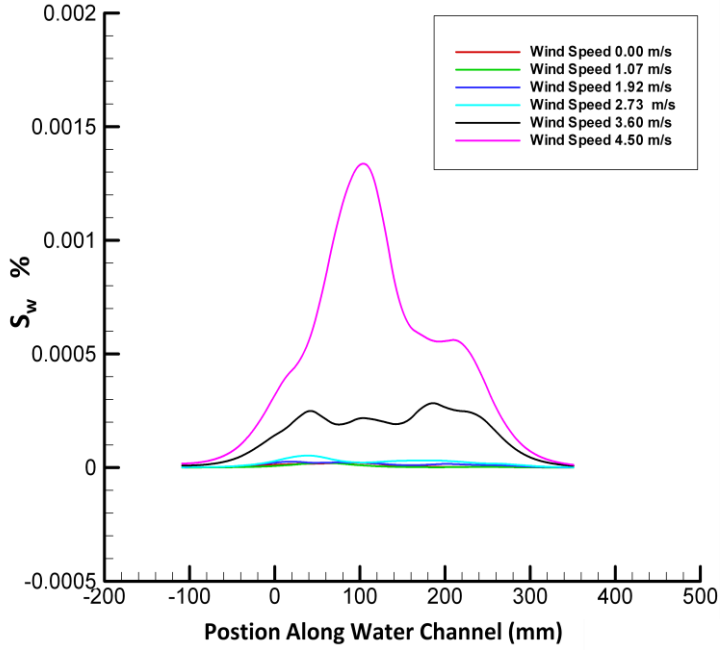

Figure (3.23): Correlation between the position along water channel and swirling strength at different wind speeds

Many studies concerning the surface wave generation under action of wind surface, for instance, Lorenz et al (2005) and Ataktürk and Katsaros (1998), discarded cases at wind speeds of less than 3 ms^{-1} because the measurement systems of wave parameters did not show any significant response when wind speed was less than 3 ms^{-1}. The intimate relationship between the characteristics of the surface wave and kinematics and dynamics of the bulk is evident. As shown in Figure (3.22) and (3.23), up to wind speeds of 2.73 m/s the transfer of wind momentum to the bulk is

not sufficient to initiate a detectable value of swirling strength and significant vorticity. For these reasons, in current measurements the waves cannot be observed at wind speeds less than 2.73 m/s. This value is not absolute, as it depends on the other parameters related to the water body and atmospheric conditions.

3.8.5 Shear strength

As shown in the first two chapters, the wind-generated surface wave phenomenon cannot be considered as a mechanical action only, as the wind transfers energy to the bulk flow and then the wave is generated. The wind generated can be understood as wind-wave interaction and due to this interaction a number of processes occur. In order to find an interpretation for some observations, for example, the time lag between the onset of the wind over the water surface and the appearance of the wave, some solid properties are studied for water bulk under action of the wind.

A Newtonian fluid is frequently defined as a medium which, as distinct from a solid, can flow at any arbitrarily small shear stress, Apakashev and Pavlov (1995). The behaviour of such fluid is considered to be completely determined by the value of a single parameter - the viscosity (μ). The solids properties such as tangential elasticity and shear strength, were observed through investigating the properties of thin liquid sheets conducted by Deryagin and Churaev (1985). However the existence of shear strength has been discussed by Bondarenko (1973) with large masses of water. Apakashev and Pavlov (1995) investigated experimentally that over a range of low strain rates the water behaves like a medium with very low shear strength and a shear modulus of the order 10^{-6} Pa.

The following algorithm of (3.7) is used to calculate the shear strength from the velocity field.

$$\max\ (0, Exy\,Eyx - ExxEyy/2 + (ExxExx + EyyEyy)/4) \quad \ldots\ldots\ldots\ldots (3.7)$$

$$\max\ (0, \frac{\partial u}{\partial y}\frac{\partial v}{\partial x} - \frac{\partial u}{\partial x}\frac{\partial v}{\partial y}/2 + (\frac{\partial u}{\partial x}\frac{\partial u}{\partial x} + \frac{\partial v}{\partial y}\frac{\partial v}{\partial y})/4)$$

i.e. only the negative part of the swirling strength λ_{ci} , the rest is set to zero to display the shear only.

The relationship between shear strength and wind speed at the given fetch is shown in Figure (3.24). The shear strength develops broadly in the same manner as swirling strength under the effect of the two higher speeds. However, the growth of shear strength at lower wind speed is insignificant but still higher than the growth of swirling strength at the same speed. The growth of the shear strength at a wind speed of 3.6 ms^{-1} is higher than the growth of swirling strength at the corresponding wind speed. Also the percentage growth of swirling strength at a wind speed of 4.5 ms^{-1} is higher than the shear strength at the corresponding wind speed. The relationship between swirl and shear will be discussed in more detail in the following section and in Chapter 4.

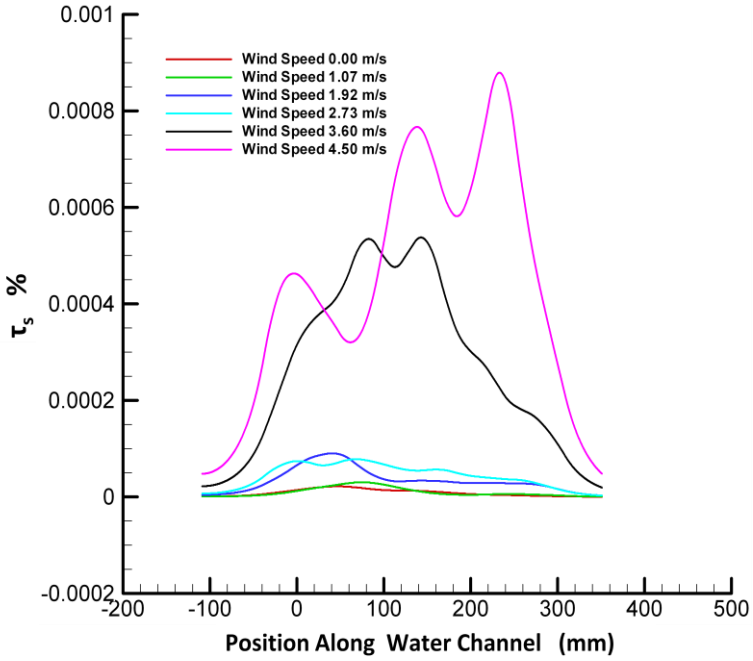

Figure (3.24): Correlation between the position along water channel and shear strength at different wind speeds

The importance of studying the properties of solids such as shear strength and Poisson ratio in studying wave generation under the action of wind is to examine the response of these parameters to the effect of wind action. This may add a new approach in studying the characteristics of the wind-water interaction and help in interpreting indistinct observations. Previous and recent studies such as Kunishi (1957), Caulliez et al (1998) and Ataktürk and Katsaros (1998) observed a time lag between the onset

of the air blowing over the water surface and the appearance of the surface wave even if the wind speed is higher than the critical wind speed. It is possible that the time lag occurs because under effect of the wind action the water particles absorb and release energy. The time between the two processes (absorption and release of energy) indicates the time lag between the onset of the air blowing and the appearance of the surface wave. The time lag seems to be a function of wind speed, density of bulk perturbations and fetch length. It is suggested that the shear strength gives an indication of the required time to transfer the effect of the bulk perturbations to the surface under action of the wind. As the shear strength attains higher magnitudes the time lag becomes less.

The consistency between the evolution of the shear strength and the other flow parameters such as vorticity and swirling strength confirms the use of this parameter in studying the effect of the wind action on the characteristics of the bulk. However, studying the characteristics of this parameter under the effect of wind action gives insight into some observations such as the time lag between the onset of the wind and the appearance of the surface wave?

3.8.6 Swirl and shear

The software used in analysing the data made it possible to study the effect of the wind on the swirl and shear through the bulk together. The equation (3.8) is used to calculate the swirl and shear strength. The swirl and shear strength is calculated by subtracting the shear strength from swirling strength.

$$-(ExyEyx - ExxEyy/2 + ExxExx + EyyEyy/4) \quad \text{..... (3.8)}$$

i.e. the imaginary portion λ_{ci} of the complex eigenvalue of the local velocity gradient tensor.

The magnitudes of swirl and shear based on equation (3.8) are shown in Figure (3.25). The effect of the swirl in the bulk is insignificant compared to the effect of the shear while the wind speed is less than or equal to 3.6 ms^{-1}. Therefore an abrupt growth in swirl strength occurs in the first half length of the PIV measuring zone. Then it decays sharply in the second half at a speed of the order of 4.5ms^{-1}. The shear strength shows

little growth as the wind speed is less than 3.6 ms^{-1}. However, a significant growth occurs at a speed of the order 3.6 and 4.5ms^{-1}. The swirl strength did not show such growth under the same conditions. The nature of swirling that requires a circular motion in the bulk to make the swirling strength significant through the flow may expalin the swirling growth pattern under the action of low wind speed. However, the shear strength does not require such motion. It is expected that the increase of surface wave growth becomes more significant at higher wind speeds, because the circular motion already exists in the bulk and the higher wind speed action will amplify the circular motion. So, the geometry of the water body that influences the nature of bulk flow motion under the action of wind should be considered when studying the generation of waves and their effects. Examples of this include studies concerning reducing the effects of scouring on water reservoir banks where the scouring on the reservoir banks is affected significantly by the surface wave growth and the waves' energy. So it is recommended that the water reservoir is designed in a way that disrupts the formation of circular motion with respect to the main wind direction. Other applications such as wave energy may need to boost the existence of circular motion to increase the wave growth rate. It may be necessary to make a modification for the natural water reservoir shape to achieve the suggested purpose. It is recommended to use the CFD to study the effect of the water reservoir design on bulk flow motion under the action of wind. The most frequent wind direction over the whole of the year should be considered in such studies.

From the discussion of the above parameters, it seems that the one which tends to follow the flow velocity most faithfully is the shear stress.

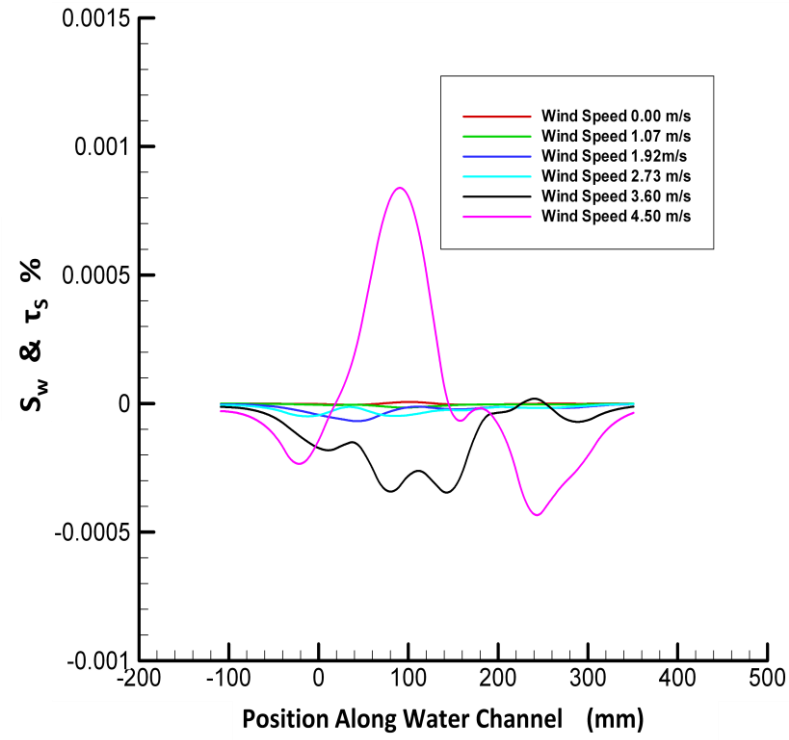

Figure (3.25): Correlation between the position along water channel and swirl and shear at different wind speeds

3.8.7 Conclusion

The effect of the wind speed on the bulk flow parameters can be categorized depending on its behaviour into four groups:

1. Parameters which are affected by the wind grow gradually from still water to a speed of the order 2.73 ms^{-1}. After that, an abrupt growth occurs in the maximum values at higher speeds. An example of this is the flow velocity.
2. Parameters, for instance the velocity vector angle, which are achieved their maximum values at very low speeds and at the high wind speeds. The trend of the plots of this parameter tends to be similar to cosine wave form.
3. Parameters which are not affected by action of the wind until a speed of the order 2.73 ms^{-1}. After which an abrupt growth in magnitude of these parameters occurs. Example of this: swirling strength.
4. Parameters which show little effect from the wind action until the speed of the order 2.73 ms^{-1}, after which an abrupt growth in these parameters occurs, for instance: vorticity and shear strength.

Analysing the velocity field images under the effect of the wind action shows that bulk flow evolution occurs as follows:

1. Vertical oscillation of the water particles (tracers) with respect to the direction of the wind; the linear motion of the water particles is insignificant. This occurs in still water conditions and when the wind speed is very low.

2. Existence of dark zones in PIV data through the bulk. This occurs as the wind speed attains different orders. The presence of the dark zones through the bulk occurs when the flow direction is changed. Also the formation of the eddies were observed in the regions of the dark zones

3. Significant changes in the flow direction with respect to the wind direction

4. Eddy formation at different depths from the water surface.

5. Growth the strength and the size of the eddies.

The inherent vorticity in the bulk being an important factor- induce circulation in the bulk to accentuate wave formation and growth.

The magnitudes of the kinetic-energy density at different orders of wind speed verify the importance of the background perturbation on the kinematics and dynamics of the flow and consequently on the surface wave initiation and evolution. On other hand it helps in understanding the discrepancy between the observed and the predicted values of the critical wind speed.

The waves attain energy from the wind that is blowing over the surface and from the eddies that propagate towards the surface. In the absence of one of these sources, the waves become weak and tend to attenuate.

The parameters that may affect the growth of the eddies size and strength, such as water depth and wind speed, affect also the growth of the surface waves. This gives insight into the intimate relationship between the characteristics of the surface waves and the characteristics of the bulk under the action of wind.

Some properties of the solid material such as shear strength can be applied to Newtonian fluid flow. The current measurements show that the property of shear strength can be measured for the water bulk under action of the wind. Also this property shows a reasonable growth when the wind speed increases gradually.

Chapter 4

Analysis and interpretation of velocity fields (II)

Introduction

In order to extend the analysis of the information that can be extracted from the PIV velocity fields and therefore enhance the understanding of the kinetics and dynamics of the bulk under effect of steadily wind action, the parameters below are analysed at three fetch lengths under the same wind speeds that were addressed in Chapter 3. The three fetch length measurement zones are located at 1.52, 212 and 272cm from the upstream leading edge of the water channel. The symbols of F1, F2 and F3 are used to indicate the first, second and third of the PIV measurements zones. Only the maximum magnitude for each parameter is considered in the following analysis. The maximum magnitudes are determined after plotting each parameter against positions along the water channel (PIV measure zone) at six different wind speeds, as shown in the first part. The maximum values of the flow velocity, vorticity, swirling strength, shear strength and strain rate are determined straightforwardly. However, the maximum values of the velocity vector angle are determined by finding the difference between max-min velocity vector angles at six wind speeds.

The aim of considering only the maximum values is to reduce the error that may occur from the inaccuracy of the measurement system or from the structure of the experiment facilities; for example, it is assumed tracers that were added to the water will follow faithfully the flow in all directions. Also, the distribution of the air flow across the wind tunnel is not uniform. The consideration of maximal values also helps to obtain the maximal effect of wind action on the kinematics and dynamics of the bulk.

4.1 Maximum flow velocity

The relationship between the maximal flow velocity, V_{max}, and th**e** wind speed U_w at F1, F2, and F3 is shown in Figure (4.1a), where U_w is the wind speed at height of 1.22 m from the surface. An exponential fit made for the Figure (4.1a) is shown in Figure

(4.1b); the measure point's trends at F1 and F2 are much closer to the exponential trend than F3. The difference in the measure point's trend at F3 may be attributable to the experiment's facility design rather than to the fetch length. As shown in Figure (3.2), the water channel is partially covered and the wind tunnel has the same cross section just over the first one third of the water channel length, while the rest is without sides and roof (the wind blows over the water surface without a tunnel as shown in Figure (3.2). The change of the wind tunnel cross section from the covered section to the uncovered section causes a sudden expansion in the wind tunnel cross section which in turn causes an increase in wind turbulence over the water surface. The turbulence in the wind side plays a key role in transferring the wind momentum to water bulk and in generating surface waves. Thus significant changes occur in the dynamics and kinematics of the bulk flow. The location of the **F3** measure zone is very close to the zone where the change in the wind tunnel cross section occurs.

The exponential profiles in the Figure (3.1b) are termed in the form of

$$V_{max} = e^{A \times U_w + B} \quad \text{..... (4.1)}$$

The values of the constants A and B are shown in table (4.1). It can be concluded that the exponential relationship between the $\boldsymbol{V_{max}}$ and $\boldsymbol{U_{1.2}}$ just occurs when the wind speed blows over water surface steadily. This observation explains the importance of the wind turbulence on the kinematics and dynamics of the water and leads to studying the relationship between the wind-velocity profile and bulk-velocity profile. The instability theory assumes a logarithmic wind-velocity profile. The investigations by people such as Kama and Donelan (1989) have proved this assumption.

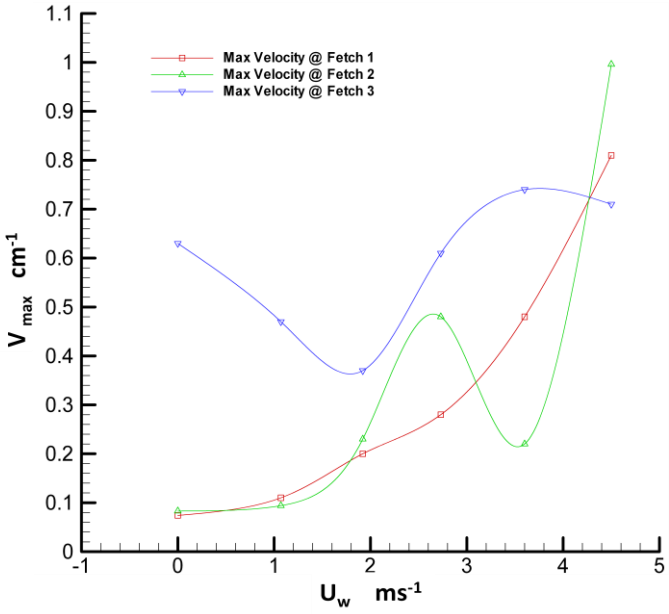

Figure (4.1a): A comparison of the max flow velocity at three fetch lengths. The max value of V_{max} occurs at the maximum wind speed for the F1 and F2. At F3 V_{max} trend is similar to cosine wave trend. F1, F2 and F3 are located at 1.52m, 2.12, and 2.72m from the upstream edge of the water channel.

Table 4.1: the values of the constants A and B of the exponential law of (3.1)

F1	A = 0.54 B = -2.68
F2	A = 0.51 B = -2.59
F3	A = 0.075 B = -0.73

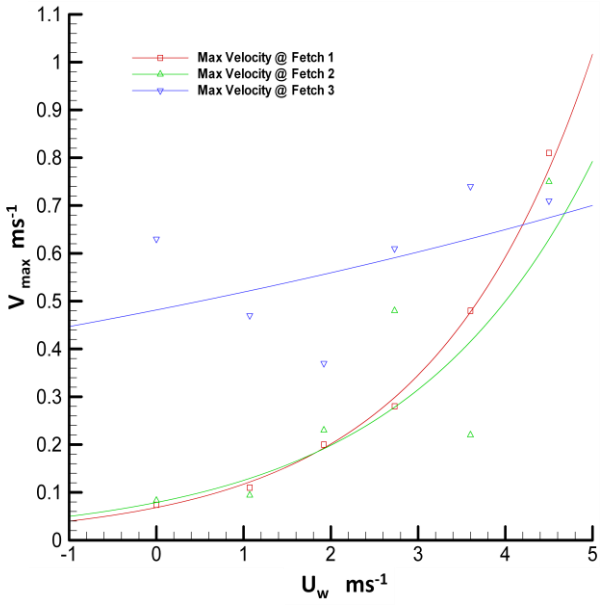

Fig (4.1b): An exponential fit data for the max flow velocity profile shown in Figure (3.1a). The measure point's trends at F1 and F2 are much closer to the exponential trend than F3 .

4.2 Vorticity Rot-z_{max}

Figure (4.2a) shows the relationship between the wind speed and maximal absolute Vorticity magnitudes (Rot -z_{max}). The absolute magnitudes of the vorticity were considered in the Figure (3.2a) irrespective of the direction of the rotation. The exponential fit for the Figure (4.2a) is shown in Figure (4.2b). As shown in the figures, the magnitudes and curve trends of the vorticity for F1 and F2 at the corresponding wind speed are nearly identical. However, the vorticity at F3 reveals higher magnitudes and shows a different trend. The vorticity at F3 fluctuates over a large scale whereas at F2 and F3 the vorticity fluctuates over a comparatively small scale. It is evident that the vorticity is a function of the flow velocity and the wind turbulence.

The exponential profiles in the figure (3.1b) are termed in the form shown below:

$$Rot\text{-}z_{max} = e^{A \times U_w + B} \quad \text{..... (4.2)}$$

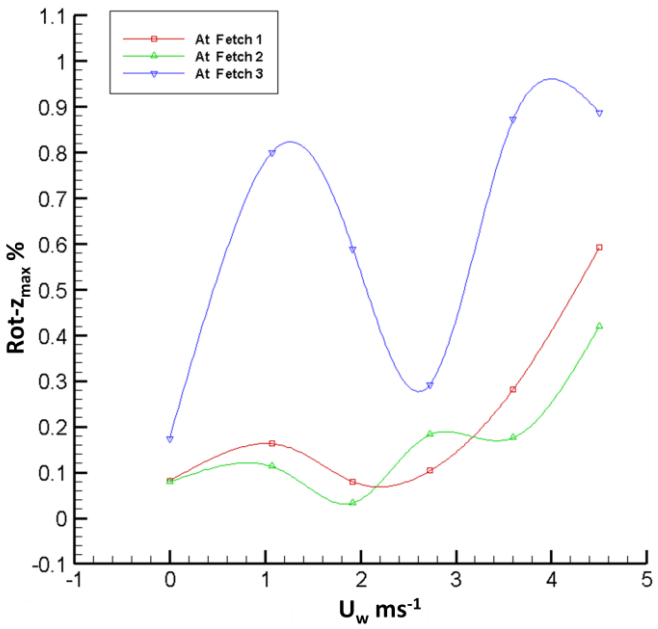

Figure (4.2a): A comparison of the max flow vorticity at three fetch lengths. The max value of Rot-z_{max} occurs at the maximum wind speed for the F1 and F2. At F3 Rot-z_{max} trend is similar to cosine wave trend.

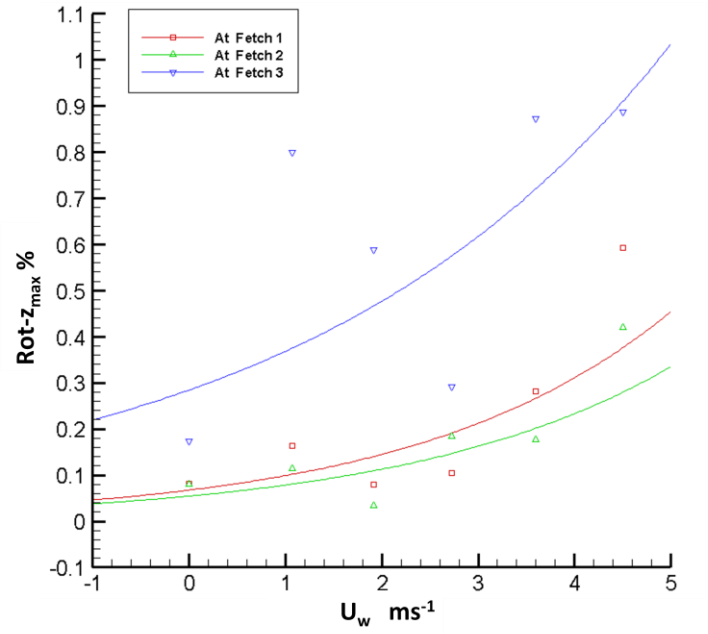

Fig (4.2b): An exponential fit for the max flow velocity profile shown in Figure (4.2a). The exponential fit data curves at F1 and F2 are approximately identical

Table 4.2: the values of the constants A and B of the exponential law of (4.2)

F1	A = 0.38 B = -2.70
F2	A = 0.36 B = -2.91
F3	A = 0.26 B = -1.26

The trend of the Rot(z) versus U_w and V_{max} versus U_w curves at F3 did not match the exponential fit curve as those at F2 and F1 did. The magnitude of the exponents A and B in the exponential equation indicates the curve curvature, i.e. the growth rate of the Y axis parameter. The higher growth rate occurs at a higher total of the exponents A and B. The total of the constants A and B at F1 is slightly higher than the total at F2. However at F3 the total of the exponents is significantly higher than the total at F1 and F2. This can be noted for the max flow velocity and max vorticity curves. This analysis illustrates the intimate relationship between the V_{max} and $Rot(z)_{max}$ under different conditions and from analysing the V -U_w the trend of the Rot-z-U_w plot can be predicted under the same conditions.

4.3 Velocity vector angle (α)

The velocity vector angle is a parameter that describes the angular movement of the velocity vectors with respect to an axis parallel to the water surface. It is obvious from Figure (4.3) that the velocity vector angle at three fetches has a minimum magnitude, α_{min} which occurs at a particular wind speed which is 1.92 ms^{-1} for F3 and 2.73 ms^{-1} for F2 and F1. The minimal velocity angle is around 10 degrees for F1 and F2 and 50 degrees for F3. Also the relationship between α and U_w is similar to the cosine wave trend particularly at F1and F3. At F3, the other flow parameters such max flow velocity, max absolute vorticity, max swirling strength and max shear strength against wind speed show significant growth compared with the same parameters at F1 and F2 as shown above and in the Figures below. Also α_{min} has attained a higher magnitude at F3, more than that it has attained at F1 and F2. All the above flow parameters show significant growth at F1 and F2 when the wind speed exceeds the speed of 2.73 ms^{-1}, where the appearance of the visible wave starts. The relationship between the flow transition from laminar to turbulent and surface wave generation was discussed in Chapter 3. It is hypothesised that fluctuations in the magnitude of α scale the flow transition from laminar flow to turbulent flow. The transition may occur at the minimum fluctuation in magnitude of the velocity vector angle if the flow is driven by the action of the wind only. It is believed that the transition from laminar flow to turbulent flow occurs at a wind speed of 2.73 ms^{-1} for F1 and F2 and at a wind speed of 1.92 ms^{-1} for F3. These results provide prospects in finding another parameter to scale the flow transition from laminar to turbulent besides the Reynolds number

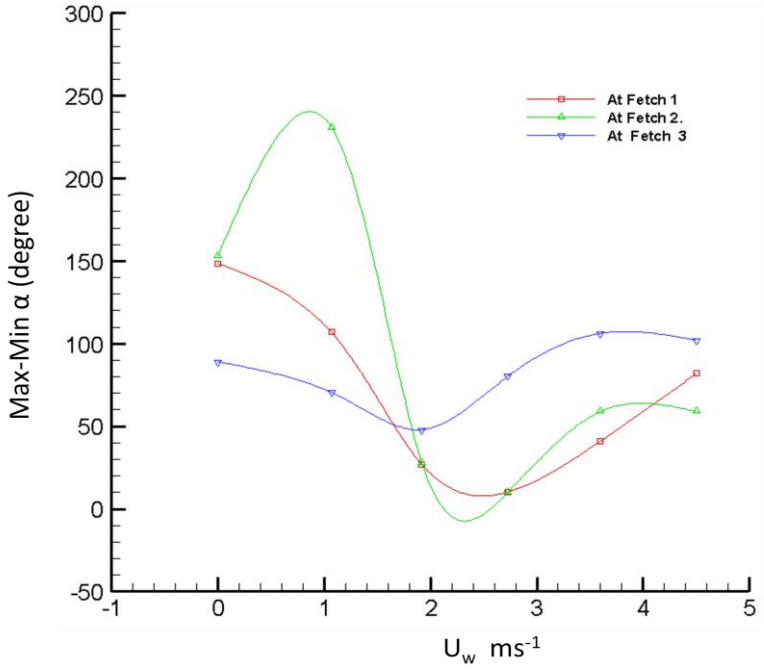

Figure (4.3): A comparison of the max-min velocity vector angle at three fetch lengths. The min value of α_{min} occurs at wind speed of 2.73 ms^{-1} for F1 and F2 and 1.92 ms^{-1} for F3.

4.4 Swirling Strength (S_w)

Figure (4.4a) shows the relationship between the wind speed and maximaum swirling strength. At F1, the increase in swirling strength is insignificant until the wind attains a speed of the order of 2.73 ms^{-1}. At a wind speed of the order 3.6 ms^{-1}a small increase occurred followed by a significant increase at a wind speed 4.5 ms^{-1}. At F2, the swirling strength oscillates, having low magnitudes until a wind speed of 3.6 ms^{-1} followed by a significant increment at a wind speed of 4.5 ms^{-1}. At F3 the swirling strength follows the trend of F2 until a wind speed attains a magnitude of the order of 2.73 ms^{-1}. A significant increment occurred at a wind speed of 3.6 ms^{-1} followed by a significant decrement at a wind speed of 4.5 ms^{-1}. The swirling strength trends at the three fetches reveal that the flow at F1 and F2 is much steadier than the flow at F3. The increase of the growth of swirling strength over the vorticity growth at F3 as shown in table (4.5) corroborates observations by Adrian et al (2000). Adrian et al visualised the water flow in a pipe and they concluded that high vorticity not only characterise the core of an eddy but also any shearing motion present in the flow. Adrian et al (2000) used several methods for analysing and interpreting the velocity

field and they found the swirling strength is more useful as a means of identifying eddies and calculating reliable eddy characteristics. They revealed additional eddies using swirling strength analysis that were not identified in analysing the vorticity.

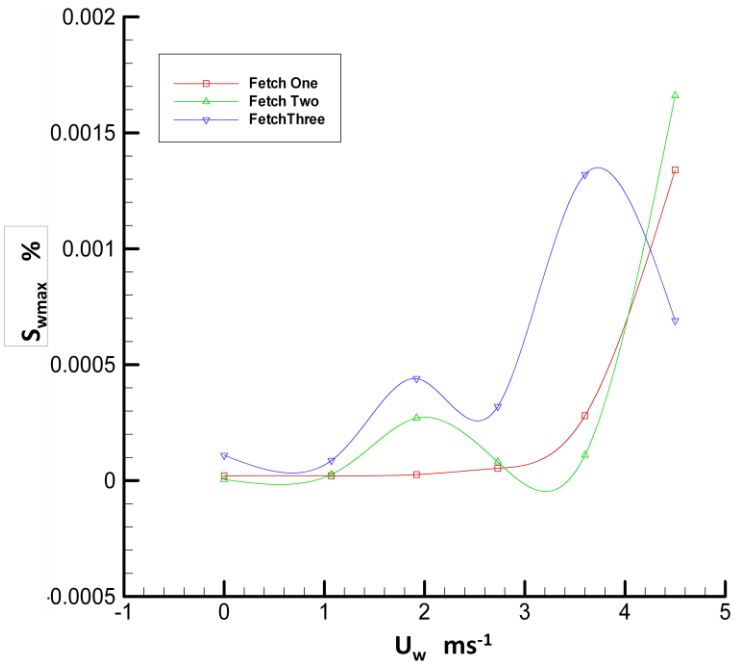

Figure (4.4a): A comparison of the max swirling strength at three fetch lengths. The max value of S_{wmax} occurs at the maximum wind speed for the F1 and F2. At F3 S_{wmax} attains lower magnitude at higher wind speed.

The exponential fit data for the Figure (4.4a) is shown in figure (4.4 b).

The exponential profiles in the figure (4.4b) are term in the form of

$$S_{wmax} = e^{A \times U_W + B} \quad \text{..... (4.3)}$$

Where the constant A and B for the three fetch are shown in the table (4.3)

Table 4.3: the values of the constants A and B of the exponential law of (3.3)

F1	A = 0.94 B = -11.61
F2	A = 1.05 B = -11.73
F3	A = 0.55 B = -9.29

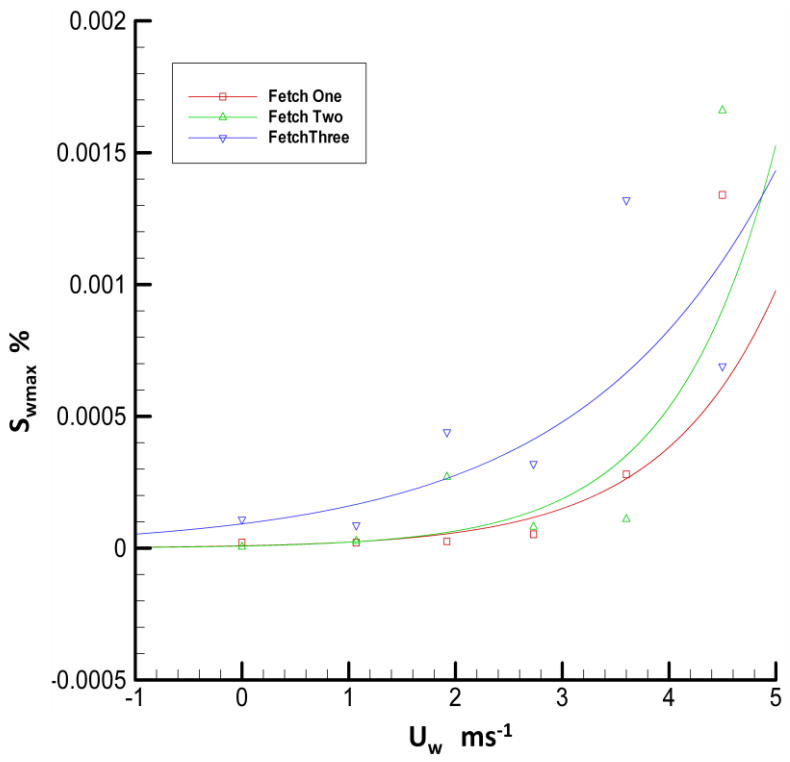

Fig (4.4b): An exponential fit for the max swirling strength shown in Figure (3.4a). The exponential fit data curves at F1, F2 and F3 is approximately identical particularly until the wind speeds of the order 2.73 ms^{-1}

4.5 Shear strength τ_s

Figure (4.5a) shows the relationship between the wind speed and the max shear strength at F1, F2 and F3. The graphs at the three fetch lengths show a similar trend, up to a wind speed of 2.73 ms^{-1} with a considerably low magnitudes followed by a significant increase at higher wind speeds. However at F3 the growth of the shear strength is comparatively high with respect to F1 and F2. Also for all fetch lengths the max shear strength at a wind speed of 1.92 ms^{-1} is higher than the corresponding value at a wind speed of 2.73 ms^{-1}. The repetition of the shear strength behaviour at particular wind speeds with different magnitudes along the fetch length gives the ability to predict the behaviour of the shear strength at higher speeds.

The trend of the shear strength-wind speed curves seem as exponential trend. The exponential fit for Figure (4.5a) is shown in Figure (3.5 b).

The three curves follow the exponential form as

$$\tau_m = e^{A \times U_W + B} \quad \text{..... (4.4)}$$

Where the constant A and B for the three fetch are shown in the table

Table 4.4: the values of the constants A and B for (3.4)

F1	A = 0.88 B = -11.10
F2	A = 0.88 B = -11.45
F3	A = 0.68 B = -9.25

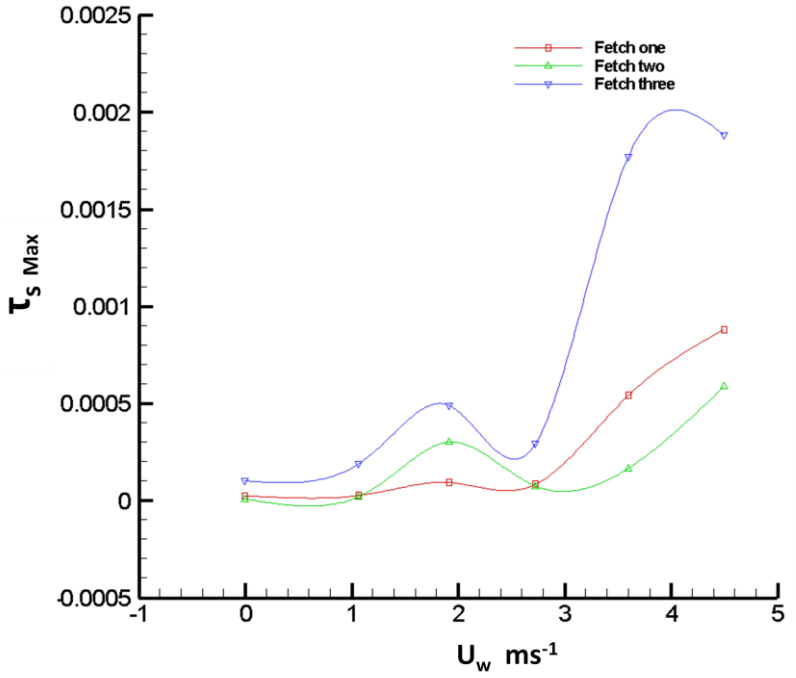

Figure (4.5a):A comparison of the max shear strength at three fetch lengths. The max value of τ_{wmax} occurs at the maximum wind speed for the F1,F2 and F3. At F3, τ_{wmax} attains higher values than F1 and F2.

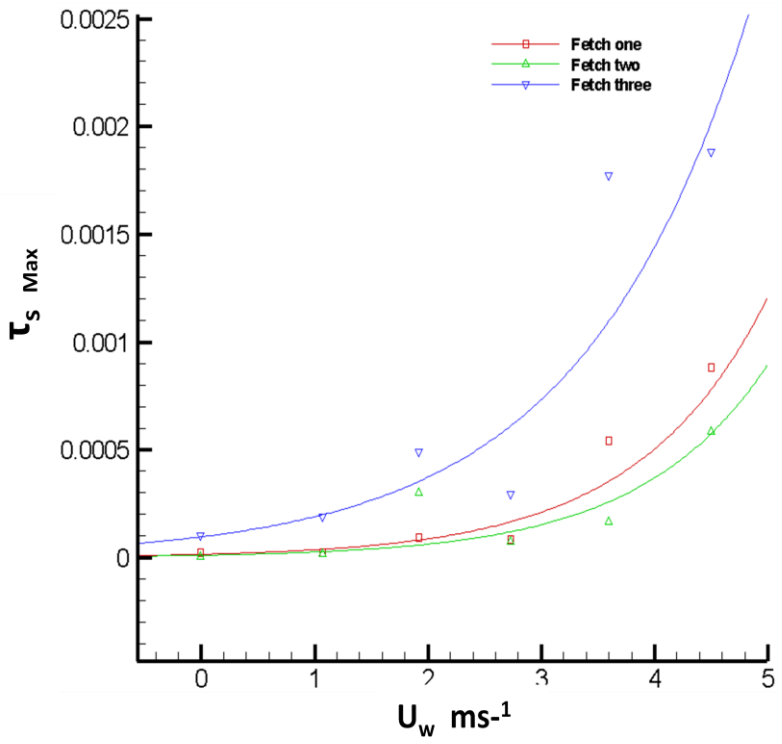

Figure (4.5 a): An exponential fit for the max shearing strength shown in Figure (3.5a). The three curves at F1, F2 and F3 are closer to the exponential fit data than the previous parameters.

The growth of the shear strength that occurring at F3 is higher than the growth of the vorticity and lower than the growth rate of the swirling strength under the effect of the corresponding conditions**.** The trend of the relationship between τ_s and U_w for F1, F2 and F3 is much closer to the exponential relationship than the relationship between Rot-z and U_w. It is concluded that the evolution of shear strength can be predicted at higher wind speeds even if the air flow is not steady. However, the evolution of the other flow parameters can be predicted only under steady air flow conditions.

In order to estimate the percentage growth of the flow velocity, vorticity, swirling strength, and shear strength that occurred due to varying the fetch length from F1 to F3, the growth was estimated using the above exponential equations in (4.1), (4.2), (4.3) and (4.4) respectively. The percentage growth for the flow parameters at F2 with respect to F1, $\gamma_{g_{2-1}}\%$ and at F3 with respect to F1, $\gamma_{g_{3-1}}\%$ are calculated by the equation (4.5) and (4.6) and tabulated in the Table (4.5).

$$\gamma_{g_{2-1}}\% = \frac{\gamma_{g2} - \gamma_{g1}}{\gamma_{g1}} \times 100\% \quad \text{..... (4.5)}$$

$$\gamma_{g_{3-1}}\% = \frac{\gamma_{g3} - \gamma_{g1}}{\gamma_{g1}} \times 100\% \quad \text{..... (4.6)}$$

$\gamma_{g=e^{A+B}}$ ..... (4.7)

Table (4.5) illustrates the significant increase in the percentage growth that occurred at F3 zone for the above flow parameters. The slight increase or decrease in the percentage growth of the same flow parameters that occurred at F2 with respect to F1 may be due to the short distance between the F1 zone and the F2 zone. At the F3 zone, the distance with respect to F1 is still short due to restriction in the experiment's facility design. However, the F3 zone is located close to a sudden expansion in the wind tunnel section zone. This expansion caused a pressure fluctuation in air flow and consequently a significant increase in wind turbulence and in the induced perturbations in the bulk flow. It is believed that the transition of the air flow from steady flow to unsteady flow causes a significant increase in the air turbulence even if the mean wind speed does not change significantly. It is postulated that the maximum growth rate of surface waves should occur where air flow transfers from steady to unsteady flow. In these conditions it is assumed that the resulting fluctuations in the air pressure cause significant fluctuations on the water surface. Such conditions make the wave formation easier and wave growth faster.

In the real fields such transition occurs when the wind speed and direction convertfrom steady wind to violent stormy wind propagation with a circular motion. The sea state converts under this action from uniform wavy to violent with high amplitude waves propagating at high speed which may be a hazard to shipping and offshore infrastructure.

Table 4.5: A comparison of the values of the percentage growth, γ_g%, at F2 and F3 with the corresponding values at F1. The percentage growth shows significant increase for all parameters at F3. Where $\gamma_{g1\%}, \gamma_{g2\%}$ and $\gamma_{g3\%}$, are the percentage growth at F1, F2 and F3

The Parameter	$\gamma_{g_{2-1}}\%$	$\gamma_{g_{3-1}}\%$
Velocity	6.18	341
Vorticity	-20	274
Swirling Strength	1	588
Shear Strength	29.53	420

Figures (4.7a-f) give insight to the effect of the sudden expansion in the wind tunnel section on the properties of the bulk flow parameters. The measurements in Figure (4.7a-f) were obtained at F3 zone; the magnitudes of the vorticity, velocity vector angle, swirling strength, shear strength and swirl and shear increase gradually at the first half length of the measure zone. However, a sharp increment occurs in the second half where the measure becomes very close to the sudden expansion zone. The flow velocity shows a distinct trend in comparison with the other parameters; the maximum values occurred at wind speeds of the order 3.6 and 4.5 ms^{-1} and extended over the whole length of the measurement zone making two peaks. The swirling strength, shear strength and vorticity show approximately the same trend; an exponential trend for these parameters can be observed where the peaks occur at the same distance from the upstream edge of the water channel. The velocity vector angle has a peak value occurring near the sudden expansion zone. The behavior of these parameters helps to predict the surface wave evolution under such conditions; as these parameters fluctuate in significant magnitudes, higher fluctuations are predicted on the surface and thus a higher wave growth rate. In general most of the parameters have a peak value which occurs near the sudden expansion zone.

The sudden expansion in the wind tunnel cross section is a proper way to generate turbulence in the air in the laboratories which may help in studying the effect of the wind-turbulence on the wave generation mechanism. The wind turbulence has a significant effect on the characteristics of bulk flow and on the formation and growth of the surface waves.

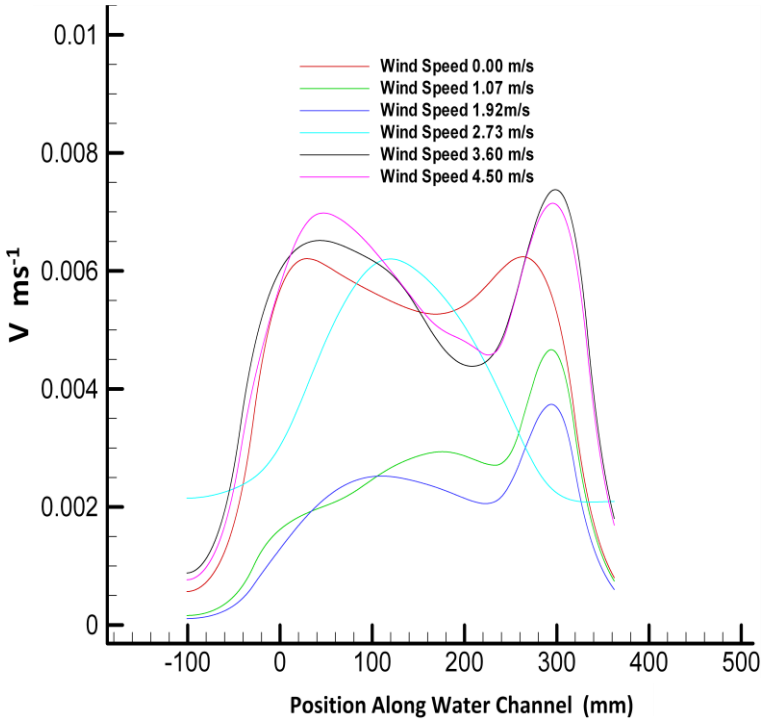

Figure (4.7a)

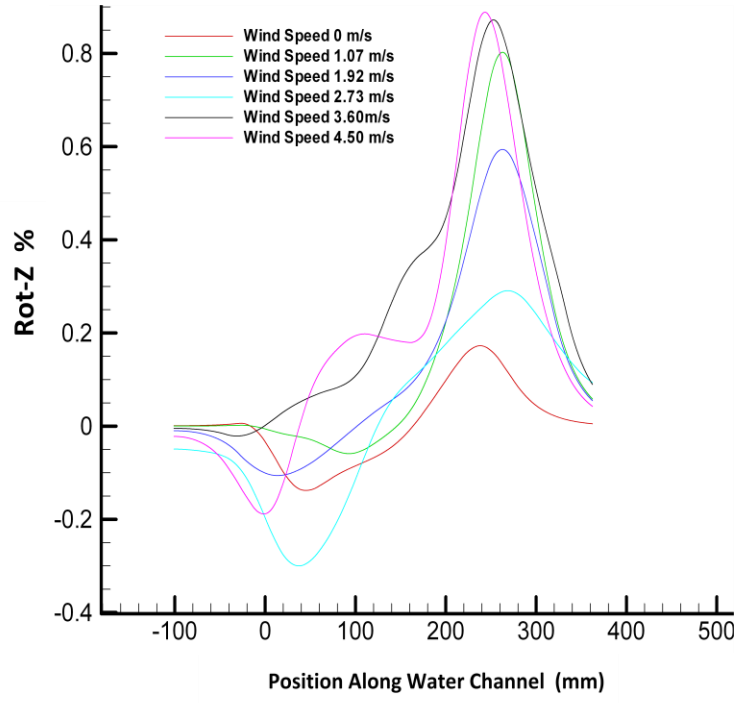

Figure (4.7b)

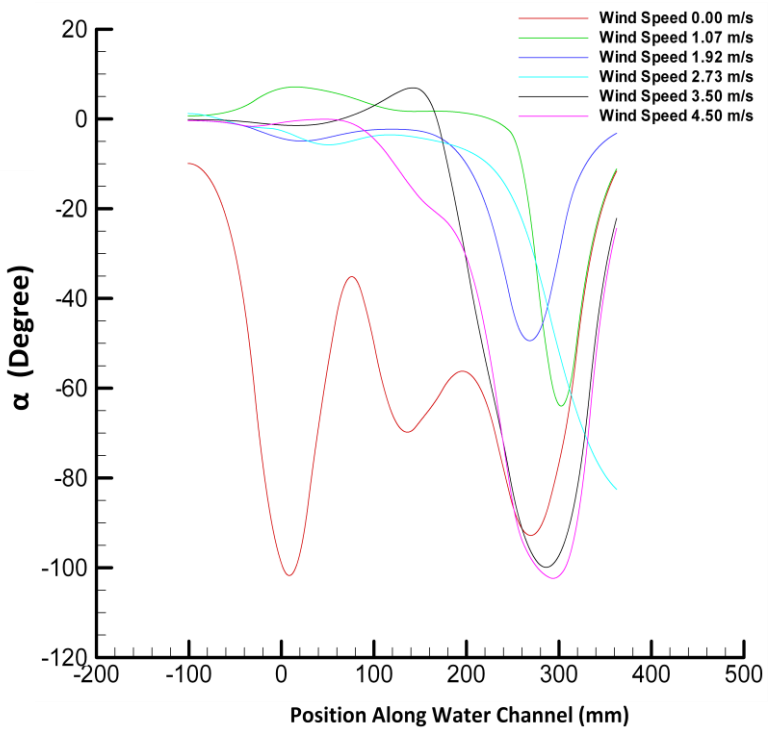

Figure (4.7c)

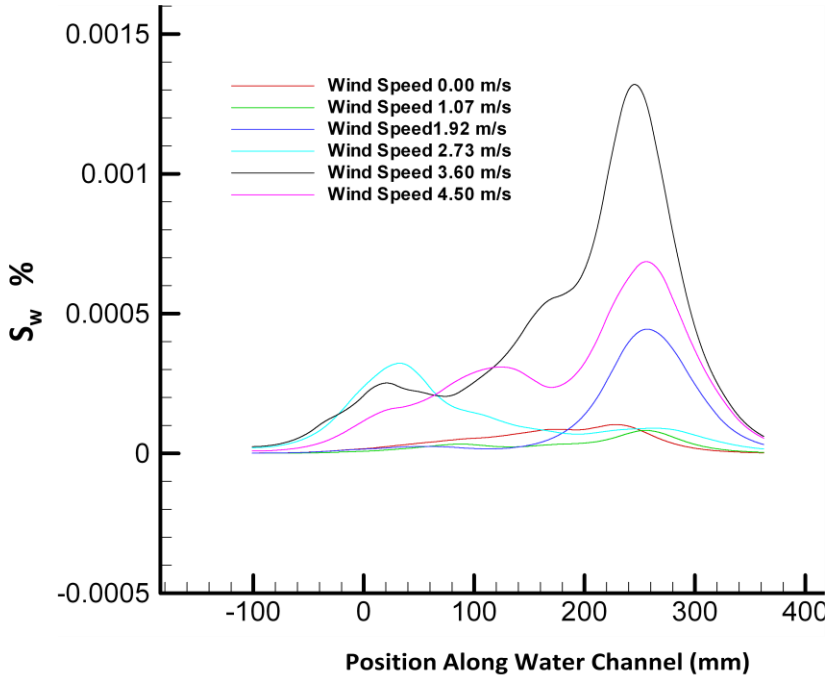

Figure (4.7d)

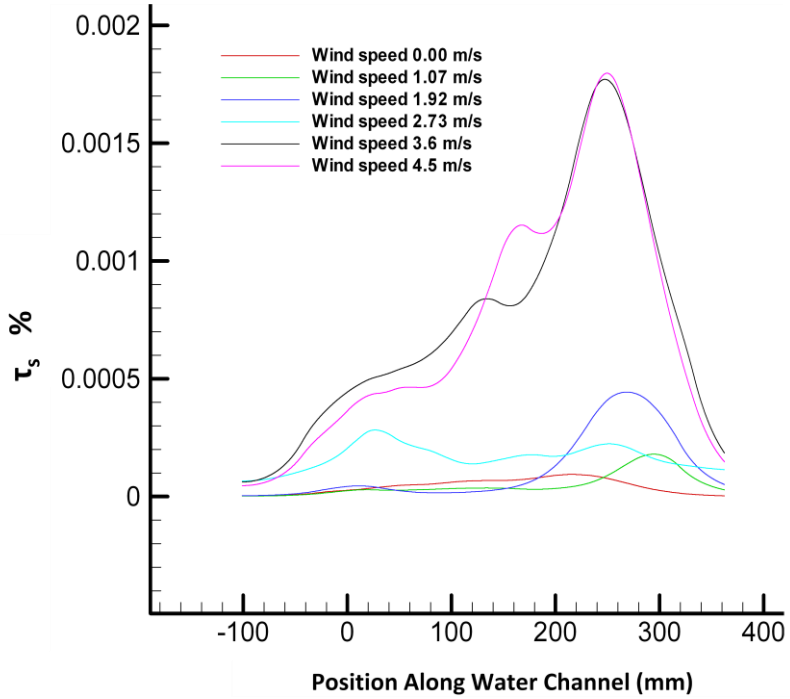

Figure (4.7e)

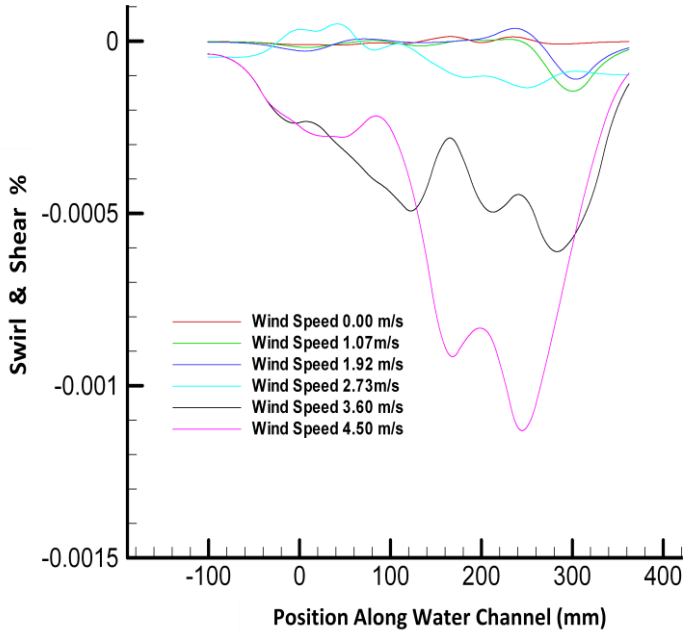

Figure (4.7f)

Figure (4.7a-f): The Flow velocity (V), Vorticity Rot-z, Velocity vector angle (α), Swirling Strength S_w, Shear strength (τ_s) and Swirling and Shear versus position along water channel. These measurements were taken under the action of the wind effect. The wind speed varied from 0 to 4.5 ms^{-1}. A notable increase occurred in the values of the above parameters at the last part of the measure zone F3 which is very close to the sudden expansion zone

4.5.1 Kinetic energy ratio

The relationship between the relative kinetic-energy of the bulk and the wind,$(\frac{V_{max}}{U_w})^2$ and the vorticity, swirling strength and shear strength under steady wind conditions at **F1** is shown in Figure (3.8a). The data points 1-5 represent the magnitudes of these parameters versus $(\frac{V_{max}}{U_w})^2$ at speeds of (1.07, 1.92, 2.73, 3.6 and 4.5 ms^{-1}) respectively. The growth of, $(\frac{V_{max}}{U_w})^2$, (Rot-(z), S_w and τ_s) is insignificant when the wind blows with a speed less than or equal to 2.73 ms^{-1}. As the wind speed increases, all the above parameters show significant growth. The three curves in Figure (4.8a) show approximately similar trends at the corresponding value of, $(\frac{V_{max}}{U_w})^2$.

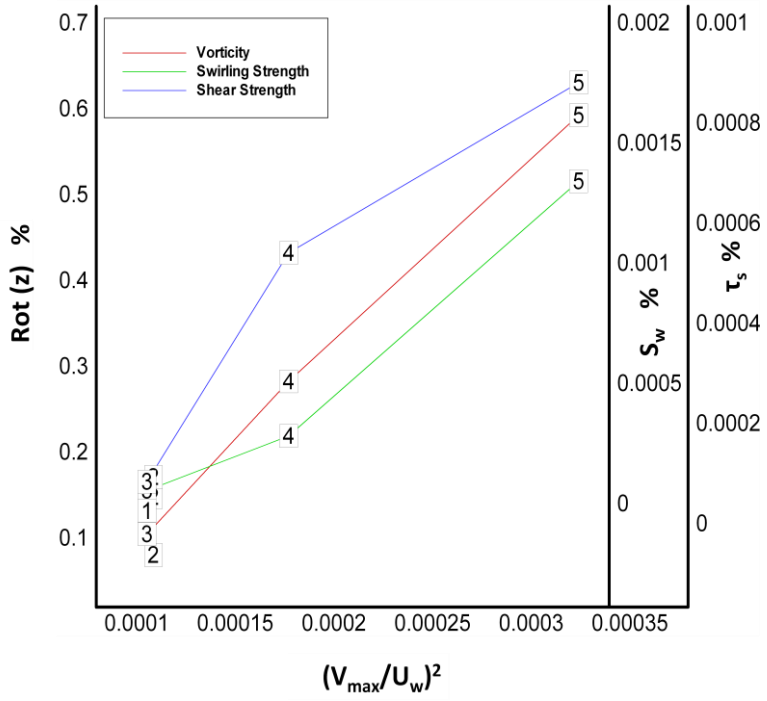

Figure (4.8a): A comparison of the max shear strength at F1 against water-wind kinetic energy ratio. The digits 1- 5 represent the wind speeds of 1.07, 1.92, 2.73, 3.6 and 4.5 ms^{-1}.

The relationship between Rot-(z), S_w and τ_s against $(\frac{V_{max}}{U_w})^2$ at F3 zone, under the effect of the same wind speeds in Figure (4.8a) is shown in Figure (3.8b). As shown in Figure (4.8b), at the **F3** zone most of the bulk parameters showed considerably higher growths under the action of wind particularly at higher wind speed when compared with the corresponding parameters at F1 and F2 except the swirling strength which did not show the same increment. The bulk parameters at F3 show distinct trends

when they are studied against $(\frac{V_{max}}{U_w})^2$. The maximum values of these parameters did not occur at the maximum magnitudes of $(\frac{V_{max}}{U_w})^2$. Rot(z), S_w and τ_s attain different magnitudes through a small range of $(\frac{V_{max}}{U_w})^2$. It is evident from the trends in Figures (4.8a) and (4.8b) that there is a difference between the growth of the bulk parameters under the action of steady wind and under the action of unsteady wind flow. In the former the bulk parameters grow steadily against $(\frac{V_{max}}{U_w})^2$ whereas the latter show different trends against $(\frac{V_{max}}{U_w})^2$.

The relationship between the kinematics and dynamic parameters between the bulk flow and the wave generation mechanism was illustrated in this chapter and in the previous chapter. It can be concluded that: the growth of the surface waves under steady wind flow conditions occurs due to the transfer of the wind momentum to the bulk, which causes steady evolution in the bulk flow parameters and therefore a steady evolution of the surface wave when the wind speed increases gradually. The behaviour and evolution of the surface waves under such conditions can be predicted even if the wind flow speed is very high. It is expected that the following relationships will be close to an exponential trend even if the wind speed is high:

1. The growth of the bulk flow parameters and the growth of the surface waves with respect to fetch length,
2. The wind velocity profile with respect to the height over water surface.

The generation and evolution of surface waves under unsteady flow conditions may occur due to the effect of the wind turbulence which causes fluctuations in the air pressure and speed over the water surface. The bulk flow parameters have different trends and growth rates based on the density of the fluctuations of the air's velocity and pressure even if the wind speed magnitude is low. The initiation and evolution of the surface waves and flow parameters under unsteady wind conditions can be predicted from analysing the wind turbulence fluctuations and from analysing the bulk flow parameters that showed different responses in term of vorticity, swirling strength, shear strength, etc.

In the light of this; the magnitudes of the flow parameters ratio are a function of $(\frac{V_{max}}{U_w})^2$ under the effect of steady wind conditions.

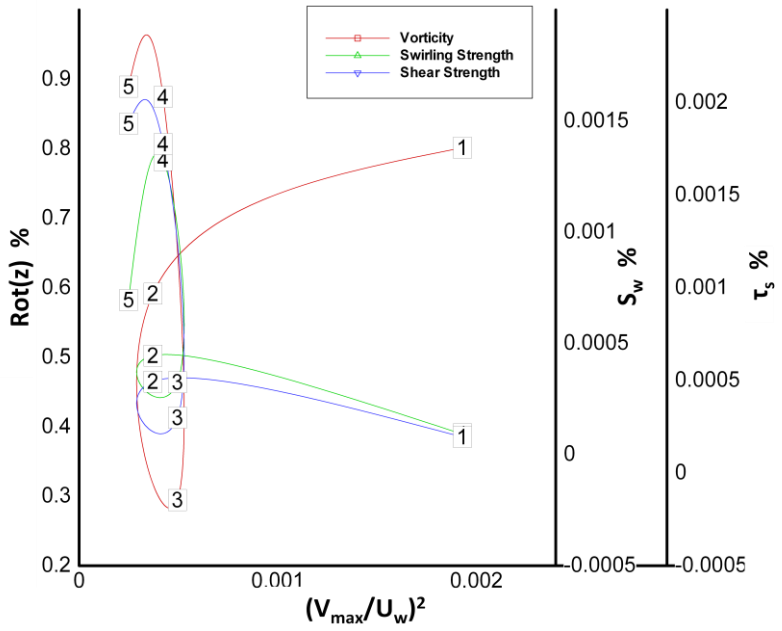

Figure (4.8b): A comparison of the max shear strength, swirling strength and vorticity at F3 against water-wind kinetic energy ratio. The digits 1- 5 represent the wind speeds of 1.07, 1.92, 2.73, 3.6 and 4.5 ms^{-1}.

4.6 Swirl and shear strength

The swirl and shear is calculated by subtracting the shear strength from swirling strength to observe the evolution of each parameter in the flow with respect to the other. However, a positive value of swirl strength & shear strength indicates that the flow is dominated by swirl action while a negative value indicates that the flow is dominated by the shear action. Figure (4.9a) is plotted based on the maximum positive value and minimun negative value of swirl and shear strength against the PIV measuring zone at F1. Figure (4.9a) shows the relationship between the maximum and minimum values of the swirl and shear against wind speed. The red line represents the positive value where the effect of swirl strength is dominant and the green line represents the negative value where the effect of the shear strength is dominant. Until to a wind speed of 3.6 ms^{-1}, the effect of the swirl on the flow is insignificant, but the effect of the swirl is significant only for a wind speed of 4.5 ms^{-1}. The shear strength

also has an insignificant effect on the flow until a wind speed of 2.73 ms^{-1} followed by a significant effect at wind speeds of 3.6 and 4.5 ms^{-1}. As shown in figure (4.9a), at wind speeds of 4.5 ms^{-1} the effect of the swirl strength and shear strength is significant, but the growth of the shear strength is higher than the swirl strength.

Figure (4.9b) is plotted on the same basis as Figure (4.9a) at F2. As shown in Figure (4.9b), the swirl strength and shear strength have the same trend as at F1; a notable effect of swirl and shear occurred at a wind speed of the order 1.92 ms^{-1}.

Figure (4.9c) shows the relationship between the maximal swirl strength and shear strength against wind speed at F3 using the same basis of plotting in F1 & F2. The growth of swirling strength is very low with respect to the growth of the shear strength until the wind speed of 2.73 ms^{-1}. At wind speeds of 3.6 ms^{-1} and 4.5 ms^{-1} the growth of swirling strength cannot be detected and only the effect of shear strength still existed. These results reveal the importance of using the shear strength in studying the effect of the wind on the characteristics of the bulk flow under different conditions.

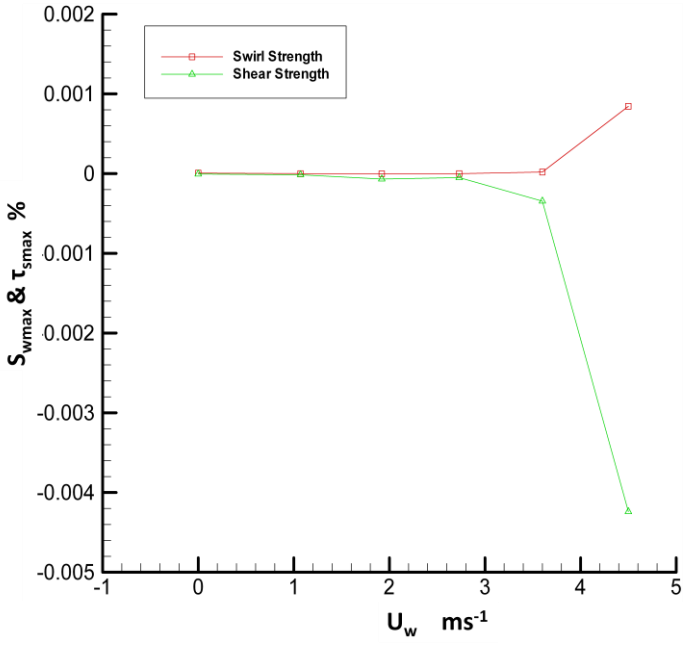

Figure (4.9a): The relationship between the swirl and shear against wind speed at F1

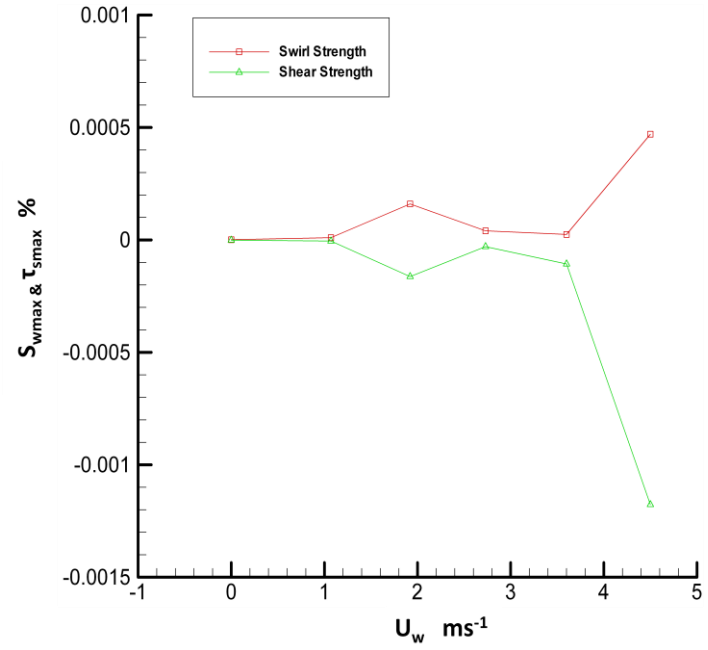

Figure (4.9a): The relationship between the swirl and shear against wind speed at F2

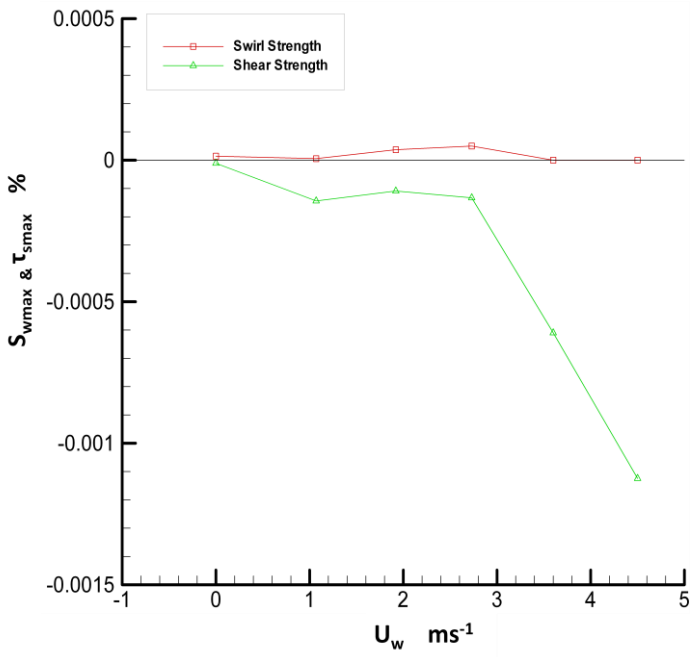

Figure (4.9a): The relationship between the swirl and shear against wind speed at F3

4.7 Conclusion

The flow parameters (flow velocity, vorticity, velocity vector angle, swirling strength, shear strength) have revealed reactions of different magnitudes and trends to the atmospheric input. The atmospheric inputs were changed in the current measurements due to changing the wind speed and the wind turbulence. The latter changed due to a sudden expansion in the wind tunnel cross-section.

The reactions of the flow parameters in terms of growth under the effect of higher air turbulence showed higher magnitudes than the corresponding parameters that grew due to the effect of the steady wind at a particular fetch length.

The behaviour of the velocity vector angle under the action of a steady wind can be understood as a parameter that may scale the flow transition from laminar flow to turbulent flow. This parameter showed the same behaviour but with different magnitudes of minimal angles even if the air-flow over the water surface is unsteady. In all cases the velocity vector angle magnitude changed from its maximum value under the effect of very low wind speed to its minimum value under the effect of a particular wind speed (as this speed the waves become visible) and then it showed gradual increase under the effect of higher wind speed action. This behaviour is understood as the flow transition from laminar flow wind speed to turbulent flow. The transition may occur as the velocity vector angle is at lower magnitudes at a particular wind speed. The existence of a lower velocity vector angle coexists with the generation of the initial waves. It is believed that the onset of the latter is due to the flow transition from laminar to turbulent.

Under effect of steady air flow the bulk flow parameter growth trends against wind speed are much closer to an exponential trend. However, this property was lost for most of the bulk parameters because of a sudden change in the air turbulence. The shear strength is one of the bulk flow parameters that maintained the exponential relationship against wind speed which gives the ability to predict the behaviour of this parameter under the action of higher wind speeds under different conditions.

The growth of the flow parameters such as vorticity, swirling strength and shear strength against the ratio of *air-bulk* kinetic energy showed a straightforward relationship under the effect of steady air flow. However, under unsteady air flow

conditions this relationship exhibited different trends. It can be concluded that the growth of the flow parameters and therefore the growth of the surface wave under the effect of steady air flow depends on the ratio of *air-bulk* kinetic energy, whereas under unsteady air flow conditions the turbulence fluctuations through the bulk is the key role of the wave generation.

Chapter five

Overall Conclusion and recommendation for future work.

5.1 Overall Conclusion

- Observing the evolution of the physical properties of the water surface under the effect of wind action to explain the wave generation mechanism is recognised as a comprehensive approach; the physical properties of the water surface and wave formation function with the same parameters.

- The surface structure and growth of capillary waves have the function of restoring forces at the surface and bulk flow regime. Since Oh number is scaled, the surface structure regime Oh number can be used to scale the evolution of the surface waves. The new formulation of Oh number is comprised of the capillary, viscous and inertia forces.

- The value of the critical wind speed for a water body can be predicted at a particular condition based on the magnitudes of the surface tension and viscosity.

- Since the characteristics of the air through viscous sublayer combine the characteristic of the water and the air, it is concluded that using the mean value of the kinematic viscosity of the wind and water surface, $\bar{\nu}$, instead of kinematic viscosity of the air, ν, in the equations that relate to the viscous sublayer zone, such as y1, $Z_{\circ}$, U_1 and $C_{D,}$ is more appropriate

- Capillary waves are instrumental in wave formation, growth once formed and the tendency of longer waves to decay. The action of the capillary waves through wind-water interaction strengthens the coupling between the wind-water and wind-wave, thus enhancing the transferring of wind momentum to water bulk and to longer waves.

- The key parameter that governs the formation and growth of the gravity waves is the wavelength. The parameters that affect the length of the capillary waves such as viscosity and surface tension should be considered when predicting the

characteristics of the gravity waves. It is suggested that the sea state can be predicted based on the magnitude of the surface tension and viscosity for a sample is taken near the sea surface.

- The evolution of bulk flow parameters are a function of the wind speed blowing over the water surface and background perturbations that exist in the flow before blowing the wind over the water surface.

- The inherent vorticity in the bulk flow is an important factor inducing circulation in the bulk to accelerate wave formation

- The significant growth of the flow parameters occurs as the flow regime is transferred to turbulent regime. After the transition, the growth becomes faster and waves attain higher magnitudes of energy.

- The behaviour of the velocity vector angle under the action of a steady wind can be understood as a parameter that may scale the flow transition from laminar flow to turbulent flow.

- Analysing the velocity field images under the effect of the wind action shows that bulk flow evolution occurs as follows:

  Vertical oscillation of water particles, existence of dark zones through the bulk, significant changes in the flow direction with respect to the wind direction, eddy formation and growth at different depths from the water surface and an increase in bulk flow fluctuations near the surface.

- The flow parameters (flow velocity, vorticity, velocity vector angle, swirling strength, shear strength) have shown reactions in different magnitudes and trends to the atmospheric input.

- The magnitudes of the kinetic-energy density at different orders of wind speed verify the importance of the background perturbation on the kinematics and dynamics of the flow and thus the wave formation and growth.

- The waves attain energy from the wind that is blowing over the surface and from the eddies that are propelled towards the surface. In the absence of one of these sources, the waves become weak and tend to attenuate.

- The growth of the flow parameters such as vorticity, swirling strength and shear strength against the ratio of *air-bulk* kinetic energy showed a straightforward relationship under the effect of steady air flow. However, under unsteady air flow conditions this relationship exhibited different trends.

5.2 Recommendations for future work.

Since the available theories and mathematical models are unable to explain observation of wave evolution over the whole range of wind and wave speeds and do not conclusively confirm the physical mechanism responsible for atmospheric input to the wave, the physical mechanism of wind generated surface waves is still a perplexing problem. It is suggested that experimental work is the solution for such problems

It is suggested that the following experimental work should be conducted in the future under specific conditions to provide more insight into the mechanism of wind generated surface waves.

The current experimental work using PIV gave insight to the effect of the wind action on the evolution of the bulk flow. It is suggested that experiments using the PIV system should be conducted to measure the bulk flow parameters simultaneously with measurements on the surface of the characteristics of the waves such as wavelength, wave amplitude, wave steepness, phase velocity. This should be done under the following conditions:

- Introduce a mechanical means to generate perturbations inside (not on the surface) the bulk under the effect of a given wind speed to observe the effect of such perturbation on energy and characteristics of surface wave. These observations should be compared with a situation using wind action only to generate surface waves. Using the same facilities it is suggested to introduce a particular mechanism to damp the flow perturbation to discover the importance of such mechanisms on reducing the effect of the scouring.
- Conducting experiments to observe the effect of the physical properties on the characteristics of the bulk flow parameters and on the surface waves using water with different physical properties (seawater, fresh water, distilled water and contaminated water)
- Conducting experiments to observe the correlation between the physical properties of the surface, wave generation and bulk evolution. In these experiments it is suggested that substances which cause a significant change in the physical properties of the water surface should be used.

- Using a particular device to increase the relative humidity to examine the effect of this parameter on the characteristics of the waves.
- Using a particular device to increase the density of the electrical charges on the wind. In these experiments it is recommended to use distilled water, tap water, sea water and water with detergents.
- Studying the characteristics of surface waves and bulk flow parameters at normal and very low temperatures where a significant increase in the bulk viscosity and significant decrease in the wind viscosity occur.
- Studying the properties of water particles in terms of solid properties to highlight the mechanism of saving and releasing energy through the water particles under the action of the wind.
- Estimate the proportional factor m in equation $\lambda_x = \mathrm{m}\lambda_w$ using water with different magnitudes of elasticity.
- Studying, using CFD, the evolution of the waves from capillary waves to gravity waves for several orders of elasticity and viscosity, in order to explain the effect of such parameters on the contraction and extension of the wavelength of capillary waves. The latter has a significant effect on the growth and evolution of the gravity waves.
- Studying the correlation between the characteristics of the eddies and the characteristics of the surface waves. It is recommended to study the characteristics of the eddies at different orders of water depth. The correlation between the wavelength and maximum wave height is one of the outcomes of such measurements.
- Studying the characteristics of the flow beneath ships while sailing in the sea, to recover the consumed energy by the ship's engines.

It is believed that the material of the tracer particles should be considered through conducting experiments in wind tunnel facilities using the PIV system as a measurements system, at least for ionic fluids (fluids containing salts and minerals) where the fluid molecules have different electrical charges. The density and type of the accumulated electrical charges on the tracer particles depend on the particle material. This may affect the evolution of the flow under action of the wind and consequently the accuracy of the velocity information at low flow velocity.

References

- Adrian, R.J. Christensen, K.T. Liu, Z.C., 2000, "Analysis and interpretation of instantaneous turbulent velocity fields", *Experiments in fluid*, 29, 275-290
- Atakürk, S.S., and, Katsaros, K.B., 1999, "Wind stress and surface waves observed on lake Washington", *Journal of physical oceanography*, 29, 633-650.
- Brown R.C., 1935, "the ripple method of measuring surface tension", *Proc phys. Soc. Lond*, 532, 312-322.
- Brutsaert, W.A., 1975, "theory for local evaporation or heat transfer from rough and smooth surface", *Water Resource. Res*. 11, 543-550.
- Carter, D. J. T., 1982 "Prediction of wave height and period for a constant wind velocity using the Jonswap results". *Ocean Eng*, 17-33.
- Caulliez, G., Ricci N., and DuPont R., 1998, "The generation of the first visible wind waves", *Physics fluids* 10, 757-759.
- Cetinbudaklar, A.G., and Jameson, G.J., 1969, "The mechanism of flooding in vertical countercurrent two-phase flow, *Chemical engineering science*, 24, 1669-1680.
- Darrigol, O., 2005,"Words of flow, A history of hydrodynamics from the Bernoullis to Prandtl", Oxford university Press, 356 pp.
- Davies, J.T. and Rideal, E.K., (1963). "Interfacial Phenomenon", Academic Press, 480 pp.
- Davis, J.T., Qidwa, A., and Hameed, A., 1968, "Surface stresses and ripple formation due to low velocity air passing over water surface", *Chemical engineering Science*, 23, 331-337.
- Donelan, A.D., Dobson F.W., Smith, S.D., Anderson R.J., 1993," On the dependence of sea roughness on wave development", *Journal of Physical Oceanography*, 23, 2143-2149
- Dragčević Dj, Vuković M and Pravdić V, 1979, "Properties of the seawater-air interface. Dynamic surface tension studies", *Limnol Oceanogr* , 24, 1022-1030
- Elsayed M.A.K., 2006, "Wavelet bicoherence analysis of wind wave interaction", *Ocean engineering*, 33, 458-470.

- Fitzgerald, L.M., 1964, "The effect of the wave-damping on the surface velocity in a wind tunnel", *Aust, J. Phys*, 17, 184-188.
- Fox Robert W., McDonald Alan T., Pritchard Philip J. (2004). "Introduction to fluid mechanics ", sixth edition. *Academic Press* New York.
- Gary A. Wick, William J. Emery, and Lakshmi H. Kantha 1996. "The Behaviour of the Bulk-skin Sea surface temperature difference under varying wind speed and heat flux. Journal of physics oceanography", 26, 1969-1988.
- Gottifredi J.C., Jameson, G.J., 1968, "The suppression of wind generated waves by surface film" *J. Fluid Mech.*, 32, 609-618
- Gottifredi, J.C., and Jameson, G.J., 1970, "The growth of short waves on liquid surfaces under the action of a wind" *Proc. Roy. Soc. Lond, A.*, 319, 373-397.
- Gaster, M., 1962," A note a relation between temporally increasing and spatially increasing disturbances in hydrodynamic stability" *J. Fluid Mech.*, 14, 222-224.
- Grassal, H., 1976, "The dependence of the measured cool skin of the ocean on wind stress and total heat flux", *Boundary- layer meteorology*, 10, 465-474.
- Handler R. A., Smith G. B., and Leighton R. I, 2001., "The thermal structure of an air-water interface at low wind speeds", *Tellus*, 53A, 233-244.
- Handler, R.A., Smith, G.B. and Leighton, R.I, 2001, "Thermal structure of an air –water at low wind speeds", *Tellus*, 53A, 233-244.
- Harris J.A, Belcher S.E and Street R.L., 1994, "Linear dynamic of wind waves in coupled air-water flow. Part 1. Theory". *J. Fluid Mec*, 308, 119-151.
- Harris J.A, Belcher S.E and Street R.L., 1996, "Linear dynamic of wind waves in coupled air-water flow. Part 2. Numerical model", *J. Fluid Mech*. 308, 219-254.
- Hasselmann Dieter and Bösenberg Jens, 1991, "Field measurements of wave-induced pressure over wind-sea and swell"., J. *Fluid Mech,* 230, 391-428.
- Hidy, G.M., and Plate, E.J., 1966, "Wind action on water standing in a laboratory channel", *J. Fluid Mech.*, 4, 651-687
- Holman J.P., (1997) Heat Transfer. 8th Ed. New York: McGraw-Hill.

- Hsiao S. V. and Shemdim O. H., 1983, "Measurements of wind velocity and pressure with a wave follower during marsen". *Journal of Geophysical Research*. 88, 9841-9849.
- http://en.wikipedia.org
- Huntley, H.E., 1952, "Dimensional analysis" Macdonald & Co Ltd,158 pp
- Hyun, B.S., Balachandar, R., Yu K., Patel V.C., 2003, "Assessment of PIV measure mean velocity and turbulence in open-channel flow", *Experiments in fluid*. 35, 262-267.
- Jeffreys, M.A., 1924, "On the formation of water waves by wind", Proc. Roy. Soc. A, 107, 189-206
- Jessup, A.T., and Phadnis, K.R., 2005, "Measurement of the geometric and kinematics properties of microscale breaking waves from infrared imagery using a PIV algorithm", *Meas. Sci. Techno*, 16, 1961-1969.
- Judd, K. P., Phongikaroon, S., Smith, G. B., and Handler, R. A., 2005, "Thermal structure of clean and contaminated free-surfaces subjected to an impinging gas Jet," Exp. *Fluids*, 38, 99–111.
- Kahma K.K., 1981, "A study of the growth of the wave spectrum with fetch", *Journal of physical oceanography*, 11, 1503-1515.
- Kahma, K.K., and, Donelan, M.A., 1988, "A laboratory study of the minimum wind speed for wind wave generation", *J. Fluid Mech*. 192 (1988) 339-364.
- Kawai, S., (1979), "Generation of initial wavelets by instability of coupled shear flow and their evolution to wind waves", *J. Fluid Mech*., 93, 661-703.
- Kawai, S., 1979b, "Discussion on the critical wind speed for wind-wave generation on the basis of shear flow", *Journal of the oceanographical Society of Japan*, 35, 179-186.
- Keulegan G.H., (1951), "Wind tides in small closed channels" *J. Res .natn. Bur. Tand*., 46, 358-381.
- Kline SJ, Robinson SK, 1989, "Quasi-coherent structures in the turbulent boundary layer", *Proceeding of Zaric Memorial Conference*,200-217,
- Lamp, H., 1932, "Hydrodynamics", Cambridge University press, 738 pp.
- Larson, T.R., Wright, J.W., 1975, "Wind generated gravity-capillary waves measurements of temporal growth rates using microwave backscatter", *J. Fluid Mech*., 3, 417-436.

- Lorenz, R.D., Kraal E.R., Eddlemon, E.E., Cheney, J., and Greeley, R., 2005, "Sea-surface wave growth under extraterrestrial atmospheres: Preliminary wind tunnel experiments with application to Mars and Titan", *ICARUS*, 175, 556-560
- Mansfield W.W., 1973, "The influence of surfactants on flow at wind-blown over water surfaces", *Chemical engineering science*, 29, 1593-1600
- Marian Muste, Jörg schöne, Jean-Dominique Creutin., 2005, "Measurement of free-surface flow velocity using controlled surface waves", *Flow measurement instrumentation*, 16, 47-55.
- Mastenbroek, Cornelis, 1996, "Wind wave interaction". PhD theses..
- Miles, J. W., 1957, "On the generation of surface waves by shear flows", *J. Fluid Mech.*, 3, 158-204.
- Miles, J. W., 1959, "On the generation of surface waves by shear flows", *J. Fluid Mech.*, 7, 469-478.
- Miles, J. W., 1962, "On generation of surface waves by shear flow. Part 4", *J. Fluid Mech.*, 13, 433-448.
- Miles, J. W., 1967, "On the generation of surface waves by shear flows", *J. Fluid Mech.*, 30, 163-175.
- Miles, J. W., 1967, "surface-wave damping in closed basins", *Proc. Roy. Soc. London, Ser. A*, 297, 459-475
- Peirson W.L., Garcia, A.W., 2003, and Pells, S.E, "Water wave attenuation due to opposing wind", *J Fluid Mech*, 487, 345-365
- Petkov, J.T., Danov K.D., and, Denkov N.D.,1996," Precise method of measuring the shear surface viscosity of surfactants monolayers", *Langmuir*, 12, 2650-2653
- Phillips, O.M., 1957, "On the generation of waves by turbulent wind" *J. Fluid Mech.*, 2, 417-445.
- Phongikaroon S, Judd, K.P., 2006, "surfactants effects on the free surface thermal structure and subsurface flow in a wind-wave tunnel", *Journal of fluid engineering*, 128, 913-920.
- Phongikaroon, S., Judd, K. P., Smith, G. B., and Handler, R. A., "The thermal structure of a wind-driven Reynolds Ridge". Exp Fluids, 37 (2004)153–158.

- Pierson, W.L.,. Gracia A.W., and, Pells, S.E., 2003, "Water wave attenuation due to opposite wind", *J. Fluid Mech.*, 487 345-365.
- Plate E.J., Chang, P.C., Hidy, G.M., (1969), "Experiments on the generation of small water waves", *J. Fluid Mech.*, 35, 625-656.
- Plate, E. J., Chang, P. C., 1969, "Experiments on the generation of small water waves by wind. *Journal of fluid mechanic*, 35, 625-656.
- Pockels, A., (1891), "Surface tension", *Nature*, 43, 437-439.
- Pokazeyev, K.V., and Voronin, L.M., 1982, "Initial stage of wind wave development", *Izv. Atoms. Ocean. Phys*, 18, 689-691
- R. A. Apakashev and V. V. Pavolv. "Determination of the shear strength and Modulus of water at low flow velocities". Fluid Dynamics, 32 (1997)
- Raffel, M., Willert, C. and Kompenhans, J., 1998, "Particle Image Velocimetry", Springer, pp 249.
- Richard Leighton and Geoffrey Smith A comparison of simulated and experimental IR measurements at low to moderate wind speed. Seattle (1998). (481-483).
- Rosen M.J., 1978, "Surfactants and interfacial phenomena", A Wiley-interscience publication, 304 pp.
- Sang-Ho Oh, Natsuki Mizutani, Kyung-Duck Suh, Noriaki Hashmito. "Experimental investigation of breaking criteria of deep water wind waves under strong action. Applied ocean research "27 (2005) 235-250.
- Satterly, J., and Turnbull, R., 1929, "The ridge at the junction of clean and contaminated liquid surface", *Trans. R. Canada*, 23, 95-118.
- Saunders, P. M., (1967) "the temperature at ocean-air interface". *J. Atoms. Sci*, 24 (269-273).
- Scott, J., C., 1982, "Flow beneath stagnant film on water: the Reynolds ridge", *J. Fluid mechanics*, 116, 283-296.
- Smolentsev, S., and, Miraghaie, R., (2005), "Study of a free surface in open channel water flows in the regime from "weak" to "strong" turbulence", *International journal of multiphase flow*, 31, 921-939.
- Snyder, R.L and Cox, C.S., 1966, "A field study of the wind generation of ocean waves", *Journal of Marine Research*, 24, 141-178.

- Teixeira, M.A.C and, Belcher, S.E., 2006, “On the initiation of surface waves by turbulent shear flow”, *Dynamics Atmospheres and Ocean*, 41, 1-27.
- Ursell, F., 1956, “Wave generation by wind, in surveys in mechanics”, *Cambridge University Press*, 216-249.
- Van Dorn, W.G., 1953, “Wind stress on an artificial pond”, *Journal of marine research*, 12, 249-276
- Volino R.J., Smith G. B., 1999, “Use of simultaneous IR temperature measurements and DPIV to investigate thermal plumes in a thick layer cooled from above”, *Experiments in fluid* 27, 70-78.
- Wamdi Group, 1988, “The WAM model-A third generation ocean wave prediction model”, *J. Phys. Oceanogr*, 18, 1775-1810.
- Young, I.R., 1999, “wind generated ocean waves”, Elsevier, 288 pp.
- Zapke A., and Kröger, D.G. 2000, “Countercurrent gas-liquid flow in inclined and vertical ducts-II: the validity of Froude-Ohnesorge number correlation for flooding”, *International Journal of Multiphase flow*, 261457-1468.

Appendix

Better Understanding of Wave Generation Mechanism near water surface

M. Janajrah[1], R. Calay[1], A.P Lewis[1] and O. Badran[2]
[1] School of Aerospace, Automotive and Design Engineering, University of Hertfordshire, Hatfield, Herts, UK, AL10 9AB, *Email: M.A.M.Janagreh@herts.ac.uk*
[2] Mechanical Engineering Department, Faculty of Engineering Technology, Al-Balqa' Applied University, Amman 11134, Jordan, Telefax; +962-6-5679773,

Abstract
The effect of wind speed on the flow parameters beneath the water surface is explored in a wind tunnel facility using a PIV system. The effect of the wind on the flow beneath the surface can be detected at very low wind speed. The plots and 2D velocity field images showed how the flow by such a system beneath the water surface develops by the action of wind characteristics. The direct relationships between the flow development beneath the water surface and the generation of surface wave are investigated. To gain better understanding of the wave generation mechanism at low wind speed, the development of the flow beneath the water surface should be considered in parallel with wave characteristic.
Key Words: PIV, flow parameter, surface wave.

Introduction

The wave generation mechanism at low atmospheric wind speed is affected by several parameters such as the wind speed, Caulliez et al (1998), physical properties of the water surface, Davies et al (1967), chemical composition of the water, Kawai (1979), wind speed to phase speed ratio Mastenbroek (1996), turbulence in the air and water Teixeira and Belcher (2005), atmospheric pressure Lorenz et al (2005), basin geometry Ataktürk and Katsaros (1999), fetch length, Plate et al (1969), heat flux on the surface, Volino and Smith (1999),etc. The large number of parameters that affect the wave generation and evolution mechanism make a complete understanding of the phenomenon very difficult. On the other hand the problems associated with measurement of direct momentum input to a water wave from the wind add further complexity to the phenomenon. The recent studies of Teixeira and Belcher (2005) showed that the turbulence in the water is more effective for wave generation at the surface than the turbulence in the air, and the waves generated by the turbulence in the air are gentler than the wave generated by the turbulence in the water. However to study the relationship between the hydrodynamics of flow beneath the water surface and surface wave generation under action of wind, a number of experiments using PIV systems were carried out in wind tunnel facilities. The measurements results of flow parameters beneath the surface are plotted against the fetch. The plots showed how the flow develops and the relationship between the flow developments beneath the surface and wave generation and evolution are observed at different wind speeds.
The clarification of the relationship between the wave evolution and flow development beneath the surface form a key role in finding better interpretation of wave generation mechanism.

Experiment setup:

The experiments were carried out using a PIV system in a water channel of 9 m length, 1.22 m width, and 0.53m depth, with wind tunnel section transitioning smoothly over the water surface, in the Fluid Mechanics Laboratory at the University of Hertfordshire. The actual water depth was 0.48m. The fan speed was adjusted at six positions to change the wind speed. The wind speed measured at height of 1.22 m over water surface. Hot wire (H.W) anemometry and Digital vane anemometry (DVA) were used for

estimation the wind speed. Comparison of wind speed at the given location from the method is given in table1. The Hot wire measurements method is used in this paper to analyse the flow at different wind speed. The reliability of HW measurements was higher than DVT.

Table (1) wind speed measurements using Hot wire (H.A) and Digital Vane Tachometer (DVA).

H.W m/s	0	1.07	1.92	2.73	3.6	4.5
DVT m/s	0	0.97	2.1	3.46	4.9	6.3

The water was seeded by hollow glass spheres with diameters $9-13\mu m$. since the density of the glass spheres is equal to 1.2 water density and the diameters of the spheres are very small, may be assumed that the spheres will follow the flow in all directions. The 15Hz PIV system includes: 2M pixel camera, high resolution 2048×2048, with the ability to control exposure time, triggering the image acquisition, and trigger schemes, 50 mJ double pulse YAGPIV laser. DaVis software was used to analyze the data. DaVis is a CCD image acquisition and processing program developed by LaVision

A laser beam used to illuminate the spheres is sited under the water channel and the camera placed parallel to the channel walls. In order to allow the laser sheet to penetrate the water from the bottom to the surface and to obtain an image the bottom and the channel sides are made from the glass. The measurements were taken at 3m from the upstream edge of the water channel and the width of the laser sheet was 40 cm.

Experiments Results:

PIV is an optical technique to measure instantaneously a 2D velocity field. The system has a capability to measure the entire flow in a plane with either two or three velocity components. In PIV experiments several hundred images are captured and processed to provide instantaneous velocity fields

The averages of instantaneous velocities fields below show the effect of the transfer of wind momentum at different wind speeds on characteristics of the flow hydrodynamics beneath the surface.

Figure (1) shows the vector velocity field under zero wind speed condition. The flow appearance is uniform from near the water surface to the bottom. However velocity vector movements as shown through the sequence of movies and the vectors shows water particles in oscillatory motion

Fig (1) Velocity at still water (zero fan speed).

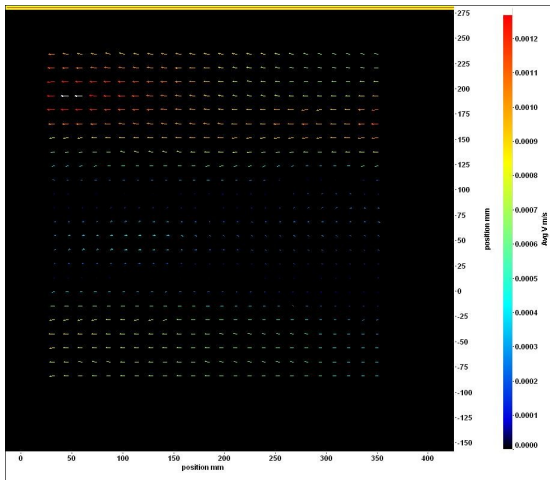

Fig (2) Velocity field at 1.07 m/s wind speed

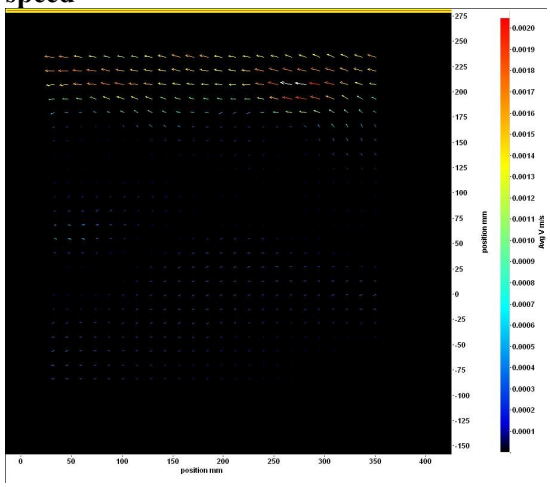

At 1.07 m/s wind speed the water flow may be seen to be forming *calm regions* having very low velocity magnitude. The

calm regions have been noted under effect of low wind by Plate et al (1969) and Caulliez et al (1998) before the surface wave become visible. These two studies were carried out at a range of wind speeds under lab conditions. Results from these papers show that *calm regions* disappear gradually by increasing the wind speed. The movement of velocity vectors is transferred at this wind speed from stationary to translational movement. It is thought that the transition from oscillatory movement to translation movement initiates the slow movement regions.

Fig (3) Velocity field at 1.92 m/s wind speed

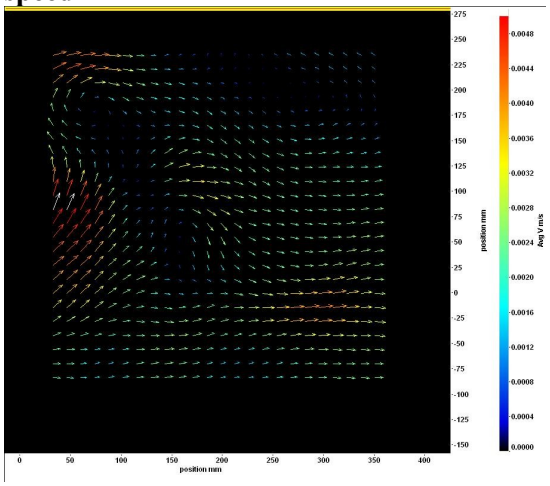

At a wind speed of 1.92 m/s, vortices start to appear at different water depths. The water flow velocity increases with wind speed at different depths. Observation of average velocity vectors at this wind speed shows that the velocity vectors rotate on vortices cores. The higher wind velocity increases the transfer of wind momentum which in turn increases the rotational vortices underneath the layer.

Fig (4) Velocity field at 2.73 m/s wind speed

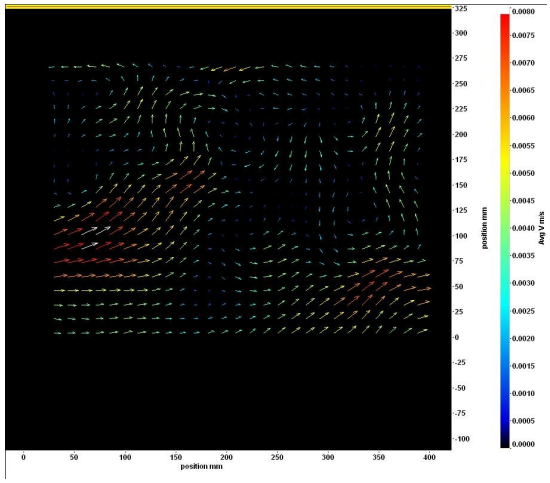

By increasing the wind speed to 2.73 m/s, the number and size of vortices is augmented, as well as the turbulence in water. The relationship between the increase in vortices size, speed and the generation of surface waves is observed. Surface wave could now be easily appreciated by the naked eye.

Fig (5) Velocity field at 3.6 m/s wind speed.

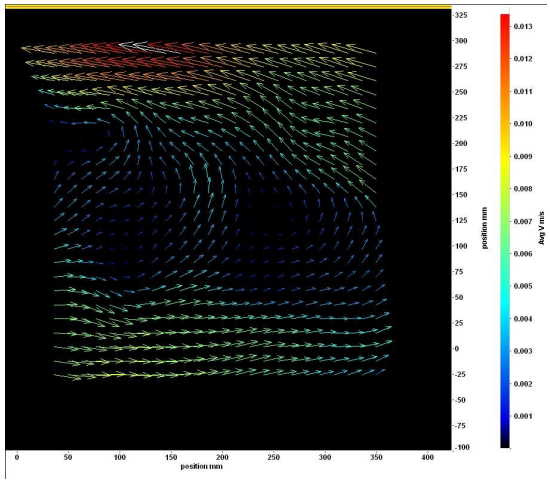

At a wind speed of 3.6 m/s the size of the vortices increased but their number decreased. The small vortices appeared to merge into a large one. At the same time an increase in surface wave's amplitude and speed are observed.

Fig (6) Velocity field at 4.5 m/s wind speed.

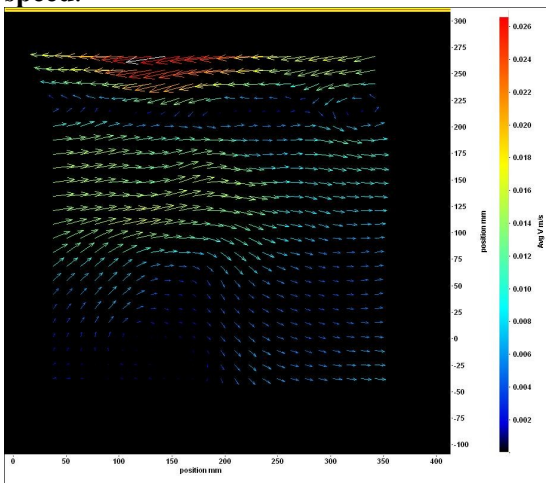

At a wind speed 4.5 m/s, a remarkable and visible augmentation of waves propagation speed is noted, and waves' amplitude becomes more visible. Waves become appreciable from the upstream edge of the channel and propagate in the wind's direction. The intensity of the turbulence beneath the surface is augmented and the speed of the water beneath the surface is increased.

Figures 1 to 6 show that the flow hydrodynamics beneath the water surface develop in a number of stages. The first stage shows that the water particles moving in oscillatory manner. The second stage showed that the water particles transition from stationary to translational movement forming calm regions at different depths from the surface. The third stage is characterized by vortices forming at different location from the surface and with an increase in flow velocity. Surface waves with small amplitude are generated at this stage. Further increases in wind speed show the flow characterized by augmentation in vortices size and speed which are accompanied with an increasing in wave's velocity and height.
To show more clearly of the effects of the wind speed on flow development below the water surface, the velocity vectors imagery format was imported by Tecplot software to generate plots.

Fig (7) Relationship between the positions along the water channel and water flow speed.

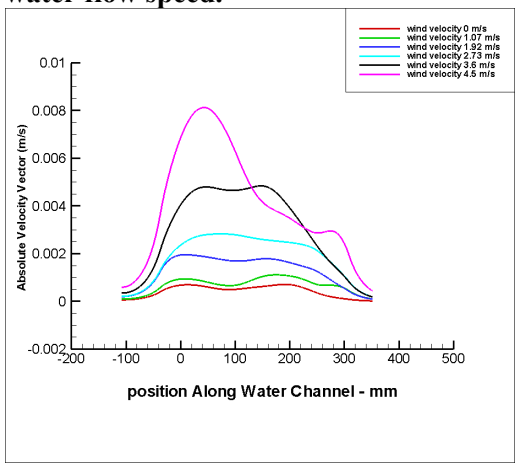

Figure (7) shows the direct relationship between water speed and wind speed at particular fetch. At wind speed of 3.6 and 4.5m/s the increased of absolute velocity vector was sharp reaching a peak followed by rapid decrease. This is in contrast with the lower wind speeds where a plateau may be seen. The maximum absolute velocity occurs at the maximum wind speed whereas at low wind speeds the absolute velocity vectors are comparative very low.

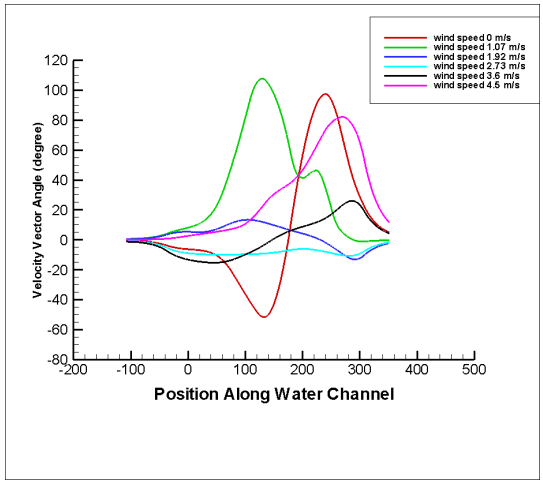

Fig(8) Relationship between the position along water channel and velocity vector angle at different wind speeds.

Figure (8) shows how velocity vectors angles vary with fetch and wind speed. The maximum velocity vector angles occur for wind speeds of 0 and 4.5 m/s.

Initially the velocity vector angle values decay with wind speed and the minimum value occurs at a wind speed 2.73 m/s, then rising to higher values at higher wind speeds. This sequence could be understood by the water particles movements from randomly in all direction at zero wind speed to a confine movement following the direction of wind shear

A visible surface wave was observed at a wind speed 2.73 m/s. It is assumed that the minimum wind speed required to generate visible waves occurs when the water particles movements translate from random behaviour to movement following the direction of wind shear.

The velocity field images showed the existence of calm regions as explained previously

Fig (9) illustrate the relation between the position along water channel and vorticity at different wind speed

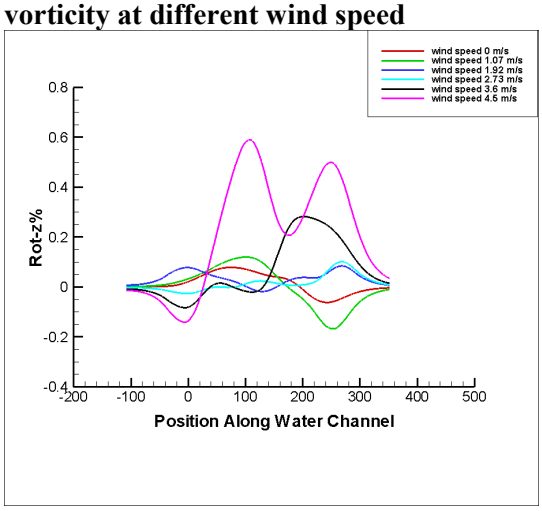

The component of vorticity perpendicular to the plane is shown. This is given by $\partial u/\partial y - \partial v/\partial x$.

As shown in figure (9) a significant increase in vorticity occurs at wind speed of 3.6 m/s and 4.5 m/s. The velocity field images also show the development of the vorticity with the wind speed.

The instantaneous relationship between the existing vortices and surface wave was observed as well as by Volino & Smith (1999). However insight wind-waves generation and evolution can be obtained from observing the vorticity. The vorticity gives an indication of the waves' generation and evolution on the water surface. The parameters that affect the vortices formation and evolution affect the wave in the same way. For instance in shallow water the friction induced by the water body base confine the vortices size and speed which in turn confines wave evolution. This is an example of one of the factors constraining the growing of the wave's amplitude at shallow or short fetch water bodies.

Fig (10) Relationship between the position along water channel and swirling strength at different wind speeds

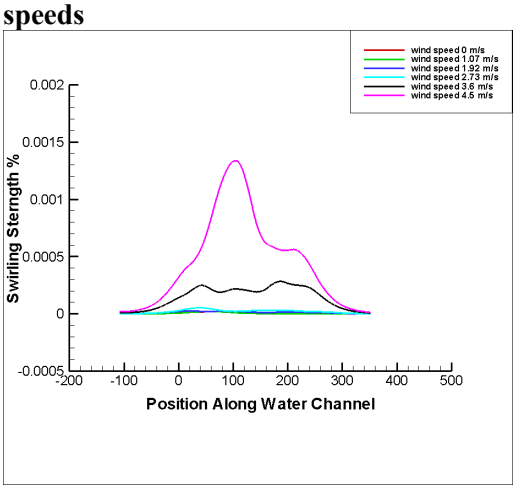

The swirling strength in Figure (10) is determined based on computation of the eigenvalues of the velocity gradient centre. In practice high levels of swirling strength indicate a location around which the streamlines are closed, which is typically the location of the vortex core. As shown in Figure (10), the swirling strength values at wind speeds less than 3.6 m/s are negligible. A noticeable increase in the swirling strength values occurs at wind speed 3.6 m/s and 4.5 m/s. Many studies of the wind wave's generation process at the water surface such as Lorenz et al (2005) and Ataktürk and Katsaros (1998) discarded cases at wind speeds of less than 3 m/s. The measurement systems of wave parameters did not show any significant response at wind speed of less than 3 m/s. These observations agree to some extent with our measurements. As shown in Figure (9) and (10), up to wind speeds of 2.73 m/s the transfer of wind momentum to the surface is not sufficient to initiates a detectable value of swirling strength and appreciable vortices. For these reasons, in

our experiments waves cannot be observed of wind speed less than 2.73 m/s. This value is not absolute, as it depends on the other water body parameters and atmospheric conditions.

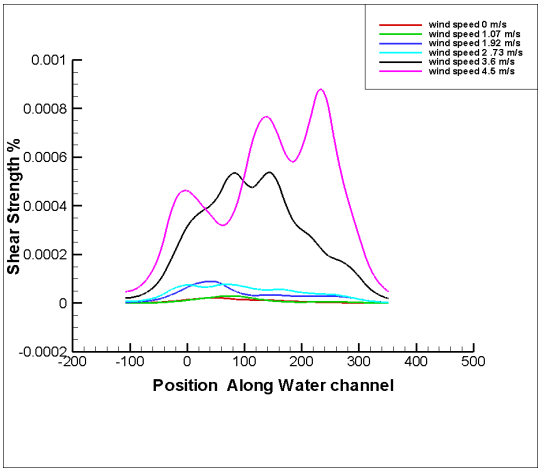

Fig (11) Relation between the position along water channel and shear strength at different wind speeds

The relationship between shear strength and wind speed at the given fetch is as shown in Figure (11). The relationship between shear strength, swirling strength, and vorticity and wind speed should be similar.

Conclusion

The effect of the wind speed on parameters of the flow below the water surface can be categorized depending on its behaviour into three groups:

1. The parameters which are affected by the wind gradually from still water to a wind speed of 2.73 m/s, after that an abrupt growth occurs in the maximum values at highest wind speed. An example is the absolute flow velocity.
2. Parameters, for instance the velocity vector angle, which attains its maximum values at very low wind speed and at the maximum wind speeds. The trend of the plots of these parameters tend to be similar to cosine wave form
3. Parameters which are not affected by wind speed until they reach 2.73 m/s, after which an abrupt grow in these parameters occurs Examples are such as: vorticity, swirling strength, and shear strength.

Understanding the generation and evolution of surface waves at different wind speeds can be obtained based on analysing the flow parameters beneath the surface.

The development behaviour of the flow verifies the idea that water waves have a long memory so that they reflect the atmospheric input integrated over the duration and fetch. The abrupt increase in some parameters can be justified based on this idea; the water particles accumulate the transfer of wind energy and momentum and release them when a certain air speed is reached. The behaviour of velocity vector angles provides a practical explanation for the process of saving and releasing the energy and momentum.

References:

[1] Cornelis Mastenbroek. Wind wave interaction. PhD theses. 1996.

[2] E. J. Plate, P. C. Chang and G. M. Hidy. Experiment on the generation of small water waves by wind. Fluid Mechanics 35 (1969) 625-656

[3] G. Caulliez, N. Ricci, and R. Dupont. The generation of the first visible wind waves. Physics fluids 10(1998) 757-759

[4] J.T. Davis, A. Qidwa, and A. Hameed. Surface stresses and ripple formation due to low velocity air passing over water surface. 23 (1967) 331-337

[5] Kawai (1979). Discussion on the critical wind speed for the wind-wave generation on the basis of shear flow instability theory. 35 (1979)179-186.

[6] K. K. Kahma and M. A. Donelan. A laboratory study of the minimum wind speed for wind wave generation. J. Fluid Mech. 192 (1988) 339-364.

[6] Ralph D. Lorenz, Erin R. Kraal, Eric E. Eddlemon, Jered Cheney and Ronald Greeley. Sea-surface wave growth under extraterrestrial atmospheres: Preliminary wind tunnel experiments with application to Mars and Titan. ICARUS. 175 (2005) 556-560

[7] R.J. Volino, G. B. Smith. Use of simultaneous IR temperature measurements and DPIV to investigate thermal plumes in thick layer cooled from above. Experiments in fluids 27 (1999) 70- 78.

[8] Sehard S. Ataktürk and Katsaros. Wind stress and surface waves observed on lake Washington. American Meteorological Society. 29 (1999) 633-650

[9] Teixeira and Belcher (2005) M.A.C. Teixeira and S.E. Belcher . On the

initiation of surface waves by turbulent shear flow, Dynamics Atmospheres and Ocean. 41(2006) 1-27

BETTER UNDERSTANDING OF WATER WAVE GENERATION BY ATMOSPHERIC WIND. PART-I

JANAJRAH. M. A [*] ***email: M.A.M.Janagreh@herts.ac.uk***

HOLDO. A. E [*] ***email: A.E.Holdo@herts.ac.uk***

LEWIS. A. P [*] ***email:A.P.Lewis@herts.ac.uk***

BADRAN. O. O [**] ***email: O_Badran@yahoo.com***

[*] Department Aerospace, Automotive and Design Engineering, University of Hertfordshire Hatfield, Herts, UK ,AL10 9AB,

[**] Al-Balqa Applied University, Faculty of Engineering Technology, Amman 11134, Jordan.

1. ABSTRACT:

This paper reviews the important studies done on the field of wave generated due to atmospheric wind and highlights the work that should be done for the purpose of initiating an experimental work.

The chemical effect which is studied in this part relates to water composition and interface lamina properties which affect the *air-water* momentum transfer mechanism. It is hypothesised that *the surface tension-dynamic viscosity ratio* gives an indication of the inception of the wave that generated on water surface due to very low wind speeds. Second it is hypothesised that the lamina dynamic viscosity determines the evolution's behaviour of the wave at high wind speed.

Keywords water composition, dynamic viscosity, surface tension, wind wave generation

2. INTRODUCTION:

The understanding of water wave generation by atmospheric wind is necessary in simulating wind-wave interaction.

There are several parameters working on wave generation through different mechanisms at different wind speeds. Some of these parameters affect wave generation and wave growth rate directly, whilst other parameters affected indirectly. Depending on this study, it is possible to

classify the process of wave generation due to three effects: Chemical effect, Thermal effect, and Mechanical effect.

The chemical effects are concerned with the effect of water composition on *air-water* interaction at the interface before the waves become appreciable by the naked eye. Whilst, the thermal and mechanical effects concern with heat flux and momentum transfer mechanism respectively. The *wind-water* interacts through the interface lamina. The lamina formation characteristics based on water composition and other conditions such as atmospheric conditions and wind speed. The nature and characteristics of the lamina play a major role in the *wind- water* momentum transfer mechanism.

Wind-water surface interactions

The water waves generated due to atmospheric wind evolves gradually from glassy (undisturbed) surface through different stages. The initial waves generation process is described by Plate and Chung (1969) where essentially two dimensional microscopic disturbances form on a nearly glassy surface. This behaviour of the waves was inferred from the appearance of the first visible waves.

Caulliez et al (1998) revealed three distinct zones within the initial wave generation area. In the first zone just downstream of the *air-water* junction, only tiny undulations, hardly perceptible by eye, propagate in the wind direction and the water surface looks perfectly smooth; in the second zone the first clearly visible wind waves can be easily seen; the third uniformly rough zone, where capillary waves cover the water surface uniformly.

According to Scot (1981) Surface-active material is present in most naturally occurring water samples, and it naturally diffuses steadily to free surfaces where it both reduces the surface tension and gives the surface elastic properties which enable it to resist compression. Phongikaroon and Judd et al (2006) showed that the surface-active materials or surfactants are naturally present in bodies of water. It diffuses to the free surface forming a thin layer that causes changing the characteristics of the interface lamina and influences wave motion.

According to Davies and Rideal (1963) the boundary between two homogeneous phases is lamina or film of characteristic thickness where the material in the' surface phase' shows properties differing from those of the material in the contiguous homogeneous phases.

According to Miles (1962) the wind and water surface becomes coupled and the momentum transfer from the wind to the surface occurs. According to Sehard et al (1999), that the water waves have a long memory; the water wave reflect the atmospheric input integrated over

duration and fetch, so the characteristics of the interface lamina affect momentum transfer mechanism and wave generation

In the light of the a above explanations It is hypothesised the following: 1.The natural active material extracted from the water bulk by wind action forming a very thin layer on the water surface consequent of the natural chemical reaction between the wind and natural active materials in the water bulk.

2. Increasing water surface viscosity enhance wind-water coupling (junction) at the interface which increases the rate of transferring momentum from wind to water surface. The water surface viscosity affected by water composition and fetch length under effect of wind

3. Increasing of water surface viscosity increases the water memory length; the water surface takes period of time before reflecting the atmospheric inputs on shape of wave growth and propagation, the surface response delay time based on surface viscosity mainly. The wind momentum and atmospheric inputs transfer to the water bulk through the water surface to different depths based on surface characteristics before reflecting the atmospheric inputs

The energy and momentum exchange through *wind-water* interface, the interface lamina properties surface such as surface tension, elasticity, and viscosity influenced by percentage of the active material in the water bulk, so the lamina properties occurred based on the type of water (sea water, fresh water, distilled water, etc.). According to Davies and Rideal (1968) the water surface lamina has a dynamic viscosity higher than water bulk and density lower than the water bulk. The water composition affects the surface characteristics which enables one to expect an effect of water composition on the *wind-water* interaction mechanism. Davies and Rideal (1968) experiments proved the diffusion of active material towards water surface occur and, the questions that arise are: *what is the active materials diffusion mechanism?*

What is the effect of the active materials diffusion mechanism on wave generation and growth?

Surface slope

According to Phongikaroon and Judd (2006) the air-water interaction mechanism causes a slight elevation in the free surface. The lamina thickness increases with wind speed and fetch, increasing lamina thickness along the wind direction generated an unsteady surface state; that the surface slope grows with fetch and wind speed. At a certain slope angle the surface starts moving.

The surface slope was measured by Scott (1982) in open water channel. A change of surface slope compared to water velocity was observed, the slope increased gradually upstream to a certain point and the sign of the slope was positive (the surface was observed to rise along the

wind direction) after which become negative. The results showed the maximum slope difference (max positive to max negative) increasing with water speed. Kahma and Donelan (1988) measured steep slopes accurately using a laser beam the X-axis increasing with fetch and z vertical and positive upwards. The spectra of surface displacement and the slope spectra measured only at wind speeds below 3 m/s, below this speed the growth rates was slightly underestimated and theory under predicts the measured growth rate. At very low wind speed the slope was very small and it was not possible to see by the naked eye, and when there was no wind at Z-slope spectrum was about ten times X-slope spectrum. It is hypothesised that the water surface slope growth is the first stage of wave generation is as a result of *wind-water* interaction. By increasing the fetch or time at very low wind speed, the surface slope grows gradually due to lamina thickness growth. Also it is hypothesised that the flow at the layer directly beneath the surface (few millimetres from the surface) flows in due the opposite wind direction causing an increase in surface roughness. The surface roughness increases the rate of the momentum that transfer from wind to water surface. Any additional increase in wind speed will change the flow direction beneath the surface towards the wind direction, and the ripple or small gravity waves start appear due to changing the flow direction beneath the surface as shown in figure (1)

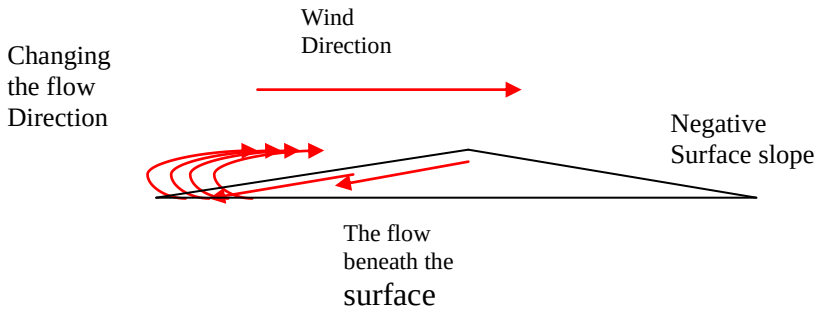

Figure (1), the surface slope grow gradually in positive and negative signs, the flow direction beneath the surface at very low wind speed opposite the wind direction, increasing the wind speed make to change the flow beneath the surface along wind direction and the surface become rougher

A simple experiment was performed in water channel- wind tunnel system at the University of Hertfordshire to study the winds effect on and beneath the water surface by spreading dye on the water surface and run the wind tunnel and specific speed. The water depth was 45 cm and the wind speeds at 1 metre above the surface vary from 1 to 5 m/s. It was found that at low wind speed the dye spreads beneath the surface directly to a few millimetres from the surface, and few amount of the dye spread across the channel toward the bottom. This experiment emphasized

that at low wind speed the water particles move towards the surface under wind action, and the vertical motion dominate the horizontal which make the vertical slope ten time the horizontal slopes in some cases. Other experiment was run in the same water channel-wind tunnel facilities using PIV system, the water seeded by hollow spheres glass with 9-13µm, the flow represented by velocity vectors image, the results showed that the water particles move with high velocity vector angle at low wind speed as shown in the figure (2)

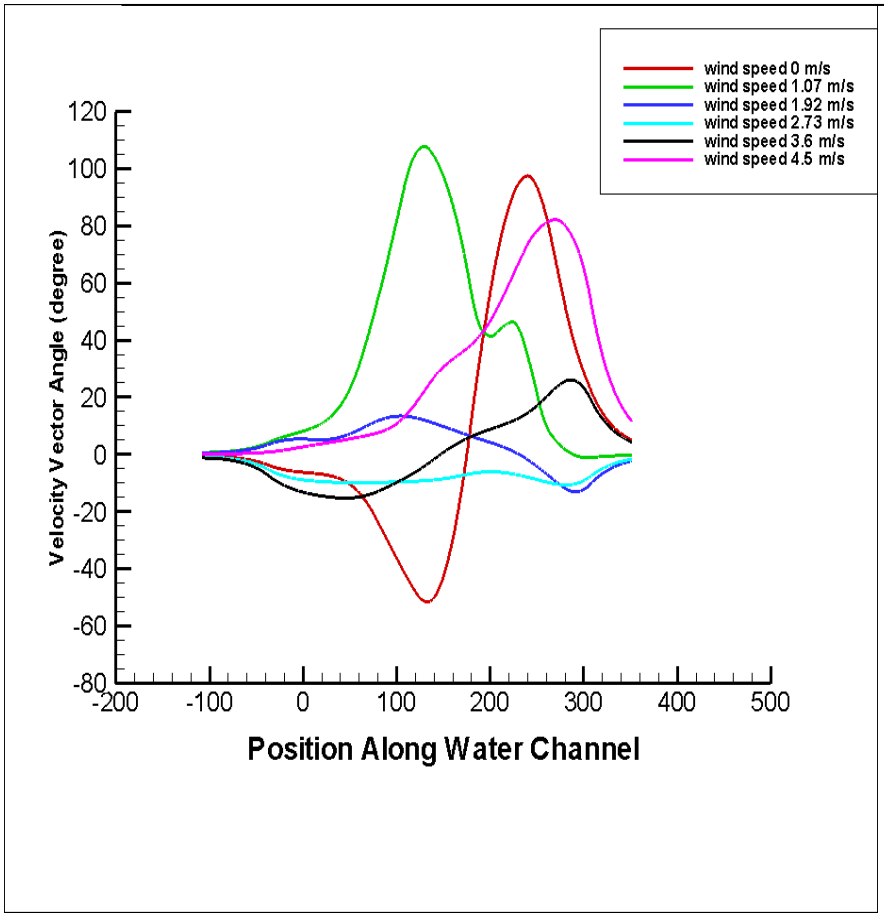

Figure (2) illustrates the relationship between the position along water channel and velocity vector angle at different wind speeds. The maximum velocity vector angle occurs at still water and at high wind speed. The water particles in still water randomly moves in all directions rather than confinement to the direction of wind flow by increasing the wind speed

The effect of water surface properties on the wave generation processes.

According to Fitzgerald (1964), the surface drift velocity of a liquid under the action of shear exerted by a wind was found to be $V_\circ \approx 0.03U_\infty$ **, where is** $V_\circ, U_\infty$ **, are drift velocity and wind**

speed respectively. However, in the presence of surfactant, at the same wind speed the surface velocity was 50 % above the previous value, the increase in drift velocity justified as a result of surface tension gradient at the interface.

In the presence of surface active agent (soap) the wave inception did not take place until wind velocity reached 12 m/s or $U_* \approx 0.6$ m/s **cm/s as showed by Keulegan et al (1951), however in the presence surfactants which has quite high values of surface elasticity wave generated at much lower velocities compared to soapy surface, at Lake Washington (nature field), Sehard (1999) found the wave inception occurred at wind velocity 3 m/s, Davies (1967) investigated that the ripple become appreciable on clean water surface at wind speed 1.6 m/s.**

Gottifredi and Jameson (1970) used artificially-generated mm-scale waves for different solutions, he found lower viscosity solutions had higher wave growth rates, and higher surface tension led to more rapid wave growth. The liquid density was not appreciably varied in his e and 1 bar air pressure was used throughout

Mansfield (1973) performed his experiments using a closed channel; he noted that when air was blown over a closed channel of water, a steady surface velocity developed as part of a flow extending to the channel bed. With concentrated solutions of surfactants, an entirely different flow is produced. The flow is confined to the boundary adjacent to the surface, and the surface velocity u_s **increases with the downwind distance x according to the following relation:**

$$u_s \propto x^{1/3} \quad \text{.....(1)}$$

The effect of the wind on water bulk investigated in our experiment in fluid mechanics laboratory at Hertfordshire University using PIV system, tab water was used without any chemical surfactant. As show in figure (3) (velocity vector imagery) the effect of the wind extend to water bulk at different depths forming vortices with size and speed based on wind speed.

Davies et al (1967) observed experimentally that the ripple becomes appreciable on the surface of the water at air velocities of about 1.60 m/s if water surface is clean, and only above 3.20 m/s if there is captive monolayer on the surface (low surface tension), and at equal air velocities the amplitude of the induced ripple when monolayer is present is only about 9 per cent of those on a clean water surface. Davies et al (1967) justified the differences between the last cases, by the surface tension gradient which makes to balances the wind stress.

The above explanations emphasize the effect of surface properties on the *wind-water* interactions mechanism. In the presence of the surfactants the momentum transfer from the wind to water

surface only, but the wind momentum effect on the surface extends to the bottom in the case of clean surface.

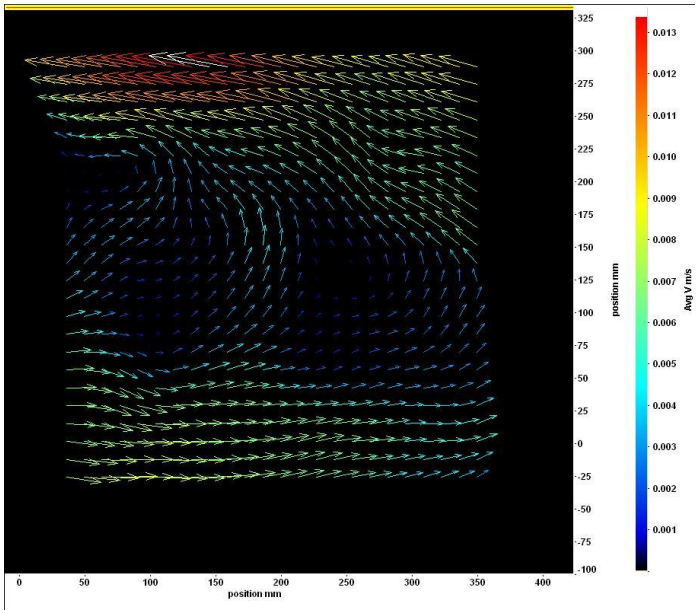

Figure (3) Velocity field computed from the single frame-duple exposure image presented above at 3.6 m/s wind seed. Number of vortices generated at different depths from the surface, the maximum velocity represented by red colour on the surface.

The surfactants affect the surface characteristics under effect of wind, by changing drift velocity, damping wave growth, increase the surface elasticity, decrease the surface tension etc.

Water contains active materials, and the percentage of those materials depends on the source of the water as explained above. The active materials diffuse from the water bulk toward the surface, the intensity of change in surface characteristics based on the percentage of the active material in the water bulk.

The effects of water source and its properties are not taken into consideration in the studies of wave generated due to atmospheric wind using water channel-wind facilities

Most of the studies that focused on the wave generation process discard the situation where the wind speed is less than 3 m/s where the ripples are not appreciable by naked eye, i.e. the resistance forces overcome wind effect on the water surface. The last two points should be taken into consideration during the future studies of wave generated by atmospheric wind

Dimensionless analysis

It is always possible to define new parameters by combining old ones or considering new effects. For example to measure the balance between viscous forces and surface tension, are such parameter is called the Ohnesorge number. According to Cetinbudaklar and Jameson (1969) the liquid film tends to become more unstable with an increase in liquid viscosity. For a given liquid flow rate, the film becomes thicker with an increase in viscosity. Smolentsev and Miraghaie (2005) explained that the Ohnesorge number is an indication of the stability of the liquid film draining down the duct wall witch increases with Ohnesorge number (i.e. increase in liquid viscosity). Apart from the effect of the liquid viscosity represented in Ohnesorge number, the stabilizing effect of the surface tension forces is also accounted for by the Ohnesorge number. From the above description of Ohnesorge number, it is hypothesised in this study that Ohnesorge number can be used to predict the water surface stability or to predict the wave generation at water surface under effect of low wind by studying *dynamic viscosity-surface tension ratio*. As explained in the previous section the surface film properties are related to water composition by the diffusion the active material from the water bulk toward the surface due to wind action. Consequently the surface tension and viscosity on the water surface change based on water composition and atmospheric conditions.

The Ohnesorge number is defined as:

$$Oh = \frac{We}{\mathrm{Re}} = \frac{\mu}{(h_m \rho \sigma)^{1/2}} \quad \text{.....(2)}$$

While the Weber number and Reynolds number are defined as follow:

$$W_e = U_m \sqrt{\rho h_m / \sigma} \quad \text{.....(3)}$$

$$\mathrm{Re} = \rho \mathrm{U}_m h_m / \mu \quad \text{.....(4)}$$

U_m and h_m are the bulk velocity and mean flow thickness in the reference cross-section, σ is surface tension, μ dynamic viscosity, and ρ is density. Another definition of Weber number can be obtained by taking the square of the previous one:

$$W_e = U_m{}^2 \rho h_m / \sigma \quad \text{.....(5)}$$

From the last Weber number definition, the new form of Ohnesorge number.

$$Oh = \frac{We}{\mathrm{Re}} = \frac{\rho h_m U_m^2 / \sigma}{\rho U_m h_m / \mu} = \frac{\mu}{\sigma} \times U_m \quad \text{.....(6)}$$

Since the kinematics viscosity and surface tension are functions of temperature, the following empirical formula is derived to calculate the ratio of σ and μ at different degrees of temperature

$$\left[\frac{\mu_w}{\sigma_w}\right]_T = 1\Big/\left[\left(\frac{\sigma_{w\ (T=0^\circ C)}}{\mu_{w\ (T=0^\circ C)}}\right)^{1/2} + AT - BT^2\right]^2 \quad ....(7)$$

$$A = 0.1$$

$$B = 2*10^{-4}$$

The kinematics viscosity and surface tension measurements with different temperature taken from Fox et al (2004)

From equation (6), it is hypothesised in this study that the *dynamic viscosity -surface tension ratio* gives an indication of surface stability or initial stages of wave generation at low wind speed. It is also hypothesised that the *dynamic viscosity surface-tension ratio* gives an indication of the minimum friction speed required to make the wave appreciable and visible by naked eye.

In wind-water facilities, Phongikaroon and Judd (2006) measured the wave height at different wind speeds for water and kerosene. They found that the wave height in kerosene for a given wind speed was larger than those formed in water and the wave become appreciable by naked eye for kerosene at a lower speed compared to water. Also they found that at higher speeds the product of wave height λ and density ρ was approximately the same for both fluids. The result of their experiments are shown in figure (4)

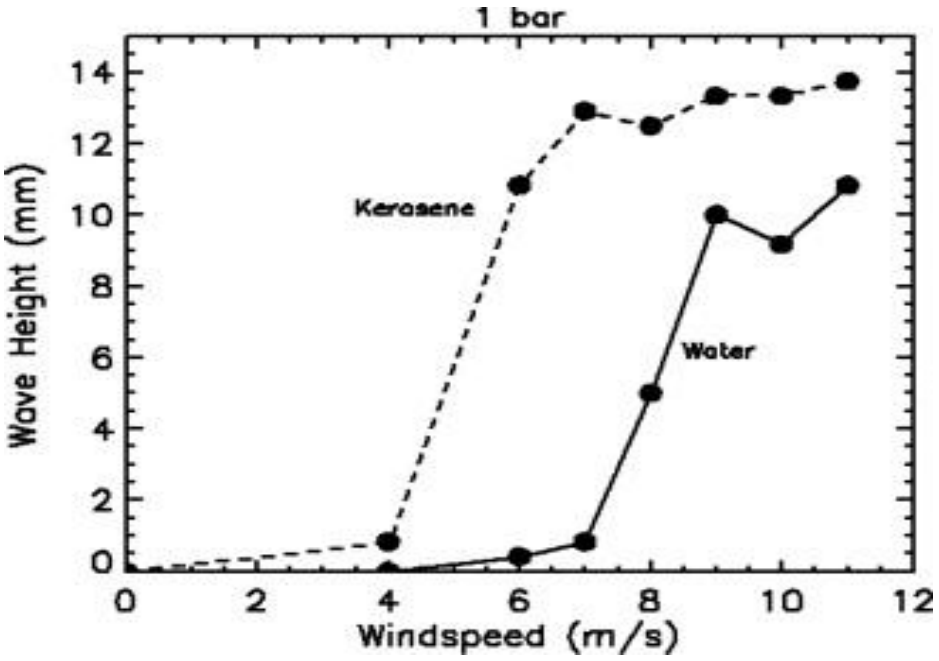

Figure (4) Water and kerosene wave height for runs at pressure 1 bar with different wind speeds. For the highest speeds, the height for waves in kerosene is ~25% larger, and at low wind speeds waves grow much more rapidly than for water, (Phongikaroon and Judd (2006))

In the last experiment the dynamic viscosity of water $\mu_w = 2.5\times10^{-3} Pa.s$ **and of kerosene** $\mu_k = 1\times10^{-3} P.s$ **and the surface tension of water** $\sigma_w = 72 mN/m$ **and of kerosene** $\sigma_k = 28 mN/m$ **. The ratio between surface tension and dynamic viscosity:**

$\sigma_k / \mu_k = 112,\ \sigma_w / \mu w = 72$

From Phongikaroon and Judd (2006) experiment results the influence of the *dynamic viscosity - surface tension ratio* on the minimum wind speed, or friction speed required to make the wave become appreciable by naked eye is obvious. It can be taken as a starting point for studying wave generation due to atmospheric wind in future work. Second the effect of fluid density on wave height at different wind speeds is recognised. The wave height increases at specific wind speed by decreasing the fluid density. Increasing the wave height at low wind speed indicate that the wave has short wave length and steeper slope compared to lower height wave at the same wind speed. So it is expected that the crests of higher wave will break first. The above explanation gives an indication that the fluid properties can be used to predict the evolution of the wave at different wind speed.

According to Kahma and Donelan (1988) the wavelength of the fastest growing waves, once β (wave growth rate) is positive, was observed to be 7-10 cm at water temperature $25^{\circ}C$, while approximately 10-15 cm at a water temperature of $5^{\circ}C$. They referred the increasing in wavelength to the fluid viscosity which is function with the temperature. The increasing in fluid viscosity acts on reducing the growth rate by increasing the wave length. Sehard et al (1999) observed at Lake Washington the wave associated with shallow depths or limited fetch were steeper (low wave length) and moving slower relative to the wind, generally presenting a rougher boundary to the atmosphere.

It is hypothesised in this study that the wave length (which is based on fluid viscosity) at low wind speed forms the base of the wave at high wind speed, which gives insight to the evolution of the wave at high wind speed. If the wave length is short at low wind speed the wave height will be limited to certain heights at high wind speed. The water composition changes wave length due to changing the viscosity, and water viscosity is related to water composition. Based on the above explanations it is hypothesised the wave length at fresh water (low viscosity) is shorter than the wave length at sea water (high viscosity), so the evolution of the wave at fresh water is limited compared to the sea water. It is hypothesised that one of the reasons that restrict the wave height on fresh water at high wind speed is wave length which wary due to water composition.

In the light of last hypothesis more investigations in the mathematical relations between wave length, maximum wave height, surface viscosity at different wind speed is necessary to add a new approach in understanding of water wave generated by atmospheric wind.

3. CONCLUSIONS

The composition of water affects water surface properties such as; drift velocity, surface tension, dynamic viscosity, wave growth rate, surface density, etc. under the effect of low wind speed. However dynamic viscosity and surface tension are the main characteristics of the water surface, which vary due to atmospheric wind and water composition and affect wave formation on water surface. It is hypothesised that dynamic *viscosity-surface tension ratio* on water surface gives an indication of water surface stability and the minimum friction velocity required to make the water waves appreciable by naked eye due to atmospheric wind.

The surface viscosity confine water wave length generated by atmospheric wind, so water viscosity can be used to predict wave height evolution and generation due to high wind speed.

The mathematical relations between wave length, maximum wave height, surface viscosity at different wind speed is necessary to formulate to add a new approach in understanding of water wave generated by atmospheric wind.

Thus it can be seen that the presence of surfactants on water surface changes the *wind-water* momentum transfer mechanism due to change surface properties. For clean water the wind momentum transfer to the surface and extends from the surface to the bottom, in presence of surfactants wind momentum confined to the surface and cause an increase in the surface velocity compare to the clean case under effect of the wind.

It is hypothesised in the case of the clean water; that the interaction between water surface and wind is a momentum transfer mechanism. The water surface and air become coupled according to the viscous theory of Miles (1962a). In the second case, where a surfactant is present, the wind water surface interaction is an energy transfer mechanism; the air energy is transferred to the surface only, so no waves appear at the surface in this case, and an increase in the surface velocity observed.

It is hypothesised that the water surface slope growth is the first stage of wave generation due to low wind speed as a result of *wind-water* interaction.

Finally decreasing the atmospheric temperature increases water viscosity and decrease air viscosity. It is hypothesised that the air-water viscosity difference enhances air- surface coupling, so the amount of momentum that transfers to the surface increases at the same wind speed compared to high temperature case.

4. RECOMMONDATION

From the previous analysis, it is recommended to take water composition as main parameter when studying wind-wave generation and interaction mechanism under laboratory conditions at low to intermediate wind speed.

5. ACKNOWLEDGMENT

This study and related experiments are prepared and performed at Hertfordshire University, in the Fluids Mechanics Laboratory Aerospace, Automotive and Design Engineering Department.

6. REFERENCES

[1]. Cetinbudaklar, A. G and Jameson G. J., (1969), "The mechanism of flooding in vertical countercurrent two-phase flow", Chemical engineering science. 24, 1669-1680

[2] Plate, E. J., P. C. Chang., (1969), "Experiments on the generation of small water waves by wind", Journal of fluid mechanic 35, 625-656.

[3] Caulliez, G., Ricci, N., and Dupont R., (1998), "The generation of the first visible wind waves", Physics fluids 10, 757-759.

[4] Scott, John. C., (1982), "Flow beneath stagnant film on water: the Reynolds ridge", J. Fluid mechanics116, 283-296.

[5] John, W. Miles., (1962)," On generation of surface waves by shear flow. Part 4", Journal of Fluid Mechanics. 433-448

[6] Gottfried, J. C., and Jameson G. J., (1970), "The growth of short waves on liquid surfaces under the action of wind", Proc. Roy. Soc. Lond, 319, 373-397

[7] Davis, J.T., Qidwa, A., and Hameed, A., (1967), "Surface stresses and ripple formation due to low velocity air passing over water surface", Chemical Engineering Science 23, 331-337

[8] Davies, J.T., and Rideal, E. K., (1968), "Interfacial Phenomenon", Academic Press, New York

[9] Kahma, Kimmo. K., and Mark, A. Donelan., (1988), "A laboratory study of the minimum wind speed for wind wave generation", J. Fluid Mech, 192 339-364.

[10] Ralph, D. Lorenz., Erin, R. Kraal., Eric, E. Eddlemon., Jered, Cheney., and Ronald, Greeley., (2005), "Sea-surface wave growth under extraterrestrial atmospheres: Preliminary wind tunnel experiments with application to Mars and Titan", ICARUS, 175 556-560

[11] Robert, W. Fox., Alan, T. McDonald., Philip, J. Pritchard., (2004), "Introduction to fluid mechanics", sixth edition, USA

[12] Sehard, S. Ataktürk., and Kristina, B., (1999), "Katsaros, Wind stress and surface wave observed on Lake Washington", American Meteorological Society 633-650

[13] Satterly, J., and Turnbull, R., (1929), "The ridge at the junction of clean and contaminated liquid surface", Trans. R. Canada 23, 95-118

[14] Sergey, Smolentsev., and Reza, Miraghaie., (2005), "Study of a free surface in open channel water flows in the regime from weak to strong turbulence", International journal of multiphase flow 31, 921-939

[15] kawai, S., (1979), "Generation of initial wavelets by instability of coupled shear flow and their evolution to wind waves", J. Fluid Mech 93 (661)

[16] Supathorn, Phongikaroon., and Peter, Judd K., (2006)," Surfactant effects on the free surface thermal structure and subsurface flow in wind-wave tunnel", Journal of Fluid Engineering 128, 913-920

[17] Mansfield, W. W., (1973), "The influence of surfactants on flow at wind-blown over water surfaces", Chemical Engineering Science 29, 1593-1600